

https://dspace.org/

Stability of planets in triple star systems

Busetti, Franco Raoul

2018

https://hdl.handle.net/10539/26052

Busetti, Franco Raoul (2018) Stability of planets in triple star systems, University of the Witwatersrand, Johannesburg, <http://hdl.handle.net/10539/26052>

Downloaded from a DSpace repository. https://dspace.org/



STABILITY OF PLANETS IN TRIPLE STAR SYSTEMS

Franco Busetti

A thesis submitted to the
Faculty of Science, University of the Witwatersrand
South Africa
in fulfilment of the requirements for the degree of
Doctor of Philosophy

Supervisors

Dr Charis Harley
School of Computer Science and Applied Mathematics
University of the Witwatersrand, South Africa

Dr Hervé Beust
Institute of Planetology and Astrophysics of Grenoble
University of Grenoble Alpes, France

April 2018

Declaration

I declare that this thesis is my own, unaided work. It is being submitted for the Degree of Doctor of Philosophy in the University of the Witwatersrand, South Africa. It has not been submitted before for any degree or examination in any other University.



Franco Busetti

1st day of April 2018

There are countless suns and countless earths all rotating round their suns in exactly the same way as the seven planets of our system. The unnumbered worlds in the universe are all similar in form and rank and subject to the same forces and the same laws.

– Giordano Bruno, *On the Infinite Universe and Worlds* (1584)

The roads by which men arrive at their insights into celestial matters seem to me almost as worthy of wonder as those matters in themselves.

– Johannes Kepler, *Astronomia Nova* (1609)

Yes, astronomy's much more fun when you're not an astronomer.

– Brian May, VOX Magazine (1991)

Abstract

This study investigates the space around triple systems to find the regions of secular stability of planetary orbits. Numerical *N*-body simulations are used to determine empirically the bounds of these regions as a function of the system's configuration.

There have been numerous theoretical studies of the stellar dynamics of triple systems, some with limited numerical checks, but the few purely empirical studies have been confined largely to binaries. Very little has been done on planetary orbits within either of these systems. There has been almost no work on generalised systems, little on retrograde planetary orbits and none on retrograde stellar orbits, with nearly all being on coplanar orbits and for a limited number of orbital parameters.

This work expands into, and investigates new areas through

1. Providing a generalised mapping of the regions of planetary stability in triples, by:
2. examining all four types of orbits – P1, P2, S1 and S3;
3. investigating these orbit types for both prograde and retrograde motion of the planets;
4. investigating them for both prograde and retrograde motion of the outer body of the triple;
5. investigating highly-inclined orbits of the outer star, stellar Kozai resonance and its effect on the region of stability for P1 and P2 orbits;
6. extending the number of parameters used to all relevant orbital elements of the triple's stars, and
7. expanding these elements and mass ratios to wider ranges that will accommodate recent and possible future observational discoveries.

This resulted in semi-analytical models describing the stability bounds of each type of orbital configuration found in triples.

These relationships can be used to guide searches for planets in triple systems and to determine quickly the feasibility of initial observational estimates of planetary orbital parameters, and to select suitable candidates for a survey of such systems. The geometry of the stable zone indicates not only where to look for planets but the most suitable search method.

To highlight how the stability of planets in triple systems differs from that for binaries, an analysis of these systems over the same parameter space was required, resulting in a contribution to the body of empirical work on binaries as well

Key words: methods: numerical – methods: *N*-body simulations – planet-star interactions – celestial mechanics – stars: hierarchical triples – planetary systems: dynamical evolution and stability

To Vivienne and Jill,
binary stars

Acknowledgments

I wish to thank my supervisors – Charis Harley, for her encouragement and ever-ready support, and Hervé Beust, for his guidance and discussions in Grenoble.

Hervé also provided the original Hierarchic Jacobi Symplectic (HJS) code and later enhancements.

The original SWIFT code was obtained from Hal Levison.

Data visualisation was done with the SwiftVis visual data-flow programming environment created by Mark Lewis.

Computations were run on the Mathematical Sciences Cluster at the University of the Witwatersrand.

This research made use of the NASA Exoplanet Archive, the Exoplanet Orbit Database and Exoplanet Data Explorer (exoplanets.org), The Exoplanet Encyclopaedia (Exoplanet.eu), the Open Exoplanet Catalogue, the Washington Double Star Catalog maintained at the U.S. Naval Observatory and bibliographic references from the Astrophysics Data System maintained by SAO/NASA.

Contents

Chapter 1 Introduction 1

1.1 Stellar Multiplicity 1
1.2 Hierarchical Orbits 3
1.3 Stability Of Triple Stellar Systems 3
1.4 Exoplanet Multiplicity 4
1.5 Exoplanet Orbits 6
1.5.1 Exoplanet orbit types 6
1.5.2 Prograde and retrograde planetary orbits 7
1.5.3 Observational discoveries 8

Chapter 2 Approaches to the problem 13

2.1 Theoretical Approaches 13
2.2 Computational Approaches 14

Chapter 3 Characteristics of triple systems 17

3.1 Overview 17
3.2 Databases 18
3.3 Triples – Stellar Characteristics 18
3.4 Triples – Planetary Characteristics 18
3.4.1 Planetary mass and orbital distances 18
3.4.2 Planetary eccentricity 20
3.4.3 The Kozai mechanism 22
3.4.4 Planetary orbital inclinations 26
3.4.5 Chaotic orbits 27
3.5 Scope And Limitations Of The Investigation 28
3.6 Selection of Parameter Space 28
3.6.1 Orbit types 28
3.6.2 Stellar configurations 30
3.6.3 Semi-major axis ratio 31
3.6.4 Inner mass ratio 34
3.6.5 Outer mass ratio 34
3.6.6 Eccentricities 34
3.6.7 Inclinations 35
3.6.8 Outer star longitude of ascending node 37
3.6.9 Outer star argument of periapsis 37
3.7 Numerical Methods And Selection Of Integrator 38
3.7.1 Swift 38
3.7.2 HJS 38
3.7.3 Mercury6 39
3.7.4 NBODY 39
3.7.5 FEWBODY 39
3.7.6 Miscellaneous 39
3.7.7 Selection of integrator 40
3.7.8 Software details and other software used 40

3.8 Computational Parameters 41
3.8.1 Time step 41
3.8.2 Integration time 41
3.8.3 The test particle cloud 43
3.8.4 Test particle removals 44
3.8.5 The Hill stability criterion 44
3.9 Orbit Stability Bounds – Edge Detection Routine 45
Chapter 4 Results 49
4.1 Orbit Types P1 And P2 49
4.1.1 Configuration 49
4.1.2 Parameter space 49
4.1.3 Computational parameters 50
4.1.4 An example integration 51
4.1.5 Prograde outer star 59
4.1.6 Retrograde outer star 67
4.1.7 Comparison with previous work on P1 and P2 bounds 77
4.1.8 Some observational examples of P1 and P2 orbits 77
4.1.9 Triples compared with binaries 78
4.1.10 Conclusions – P1 and P2 orbits 86
4.2 Orbit Types P1 And P2 In Highly Inclined Triple Systems 87
4.2.1 Vertical characteristics of the stability region 87
4.2.2 Stellar Kozai resonances in the triple 94
4.2.3 Analysis of stellar Kozai resonances 99
4.2.4 Planetary stability bounds and the outer star's inclination 101
4.2.5 Comparison with previous work on non-coplanar orbits 109
4.2.6 Observational examples of stellar Kozai resonance in triples 110
4.2.7 The limitations of a theoretical approach 110
4.2.8 Conclusions – highly inclined triple systems 115
4.3 Orbit Type S1/S2 116
4.3.1 Configuration 116
4.3.2 Parameter space 117
4.3.3 Computational parameters 119
4.3.4 Prograde outer star 120
4.3.5 Retrograde outer star 124
4.3.6 Comparison with the Hill stability criterion 130
4.3.7 Comparison with previous work on S1 bounds 131
4.3.8 Some observational examples of S1 orbits. 132
4.3.9 Triples compared with binaries 132
4.3.10 Conclusions – S1/S2 orbits 137
4.4 Orbit Type S3 137
4.4.1 Configuration 137
4.4.2 Parameter space 138
4.4.3 Computational parameters 138
4.4.4 Prograde outer star 141
4.4.5 Retrograde outer star 145
4.4.6 Comparison with previous work on S3 bounds 149
4.4.7 Some observational examples of S3 orbits. 149
4.4.8 Triples compared with binaries 150

4.4.9 Conclusions – S3 orbits 153
4.5 Orbit Types S1 And S3 In Triples Compared 153
4.5.1 Prograde stellar orbits 154
4.5.2 Retrograde stellar orbits 155
4.5.3 Conclusions 156
4.6 Summary Of Results 156
4.6.1 Summary of differences between triples and binaries 156
4.6.2 Summary of results for triples 158
4.7 Comparison With Previous Work 163
4.7.1 Comparison of scope 163
4.7.2 Comparison of results 166
4.7.3 New binary data 168
Chapter 5 Conclusions 169
5.1 What Was Done In This Study 169
5.2 How This Extended Previous Work 169
5.3 New Findings 170
5.4 How The Results Can Be Used 173
Chapter 6 Further work 174
Appendices 175
A.1 Summary Of Stellar Parameters 175
A.2 Summary Of Computational Parameters 175
B.1 Comparison With Theory – Outer Restricted Model 176
C.1 Regressions – Highly-Inclined Triple Systems 178
D.1 Regressions – Binary Systems 179
References 180

List of Figures

Figure 1. A planet in a binary system, where ⊗ is the stellar centre of mass: a) the planet orbits one component of the stellar binary; b) the planet is in a circumbinary orbit around both stellar components (Perryman 2011).....6
Figure 2. Stability limits for a three-body system as a function of orbital inclination. The lines overlaid on the numerical solution are various theoretical solutions (Grishin et al. 2017).....13
Figure 3. Planet mass versus semi-major axis, with stellar multiplicity.....19
Figure 4. Planet mass versus semi-major axis, with stellar multiplicity and orbit type.....19
Figure 5. Planet eccentricity versus semi-major axis, with stellar multiplicity.....21
Figure 6. Planet eccentricity versus semi-major axis, with stellar multiplicity and orbit type.....21
Figure 7. Observed exoplanet eccentricities (Kaib, Raymond & Duncan 2013).....22
Figure 8. Triple system nomenclature with S-type and P-type orbits.....29
Figure 9. Triple systems – orbit types.....30
Figure 10. Stability criterion for triples. a) semi-major axis ratio and outer eccentricity b) period ratio and outer eccentricity.....33
Figure 11. Triple systems – distribution of eccentricities.....35
Figure 12. Distribution of mutual orbital inclinations for triple systems. The peak between 0° – 5° contains 21 systems (off scale). (Borkovits et al. 2015).....37
Figure 13. Relative energy error of a typical integration.....42
Figure 14. a) Cartesian plot of final particle positions, b) corresponding density function.....45
Figure 15. a) Cartesian plot of final particle positions over the last 5% of the integration time b) corresponding density function.....46
Figure 16. The particle density function and edge detection algorithm.....46
Figure 17. Test particle cloud and density function of: a) prograde planets b) retrograde planets, with all other parameters identical.....47
Figure 18. P1 and P2 orbits. Triple system configuration.....49
Figure 19. P1 and P2 orbits. Progression of the clearing of the inner area, at times $t = 0$ yr, 170 yr, 290 yr, 1 380 yr and 10 000 yr.....52
Figure 20. P1 and P2 orbits. Semi-major axes and eccentricities of test particles after 100 000 yr.....53
Figure 21. Keplerian outer P2 orbits and chaotic and eccentric inner P1 orbits.....54
Figure 22. Selected orbital elements of test particle #942.....54
Figure 23. Selected orbital elements of test particle #902.....55
Figure 24. Selected orbital elements of test particle #727.....55
Figure 25. Decline in the number of surviving test particles over time.....56
Figure 26. P1 and P2 orbits. a) prograde planetary orbits b) retrograde planetary orbits.....57

Figure 27. P1 and P2 orbits, prograde outer star, prograde planets. a) inner bounds b) outer bounds 59
Figure 28. P1 and P2 orbits, prograde outer star, retrograde planets. a) inner bounds b) outer bounds 59
Figure 29. Regression plot of outer critical semi-major axis ratio against outer star eccentricity 63
Figure 30. P1 and P2 orbits, retrograde outer star, prograde planets. a) inner bounds b) outer bounds 67
Figure 31. P1 and P2 orbits, retrograde outer star, retrograde planets. a) inner bounds b) outer bounds 68
Figure 32. P1 and P2 orbits. Regression coefficients for various combinations of orbital motions. Upper panel a) prograde outer star, lower panel b) retrograde outer star 74
Figure 33. P2 orbits. Outer stability bound as a function of outer star eccentricity 76
Figure 34. P1 orbits. Inner stability bound as a function of outer star eccentricity 76
Figure 35. For $m3 = 0.001\ Ms$ (upper panel) a) outer orbit b) inner orbit. For $m3 = 6\ Ms$ (lower panel) c) outer orbit d) inner orbit 79
Figure 36. For $m3 = 0.001\ Ms$ (upper panel) a) test particle cloud b) zoomed in. For $m3 = 6\ Ms$ (lower panel) c) test particle cloud d) zoomed in 79
Figure 37. Reducing the inner binary. a) upper panel: $m1 = 2.5\ Ms,\ m2 = 2.5\ Ms, a1 = 1$ AU b) lower panel: $m1 = 4.999\ Ms,\ m2 = 0.001\ Ms, a1 = 0.01$ AU 81
Figure 38. Binary P1 and P2 orbits, prograde outer star, prograde planets: a) inner bounds b) outer bounds 82
Figure 39. Binary P1 and P2 orbits, prograde outer star, retrograde planets: a) inner bounds b) outer bounds 83
Figure 40. Binary P1 and P2 orbits. Regression coefficients, triples compared with binaries 86
Figure 41. The invariable plane in a triple system 88
Figure 42. P1 and P2 orbits, using coordinate system of the inner orbital plane. a) upper panel: $t = 0$ yr b) lower panel: $t = 100$ kyr 90
Figure 43. P1 and P2 orbits, using coordinate system of the outer orbital plane. a) upper panel: $t = 0$ yr b) lower panel: $t = 100$ ky 91
Figure 44. Position in space of surviving test particles after 100 kyr. P1 and P2 prograde orbits 92
Figure 45. P1 and P2 orbits. Single prograde test particle cloud after 1 Myr, $a = 40$ AU, $e1 = e2 = 0, i1 = 0, \mu1 = 0.5, \mu2 = 2.0, i2 = 65°$ 93
Figure 46. Number of stable P1 and P2 prograde orbits remaining after 1 Myr as a function of initial planetary inclination, for various triple configurations 94
Figure 47. P1 and P2 orbits, base case, no Kozai resonance, $\mu1 = \mu2 = 0.5, i2 = 30°, a = 40$ AU 95
Figure 48. P1 and P2 orbits, higher outer star inclination, $\mu1 = \mu2 = 0.5, i2 = 65°, a = 40$ AU 96
Figure 49. P1 and P2 orbits, closer outer star, $\mu1 = \mu2 = 0.5, i2 = 65°, a = 20$ AU 97

Figure 50. P1 and P2 orbits, higher outer star inclination, $\mu 1 = 0.5, \mu 2 = 0.5, i2 = 90°, a = 40$ AU 97
Figure 51. P1 and P2 orbits, higher outer star mass, $\mu 1 = 0.5, \mu 2 = 2.0, i2 = 65°, a = 40$ AU 98
Figure 52. P1 and P2 orbits, retrograde outer star, $\mu 1 = 0.5, \mu 2 = 2.0, i2 = 115°, a = 40$ AU 98
Figure 53. P1 and P2 orbits, higher outer star mass and lower inner star mass, $\mu 1 = 0.25, \mu 2 = 2.0, i2 = 65°, a = 40$ AU 99
Figure 54. Angular momentum ratio distribution for Kozai integrations 102
Figure 55. P1 and P2 orbits. Critical semi-major axis ratios versus outer star inclination a) inner stability bound b) outer stability bound 103
Figure 56. P1 and P2 orbits. Regression results for non-Kozai and Kozai regimes 105
Figure 57. P1 and P2 orbits. Outer critical semi-major axis ratio versus outer star inclination (smoothed) 106
Figure 58. P1 and P2 orbits under Kozai resonance, $a = 30$ AU, $\mu 1 = 0.5, \mu 2 = 0.5$ 107
Figure 59. P1 and P2 orbits under Kozai resonance, $a = 20$ AU, $\mu 1 = 0.5, \mu 2 = 0.5$ 108
Figure 60. P1 and P2 orbits under Kozai resonance, $a = 15$ AU, $\mu 1 = 0.25, \mu 2 = 2.5$ 108
Figure 61. Outer restricted approximation, Hamiltonian surface 111
Figure 62. Outer restricted approximation, curves of constant Hamiltonian for values of k of a) 0.02 b) 0.5 c) 1.0 d) 5.0. Contours cover the range $H = -8, 8$ 112
Figure 63. P1 and P2 orbits. High-inclination example, $a = 20$ AU, $\mu 1 = 0.5, \mu 2 = 0.5, e1 = 0.5, e2 = 0.5, i1 = 0°, i2 = 60°, \Omega 2 = 90°, \omega 2 = 0°$ 113
Figure 64. P1 and P2 orbits. a) final distribution in the *p*-*q* plane of test particles from an initial spherical cloud b) test particle distribution overlaid with curves of constant Hamiltonian 113
Figure 65. P1 and P2 orbits. Final distribution in the *p*-*q* plane of test particles from an initial disc aligned with the invariable plane 114
Figure 66. P1 and P2 orbits. Final distribution in the *p*-*q* plane of test particles from initial discs aligned with the invariable plane, for various outer mass ratios and inclinations 115
Figure 67. S1/S2 orbits, triple system configuration 117
Figure 68. S1 orbits, prograde outer star, test particle survival rates 121
Figure 69. S1 orbits, prograde outer star. a) prograde bounds b) retrograde bounds 121
Figure 70. S1 orbits, retrograde outer star, test particle survival rates 124
Figure 71. S1 orbits, retrograde outer star. a) prograde bounds b) retrograde bounds 125
Figure 72. S1 orbits. Regression coefficients for various combinations of orbital motions a) prograde outer star, b) retrograde outer star 128
Figure 73. S1 orbits. Critical semi-major axis ratios versus (1-$\mu 1$) 131
Figure 74. S1 orbits. Critical semi-major axis ratio versus mass of outer star 133
Figure 75. S1 orbits. All stability bounds a) binary bounds b) triple bounds 134
Figure 76. Binary S1 orbits. Distribution of critical semi-major axis ratios 134

Figure 77. S1 orbits. Regression coefficients, triples versus binaries – a) prograde planets b) retrograde planets 136
Figure 78. Triple system configuration – S3 orbits.....137
Figure 79. S3 orbits. a) orbit of close binary pair Star 1 and Star 2 b) orbit of binary pair around Star 3. Parameters $a1 = 1$ AU, $a2 = 62$ AU, $\mu1 = 0.176, \mu2 = 0.375, e1 = 0.042, e2 = 0.651, \Omega2 = 32°$ 139
Figure 80. S3 orbits. a) test particle density function at aphelion b) test particle cloud at centre with captured sub-cloud at aphelion 139
Figure 81. S3 orbits. a) test particle density function at perihelion b) test particle cloud at centre with captured sub-cloud at perihelion 140
Figure 82. S3 orbits, prograde outer star, test particle survival rates.....141
Figure 83. S3 orbits, prograde outer star a) prograde bounds b) retrograde bounds 142
Figure 84. S3 orbits, prograde outer star. Relationship between critical semimajor axis ratio and $\mu2$, linearised 144
Figure 85. S3 orbits, retrograde outer star, test particle survival rates.....145
Figure 86. S3 orbits, retrograde outer star. a) prograde bounds b) retrograde bounds 146
Figure 87. S3 orbits. Regression coefficients for various combinations of orbital motions a) prograde outer star, b) retrograde outer star 148
Figure 88. Binary S3 orbits. a) all stability bounds b) test particle survival rates 150
Figure 89. S3 orbits. Regression coefficients, triples versus binaries – a) prograde planets b) retrograde planets 153
Figure 90. S1 and S3 orbits compared. Regression coefficients for a) prograde and b) retrograde outer star/s 156
Figure 91. Summary of mean and standard deviation of critical semi-major axis ratios for P1, S1 and S3 orbits 159
Figure 92. Summary of mean and standard deviation of critical semi-major axis ratios for P2 orbits 159
Figure 93. Summary of mean and range of critical semi-major axis ratios for non-Kozai and Kozai cases, for both stellar motions.....162
Figure 94. Comparison of results for binaries – regression constants 167
Figure 95. Comparison of results for binaries – critical semi-major axis ratios.....168

List of Tables

Table 1. Stellar multiplicities per Tokovinin (2014).....2
Table 2. Multiplicities of solar-like stars and exoplanet host stars.....5
Table 3. Frequencies of multiplicities (references refer to those in Table 2) 5
Table 4. Frequency of exoplanets by type of orbit.....9
Table 5. Exoplanets discovered in stellar systems of multiplicity three and higher.....11
Table 6. Compact triples from the Eggleton & Tokovinin 2008 survey.....32
Table 7. Triple systems –inclinations. All systems where two visual orbits are known, from the Multiple Star Catalog (Tokovinin 1997) 36
Table 8. Edge detection parameters for triple system P1 and P2 orbits.....48
Table 9. P1 and P2 orbits – parameter space 50
Table 10. P1 and P2 orbits – computational parameters.....50
Table 11. P1 and P2 orbits, prograde outer star. Number of bounds found.....60
Table 12. P1 and P2 orbits, prograde outer star – mean critical semi-major axis ratios 60
Table 13. P1 and P2 orbits, prograde outer star – expected signs of regression coefficients.....61
Table 14. P1 and P2 orbits, prograde outer star. Regression coefficients – outer region, prograde planetary orbits 63
Table 15. P1 and P2 orbits, prograde outer star. Regression coefficients – outer region, retrograde planetary orbits.....64
Table 16. P1 and P2 orbits, prograde outer star. Regression coefficients – inner region, prograde planetary orbits 65
Table 17. P1 and P2 orbits, prograde outer star. Regression coefficients – inner region, retrograde planetary orbits.....66
Table 18. P1 and P2 orbits, prograde outer star. Critical semi-major axis ratio versus direction of planetary motion and outer star eccentricity 67
Table 19. P1 and P2 orbits, retrograde outer star. Number of bounds found.....68
Table 20. P1 and P2 orbits, retrograde outer star. Mean critical semi-major axis ratios 68
Table 21. P1 and P2 orbits. Difference in mean critical semi-major axis ratios for prograde and retrograde stellar orbits.....69
Table 22. P1 and P2 orbits, retrograde outer star. Regression coefficients – outer region, prograde orbits.....70
Table 23. P1 and P2 orbits, retrograde outer star. Regression coefficients – outer region, retrograde orbits.....71
Table 24. P1 and P2 orbits, retrograde outer star. Regression coefficients – inner region, prograde orbits.....72
Table 25. P1 and P2 orbits, retrograde outer star. Regression coefficients – inner region, retrograde orbits.....73
Table 26. P1 and P2 orbits. Mean critical semi-major axis ratios for various combinations of orbital motions.....73
Table 27. P1 and P2 orbits. Differences in regression coefficients for prograde and retrograde motions of the outer star 75

Table 28. P1 and P2 orbits. Edge detection parameters for reduced binary system....82
Table 29. Binary P1 and P2 orbits, prograde outer star. Number of bounds found....83
Table 30. Binary P1 and P2 orbits, prograde outer star – mean critical semi-major axis ratios....83
Table 31. Binary P1 and P2 orbits. Difference between mean critical semi-major axis ratios in triples and binaries....84
Table 32. Binary P1 and P2 orbits. Regression coefficients and model fits, triples compared with binaries....85
Table 33. Highest and lowest contributions to system angular momentum for high-inclination integrations....89
Table 34. P1 and P2 orbits. Summary of Kozai characteristics....100
Table 35. P1 and P2 orbits. Comparison of libration periods, Kozai resonance periods and maximum eccentricity....101
Table 36. Non-Kozai and Kozai cases, mean critical semi-major axis ratios for prograde and retrograde stellar orbits....104
Table 37. P1 and P2 orbits. Regression constants for non-Kozai and Kozai regimes....106
Table 38. S1 orbits. Scaling of inner binaries....118
Table 39. S1 orbits. Parameter space used....118
Table 40. S1 orbits. Edge detection algorithm parameters....120
Table 41. S1 orbits. Computational parameters....120
Table 42. S1 orbits, prograde outer star. Number of bounds found....122
Table 43. S1 orbits, prograde outer star. Mean critical semi-major axis ratios....122
Table 44. S1 orbits, prograde outer star, expected signs of regression coefficients....122
Table 45. S1 orbits, prograde outer star. Regression coefficients – prograde planetary orbits....123
Table 46. S1 orbits, prograde outer star. Regression coefficients – retrograde planetary orbits....124
Table 47. S1 orbits, retrograde outer star. Number of bounds found....125
Table 48. S1 orbits, retrograde outer star. Mean critical semi-major axis ratios....125
Table 49. S1 orbits, retrograde outer star. Regression coefficients – prograde planetary orbits....126
Table 50. S1 orbits, retrograde outer star. Regression coefficients – retrograde planetary orbits....127
Table 51. S1 orbits. Mean critical semi-major axis ratios for various combinations of orbital motions....128
Table 52. S1 orbits. Relative stability of combinations of stellar and planetary orbital motions....129
Table 53. S1 orbits of planets discovered in triple-star systems....132
Table 54. Binary S1 orbits. Number of bounds found....135
Table 55. Binary S1 orbits. Mean critical semi-major axis ratios....135
Table 56. Binary S1 orbits. Difference between average planetary bounds in triples and binaries....135
Table 57. S1 orbits. Regression coefficients and model fits, triples versus binaries....136
Table 58. S3 orbits. Parameter space used....138

Table 59. S3 orbits. Computational parameters 141
Table 60. S3 orbits. Edge detection algorithm parameters 141
Table 61. S3 orbits, prograde outer star. Number of bounds found 142
Table 62. S3 orbits, prograde outer star. Mean critical semi-major axis ratios 143
Table 63. S3 orbits, prograde outer star. Expected signs of regression coefficients 143
Table 64. S3 orbits, prograde outer star. Regression coefficients – prograde planetary orbits 144
Table 65. S3 orbits, prograde outer star. Regression coefficients – retrograde planetary orbits 145
Table 66. S3 orbits, retrograde outer star. Number of bounds found 146
Table 67. S3 orbits, retrograde outer star. Mean critical semi-major axis ratio 146
Table 68. S3 orbits, retrograde outer star. Regression coefficients – prograde planetary orbits 147
Table 69. S3 orbits, retrograde outer star. Regression coefficients – retrograde planetary orbits 147
Table 70. Mean critical semi-major axis ratios for S3-type orbits 148
Table 71. S3 orbits. Selected planets found in these orbits in triple-star systems 149
Table 72. Binary S3 orbits. Number of bounds found 151
Table 73. Binary S3 orbits. Mean critical semi-major axis ratios 151
Table 74. Binary S3 orbits. Difference between mean planetary bounds in triples and binaries 152
Table 75. S3 orbits. Regression coefficients and model fits, triples versus binaries 152
Table 76. S1 and S3 orbits compared. Mean critical semi- major axis ratios, prograde outer star/s 154
Table 77. S1 and S3 orbits compared. Difference in regression coefficients, prograde outer star/s 154
Table 78. S1 and S3 orbits compared. Mean critical semi- major axis ratios, retrograde outer star/s 155
Table 79. S1 and S3 orbits compared. Difference in regression coefficients, prograde outer star/s 155
Table 80. Summary of differences between mean critical semi-major axis ratios in triples and binaries – all orbit types 157
Table 81. Summary of mean critical semi-major axis ratios for various orbital configurations 158
Table 82. Summary of differences in mean critical semi-major axis ratios and regression constants, for retrograde relative to prograde stellar motion, with the same planetary motion 160
Table 83. Summary of differences in mean critical semi-major axis ratios and regression constants for retrograde relative to prograde planetary motion, with the same stellar motion 161
Table 84. Summary of differences in S1 and S3 mean critical semi-major axis ratios 161
Table 85. Summary of regression statistics for all triple orbital configurations 164
Table 86. Comparison with variable ranges used in previous empirical studies 165

Table 87. Comparison with mean critical semi-major axis ratios and regression constants from previous empirical studies.....166

List of Symbols

Orbital

Numerical subscripts usually refer to stars 1, 2 and 3

m	mass
$\mu = \frac{m_1 m_2}{m_1 + m_2}$	reduced mass of a system comprising masses m_1, m_2
a	semi-major axis
P	period
e	eccentricity
i	inclination
a_1	semi-major axis of star 2
a_2	semi-major axis of star 3
$a = a_2/a_1$	stellar semi-major axis ratio
a_{io}/a_2	planetary semi-major axis ratio – inner
a_{oi}/a_2	planetary semi-major axis ratio – outer
$\mu_1 = m_2/(m_1 + m_2)$	mass ratio, inner
$\mu_2 = m_3/(m_1 + m_2)$	mass ratio, outer
Ω	longitude of ascending node or line of nodes
ω	argument of periapsis
ν	true anomaly
L	angular momentum
G	the gravitational constant
L_z	conserved quantity in the Kozai relationship
t_{K}	characteristic Kozai time
R_{H}	Hill radius
$p = i_2 \cos \Omega_2$	transformed variable used in Hamiltonian
$q = i_2 \sin \Omega_2$	transformed variable used in Hamiltonian
M_s	Solar mass

Computational

$rmin$	heliocentric distance at which a test particle collides with the central star
$rmax$	heliocentric distance at which a test particle is ejected from the system

$amin$	minimum semi-major axis of the test particle cloud
$amax$	maximum semi-major axis of the test particle cloud
$dt, \Delta t$	integration time step
f_t	fraction of integration time used to generate the test particle density function
max	maximum of the inner orbit density function
f_i	fraction of the maximum used as the inner orbit density function's cutoff limit
avg_i	mean density of the inner orbit density function
$peak = max/avg_i$	"peakiness" of the inner orbit density function
f_p	cutoff value of the "peakiness" of the inner orbit density function
l_s	fraction of the outer star's semi-major axis, set as a minimum inner orbit semi-major axis
avg_o	mean of the outer orbit density function
f_o	fraction of the average, used as the outer orbit density function's cutoff limit
a_a	ratio of the mean density of the inner orbits to the outer orbits

Statistical

B	regression coefficients
t	t-statistic
R^2	coefficient of determination
SD or σ	standard deviation
SE	standard error
F	F-statistic for overall significance
MAPE	mean absolute percentage error

Abbreviations

CCDM	Catalogue of Components of Double and Multiple Stars
EOD	Exoplanet Orbit Database
EPE	The Extrasolar Planets Encyclopaedia
MSC	Multiple Star Catalogue
MMR	mean motion resonance

MCSAR	mean critical semi-major axis ratio
MSSAR	mean stable semi-major axis ratio

Note that the previous two terms and “stability bound” or “bound” are used fairly interchangeably in the text.

NEA	NASA Exoplanet Archive
OEC	Open Exoplanet Catalogue
PDF	particle density function
TP	test particle
WDS	Washington Double Star Catalog

Chapter 1

Introduction

There have been numerous theoretical studies of the stellar dynamics of triple systems, with some including limited numerical checks. Theoretical approaches have some significant limitations. The few studies that are a) numerical/empirical and b) apply to planets, have been confined almost exclusively to binaries. There has been only one study of the four-body problem of planets within a triple. There has been almost no work on generalised, rather than specific, systems. Few studies have looked at retrograde planetary orbits (which should be entirely possible in triples, like HAT-P-7b, in a binary system) and none at retrograde stellar orbits (of which four have already been discovered). Nearly all have been for coplanar orbits and for a limited number of orbital parameters.

The objective of this work was to comprehensively map the regions of planetary stability in triples and address some of these limitations.

For a comprehensive analysis, one needs to examine all four types of planetary orbits in triples, i.e. P1, P2, S1 and S3 orbits. One also needs to address retrograde planetary orbits, as planets with these motions have been discovered, and also retrograde orbits of the outer star, a rarer occurrence. It is also necessary to touch on highly-inclined orbits of the outer star, with the resulting stellar Kozai resonance and its sculpting of the geometry of the stable region.

We also extended the number of parameters used in previous work to all the orbital elements of the triple's stars, and widened the ranges of both these and the relevant mass ratios, in order to encompass recent observations as well as potential future discoveries.

The remainder of this chapter provides a contextual overview, ending with an outline of the thesis.

1.1 Stellar Multiplicity

Some time ago it was recognized that a large fraction of systems in the Galaxy are composed of multiple stars. For example, an examination of the 164 nearest G-dwarfs by Duquennoy and Mayor (1991) showed that 38% of these stars were in binaries, 4% in triples, and 1% in quadruple star systems. It has been variously estimated that 12% – 40% of the stars in our Galaxy are binary or multiple systems, that multiplicities of three and higher can occur in 2% – 25% of all stellar systems and that many, if not most, close binaries have distant tertiary components (Tokovinin 2004; Alexander 2012; Kane & Hinkel 2013). Binary frequency appears to correlate well with stellar ages, with low-mass pre-main sequence stars having very high binary frequencies of 80% – 100%. More recently, the Kepler Eclipsing Binary Catalog has listed more than 2 100 eclipsing binaries (Slawson et al. 2011) among which approximately 20% are in triple systems.

Most known multiple stars result from random discoveries. One early catalog of physical stellar multiplicity data is the Multiple Star Catalogue (MSC) (Tokovinin

1999), which was complete to a distance of around 10 pc and was updated (up to April 2010) to contain 1 359 stellar systems of multiplicity 3 to 7. However, it has strong observational biases and is not usable for unbiased statistical studies. Tokovinin attempted a comparative analysis of triples and quadruples based on the MSC (Tokovinin 2008). A similar effort was undertaken by Eggleton, using bright stars and an ad hoc model of observational selection (Eggleton 2009).

A joint study by Eggleton and Tokovinin (2008) that considered stellar systems with multiplicities ranging from one to seven in the set of stars with combined magnitude brighter than 6.00 on the Hipparcos scale (which was effectively limited to systems with mass above about 1 M_s, since very few systems of lower mass are included among the bright stars) identified 4 558 such bright systems, of which 60% were single stars, 32% binaries and 6% triples, with an observed mean multiplicity of 1.53. Although reasonably representative of stars more massive than the Sun, this study is unlikely to be representative of the Galaxy as a whole because of its magnitude constraint. Raghavan et al. (2010) came to a similar conclusion with observed fractions of single, double, triple, and multiple systems of 56%, 33%, 8% and 3% respectively, if all confirmed stellar and brown dwarf companions are accounted for.

A more comprehensive survey is based on a volume-limited sample of 4 847 unevolved or moderately evolved stars with masses from 0.9 to 1.5 M_s within 67 pc of the Sun (Tokovinin 2014a, 2014b). The multiplicities found are shown in Table 1.

Stellar type	Fraction
Single	54%
Binaries	33%
Triples	8%
Quadruples	1%
2+2 quadruples	3%
Quintuples	1%
Total	100%

Table 1. Stellar multiplicities per Tokovinin (2014)

Some key findings were that:

1. Periods of all binaries are distributed log-normally with a median $ln\,P = 4.54$ (~100 yr).
2. The mass ratio is distributed uniformly and is effectively independent of the period.
3. The multiplicity fraction is 0.46 ± 0.01. The fraction of hierarchical systems is 0.13±0.01.
4. There is a lack of outer systems with periods shorter than ~1 000 d.
5. There is an excess of tight inner binaries with P < 10 d compared to the smooth Gaussian distribution, presumably caused by tidal evolution.
6. The mass ratios in the inner and outer systems of triple stars are uncorrelated. In triple stars, the system mass ratio of the outer binary does not depend on its period and has a median value of 0.39, meaning that the masses of tertiary components are comparable to the masses of stars in the inner binary.

A comprehensive study of 2 600 targeted main-field Kepler binaries found evidence for a third body in 222 systems (Borkovits et al. 2015); this implied that at least 30% of binaries are in triple or higher multiple systems and the authors concluded that a much larger fraction of the binaries in their sample were likely to be bound with one or more other bodies.

According to the Open Exoplanet Catalogue (May 2017), out of the 185 multiple star systems with planets, 37 or 20% are triple star systems. This is consistent with the finding that triple star systems represent less than a fifth of multiple star systems (Raghavan et al. 2010).

Some quadruple systems have been found, of which AD1652 is one of the few systems where orbital fits were found for multiple orbits (Tokovinin, Gorynya & Morrell 2014).

A quintuple system, consisting of a contact binary and a detached binary together with a fifth star, probably all gravitationally bound in a single system has also been confirmed (Lohr et al. 2015).

1.2 Hierarchical Orbits

A hierarchical triple can be loosely defined as a close binary that is orbited by a distant companion. More formally, strong hierarchy has been described by Zhuchkov, Orlov and Rubinov (2006) as "when the ratio of the orbital periods of the outer and inner subsystems following along the hierarchy are $\sim 10^2$ or higher, the hierarchy will be strong, and the system itself will probably be stable, with motions close to Keplerian in each hierarchical level. Only systems with strongly elongated orbits for their outer subsystems can be exceptions to this rule. Secular perturbations (similar to Kozai resonances in triple systems) can certainly alter the orbital eccentricities and inclinations in inner subsystems; however, these are unable to affect substantially the dynamical stability of the system as a whole." They also noted that "in some systems with strong hierarchy whose closest subsystems have periods shorter than 10 days, tidal interactions between the components must be taken into account, and these depend substantially on the structure of the stars."

Most triples are hierarchical simply because if they were not, the system is likely to be unstable and fragment into a binary and an ejected third star.

1.3 Stability Of Triple Stellar Systems

Hierarchical triple systems normally comprise three bodies of comparable mass, with the semi-major axis between two of them being quite small and the third body moving in an approximately Keplerian orbit around the centre of mass of the binary pair, at a distance large compared to the binary's separation. A system of three or more bodies with comparable separations was shown to be dynamically unstable by Harrington (1972). The orbital behavior of hierarchical triple systems has been the subject of many theoretical investigations in the last half century (Harrington 1968; Mazeh & Shaham 1979; Soderhjelm 1984; Krymolowski & Mazeh 1999). A succinct summary of work done on three-body stability criteria prior to 1999 is provided by Donnison (1999). At that stage, the criterion for three equal masses and circular orbits was $3.1 \leq q_{out}/a_{in} \leq 3.5$, where q_{out} is the closest approach of the third mass to the centre of mass of the binary and a_{in} is

the semi-major axis of the binary orbit. More recent theoretical approaches, some incorporating numerical checks of their results, are discussed in later sections and include Ford, Kozinsky and Rasio (2000), Mardling and Aarseth (2001) and Hamers, Perets and Portegies Zwart (2015).

Retrograde orbits for the outer binary are more stable than perpendicular or prograde orbits. The reason for this is that from the perspective of the inner binary, at each periastron passage between the two binaries the relative motion is more rapid, so perturbations are better averaged over the orbital motions, making the system more stable. However, for prograde orbits the motion of the outer binary relative to the inner binary is more synchronous at each periastron passage, with the result that the tidal pull is much stronger, making the outer binary less stable. This result has been known for over one hundred years (Moulton 1914) and was investigated further by e.g. Harrington (1972), Donnison and Mikulskis (1994) and Gayon and Bois (2008). A different interpretation is that the phase-space topological structures of mean-motion resonances for prograde and retrograde motion are simply different (Morais & Giuppone 2012).

For example, an early study by Donnison and Mikulskis (1995) on triples found that retrograde stellar systems are more stable than prograde for all mass ranges, with stability of the system decreasing as the eccentricity of the binary pair increases for small outer-body eccentricities and stability increasing for large eccentricities, with little effect for intermediate eccentricities. For triples with small binary eccentricities, retrograde orbits are more stable, while for systems with large eccentricities for both the inner binary and the outer-star, prograde orbits are more stable (Donnison & Mikulskis 1995).

In our study both prograde and retrograde planetary orbits were investigated.

Previous studies have used a fairly wide range of mass ratios for the outer star relative to the inner binary, as there are triples where the inner and outer components are of comparable mass. These have been widened even further in this study since systems with an inverted mass ratio (i.e. the outer star is more massive than the aggregate inner binary) have been found, such as HD 181068 (Derekas et al. 2011; Borkovits et al. 2013).

1.4 Exoplanet Multiplicity

Per the NASA Exoplanet Archive, (to June 2017) there are 2 600 stellar hosts and 3 486 confirmed extrasolar planets, of which 2 335 were contributed by the Kepler mission, with a further 2 250 unconfirmed candidates. Of the planet candidates, only 5% – 10% are likely to be false positive detections. In addition, 2 876 eclipsing binary stars have been identified.

A 2010 detailed analysis of companions to solar-type stars, based on a sample size of 454 concluded that 9% ± 2% of the single stars had planets, compared with 7% ± 2% of binaries and 3% ± 3% of triples (Raghavan et al. 2010). The results also showed that these fractions were statistically similar, suggesting that single stars and stars with companions are equally likely to harbour planets.

A later study by Roell et al. (2012) of 477 stellar systems, identified 57 multiple systems (47 double and 10 triple systems) with at least one planet. Some data from this study is shown in Table 2. The resulting multiplicity of about 12% was lower than previously published values. A suggested reason was the increasing

number of transiting planets found in recent years, which were excluded by earlier studies.

Multiple	Single	Double	Triple or higher	Reference
Solar-like stars				
46%	54%	34%	9%	1
44%	56%	38%	4%	2
Exoplanet host stars				
22.90%	77.10%	19.80%	3.10%	3
17.20%	82.80%	14.80%	2.40%	4
11.95%	88.05%	9.85%	2.10%	5

1: Raghavan et al. (2010), 2: Duquennoy & Mayor (1991)

3: Raghavan et al. (2006), 4: Mugrauer & Neuhauser (2009)

5: Roell et al. (2012)

Table 2. Multiplicities of solar-like stars and exoplanet host stars

The multiplicity for exoplanet host stars of 12% is also approximately a quarter of the multiplicity of solar-like stars. To date, no S-type planet has been found in a binary with a (projected) separation of under 10 AU and S-type multi-planet systems have only been found in stellar systems with (projected) separations larger than 100 AU. The equivalent range for triples is 20 AU and 65 AU.

Combining the Eggleton (2009) and Roell et al. (2012) data results in the mean frequencies shown in Table 3. These are approximate because of different binnings of the data.

Reference	Multiplicity			
	1	2	3+	4+
1	54	34	9	
2	56	38	4	
3	77.1	19.8	3.1	
4	82.8	14.8	2.4	
5	88.05	9.85	2.10	
Eggleton[1]	59.61	31.53	6.30	2.60
Average	69.59	24.66	4.48	2.60

[1] Excluding the Sun

Table 3. Frequencies of multiplicities (references refer to those in Table 2)

The table clearly shows that multiplicity rates are still quite uncertain if not contradictory (Wang et al. 2014). We will use the multiplicities from Raghavan et al. (2010) – 54% for single stars, 34% for binary stars and 9% for triple stars.

Eggleton found that the frequencies of various multiplicities follow a power law up to septuple multiplicity.

The frequency of occurrence of circumbinary planets orbiting close to non-contact binaries (periods of less than 60 d) depends strongly on the planetary inclination distribution. If circumbinary planetary orbits are preferentially coplanar, then the rate of occurrence of circumbinary planets is 10% with 95% confidence, which is higher than, but consistent with, single star rates. If the planetary inclination

distribution is isotropic, then the frequency increases to 47%. This implies that formation and evolution in circumbinary disks must either lead to largely coplanar planets, or proceed with much greater facility than in circumstellar disks (Armstrong et al. 2014). It is likely that this conclusion applies to triples as well.

To date, 30 confirmed and 37 unconfirmed planets have been found in triple systems.

Putting together all the results of planet frequency studies, it appears that, on average, every star should harbour at least one planet. Our Galaxy has at least 10^{11} stars, implying approximately the same number of planets. With the visible universe containing a current estimate of 2×10^{12} galaxies, the number of planets therein is of the order of 10^{23}. Of these, approximately 10^{22} will therefore be in triple systems.

While Kepler's capabilities have been severely diminished, analysis of its accumulated data over the next few years is expected to reveal possibly thousands of additional planet candidates, and extend their range to smaller sizes and longer periods. Follow-up and continuing searches for exoplanets from the ground and from space continues, with surveys from GAIA (first data release September 2016), TESS (2018), CHEOPS (2018) the JWST (2018) and PLATO (2025).

1.5 Exoplanet Orbits

1.5.1 Exoplanet orbit types

A planetary orbit around one stellar component of a binary or triple is denoted an S-type orbit, while an orbit around both stars of a binary or all three stars of a triple system is a P-type orbit. (There is a further type of orbit, the L-type, where the planet co-orbits with one of the stars, i.e. librates about the triangular Lagrangian points like the Trojan asteroids in the Solar System. However, these orbits are less important in binary and triple systems as they require an outer mass ratio $\mu_2 = m_2/(m_1 + m_2) \leq 1/26$, which is more likely to be met by an outer planet than an outer star. These orbits are therefore ignored in this study.)

These two orbit types are shown diagrammatically in Figure 1 for the binary case. A triple system simply consists of a third star orbiting this inner binary.

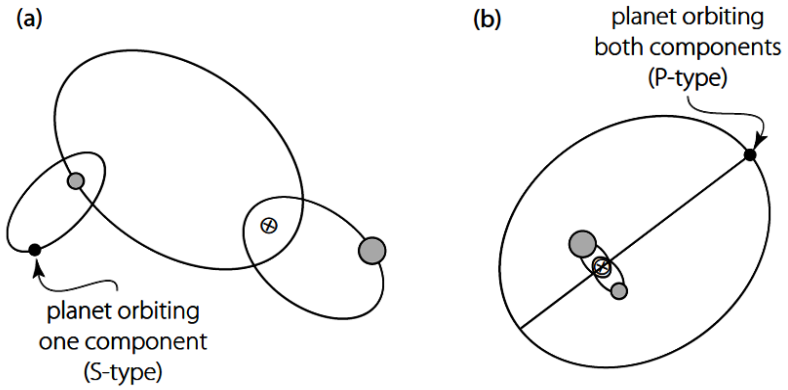

Figure 1. A planet in a binary system, where ⊗ is the stellar centre of mass: a) the planet orbits one component of the stellar binary; b) the planet is in a circumbinary orbit around both stellar components (Perryman 2011)

In a triple system five planetary orbits are possible – three S-type orbits around each of the stars, and two P-type orbits, one around the inner binary and one around all three stars of the triple. These are discussed in Section 3.6.1.

While planets have been found in S-type orbits around the binary components of triples as well as around the outer star, only two P-type orbits have been found, both being circumbinary (with one being in a quadruple system). The discovery of a planet in a circumtriple orbit has not yet been made, but appears inevitable – *a priori*, there is no reason for planetary formation not to occur in a circumtriple disk just as in a circumbinary disk.

However, hierarchical triple systems that are compact enough to possibly harbour planets in P-type circumtriple orbits form a small minority of hierarchical triples, with only 7 of 724 catalogued systems in one survey appearing suitable (Tokovinin 2008).

The dynamics of a planet in a triple system are potentially much richer than for a planet in a binary system. The two orbits constituting the triple system may interfere with each other and therefore exhibit secular change. A circumtriple planet could therefore interact resonantly with the orbital motion of the stars of this stellar system, i.e. show mean motion resonance (MMR). It is these resonances that set bounds on the orbits within the system and define the chaotic region. A circumtriple planet may also interact with the slower secular precession of the two stellar orbits that perturb each other, i.e. secular resonance. A secular resonance can create unstable areas within stable regions, as with the asteroid belt in the Solar System. Furthermore, for triple star systems that are not coplanar, the planet will experience gravitational perturbations not limited to its orbital plane – its orbital inclination will also be subject to secular change. Also, a triple system with a high mutual inclination will tend to exhibit Kozai resonance, with very large fluctuations in eccentricity and inclination. A planet orbiting such a system will be affected by all these gravitational effects, with a potentially strong influence on its orbital stability.

1.5.2 Prograde and retrograde planetary orbits

The stability of prograde versus retrograde planets in circular binary systems has been investigated by, for example, Morais and Giuppone (2012) who used numerical simulations of S-type systems to produce detailed maps of the (a, μ_1) stability boundary and showed that retrograde planets are stable at distances up to 1.5x closer to the perturber than prograde planets (compared with the 1.2x found in this study). They also concluded that instability is a result of either increasing eccentricity caused by single mean motion resonance forcing, or the chaotic diffusion of eccentricity and semi-major axis, as a result of overlapping adjacent mean motion resonances.

Although none have yet been confirmed, planets in retrograde orbits around a binary or triple system should be quite possible. For example, the Rossiter–McLaughlin effect has been used to show that as many as 25% of hot Jupiters are orbiting in a retrograde direction with respect to their parent stars (Triaud et al. 2010), strongly suggesting that dynamical interactions rather than planetary migration produce these objects.

In this study both prograde and retrograde planetary orbits were investigated.

1.5.3 Observational discoveries

Initial exoplanet discoveries were of planets orbiting single stars. Later, stellar companions were discovered around several dozen exoplanet host stars formerly believed to be single. Most of these exoplanet candidates are in S-type orbits. However, the existence of circumbinary planets had been suspected and Kepler provided the first confirmed identifications of transiting circumbinary planets.

To date (May 2017) 3 468 confirmed exoplanets have been found in 2 632 planetary systems (i.e. a multiplicity of 1.3), including 133 binary systems, 25 triple systems and two quadruple systems. Kepler/K2 has contributed 2 483 confirmed planets, over 70% of the total. Discoveries comprise both S-type orbits (beginning with HD 114762 b in 1992) and P-type orbits (PSR B1620 – 26 b in 1994). P-type circumbinary orbits have been found around both wide binaries (e.g. NN Ser (AB) c, d, DP Leo b, HU Aqr (AB) c and UZ For (ab) d) and close binaries (e.g. HWVir (AB) b, Kepler-16 (AB) b, dubbed the first "Tatooine" planet, Kepler-34 (AB) b, Kepler-35 (AB) b, Kepler-38 (AB) b, and Kepler-47 (AB) b, c, which are all Neptune-like or Jupiter-like planets). The Kepler team estimates that about 1% of binary stars of close separations have giant planets in nearly coplanar P-type orbits. The 30 confirmed planets in triple star systems began with 16 Cygni Bb in 1996, with the most recent discovery being Proxima Centauri b in 2016.

Two planets have been discovered in two quadruple star systems. PH-1 A(ab) b or Kepler-64b is in a P-type orbit outside a 20-day period eclipsing binary, with another visual binary orbiting ~1 000 AU away (Schwamb, Orosz et al, 2012) and 30 Ari Bb is in an S-type orbit around one star of a double-binary system (Kane et al. 2015).

Roell et al. (2012) defined the multiplicity of an exoplanet host star by its inclusion in the Catalogue of Components of Double and Multiple Stars or CCDM (Dommanget & Nys 2002). The current number of discovered planets by configuration of star system and hence orbit type, compiled from various sources, is shown in Table 4. The exoplanet data was extracted from the Open Exoplanet Catalogue (OEC) (Rein 2012) and the NASA Exoplanet Archive database (Akeson et al. 2013). The planet orbit code used in the table denotes [number of stars in system, number of stars orbited].

It should be noted that exoplanet host star multiplicity suffers from strong observational bias and selection effects produced by the original planet search programmes. For example, the Kepler input catalog was selected for certain stellar spectral types and radii.

Comparing stellar multiplicity frequencies with those for exoplanets, approximately 70% of stellar systems are single, while 97% of exoplanet discoveries have been of this type. Binaries comprise 25% of stellar systems but only 2.2% of exoplanets discovered have been of this type. While triple systems account for almost 5% of stellar systems, the frequency of exoplanet discoveries in these has been only 0.5%. The ratios of these frequencies suggest that, on the assumption that the true occurrence of exoplanets is not skewed as acutely as this, a large potential exists for future discoveries in binary and higher multiple systems, with this potential increasing with increasing multiplicity.

Stellar multiplicity	Freq. (%)	Orbit type Code	Type	Number (no.)	Freq. (%)	Exoplanets Number (no.)	Freq. (%)	Relative freq.[1]
Singles	69.6	1,1	P	3157	96.4	5657	97.2	1.40
Binaries	24.7			94	2.9	129	2.2	0.090
		2,1	S	77	2.4	110	1.9	
		2,2	P	17	0.5	19	0.3	
Triples	4.5			22	0.7	32	0.5	0.123
		3,1	S	21	0.6	31	0.5	
		3,2	P	1	0.0	1	0.0	
		3,3	P	-	-	-	-	
Higher	2.6			2	0.1	2	0.0	0.013
		4,1	S	1	0.0	1	0.0	
		4,2	P	1	0.0	1	0.0	
Total	101			3275	100	5820	100	

[1] Ratio of stellar frequency to exoplanet frequency. Note some rounding has occurred.

Table 4. Frequency of exoplanets by type of orbit

To support this view, comparing the exoplanet orbit type frequencies with the planet number frequencies shows that they are broadly similar for single and binary stars. It has been found that the frequency of planets in binaries is not statistically different from planets orbiting single stars and that it cannot be lower by more than a factor of three compared to planets orbiting single stars (Bonavita & Desidera 2007). This study also found that for moderately wide binaries, the frequency of planets is independent of separation and the wide companion plays only a marginal role in the formation and evolution of giant planets. It has also been reported that the presence of distant companions (of separations >300 AU – 500 AU) does not significantly affect the process of planet formation, as the mass and period distribution of planets in such wide binaries are similar to those of planets orbiting single stars (Desidera & Barbieri 2007). However, comparing the frequency of S-type orbits with P-type orbits in binaries in Table 4 shows that the former are over six times more common.

It should nevertheless be noted that while the global frequency of planets in binaries may be close to that of singles, several studies have shown that this is only true for relatively wide binaries of separation greater than 50 – 100AU. For binaries tighter than 50AU, there is a clear deficit of exoplanets (e.g. Kraus et al. (2016)).

The planet frequencies for triples and higher (hidden by rounding) are also roughly similar to those for the orbit frequencies, with a large preponderance of S-type orbits. However, one must again be aware of the small sample size and selection effects.

Most binary and multiple stellar systems found to be harbouring planets are wide, with separations larger than 100 AU (Eggenberger, Udry & Mayor 2004), and nearly half of the planets found are in very wide binaries with average stellar separations greater than 1 000 AU (Roell et al. 2012). However, several systems with separations as low as ~20 AU, such as HD 196885, have been shown to contain giant planets. Close binaries tend to be found in higher-multiplicity

systems, implying that wide and close binarity are related statistically (Tokovinin 2001).

Many planetary configurations are possible, e.g. two hot Jupiters have been discovered orbiting each star of a wide binary system (Neveu-VanMalle et al. 2014). Only three stellar binaries are known to host pairs of circumprimary planetary systems, and all are wide: HD 20781/2, XO-2 and Kepler-132, where dynamical analysis show that its two planets cannot be orbiting the same star.

Of the 185 exoplanets in 133 binary systems, the closest P1-type orbit (Kepler-47b) is ≃0.3 AU, with a stellar separation of just 0.0836 AU (Orosz et al. 2012). An example of a close S3 orbit is KOI-2939, a compact triple system with a close binary orbited by a large planet 2.7 AU away. (For the definitions of P1, P2, S1/S2 and S3 orbits, see Section 3.6.1.)

Most multiple star systems are triple, with systems of four or more components far less likely to occur. Some researchers expect that there will be more cases discovered of planets orbiting outside compact binaries than inside wide binaries, and this may also hold true for triples. It appears that most triples are hierarchical, consisting of a close binary with the third star in a wide orbit.

Systems with multiplicities of three or higher containing planets are shown in Table 5, extracted from the OEC, where a and e are the planets' semi-major axis and eccentricity respectively. Although stellar systems up to septuples are known, to date planets have only been found in systems up to quadruples, of which there are two.

The 26 triple systems contain 35 (confirmed and unconfirmed/controversial) planets, giving a multiplicity of 1.3. (There is some uncertainty whether Fomalhaut b is a planet; it may be a dust cloud or disc possibly surrounding a compact inner object.)

In stellar systems of multiplicity three or greater, only two P-type orbits have been found to date, and both are circumbinary rather than circumtriple. PH-1 is a multiple star system of at least four components, hosting at least one planet, PH-1 (AaAb) b, found through the citizen science project Planet Hunters. The planet is in a circumbinary orbit around a binary that in turn is being orbited by a second binary approximately 1 000 AU away. HW Virginis is a multiple star system of at least three stellar components, which hosts at least one planet, HW Vir (AB) b, detected by eclipse timing variations. An additional object orbits the binary every 16 – 55 yr; at around 20 – 65 M_J it is classified a brown dwarf.

A planet in a circumtriple P2 orbit around a triple system has not yet been discovered, but it appears inevitable that this configuration will eventually be found.

For S-type orbits, S3 orbits predominate with 29 cases, while there are only four S1 orbits.

The object of this study was to establish the orbital stability landscape for planets around triple systems. This would help to guide searches for this type of planet. It should also provide a quick stability check for any orbits that are postulated for planets found in triples.

No.	Planet name	Year	Distance [pc]	Mass [M_{Jup}]	Radius [R_{Jup}]	a [AU]	e	Stars	Planets	Orbit type
Quadruples										
1	30 Ari B b	2009	41.8	6.6	-	1.010	0.18	4	1	S1
2	PH-1 A(ab) b	2012	1500	-	0.563	0.634	0.0539	4	1	P1
Triples										
1	HW Vir (AB) b	2008	181	14.3	-	4.69	0.4	3	1	P1
2	HD 2638 b	2005	53.7	0.48	-	0.044	0.0	3	1	S1
3	Fomalhaut b	2008	7.7	-	-	177	0.80	3	1	S1
4	HD 126614 A b	2010	73	0.38	-	2.35	0.41	3	1	S1
5	Alpha Centauri B c	2015	1.295	N/A	0.084	N/A	<0.24	3	2	S1
6	16 Cygni B b	1996	21.146	1.77	-	1.720	0.689	3	1	S3
7	HD 178911 B b	2001	46.7	6.29	-	0.32	0.1243	3	1	S3
8	HD 196050 A b	2002	46.9	2.83	-	2.47	0.21	3	1	S3
9	HD 40979 A b	2002	33.3	3.28	-	0.83	0.25	3	1	S3
10	91 Aquarii A b	2003	45.9	3.2	-	0.7	0.03	3	1	S3
11	HD 41004 A b	2004	43	2.54	-	1.7	0.74	3	1	S3
12	HD 185269 b	2006	50.3	0.94	-	0.077	0.30	3	1	S3
13	HAT-P-8 b	2008	230	1.275	1.321	0.0439	0.0	3	1	S3
14	WASP-12 b	2008	250	1.404	1.736	0.0229	0.0	3	1	S3
15	Gliese 667 C b	2009	6.97	0.018	-	0.051	0.13	3	7	S3
16	Gliese 667 C c	2009	6.97	0.012	-	0.125	0.02	3	7	S3
17	2M 044144 b	2010	145	9.8	-	-	-	3	1	S3
18	HD 132563 B b	2011	96	1.49	-	2.62	0.22	3	1	S3
19	Kepler-13 A b	2011	530	9.28	1.51	0.0342	-	3	1	S3
20	Gliese 667 C d	2013	6.97	0.016	-	0.28	0.03	3	7	S3
21	Gliese 667 C e	2013	6.97	0.008	-	0.213	0.02	3	7	S3
22	Gliese 667 C f	2013	6.97	0.008	-	0.156	0.03	3	7	S3
23	Gliese 667 C g	2013	6.97	0.014	-	0.55	0.08	3	7	S3
24	Gliese 667 C h	2013	6.97	0.003	-	0.089	0.06	3	7	S3
25	51 Eri b	2015	29.4	2.0	1.0	14	0.21	3	1	S3
26	HAT-P-57 b	2015	303	< 1.85	1.41	0.0406	0.0	3	1	S3
27	KELT-4A b	2015	210	0.9	1.70	-	-	3	1	S3
28	Kepler-444 b	2015	35.7	-	0.0367	0.0418	0.08	3	5	S3
29	Kepler-444 c	2015	35.7	-	0.0453	0.0488	0.12	3	5	S3
30	Kepler-444 d	2015	35.7	-	0.0483	0.06	0.18	3	5	S3
31	Kepler-444 e	2015	35.7	-	0.0498	0.0696	0.02	3	5	S3
32	Kepler-444 f	2015	35.7	-	0.068	0.0811	0.29	3	5	S3
33	KOI-2939 b	2015	-	1.5	1.059	2.720	0.06	3	1	S3
34	Psi-1 Draconis B b	2015	22.93	1.53	-	4.43	0.40	3	1	S3
35	Proxima Centauri b	2016	1.295	0.0041	N/A	0.049	<0.35	3	3	S3

Table 5. Exoplanets discovered in stellar systems of multiplicity three and higher

The rest of this document is organized as follows:

Chapter 2 outlines previous theoretical and computational approaches to the problem of triples.

Chapter 3 deals with the preparations for the research, including a review of the observed ranges of parameters for triple stars and their planets; the ranges to be investigated; the selection of the types of orbit to be investigated; Kozai resonances; the selection of numerical method and integrator; the choice of computational parameters and their ranges for planetary orbits and the development of code for the detection of the planetary stability bounds.

Chapter 4 comprises the major portion of the work, in which we investigate the generalised stability of planets for the various triple configurations, for all S-type and P-type orbits, for prograde and retrograde planetary orbits and prograde and retrograde stellar orbits. We then reduced the triple configurations to binaries and re-ran the integrations, to highlight how the results for triples differ from those for binaries. The results for triples are then compared with any previous work and with observational examples.

Chapter 5 consists of a discussion of these results, and the main conclusions that may be drawn from them, followed by Chapter 6 in which we suggest the direction of further work on this topic.

Chapter 2

Approaches to the problem

2.1 Theoretical Approaches

There have been many theoretical approaches to determining stability criteria for three-body stellar systems. For example, Ford, Kozinsky and Rasio (2000) derive octupole-level secular perturbation equations for hierarchical triple systems, using classical Hamiltonian perturbation techniques that describe the secular evolution of eccentricities and inclinations as functions of the relevant masses and orbital elements of triples. Their analytical results were tested by direct numerical integrations using, among others, the Swift code described in Section 3.7.1. These equations have been re-derived by Naoz et al. (2013), showing that the simplified Hamiltonian found can be used as long as the equations of motion for the inclinations are calculated from the total angular momentum.

Most analytical solutions of the equations of motion use linear expansions, but the interactions of large, massive bodies close to one another, such as the compact triples in this study, are nonlinear. Therefore, while these theoretical approaches can be qualitatively useful for the broad understanding of a problem, and for establishing approximate bounds, their accuracy can be quite poor, making numerical solutions almost obligatory. A good illustration of the degree of qualitative and quantitative differences between the two approaches is shown in Figure 2.

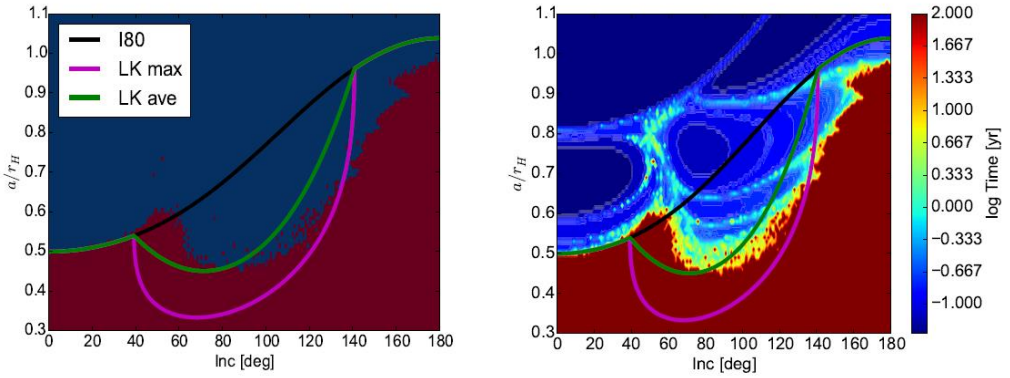

Figure 2. Stability limits for a three-body system as a function of orbital inclination. The lines overlaid on the numerical solution are various theoretical solutions (Grishin et al. 2017)

The quantitative accuracy is poor and even the qualitative correspondence holds only in the broadest sense.

To further emphasise the necessity of a numerical approach, in Section 4.2.7 we solve the theoretical equations for high-inclination stellar orbits and compare these with the numerical results, while in Section 4.3.6 we check the Hill stability

criterion against the results of numerical simulations. Both theoretical results fare poorly.

The focus of this work was therefore on a computational approach to the determination of stable planetary regions in triples.

2.2 Computational Approaches

The three-body problem requires the computation of the mutual gravitational interaction and motion of three interacting masses. Unlike the two-body problem, an analytic solution is not generally possible.

In 1887 Heinrich Bruns and Henri Poincaré proved that only specific solutions to the generalised three-body problem were possible. The motion of three bodies is generally nonrepeating, although some specific repeating solutions were found, e.g. by Lagrange (1772). However, these were sparse, consisting of just three families. The best-known family is the equilateral configuration where three stars of different masses orbit around their common center of mass, always preserving an equilateral triangle, with the orbits being circular or elliptical. Another unusual family is where three bodies of equal mass revolve around their center of mass in a figure-eight orbit (Moore 1993; Chenciner & Montgomery 2000). Surprisingly, 13 new families were recently discovered (Suvakov & Dmitrasinovic 2013). It remains to be established which of these new solutions are stable and may represent actual systems, of both stars and planets.

A simplification of the problem is the restricted three-body problem, where one body is assumed to be of negligible mass – it is under the influence of the other two primary bodies, but too small to affect the motion of these primary bodies, which are assumed to be in coplanar, circular orbits about their center of mass. If they are in elliptical rather than circular orbits, it is labelled the elliptic restricted problem. Famous mathematicians tackled this problem, such as Euler (1772), who introduced a rotating coordinate system; Lagrange (1772); Jacobi (1836), who discovered the eponymous integral of motion in this coordinate system; Hill (1878); Tisserand (1899); Poincaré (1899); Levi-Civita (1905) and Birkhoff (1915).

Three-body orbits therefore have to be solved numerically. The first tentative numerical study of the hierarchical three-body problem, where all masses are large, was in 1909 by Danish astronomer Elis Strömgren, followed in 1923 by Swedish astronomer Karl Bohlin. Later numerical simulations first investigated long-term orbital stability within the coplanar, circular, restricted three-body problem – mainly circumstellar and circumbinary orbits. The Laplacian interpretation of stability is that the orbits are bounded such that the orbital elements (semi-major axes and eccentricities) show no secular or large periodic variations during the time covered by the integrations. With improvements in computing power, the circular constraint was relaxed to model eccentric binary systems, e.g. (Holman & Wiegert 1999; Haghighipour 2008) and then to relax the coplanar constraint and investigate inclined orbits. There is now sufficient computing power to model extremely large *N*-body problems.

One of the earlier numerical approaches, by Eggleton and Kiseleva (1995), offered an empirical stability criterion in terms of a critical ratio of the outer orbit's periastron to the inner orbit's apastron distances in a binary. After deriving

the critical semi-major axis for binary dynamical stability in this way, the authors also noted that highly mutually inclined orbits are unstable.

Mudryk and Wu (2006) also analyzed the low-resolution numerical results of Holman and Wiegert (1999) and investigated the instability boundary, finding that the Hill criterion yields a bound that is very similar to that obtained by resonance overlap arguments, making this criterion a necessary and sufficient condition for planetary instability.

Similar subsequent work on S-type and P-type planetary orbits in binary systems was done by Musielak et al. (2005) for circular orbits, showing that the regions of stability for S-type orbits depend on the semi-major axis ratio between the star and planet being in the range 0.22 – 0.46, depending on the mass ratio. For P-type orbits, the regions of stability also depend on that distance ratio, and are in the range 1.75 – 2.45, again dependent on the mass ratio.

Cuntz, Eberle and Musielak (2007) later established analytical stability criteria using Jacobi's integral for the coplanar circular restricted three-body case, with results in good agreement with those of Holman & Wiegert and Misielak.

In a different approach, stable configurations for circumstellar and circumbinary discs in eccentric binary systems were found by using "invariant loops", which are closed curves that change shape with the orbital phase of the binary as test particles (TPs) in them move under the influence of the binary potential (Pichardo, Sparke & Aguilar 2005; Pichardo, Sparke & Aguilar 2008). These are analogous to stable periodic orbits in time-independent potentials. This method is more demanding than that of Holman & Wiegert, whose orbits can intersect themselves or neighbouring orbits. The authors compared their results with those of Holman & Wiegert and found that the two methods provided similar results when the binary eccentricity is small, but when the binary's eccentricity is large, Holman & Wiegert found fewer stable orbits close to the binary, resulting in larger inner gaps.

Numerical stability studies are a powerful tool to guide the search for new planets, or additional planets in known planetary systems. For example, over the last decade a number of studies have shown that, for systems that contain more than one planetary body, the orbits proposed initially were simply not dynamically feasible, "illustrating the critical importance of performing dynamical analyses as a part of the discovery process for multiple-planet exoplanetary systems." (Horner et al. 2012).

Also, in recent years, numerous numerical investigations have estimated stability zones in known systems that might harbour undiscovered planets. However, only one of these addressed triple systems and attracted only six citations (Verrier & Evans 2007). This work was an extension to triples of the important empirical study by Holman and Wiegert (1999) of planetary stability in binaries (466 citations). It extended Chambers's symplectic integrator algorithm (Chambers et al. 2002) to a triple system by deriving the split Hamiltonian required for each of three hierarchical cases. Verrier & Evans used only one case, that of a circumbinary situation, to determine the stable zone for long-lived planetary orbits, providing fits to the inner and outer bounds. They concluded that the addition of a stable third star does not distort the original binary stability boundaries and that binary stability criteria can be used to quite accurately predict

the stability zones in any hierarchical stellar system, irrespective of the number of stars. They also suggested that circumbinary planets are unlikely to exist in at least 50% of observable systems. However, they did not apply their analysis to P-type circumtriple orbits.

They also found that, in the dynamics of planetesimals in the quadruple star system HD 98800, there were significant numbers of stable test particles in circumbinary polar orbits about the inner binary pair, which were apparently able to evade the Kozai instability (Verrier & Evans 2009). (The Kozai or Lidov-Kozai mechanism (Kozai 1962; Lidov 1962) often destabilizes high-inclination orbits. It couples changes in stellar eccentricity and inclination, with high-inclination circular orbits oscillating to low-inclination eccentric orbits, and is discussed in Section 4.2.) They concluded that high mutual planet-star inclinations are very likely, and that if there are regions of stability, then the outlook for planetary systems in these environments is more promising than previously thought. The numerical results of Verrier and Evans were later explained purely analytically by Farago and Laskar (2010), and other researchers in turn expanded on this work numerically, investigating the dynamics and stability of orbits in three-dimensional circumbinary phase space as a function of binary eccentricity and mass fraction. They found that these orbits are surprisingly stable. In the words of one team of researchers, "circumbinary phase space is rich and dynamic, full of remarkable and stable orbits which do not behave simply. We should not presume any given binary system to lack a circumbinary component unless otherwise demonstrated." (Doolin & Blundell 2011).

Interestingly, an earlier study by Verrier and Evans (2006) is of use to us. It examined the γ Cephei system, which consists of a close binary with a hot Jupiter orbiting one component. This is conceptually no different to a triple with a very low-mass inner binary component. It has therefore been used as an extreme example to compare with this study's results.

A further development has been an analytical theory to model the motion of the recently discovered circumbinary planets Kepler-16 b, Kepler-34 b and Kepler-35 b (Leung & Lee 2013). Their orbits are significantly non-Keplerian due to the large outer mass ratio and the orbital eccentricities of the binaries, as well as the proximity of the planets to the binaries.

A summary of analytical, numerical and chaos-derived stability criteria from the Sixties to 2007 is provided by Georgakarakos (2008).

However, formal stability analyses have not yet been applied to all the possible orbit types in triples

The fact that a meaningful proportion of stars in the Galaxy are triple systems, and the anticipated discovery of new (e.g. circumtriple) orbits in these systems, is one of the motivations for this investigation.

Chapter 3

Characteristics of triple systems

3.1 Overview

Some multiple stars, termed trapezian, are very young, unstable systems. The relative distances between these bodies are comparable and they are usually unstable on time-scales of a few million years or less. They are thought to form in stellar nurseries and quickly fragment into stable multiple stars, which may eject components as galactic high-velocity stars in the process. An example of such a system is the Trapezium at the centre of M42, the Orion nebula.

However, most multiple stars are hierarchical. A gravitational three-body system is called hierarchical if its motion is well approximated by a pair of non-crossing elliptic orbits. In these systems there is little interaction between the orbits and, as for binary stars, they tend to be stable – as a first-order approximation, the dynamic effects of the distant pair can be considered as a single star with a mass equal to the sum of the masses of the individual components. In a triple star system, each star orbits the center of mass of the system. Usually, two of the stars form a close binary and the third orbits this pair at a distance much larger than that of the binary orbit. The reason for this is that if the inner and outer orbits are comparable in size, the system may become dynamically unstable, leading to one star being ejected from the system. Hierarchical triple systems are important for testing theories of star formation and of stellar evolution in the presence of nearby companions.

While triple systems are less common than binaries, as previously discussed, and compact triples are fewer still, their prevalence is not insignificant. One study of the photometric database of eclipsing Kepler binaries estimated that at least 20% of all close binaries have tertiary companions and that at least 8% have tertiary companions with periods less than ~7 yr (Rappaport et al. 2013).

One investigator summarised this (regarding an S3 orbit) as follows: “It seems that hierarchical triple systems do not represent a hostile environment for planet formation around the isolated component, regardless of the mass ratio between the planet host and the sum of the masses of the other components. …In all but one stellar triple with planets, the separation of the stellar pair is larger than the planet semi-major axis. While selection effects certainly play a role, a moderately wide pair in a triple system guarantees that the present stellar orbits are not disruptive for the planetary system around the isolated component. A wide stellar triple might also indicate a rather unperturbed dynamical history for the system.” (Desidera et al. 2011).

In comparison, the circumbinary planets around eclipsing binaries that have been found to date are all rather massive and have long periods.

3.2 Databases

The main sources of exoplanetary data are the NASA Exoplanet Archive (NEA), the Open Exoplanet Catalogue (OEC), the Exoplanet Orbit Database (EOD or exoplanets.org) (Wright et al. 2011), The Extrasolar Planets Encyclopaedia (EPE or Exoplanet.eu) (Schneider et al. 2011) and the Catalogue of Exoplanets in Binary and Multiple Star Systems (Richard Schwarz).

The open-source OEC database was created because of perceived deficiencies in the EOD and EPE and claims to be the only catalogue that can correctly represent the orbital structure of planets in arbitrary binary, triple and quadruple star systems, as well as orphan planets (Rein 2012).

The EOD only lists exoplanets that are validated in peer-reviewed journal articles, whereas the EPE also includes candidate and unconfirmed planets, and the NEA lists and distinguishes planets at various stages of the confirmation process. Also, the NEA uses the Washington Double Star Catalog (WDS) catalog for its stellar multiplicities, and the WDS also contains optical systems, i.e. stars that are not actually physically associated. Therefore, the fact that a star is listed as having multiple components in the NEA does not necessarily mean it is a true multiple system.

All these databases were used in the study.

3.3 Triples – Stellar Characteristics

The characteristics of triple stellar systems, together with the parameters chosen for these in the integrations, are discussed in Section 3.6.

3.4 Triples – Planetary Characteristics

3.4.1 Planetary mass and orbital distances

The mass versus semi-major axis diagram for all confirmed planets is shown in Figure 3. The diameter of the circles is proportional to the number of stars in the system (from 1 to 4) and the solid circles represent the planets in the Solar System for comparison.

Our definition of a planet in terms of mass will be from a fairly arbitrary $0.03 M_{\oplus}$, which is roughly halfway between the masses of dwarf (non-)planet Pluto and Mercury, up to $30 M_J$ or approximately twice the mass of a brown dwarf, commonly defined to be $13 M_J$.

The planets' semi-major axes span 0.0044 AU to 177 AU, with masses ranging from $6.3 \times 10^{-5}\ M_J$ to $30\ M_J$. The exoplanet sample shows observational and selection biases – the sample consists of planets generally more massive than most planets in the Solar System and with semi-major axes that are mostly smaller, although there is a clear bimodal distribution in both variables, with semi-major axis peaks at around 2 AU and 0.05 – 0.10 AU.

There is a dearth of exoplanets in the region where the Solar System planets lie, since smaller planets are more difficult to detect. There are few semi-major axes smaller than 0.02 AU or larger than 10 AU. The first implies very short orbital

periods while the second corresponds to long periods, with many years of observation required to confirm just a few planetary orbits.

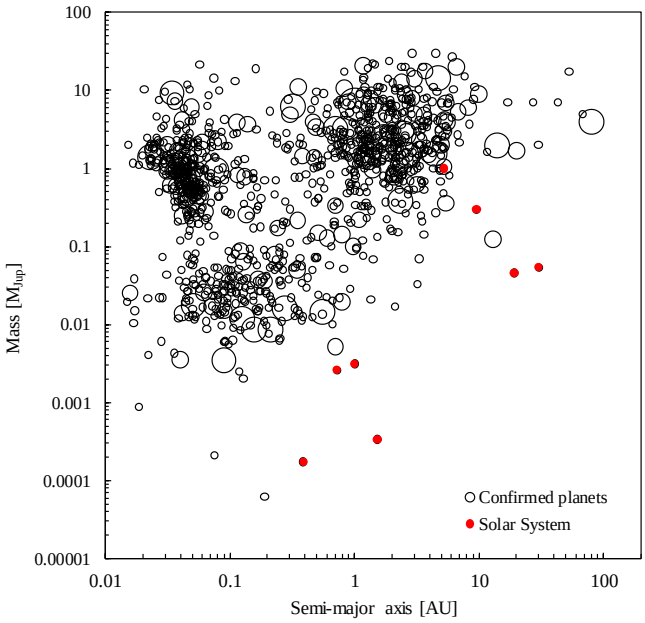

Figure 3. Planet mass versus semi-major axis, with stellar multiplicity

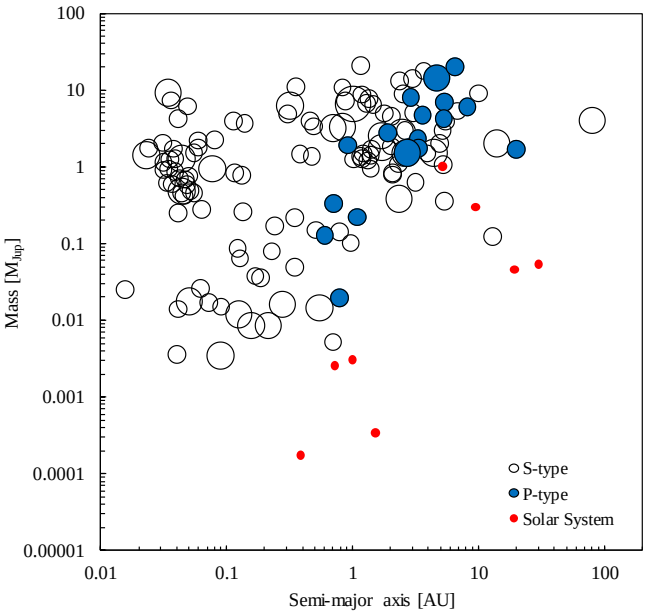

Figure 4. Planet mass versus semi-major axis, with stellar multiplicity and orbit type

Although the sample size is small, there appears to be no obvious difference in distribution between the different stellar multiplicities shown in the graph. This is highlighted in Figure 4, which shows, on an identically scaled graph, the confirmed planets discovered in stellar systems of multiplicities greater than one.

It also identifies those in S-type and P-type orbits, again together with the Solar System planets.

These exoplanets have semi-major axes spanning 0.016 AU to 80 AU, with masses ranging from 0.0035 M_J to 20.6 M_J. Again, they tend to be more massive than the Solar System planets.

Here a difference in distribution becomes more apparent, with planets in P-type orbits being of higher mass and in wider orbits than for S-type orbits. The mean mass of planets in P-type orbits is 8.8 M_J, almost twice the 4.8 M_J for planets in S-type orbits, while the corresponding mean semi-major axes are 4.0 AU and 2.9 AU respectively.

Alexander and Pascucci (2012) suggested that disks around close binaries with semi-major axes less than 1 AU live longer than those around single stars, but disk lifetimes decline as photoevaporation increases at larger binary semi-major axes. As a result, they predicted a dearth of circumbinary planets around wide binaries with $a > 10$ AU and an abundance of circumbinary planets in stellar binaries with $a < 1$ AU.

In our analysis we are unconcerned with planet masses *per se*, since they are represented by massless test particles, but we are able to compare the stable regions found with the above semi-major axis ranges.

3.4.2 Planetary eccentricity

Eccentric orbits are a consequence of strong gravitational interactions; eccentric planetary orbits in systems with no other detected planets suggest prior scattering events in which their siblings were ejected. Planets in multiple systems tend to have lower eccentricities, suggesting these interactions did not occur. Planets orbiting their central star very closely tend to have very low eccentricities as tidal interaction with the star circularises their orbits over long timescales.

Figure 5 shows the orbital eccentricity of all the confirmed planets against their semi-major axes, again with the Solar System planets for comparison.

Exoplanet eccentricities display a more uniform distribution than mass, ranging from close to zero to almost one, averaging 0.17 against the Solar System's 0.08. The distribution of eccentricities for planets orbiting in multistellar systems is shown in Figure 6.

The exoplanets are generally in smaller orbits than the average Solar System planet and their eccentricities are higher. The mean eccentricity of S-type orbits is 0.21 and that for P-type orbits is a smaller 0.13.

For S-type orbits the gravitational force of the secondary star (or stars) is the main source of orbital perturbation, while the stability of P-type orbits is determined by the orbital geometry of the stars being orbited.

One of the proposed explanations is that when the orbit of a close-in planet is excited by an outer companion planet, the planet's gravitational interaction combined with tidal effects between the host star and the close-in planet can give rise to an increasing growth in the eccentricity of the close-in planet (Alexander 2012).

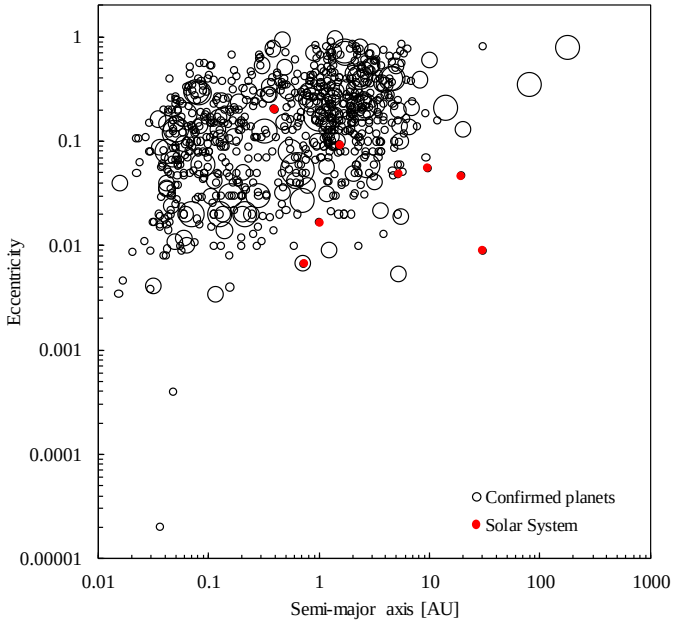

Figure 5. Planet eccentricity versus semi-major axis, with stellar multiplicity

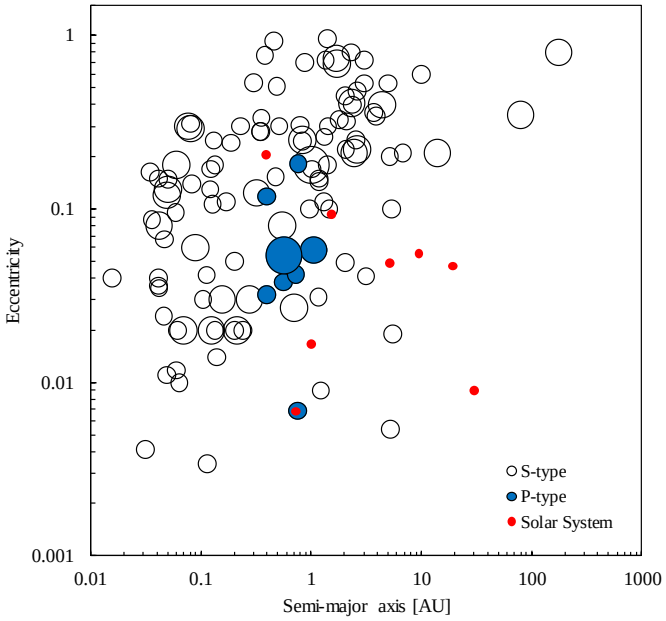

Figure 6. Planet eccentricity versus semi-major axis, with stellar multiplicity and orbit type

Statistically it has been found that the orbits of large exoplanets within wide binaries have higher eccentricities than those around single stars (Kaib, Raymond & Duncan 2013). This is because, even though the companion star in a wide binary is far away, this in fact makes it vulnerable to perturbations such as those from the galactic tide and passing stars, with the result that its pericentre can become quite small given sufficient time and strongly perturb the planetary

system. So, counterintuitively, wide binary companions can affect planetary systems at least as strongly as tight binaries, causing ejections and increasing the eccentricities of the remaining planets. The significant differences in eccentricity with size of binary are illustrated in Figure 7, which shows eccentricities within tighter ($a_* < 10^3$AU) binaries and those in very wide ($a_* > 10^3$AU) binaries and isolated systems, where a_* denotes the binaries' semi-major axis. Although our focus will be on relatively close triples, similar behaviour may be expected for wide triples.

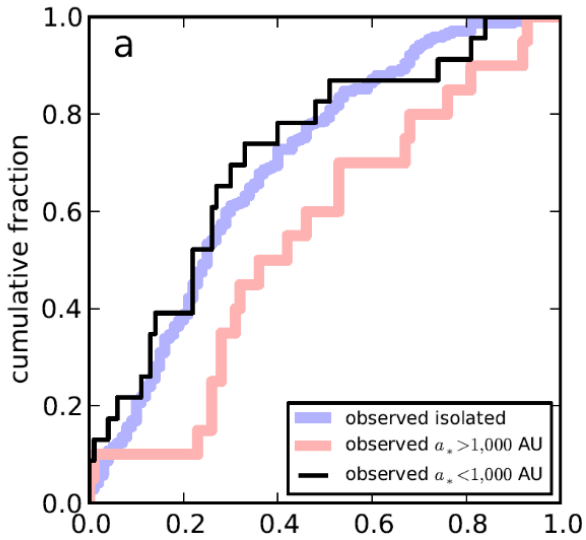

Figure 7. Observed exoplanet eccentricities (Kaib, Raymond & Duncan 2013)

3.4.3 The Kozai mechanism

One important perturbation which is addressed is that of orbital eccentricities. As the two orbits exchange angular momentum, their eccentricities will undergo periodic oscillations over secular timescales.

For non-coplanar systems, corresponding oscillations occur in the orbital inclinations. This influence, which can be a large contributor to stellar and planetary orbital inclination, is the Kozai or Lidov–Kozai mechanism (Kozai 1962; Lidov 1962), which refers to the orbit of a body that is perturbed by another body orbiting farther out. Due to the perturbation, the orbit of the small body experiences libration of its argument of pericentre. Also, as the orbit librates, there is a periodic exchange between its inclination and its eccentricity. This often destabilizes high-inclination orbits, driving high-inclination circular orbits into low-inclination eccentric orbits. A planetary system can be affected strongly by the presence of a companion star, even if the semi-major axis of the companion's orbit is large. However, this is only true if the initial inclination between the orbital planes of the planet and the companion star is larger than a critical angle of 39.2°.

Generally, it has been found experimentally that if the ratio of the initial angular momenta of the inner orbit and inclined outer orbits of a triple are greater than ~4, the angular momentum of the outer star will dominate and significant Kozai

resonance arises. This will tend to occur if the outer mass ratio μ_2 (defined in Section 3.6.2) is greater than ~ 2.

A concise description of this mechanism is provided by Fabrycky and Tremaine (2007), which is paraphrased and expanded in the following paragraphs.

The long-term stability of three bodies interacting only through gravity requires that the system is hierarchical and also that the eccentricity of the outer body cannot be so large that it makes close approaches to the inner binary, i.e. the gravitational perturbations on the inner binary must be small. However, even small perturbations from the outer body can have important secular effects on this binary.

The first effect is precession of the orbital plane, which occurs if the orbital planes of the inner binary and outer body are unaligned. If the inner and outer orbits are circular, both the mutual inclination and the scalar angular momenta of the two orbits remain fixed, while the two angular momentum vectors precess around the direction defined by the total angular momentum vector of the triple system.

However, if the orbit of the inner binary is initially circular, with the initial mutual inclination between inner and outer binaries equal to $i_{initial}$, Lidov and Kozai found there is a critical angle i_c such that if $i_{initial}$ is between i_c and $180 - i_c$, then the orbit of the inner binary does not remain circular as it precesses, but both the eccentricity of the inner binary e_{in} and the mutual inclination i exhibit periodic oscillations known as Kozai cycles. The amplitude of the oscillations in eccentricity and inclination is independent of the magnitude of the perturbation from the outer body, which depends on its mass m_3, its semi-major axis a_{out} and eccentricity e_{out}. However, the oscillation amplitude does depend on $i_{initial}$ – for initially circular orbits with $i_{initial} = i_c$ or $180° - i_c$, the maximum eccentricity is zero, but if $i_{initial} = 90°$ the maximum eccentricity is one, i.e. the two inner bodies collide.

Kozai cycles can be investigated with various degrees of approximation, from analytic equations for the secular evolution of the orbital elements to fully numerical approaches.

The analytical method is to average over the orbital phases of the inner and outer binaries (Kozai 1962; Ford, Kozinsky & Rasio 2000). This secular approximation can be used since the precession time is usually much longer than the periods of the two orbits. In this averaged problem the semi-major axes of the inner and outer binary are both conserved. The analysis is simplest in the limiting case when $a_{out} \gg a_{in}$ (so that the perturbing potential of the outer body can be written in the quadrupole approximation) and the angular momentum of the outer binary is much greater than that of the inner binary (so that the orientation of the outer binary is a constant of the motion). With these approximations, the following results hold:

1. The averaged quadrupole potential from the outer binary is axisymmetric relative to its orbital plane.
2. The averaged problem can be described by a Hamiltonian with one degree of freedom.
3. The eccentricity of the outer binary is constant.

4. The critical inclination is

$$i_c = \arccos\left[\left(\frac{3}{5}\right)^{\frac{1}{2}}\right] = 39.2° \quad (1)$$

It is important to note that this critical inclination is, first, theoretical and second, applicable only to test particles. For real bodies the critical inclination is larger than 39.2°.

If the inner orbit is initially circular the maximum eccentricity achieved in a Kozai cycle is

$$e_{in,max} \cong \left[1 - \left(\frac{5}{3}\right)\cos^2(i_{initial})\right]^{\frac{1}{2}} \text{ for } i_{initial} > i_c \quad (2)$$

5. Depending on the initial conditions, the argument of pericentre ω_1 (the angle measured in the orbital plane between the pericentre of the inner binary and the orbital plane of the outer binary) can either librate (oscillate around 90° or 270°) or circulate. The system may remain at a fixed point i_{fix} with $\omega_1 =$ 90° or 270° and

$$e_1 = \left[1 - \left(\frac{5}{3}\right)\cos^2 i_{fix}\right]^{\frac{1}{2}} \text{ for } i_c < i_{fix} < 180° - i_c \quad (3)$$

6. The only property of the Kozai oscillation that depends on the masses of the three bodies, their semi-major axes or the eccentricity of the outer binary is the period of the eccentricity oscillations, given by Ford, Kozinsky and Rasio (2000) as (in our notation)

$$P_e \cong P_{in}\left(\frac{m_1+m_2}{m_3}\right)\left(\frac{a_2}{a_1}\right)^3 (1 - e_2^2)^{\frac{3}{2}} \quad (4)$$

where P_{in} is the orbital period of the inner binary. This expression is a quadrupole derivation, is approximate and should be multiplied by a coefficient of order unity that can be obtained using Weierstrass's zeta function, as shown by Kozai (1962).

These oscillations are of the order of the timescale period given by Kiseleva, Eggleton and Mikkola (1998) as

$$\tau = \frac{2}{3\pi}\frac{P_{out}^2}{P_{in}}(1 - e_{out}^2)^{\frac{3}{2}}\left[\frac{m_1+m_2+m_3}{m_3}\right] \quad (5)$$

The small-amplitude libration about the fixed point takes place with a period

$$P_{lib} = \tau\frac{2\pi}{\sqrt{30}\left[1-\left(\frac{5}{3}\right)\cos^2 i_{fix}\right]^{\frac{1}{2}}\sin i_{fix}} \quad (6)$$

Combining the last two equations yields

$$P_{lib} = \frac{4}{3\sqrt{30}}\frac{P_{out}^2}{P_{in}}\frac{(1-e_{out}^2)^{\frac{3}{2}}\left[\frac{m_1+m_2+m_3}{m_3}\right]}{\left[1-\left(\frac{5}{3}\right)\cos^2 i_{fix}\right]^{\frac{1}{2}}\sin i_{fix}} \quad (7)$$

In general, for large inclinations with large initial eccentricities of the inner orbit, the initial argument of periapsis of the inner binary has a large influence on whether the system undergoes circulation or libration (libration occurs when ω oscillates between fixed limits while for circulation ω increases or decreases without reversing). But if the inner orbit is nearly circular initially, then the initial values of these orbital angles have little effect, since the inner orbit can switch from circulation to libration and vice versa (Ford, Kozinsky & Rasio 2000).

7. Octupole and higher order terms in the perturbing potential introduce a narrow chaotic zone around the separatrix between circulating and librating solutions as determined by the quadrupole approximation (Holman, Touma & Tremaine 1997).

For a sequence of triple systems in which the semi-major axis a_{out} of the outer binary becomes larger while its mass, inclination, and eccentricity remain the same, the maximum eccentricity of the inner binary in the Kozai cycle will remain fixed, but the period of the Kozai cycle will increase as a_{out}^3. This behaviour will continue as long as the perturbation from the outer body is the dominant cause of apsidal precession in the inner binary orbit. Even weak perturbations from distant third bodies can therefore result in large eccentricity and inclination oscillations. However, small additional sources of apsidal precession in the inner binary, such as general relativity, tides or the quadrupole moments of the two members of the inner binary or planetary companions can suppress Kozai oscillations caused by a distant third body completely, if they dominate the apsidal precession.

The above formulas are for the case of a test particle and are theoretical. Under more realistic assumptions the dynamics become more chaotic and the restrictions of the previous simple case do not apply, particularly the maximum eccentricity. For example, in triple systems with different inner binary masses, higher-order terms of the Hamiltonian give rise to the eccentric Kozai mechanism or EKM, which induces arbitrarily high eccentricities over a wider range of $cos\ i$ than in equal-mass systems and can flip the orientation of the inner orbit between retrograde and prograde (Lithwick & Naoz 2011; Naoz et al. 2011; Dong, Katz & Socrates 2013; Naoz et al. 2013). In addition, the behaviour of real bodies differs from theory.

It has also been shown with direct integration that for a small fraction of triples the angular momentum of the inner binary can go from a finite value to essentially zero very quickly, which can produce stellar collisions with no prior tidal interaction (Katz & Dong 2012).

Although the full parameter space exploration of Kozai cycles in triple systems with direct three-body integrations remains to be explored, the basic principle that systems with lower initial $|cos\ i|$, i.e. higher i, reach higher eccentricities remains valid.

For inner binaries in triple systems, when their separation at periastron becomes approximately the same as the stellar radii, tidal friction absorbs the orbital energy and the period of the inner binary shortens to $P_{in} \lesssim 10$ d. This mechanism, known as Kozai cycles with tidal friction or KCTF (Eggleton 2006), works well when the period ratio P_{out}/P_{in} is not too high and the initial inner period P_{in} is not too long.

It causes migration of inner periods from P_{in}~100 d to $P_{in} \leq 10$ d (Fabrycky & Tremaine 2007), while some inner binaries can merge.

The Kozai mechanism's influence on planetary orbital inclinations is mentioned in the next section and that on stellar configurations is investigated in Section 4.2, where inclined orbits of the outer star were used and numerical integrations were compared with the above equations.

It is worth noting that Kozai resonance is not inevitable. The mechanism has known limitations, specifically that it can be suppressed when there is a faster perturbation acting on a planet. For example, in planet-forming disks, Batygin, Morbidelli and Tsiganis (2011) showed that the disk's self-gravity tends to induce fast apsidal recession that erases the Kozai effect, which can remain inhibited as a result of orbital precession caused by planet-planet interactions. In multiple planet systems the dynamical interaction of the planets, or any additional effect resulting in additional precession of the pericenter, can inhibit the Kozai effect, and such systems can be classified as dynamically rigid (Innanen et al. 1997). Although Kozai evolution is inhibited, the planetary mean plane still precesses if it is inclined relative to the orbit of the companion (Mardling 2010; Kaib, Raymond & Duncan 2011; Boué & Fabrycky 2014a, 2014b).

3.4.4 Planetary orbital inclinations

Planetary orbits in the Solar System are close to coplanar and stable. If multiple stars form by hierarchical fragmentation of a rotating cloud (Bodenheimer 1978) or by fragmentation of a circumbinary disk (Bonnell & Bate 1994), similarly coplanar configurations would be expected.

Close to 85% of Kepler's multi-planet systems are coplanar to within 3° because of the transit technique used. However, several other studies from radial velocity searches reach a similar conclusion: that planets in multiple systems usually have very low mutual inclinations. For example, Fang and Margot (2012) also found that most (85%) multi-planet systems have mutual inclinations of less than 3°. This implies that these planets formed together inside a protoplanetary disc and did not experience any large gravitational perturbations, which would have increased their orbital inclinations.

The relative orientation of inner and outer orbits in a triple or higher multiplicity system can be measured by the angle ∅ between the angular momenta of their orbits. One expects totally uncorrelated orbital spins ($\emptyset = 90°$) for purely dynamical processes and correlated spins ($\emptyset = 0°$) for a cascade fragmentation of a rotating protostellar cloud. A coplanar system ($\emptyset = 0°$) will stay coplanar forever in the absence of any external disturbance. Early studies, such as by Tokovinin (1993) showed that the available data could only be interpreted by involving a small degree of orbital momentum alignment. A later study of ∅-statistics showed that both extreme hypotheses (co-aligned and random orbital spins) could be rejected. The mean ∅ was around 50° (Tokovinin 2000).

If a planetary system forms in a primordial binary system, the orbits of the planets and the companion star may be expected to be essentially coplanar. However, while close binaries are likely to have aligned circumbinary disks, wider binaries can have misaligned disks (Foucart & Lai 2013).

If a planetary system forms around an initially single star, which becomes a binary later through an encounter, the orientation of the orbits of the planets is random with respect to the orbit of the companion star (Malmberg, Davies & Chambers 2007).

Alexander (2012) predicted that circumstellar disks around binaries with $a < 100$ AU should be coplanar to the orbit of the binary. Thus any planets formed from such a disk are expected to be aligned with the binary's orbit (Bate et al. 2000).

Malmberg, Davies and Chambers (2007) showed that for systems which have formed from a single star, which is later exchanged into a binary, around 80% will have an initial inclination above 39.2° and hence be in the region where the Kozai mechanism can be important. The Kozai mechanism will lead to an increase in the eccentricity of an outer planet, if the binary is not too wide. The increased eccentricity of the outer planet leads to strong planet-planet interactions in the system, which can lead to the ejection of one or more planets and also result in the remaining planets being left on more eccentric orbits than before.

It has been pointed out by Perryman (2011) that, based on limited data, planets with the highest eccentricities ($e > 0.8$) tend to be accompanied by a stellar or brown dwarf companion. This suggests eccentricities are caused by the Kozai mechanism, in which hierarchical triple systems with high mutual inclinations cause large-amplitude periodic oscillations of the eccentricity of the inner orbit. The coupling of these Kozai oscillations with tidal friction (Kozai migration) may also lead to circular orbits for short-period planets. In multiple systems this may bring massive planets close to their stars and may explain why the most massive short-period planets are found in binary or multiple systems.

In their simulation of planetary orbits around triples, Verrier and Evans (2007) assumed all orbits to be coplanar, justifying this assumption on the basis that higher inclinations will be subject to Kozai instability, causing large variations in the stellar orbits, which would be expected to destabilize test particles rapidly. Their integrations always kept one star in a circular orbit. However, their later empirical investigation of small particles around a highly eccentric binary star in a hierarchical triple system found that while such particles might be expected to be disrupted by the Kozai instability, test particles existed in stable, high inclination circumbinary orbits. They owed their stability to the high eccentricity of the inner binary, which instead of inducing Kozai cycles, caused smooth inclination variations and nodal precession for certain initial longitudes. This suppressed the Kozai cycles that would be expected to be induced by the outer star in the triple (Verrier & Evans 2009).

3.4.5 Chaotic orbits

Chaos is a term used to describe a system with nonrepeating motion over a given timescale – it is deterministic but unpredictable because of high sensitivity to initial conditions. For example, even small differences in estimated orbital parameters may result in large differences in orbital trajectories. Since these orbits are variable, the initial orbital configurations may not define stable regions well. This could lead to different stability landscapes for different planets in the system.

Stability describes the “boundedness” of a system – a system is stable if changes in its evolution are confined within a certain range. For example, a chaotic system

can be stable in that the orbits of the bodies do not interchange or become unbound, and the oscillations of orbital elements such as eccentricity occur over a finite range. This illustrates an important dichotomy in chaotic systems – a system may be formally unstable, but for all practical purposes it is stable. With "bounded chaos" one can predict the general orbital evolution reasonably well, but not the exact positions of the bodies in their orbits.

While all the stellar orbits we found for triples were well-behaved, this would not necessarily be true for planets. Their orbits could be chaotic, but if they completely fill an orbital space, although they may not be "stable" in the traditional sense, they are bounded. To determine the type of motion of the computed orbits, one has to use either long-term orbital computations and analysis, or a chaos indicator, such as the fast Lyapunov indicator, which is a quick tool to distinguish between regular and chaotic motion. In our investigations we used the former, together with many integrations, which would have statistically smoothed out these effects.

3.5 Scope And Limitations Of The Investigation

Our aim was to determine the orbital stability of both the host stars and their planets, where collisions between the stars or the ejection of one of the three stars (typically the least massive body) does not occur over secular timescales that are very long compared to the orbital periods.

Our treatment of secular perturbations in this work was based on classical Newtonian dynamics and assumed that all three bodies are point masses that do not interact other than through gravitation and do not evolve in any way.

General relativity and tides and can modify such results significantly. General relativity can lead to resonant behaviour of the inner orbits' eccentricity (Ford, Kozinsky & Rasio 2000; Naoz et al. 2013), while tidal effects can suppress changes in their eccentricity, changing the system's dynamics materially (Soderhjelm 1984; Kiseleva, Eggleton & Mikkola 1998). A combined theoretical treatment of these two effects is given by Correia, Boué and Laskar (2016). A possible additional perturbation is the general relativistic precession of the inner orbit if the inner binary contains compact objects such as white dwarfs or neutron stars. When the precession periods from general relativity and from Newtonian perturbations become comparable, a resonant effect that leads to larger orbital perturbations is possible.

Also, for triple systems containing very close inner binaries, tidal dissipation in the inner components provides a sink of energy and angular momentum that can substantially change the character of the secular perturbations.

Relativistic and tidal effects, as well spin, were not addressed in this study.

3.6 Selection of Parameter Space

3.6.1 Orbit types

The triple system's nomenclature is shown in the schematic illustration in Figure 8.

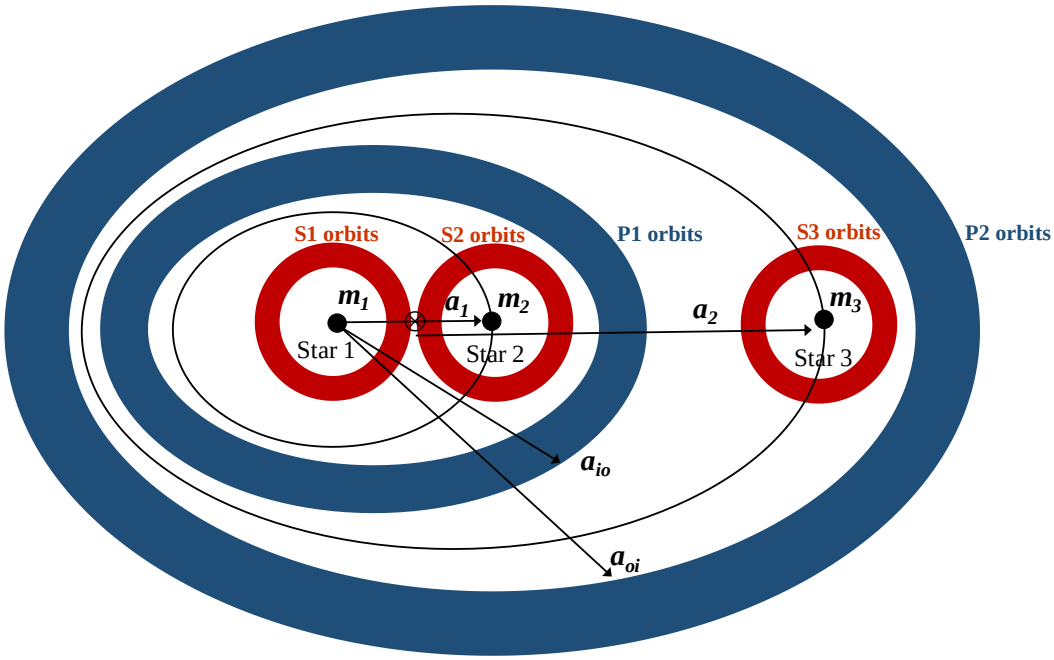

Figure 8. Triple system nomenclature with S-type and P-type orbits

Star 2 orbits Star 1 to form the inner binary and the outer Star 3 orbits the centre of mass ⊗ of this binary. Within the inner binary we define m_1 to be the primary (and usually heavier) star. There are three S-type orbits, around each of the three stars, and two P-type orbits, one circumbinary and one circumtriple. A cloud of test particles in circumbinary (P1) orbits will have an inner and outer stability bound, while a circumtriple (P2) cloud will have an inner bound only. Circumstellar (S1, S2, S3) clouds around the stellar components will have their outer edges bounded. Our objective is to determine the regions of orbital stability for planets within the system, specifically the outer bound a_{io} of the stable region for S1, S2, S3 and P1 orbits (shown for P1 orbits only) and the inner bound a_{oi} of the P2 orbits.

The diagram shows a coplanar case, but the orbit of Star 3 (and the test particle clouds) can be inclined relative to the orbital plane of Star 1 and Star 2 and the invariable plane of the system, as discussed in a later section.

The outer star in a triple can be in a prograde orbit or a retrograde orbit. In Sterzik and Tokovinin (2002), of the 22 triples from the MSC catalogue where sufficient orbital data was available, four orbits were retrograde (see Table 7). Retrograde planetary orbits in triples have not been studied much, and this is therefore one of the new areas investigated in this work.

From the five types of stellar orbits in Figure 8, some reduction in complexity is possible. First, the orbits S1 and S2 are interchangeable so only one case needs to be examined. Second, since in many triples the binary is very close, the total number of possible orbits often reduces to three, being the two P-type orbits and the S3 orbit around the outer star, as shown schematically in Figure 9. So there is a maximum of four orbit types to be investigated and effectively only three in many cases.

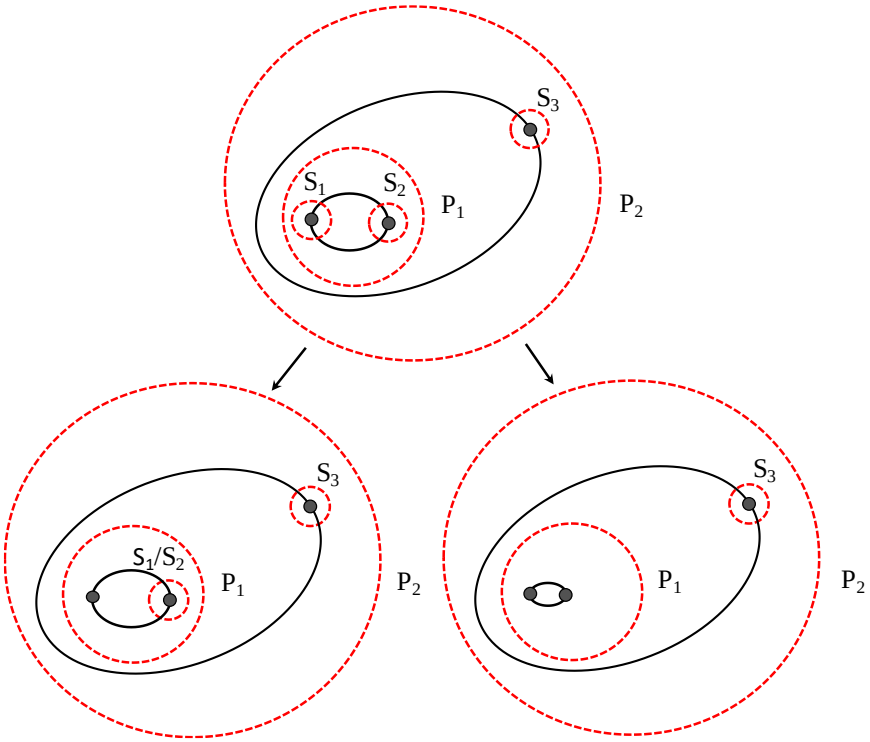

Figure 9. Triple systems – orbit types

To date, 37 triple systems have been found to contain planets, as previously shown in Table 5, extracted from the Open Exoplanet Catalog.

The vast majority, 31, contain S3 orbits, with only five systems hosting S1 orbits. Only one P-type orbit has been found, a P1-type. No planets in P2 orbits have been found to date.

In Chapter 4 we investigate the stable regions of a generalised triple system for each of these orbit types.

3.6.2 Stellar configurations

The system's configuration is defined by:

1. Size: semi-major axes a_1, a_2
2. Shape: eccentricities e_1, e_2
3. Orientation: inclinations i_1, i_2; longitudes of ascending nodes Ω_1, Ω_2; arguments of periapsis $\omega_1, \omega_2$and mean anomalies $\mathrm{M}_1, \mathrm{M}_2$.
4. Mass ratios: m_2 relative to m_1 and m_3 relative to m_1 and m_2

The expressions we derive for the regions of stability should be in terms of these parameters.

The triple system consists of three stars, each with one mass and six orbital elements, so there are 21 variables in the system and the dimensionality of the problem is high. However, using Star 1 as the centre of the coordinate system removes its orbital elements. We can then define three dimensionless parameters:

Stellar semi-major axis ratio $a = \frac{a_2}{a_1}$

Inner mass ratio $\mu_1 = \frac{m_2}{m_1+m_2}$

Outer mass ratio $\mu_2 = \frac{m_3}{m_1+m_2}$

where semi-major axis ratio subscripts 1 and 2 refer to the inner and outer orbits respectively and mass subscripts 1 and 2 refer to the inner binary stars and 3 to the outer star. Mass ratio definitions in the literature are quite inconsistent. We have used the original Holman & Wiegert (1999) inner ratio definition and kept the same denominator for the outer ratio.

Then, since we are interested only in the mutual inclination of the outer star relative to the inner binary, the inclination and argument of periapsis of the inner binary are free parameters and can be set to zero. Also, since its inclination is zero, the longitude of the ascending node for the inner binary does not exist. For our purposes the true anomalies were ignored. With these simplifications the number of variables falls to eight.

The following sections discuss the ranges selected for the various configuration parameters.

3.6.3 Semi-major axis ratio

This ratio a cannot be made arbitrarily small as the Swift-HJS algorithm requires that $a_2/a_1 \gg 2$. In the case of compact triples this would appear to put a lower limit on the compactness that can be modelled. However, this does not appear to be a practical limitation. Of the 285 triples in the Eggleton and Tokovinin (2008) catalogue, the dozen most compact systems are shown in Table 6 and the smallest semi-major axis ratio was 4.1, with a corresponding outer period of 33 d. Short outer periods such as these are unusual, and there is generally a notable absence of outer periods of under 10^3 d (Tokovinin 2014b). In the case of binaries, the smallest ratio found to date of a P1-type planet's semi-major axis to its binary's semi-major axis is currently 3.14, in Kepler-16 b (Doyle et al. 2011)

The dependence of the stability limits of stellar orbits on the inner and outer mass ratios and eccentricities are generally not strong. The stability criterion for triples is given by Mardling and Aarseth (2001) as

$$\frac{a_{trip}}{a_{bin}} \gtrsim C \left(\frac{M_{trip}}{M_{bin}}\right)^{\frac{2}{5}} \frac{(1+e)^{\frac{2}{5}}}{(1-e)^{\frac{6}{5}}} \quad (8)$$

where a_{trip} and e are the semi-major axis and eccentricity of the outer star (our a_2 and e_2), a_{bin} is the orbital separation of the two stars in the binary and M_{trip} and M_{bin} are the aggregate masses of the triple and binary respectively, while $C \cong 2.8$ is determined empirically. The ratio a_{trip}/a_{bin} is equivalent to our semi-major axis ratio a. This criterion is valid only for coplanar prograde stellar orbits and for $q_{out} \leq 5$, where $q_{out} = m_3/(m_1 + m_2)$, i.e. equivalent to our μ_2. This criterion has not been tested in systems with planetary masses (Aarseth & Scarfe 2004).

No.	System name	Configuration (per Eggleton & Tokovinin 2008)	Inner period (d)	Outer period (d)	Period ratio	Semi-major axis ratio a
1	Lam Tau	((A4IV + B3V; 3.953d SD) + ?; 33.03d, e=0.15)	4.0	33	8	4.1
2	Phi Phe	((A3V + ?; 41.49d e=.32) + ?; 2.403y)	41.5	878	21	7.6
3	15Eta Vir	((A2IV + A4V; 71.79d e=.27) + A8-F0; 4791d, e=.08)	71.8	4791	67	16.5
4	VV Ori	((B1V + B5-9V; 1.485d) + A7V:; 119.1d e=.29)	1.5	119	80	18.6
5	Lam Sco	((B1.5IV + ?; 5.953d e=.26) + B2IV; 1053d, e=.12)	6.0	1053	177	31.5
6	Bet Per	((6.0G8IV + 2.2B8V; 2.87d SD) + 4.72F1; 1.86y, e=0.23)	2.9	679	237	38.3
7	64 Ori	((B7III + B8III; 14.57d e=.39) + B5V; 13.22y, e=0.73)	14.6	4829	331	47.9
8	The Car	((B0.2Vp + ?; 2.139d e=.24) + 13.0; 2.242:y)	2.1	819	383	52.7
9	B Per	((A2V + ?; 1.527d e=.02) + ?; 1.921y, e=.24)	1.5	702	459	59.5
10	1 Gem	(4.77(G6III + ?; 9.597d) + K0III; 13.20y e=.34)	9.6	4821	502	63.2
11	HR 6469	((F2V + F8:; 2.23d) + G8III-IV; 2019d e=.67)	2.2	2019	905	93.6
12	4 Dra	((WD + M4V; 0.16d, SD, CV) + M3III; 1703d, e=0.30)	0.2	1703	10644	483.9

Table 6. Compact triples from the Eggleton & Tokovinin 2008 survey

For a retrograde outer star, the stability criterion for triples given by Mardling and Aarseth (2001) and shown earlier in equation (8) was modified by them by the addition of an ad-hoc factor $f = 1 - (0.3i/180)$ (with inclination i in degrees) as follows:

$$\frac{a_{trip}}{a_{bin}} \gtrsim \left(1 - \frac{0.3i}{180}\right) C \left(\frac{M_{trip}}{M_{bin}}\right)^{\frac{2}{5}} \frac{(1+e)^{\frac{2}{5}}}{(1-e)^{\frac{6}{5}}} \quad (9)$$

This factor was derived from numerical experiments by Mardling (1999) and was similar to the findings of Harrington (1972) for retrograde coplanar orbits. The empirical constant C retains its value of 2.8.

Converting equation (8) to orbital periods,

$$P_{trip} \gtrsim 4.7 \left(\frac{M_{trip}}{M_{bin}}\right)^{\frac{1}{10}} \frac{(1+e)^{\frac{3}{5}}}{(1-e)^{\frac{9}{5}}} P_{bin} \quad (10)$$

where P_{trip} and P_{bin} are the orbital periods of the outer and inner binary respectively.

These relationships are shown in Figure 10, which plots the semi-major axis ratio and the period ratio against the triple's outer eccentricity for various mass ratios.

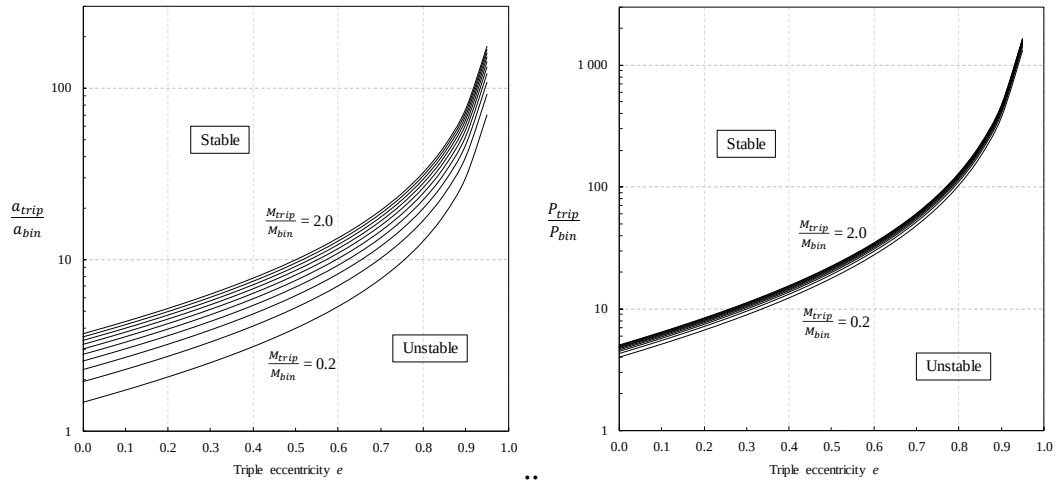

Figure 10. Stability criterion for triples. a) semi-major axis ratio and outer eccentricity b) period ratio and outer eccentricity

The relationship becomes super-exponential for higher eccentricities. For example, increasing eccentricity from 0.5 to 0.9 raises the required semi-major axis ratio an order of magnitude, from 10 to 100.

Although observational errors in the estimated masses of binaries and triples may be large, the small exponent on the mass ratio of 1/10 in equation (10) means the dependence of period on these masses is very weak.

For each triple configuration integration, we set the lower limit of a at the Mardling stability limit. In every case this lower stability bound was greater than that required by the Swift-HJS algorithm. The occasional stellar instability that was found corresponded well with the Mardling limit. Large separations can still result in a small semi-major axis ratio. For example, in 2013 the Fomalhaut system was found to be triple, with new discovery Fomalhaut C's current separation being ~160 000 AU from Fomalhaut A and ~200 000 AU from Fomalhaut B. Given the separation between A and B of 58 000 AU, the semi-major axis ratio is only ~3. (Fomalhaut b may not be a planet, but a dusty disc surrounding the inner object.)

Regarding the choice of upper limit for the semi-major axis ratio, recent research by Reipurth and Mikkola (2012) has suggested that, with wide ranges, stable bound triples show mean inner and outer semi-major axes of ~100 AU and ~2 000 AU respectively, giving a mean semi-major axis ratio of around 20. (However, their mean initial separations ranged from 40 AU to 400 AU, guided by observations, giving a mean semi-major axis ratio of 10.)

The semi-major axis ratio was therefore varied from slightly inside the Mardling limit, denoted a_m, to 100. The vast majority of semi-major axis ratios for triple systems fall within this range. Values for a were usually generated randomly within this range. Where increments were used, they were fairly coarse given the insensitivity to this variable, commonly being 20 AU.

Generally, the stability boundaries were well modelled as functions of mass ratios and eccentricities (with only weak contributions from the other orbital elements) and scale with a except for very small separations. Since its regression coefficient should be zero, this parameter was included in all models as an error check.

3.6.4 Inner mass ratio

The range for this ratio, μ_1, is between zero and one. However, only the range $0 < \mu_1 < 0.5$ needs to be studied, as mass ratios of μ_1 and $1 - \mu_1$ are equivalent, other than for a 180° change in the longitude of the ascending node. Lower limits of 0.001 or 0.1, depending on the orbit type, were used in different integrations. When not randomly generated, increments of 0.05 – 0.10 were usually used; again, the influence of this variable is relatively weak.

For any selected μ_1, m_2 was calculated from

$$m_2 = \frac{\mu_1}{1 - \mu_1} m_1$$

3.6.5 Outer mass ratio

The lower limit for this ratio, μ_2, is again zero.

Interestingly, no evidence has been found that distant tertiary components are generally less massive than the components of the inner binaries (Tokovinin 2014a). Analysing the data from this survey, the largest mass ratio (here defined as m_3/m_1, where m_3 refers to the distant tertiary component and m_1 to the more massive component of the close binary) found was 8.9 (for HIP 29860). However, 94% of mass ratios are below two and 99% are below five. An upper limit for this ratio of around five therefore appears reasonable. If it is assumed that the masses of the binary pair are broadly comparable, the equivalent value for our ratio $\mu_2 = m_3/(m_1 + m_2)$ is $\sim 5/2 = 2.5$. A mass ratio greater than one implies an inverted system, where the outermost star is more massive than the aggregate inner binary. An example is the triple system HD 181068 (Derekas et al. 2011; Borkovits et al. 2013), which has a mass ratio of ~1.7. The integrations need to cater for this (less usual) situation.

The lowest mass ratio found in the Tokovinin (2014) survey was 0.07.

We therefore used values for the outer mass ratio μ_2 ranging from either 0.2 or 0.001 (depending on the orbit type) to 2.2 – 2.5.

Previous studies have found that the influence of mass ratio on stability is weak, so a relatively coarse increment of 0.2 was used if these values were not randomly generated. Tokovinin also showed that the mass ratios are distributed almost uniformly at all periods, so equal increments across the above range were used.

For any selected μ_2, m_3 is calculated from

$$m_3 = \frac{\mu_2}{\mu_1} m_2 = \frac{\mu_2}{1 - \mu_1} m_1$$

3.6.6 Eccentricities

The only data on both inner and outer stellar eccentricities in triples is from Sterzik and Tokovinin (2002), although an updated and larger sample is being planned (Tokovinin, private communication 8/11/16). The existing and rather modest sample of inner and outer orbital eccentricities is shown in Figure 11, ranked in order of largest differences between them.

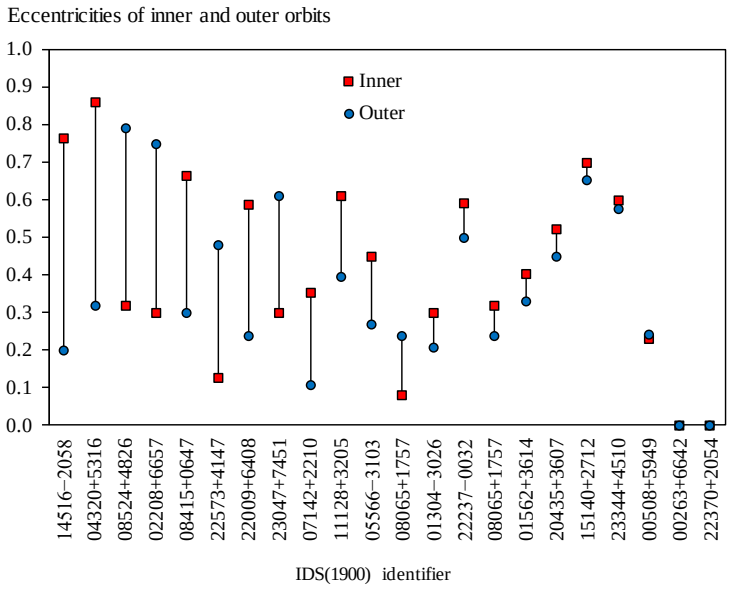

Figure 11. Triple systems – distribution of eccentricities

The mean eccentricity of both inner and outer orbits is quite high at 0.39 and in most (70%) of the systems the inner orbit is more eccentric than the outer orbit. The difference in eccentricities within these systems ranges from effectively zero to 0.57.

The integrations therefore covered eccentricities in both orbits ranging from zero to 0.7 – 0.9, randomly generated or with increments of 0.05 – 0.10.

Inner binary eccentricity e_1

The integrations therefore covered eccentricities in the inner orbit ranging from zero to 0.7 – 0.9, randomly generated or with increments of 0.05 – 0.10.

Outer star eccentricity e_2

A study of 222 Kepler triples found outer eccentricities spanning the full range, with a broad peak in the middle of the range and an unexplained narrow peak near $e_2 \simeq 0.28$ (Borkovits et al. 2015).

Tokovinin and Kiyaeva (2016) found that the eccentricities of wide (median separation ~120 AU) low-mass binaries are distributed approximately as $f(e) \approx 1.2e + 0.4$, with $\langle e \rangle = 0.59$. High eccentricities should therefore not be ignored.

Eccentricities for the outer binary also from zero up to 0.7 – 0.9 were used, randomly generated or with increments of 0.05 – 0.10.

3.6.7 Inclinations

The first list of hierarchical triples published, by Fekel (1981), noted that at least one third of triple stars have non-coplanar orbits.

For triples we will define mutual inclination as the angle of an orbit relative to the plane of the inner binary, so mutual inclinations of over 90° represent retrograde orbits. Most planetary inclinations are not known. Transiting planets around

eclipsing binaries have $i \cong 90°$ to the line of sight, but that does not say anything about their mutual inclinations (although most are probably coplanar).

The data shown in Table 7 for 22 triple systems is also from Sterzik and Tokovinin (2002). The mutual inclination Δi between two orbits is given by e.g. Martin and Triaud (2015) as

$$\cos \Delta i = \sin i_1 \sin i_2 \cos \Delta\Omega + \cos i_1 \cos i_2 \qquad (11)$$

where $\Delta\Omega = \Omega_1 - \Omega_2$ and the inclinations have their usual subscripts.

We have calculated and inserted Δi as the last column in the table, in which subscripts *in* and *out* were set to 1 and 2 respectively in the previous equation.

No.	Identifier	Primary	log P_{out}	e_{out}	Ω_{out}	i_{out}	log P_{in}	e_{in}	Ω_{in}	i_{in}	Remark	Δi
	IDS(1900)	Sp(A)	(d)		(°)	**(°)**	(d)		(°)	**(°)**		(°)
1	00263+6642	dM2.5	5.07	0	168	**51**	3.75	0	24	**27**		**74.0**
2	00508+5949	A1V	4.48	0.24	175	**54.9**	3.25	0.23	185	**55**	Inner astrom. orbit weak	**8.2**
3	01304− 3026	K3V	4.61	0.21	142	**29.3**	3.22	0.301	57.4	**21.8**		**34.2**
4	01562+3614	G9V	5.08	0.33	159	**140**	3.67	0.404	191.4	**67**		**78**
5	02208+6657	A5pSr	5.35	0.75	0.8	**115**	4.28	0.3	175	**106**	Outer orbit uncertain	**139**
6	04320+5316	A8V	5.2	0.32	113	**133**	3.99	0.86	20.8	**141**		**59**
7	05566− 3103	K5V	5.15	0.27	143	**110**	4.39	0.45	125	**103**		**18**
8	07142+2210	F2IV	5.64	0.11	18.4	**63.3**	3.35	0.353	70	**92.4**	Inner orbit controversial	**57.6**
9	08065+1757	F7V	5.61	0.24	74.2	**146**	4.34	0.32	13	**167**		**30**
10	08065+1757	F7V	5.61	0.24	74.2	**146**	3.8	0.08	77	**142**		**4**
11	08415+0647	G5III	5.56	0.3	229	**39**	3.74	0.665	284.8	**50**	Quintuple	**39**
12	08524+4826	A7IV	5.47	0.79	4.8	**57.8**	4.16	0.32	21	**108**	Outer orbit uncertain	**52.5**
13	11128+3205	G0V	4.34	0.4	102	**122**	2.83	0.61	318	**91**		**132**
14	14516− 2058	K4V	5.89	0.2	317	**72.5**	2.49	0.765	18	**110**	Outer orbit uncertain	**70.4**
15	15140+2712	G0V	4.87	0.65	64	**58.2**	4.26	0.7	135	**90**	Inner system controversial	**73.9**
16	20435+3607	B5Ve	5.15	0.45	139	**134**	3.63	0.524	150	**135**		**8**
17	22009+6408	A3Vm	6.14	0.24	85	**109**	2.91	0.589	93.5	**71.9**	Outer orbit uncertain	**38**
18	22237− 0032	F3V	5.44	0.5	305	**136**	3.97	0.59	202.7	**34.3**		**132**
19	22370+2054	G0	5.37	0	27.1	**127**	4.48	0	13.8	**42.2**		**86**
20	22573+4147	B6III	4.4	0.48	191	**104**	3.51	0.127	15	**81**		**174**
21	23047+7451	K0III	4.79	0.61	81	**30**	2.75	0.3	107.9	**99**		**72**
22	23344+4510	A2	4.74	0.58	128	**130**	3.74	0.6	129.7	**127.4**	Both orbits uncertain	**3**

Table 7. Triple systems –inclinations. All systems where two visual orbits are known, from the Multiple Star Catalog (Tokovinin 1997)

The mean mutual inclination was high at 63°. There were four systems with retrograde orbits and six with inclinations greater than 70°.

A later study by Borkovits et al. (2015) found that the distribution of mutual inclinations for 62 Kepler triples had a large peak at 0° – 5°, indicating predominantly close-to-coplanar configurations, but with a significant 38% portion of the systems in a secondary peak centred at 40°, indicating Kozai effects, as shown in Figure 12.

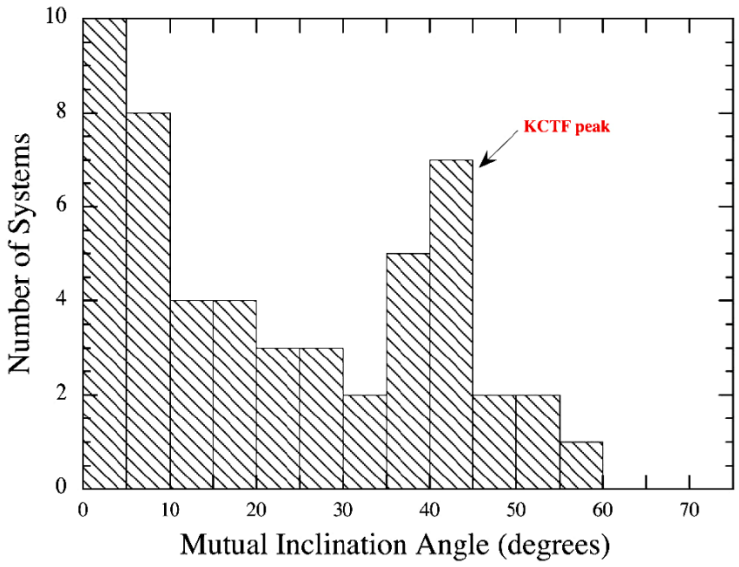

Figure 12. Distribution of mutual orbital inclinations for triple systems. The peak between 0°– 5° contains 21 systems (off scale). (Borkovits et al. 2015)

Tokovinin (2017) found that the two orbits in close triples tend to be aligned, with a mean Δi of around 20° for outer star separations of $\lesssim 50$ AU but no alignment for outer orbits $> 1\,000$ AU. Orbit alignment appears to decline for higher inner binary masses and the distribution of Δi is such that 80% of triples have $\Delta i < 70°$ and the remainder is aligned randomly.

Outer star inclination i_2

In our integrations the inclination of the inner stellar orbit is set at zero and that of the outer orbit varies from zero (coplanar) to 180° (fully retrograde), encompassing the ranges found above. Values were usually randomly generated within the desired ranges or increments of 10° were used.

For the coplanar integrations, small ranges of outer inclination of 0°- 60° for prograde orbits and 120°- 180° for retrograde orbits were selected. In the high-inclination integrations the full range of 0°- 180° was used.

Both prograde and retrograde planetary orbits were also investigated.

3.6.8 Outer star longitude of ascending node

The longitude of ascending node Ω_2 was varied from 0° to 270°. The longitude of ascending node did not affect the secular evolution of the system significantly. Increments were usually 60° or 90°.

3.6.9 Outer star argument of periapsis

The argument of periapsis ω for the inner orbit was normally set at zero, with that for the outer orbit ranging from zero to 270°. Increments of 60°- 90° were used. A value of 90° was often used as this lead to the maximum induced eccentricity in the inner binary.

3.7 Numerical Methods And Selection Of Integrator

The fastest algorithms that are reliable for long-term numerical orbit integrations are symplectic integrators. A symplectic integrator is a numerical integration scheme for a specific group of differential (in this case, Hamiltonian) equations, using classical mechanics and symplectic geometry. One of the earliest symplectic integrators was developed by Wisdom and Holman (1991). In particular, mixed-variable symplectic integrators exhibit substantially faster speed than conventional *N*-body algorithms. However, they become inaccurate when two bodies approach one another closely. This occurs because the potential energy term for the pair undergoing the encounter becomes comparable to the terms representing the unperturbed motion in the Hamiltonian. The problem can be overcome by using a hybrid method in which the close encounter term is integrated using a conventional integrator whilst the remaining terms are solved symplectically. Symplectic integrators may also give spurious results if some objects have or develop highly eccentric orbits during an integration.

Some of the codes investigated include (in approximate order of development):

3.7.1 Swift

Swift was created in 1993 (Levison & Duncan 1994; Levison & Duncan 2013). The code was designed to symplectically integrate the motion of massive bodies and test particles orbiting a more massive center, and is well suited for studying the dynamics of planetary systems. A later version for orbital simulation was SyMBA (Duncan, Levison & Lee 1998), an extension of Swift that uses a multiple time step technique and can symplectically integrate a full *N*-body system including close approaches between massive bodies. However, it fails in integrating close encounters with the central star. A further development has been Swifter, written by David Kaufmann, where the SyMBA integrator supports a second class of bodies of specified maximum mass. These bodies interact gravitationally with the more massive bodies, but not with one another. It offers seven integration techniques, including the first three listed for Mercury6, below.

3.7.2 HJS

Beust (2003) developed an add-on for Swift designed to handle the dynamics of hierarchical systems of any size and structure, provided the hierarchy is preserved. It comes in the form of the HJS (Hierarchic Jacobi Symplectic) package, a set of routines that can be added to the Swift package and specifically allow one to integrate the dynamics of multiple stellar systems, i.e. systems with more than one massive centre, if they have a hierarchical structure. For example, for a circumbinary planet, the main dynamic part will be the Keplerian motion around the center of mass of the two stars, with its effective mass the sum of the two component masses, and the second part will consist of the rest of the disturbance. This code was used by its author in various applications (Beust & Dutrey 2005, 2006; Reche, Beust & Augereau 2009). It was made public and was subsequently used successfully by various researchers (Mudryk & Wu 2006; Lithwick & Wu 2008a, 2008b; Domingos, Winter & Carruba 2012; Kennedy et al. 2012; Wiegert, Faramaz & Cruz-Saenz de Miera 2016).

3.7.3 Mercury6

The code probably used most frequently for problems involving a dominant central mass has been Mercury6 (Chambers 1999). However, dealing with planetary orbits in a binary system is problematical since the system no longer contains just one single dominant body. Fortunately, all long-lived planetary systems around binary and triple stars are likely to be hierarchical, in which case one can modify symplectic schemes while still permitting close encounters. The original Mercury6 was later expanded to do this (Chambers et al. 2002).

Although this package cannot incorporate collisions, since these cannot be modelled symplectically, it performs well on most metrics, especially for modelling relatively few bodies (where it is very accurate) and the handling of close encounters. It is written in Fortran 77 and uses various *N*-body algorithms: a second-order mixed-variable symplectic algorithm, a general Bulirsch-Stoer algorithm, Everhart's RA15 Radau algorithm and a hybrid symplectic/Bulirsch-Stoer integrator. The Bulirsch-Stoer algorithm will work with any system, but it may, however, be slow (Chambers, private communication 7/8/13).

3.7.4 NBODY

A suite of *N*-body algorithms (e.g. NBODY6), has been developed by Sverre Aarseth, as described in his book (Aarseth 2003). While focused mainly on modelling clusters and galaxies, some programs (e.g. Triple) may be applied to planetary systems and small-*N* experiments.

3.7.5 FEWBODY

Another code is FEWBODY (Fregeau et al. 2004), which uses the approximate analytical criterion of Mardling and Aarseth (2001) for the dynamical stability of hierarchical systems and is particularly suited to performing scattering experiments. It has been used in the modelling of quadruple systems and their comparison with triples (Pejcha et al. 2013).

3.7.6 Miscellaneous

In 2007 Verrier & Evans developed a stand-alone program for triple systems, Moirai, based on the Chambers et al. (2002) algorithm, and tested it on the three main orbital configurations for triples (Verrier & Evans 2007). However, the code was not made public.

Another integrator, written by Piet Hut to investigate a planet bouncing between the two stars of a binary, was built on a fourth-order Hermite integrator; it is a robust and flexible integrator for small-*N* systems as it has no preferred dominant force or geometry (Moeckel & Veras 2012).

Some of the more recent integrators have been designed for parallel or multicore/GPU implementation, such as QYMSYM (Moore & Quillen 2011) and GENGA (Grimm & Stadel 2014). Both codes are hybrid symplectic integrators based on Mercury6. At a low number of integrations (~30), the GPU overhead dominates and Mercury6 is faster. At a high number of integrations, GENGA begins to benefit from the large number of GPU cores, until at around 1 000 integrations the GPU is fully occupied and the computation time begins to

increase again. At 16 000 integrations the GPU is about 40 times faster than one CPU.

Other codes include the HNBody package, for the symplectic integration of hierarchical systems, which offers explicit support for three classes of particles – heavy, light, and massless (Rauch & Hamilton 2012).

3.7.7 Selection of integrator

Of these scientific-grade symplectic integrators, perhaps the most popular and well-used small-*N* codes are Swift and Mercury6, with the former's HJS extension being particularly appropriate for the triple star system to be investigated. For a compact triple, close encounters are likely.

Mercury6's Wisdom and Holman algorithm only uses Jacobi coordinates for massive objects. For masses around a hierarchical triple these would in theory be the same as Beust's hierarchical Jacobi coordinates, if one of the binary pair from the triple was specified as the central object. (As Chambers et al. (2002) have pointed out, the technique is identical to the Beust algorithm if only one planet is present in the system.) However, use of this code for the integration of the dynamics in multiple stellar systems becomes potentially problematic. Even taking the interaction with the most massive object as the main part of the Hamiltonian, if the masses of different stars are of the same order of magnitude this no longer guarantees that one party dominates the other, and the symplectic integration method does not work well unless an extremely small time step is adopted.

Previous work (Busetti, F.R., Masters dissertation, 2013) found that Mercury6 worked well for a triple configuration such as HW Virginis with $a = 1\,326$ and $\mu_2 = 0.03$ (Beuermann et al. 2012), but did not model the closer proximity and inverted mass ratio of a configuration such as HD 181068 with $a = 19$ and $\mu_2 = 1.7$ (Borkovits et al. 2013) well, and the addition of further bodies, in the form of test particles, was unsuccessful.

Beust's hierarchical Jacobi coordinate scheme is therefore the most appropriate for the triple systems to be investigated and the HJS code was selected. Much research that looks at hierarchical systems uses this code.

3.7.8 Software details and other software used

SWIFT and HJS are written in ANSI standard Fortran 77. For the OPEN function and in recursive routines SWIFT makes use of the C pre-compiler, *cpp*. For consistency, the edge-detection routine described in Section 3.9 was also written in Fortran 77. The Intel Fortran Compiler for Linux, *ifort*, was used for compilation.

An attempt was made to parallelize the code, first profiling it by compiling with -*profile*- loops for both functions and loops. Since many loops had little computational content but their parallelization introduced substantial overhead, only the top 11 functions, accounting for 76% of the run time, were then auto-parallelized using OpenMP. However, no speedup was achieved. Lower-level parallelization using MPI was not attempted.

Program output is written to a binary output file. Fortran code was written to read data from this file as part of the edge-detection routine. This binary output file was also input to SwiftVis, a powerful and very flexible visual data-flow programming package by Mark Lewis, which was used to visualise and analyse the data and generate some of the graphics.

Data filtering, visualisation and graphics were also done in OriginsPro and Excel. Statistical analyses were carried out with SPSS. Mathematical manipulations such as solving the Hamiltonian were done using Mathematica.

The Bash shell was used extensively for scripting and automating integrations for the cluster. Cluster jobs were submitted using the PBS administrative interface system.

Integrations were run on the Mathematical Sciences Cluster at the University of the Witwatersrand, using up to 300 cores.

3.8 Computational Parameters

3.8.1 Time step

An early study by Ford, Kozinsky and Rasio (2000) that utilized SWIFT used a time step of $1/40$ of the orbital period of the inner binary, reducing to 1/600 for high-eccentricity systems. Energy and angular momentum were typically conserved to 1 part in 10^6 and 10^{12}, respectively. A larger time step, of $1/20$ of the orbital period of the inner binary is more commonly used, e.g. Beust (2003). Symplectic integration schemes usually ensure energy conservation with 10^{-6} relative accuracy using this time step (Levison & Duncan 1994).

An integration time step of 1/20 of the orbital period of the inner binary was therefore normally used in our integrations. The time step also needs to be varied to verify that results are not affected by numerical errors. For each batch of integrations, we checked that the use of a significantly smaller time step did not change our results.

The time interval between data outputs and dumps was normally set at $1/1\,000$ of the total integration time, which usually translated to $100 - 1\,000$ yr.

3.8.2 Integration time

In stability analyses an integration time of 10^8 years is often used, as this typically applies to systems with dimensions comparable to the Solar System because it corresponds roughly to the bulk Lyapunov time for the major planets. However, in general the more compact the system, the shorter the required integration time as most of the characteristic features of the secular evolution of the orbital parameters occur on a shorter time scale. Short orbital periods of the test particles (i.e. planets) and high precession frequencies can reduce the required integration time by some orders of magnitude.

The characteristic Kozai times t_K for the inner binary can be defined, in terms of our notation, as per Pejcha et al. (2013):

$$t_{\mathrm{K}} = \frac{4}{3}\left(\frac{a_1^3\ m_1}{G m_2^2}\right)^{\frac{1}{2}}\left(\frac{a_2\left(1-e_2^2\right)^{\frac{1}{2}}}{a_1}\right)^3 \tag{12}$$

where a refers to semi-major axes, m to masses, e to eccentricity and the subscripts to stars 1 and 2 of the inner binary.

As higher-order effects in Kozai cycles become important only on longer timescales than this, this time is used to indicate which are the relatively worst (i.e. least compact) cases in a set of integrations. One can plot the width of the evolution ranges obtained over, say, 10^5 yr for both the semi-major axes and the eccentricities of the three bodies to ensure that the integration time comfortably exceeds the precession periods of the system.

The secular evolution of orbital parameters was sampled for each of the configurations used, and an integration time of 10^5 yr was found to be sufficiently long in most cases examined. Each batch of integrations included at least one run with an integration time of 10^6 yr or 10^7 yr on the least compact configuration, to confirm this.

To check the accuracy of the planetary integrations we monitored conservation of total energy for the integrations. Using time steps of the above order lead to an overall fractional change in the system energy $\Delta E/E_0$ of about 10^{-7} over a 10^5 yr integration. The relative energy error $\Delta E/E_0$ of a typical integration is shown in Figure 13.

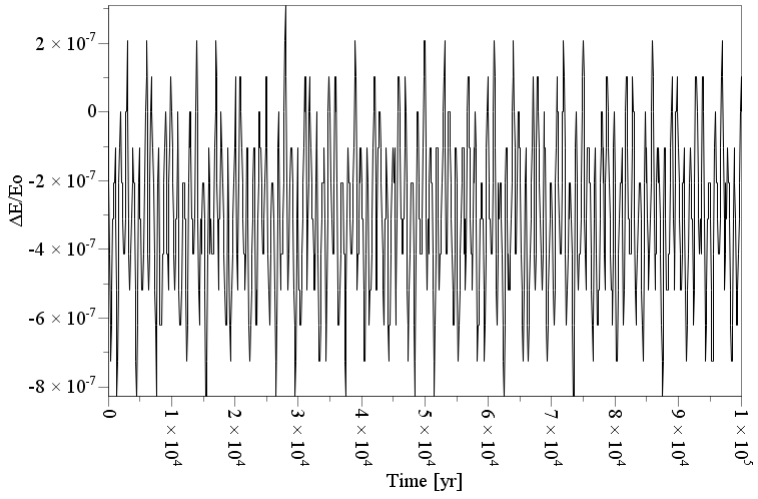

Figure 13. Relative energy error of a typical integration

Orbital failures tended to occur quickly – if an orbit did not fail within as little as 10 – 100 yr, it was usually stable up to 10^5 yr. While long integration times are always desirable, the fact that the stellar systems we investigated were compact worked in our favour: 10^5 yr was often equivalent to hundreds of thousands of orbits of the outer star.

3.8.3 The test particle cloud

The number of test particles used varied from 1 000 to 10 000, with higher numbers being used when rates of ejection were high. In most cases 2 000 or 3 000 test particles were sufficient.

The particles' eccentricities and maximum inclination could be set to any desired values (with inclinations of greater than 90° describing retrograde orbits).

For most stellar configurations, which were close to coplanar, the initial test particle cloud took the form of a disc, with the plane of the disk aligned with the plane of the inner binary. For configurations where the outer star was of high inclination, the test particle disc was aligned with the invariable plane, as explained in more detail in Section 4.2.1.

The inner and outer limits of the particle cloud also need to be specified. To avoid making the cloud unnecessarily large for certain configurations and save on computation time, the outer limit for P-type orbits needs to be set at a reasonable distance. Our approach was to define this relative to the chaotic zone and main mean-motion resonances. For example, knowing the period of the outermost star enables one to calculate the distance at which the, say, 5:1 MMR occurs; a test particle should orbit the whole system stably at that distance. Twice this value would be a conservatively large value for the outer boundary, and this criterion was generally used. For S-type orbits the maximum outer distance will be approximately to the nearest star, some further tweaks are discussed in the relevant sections.

In both cases some computation time can theoretically be saved if, instead of abruptly truncating the disk of test particles at a (relatively short) distance, one decreases the density of particles moving outwards, for example by using a power law where the density of test particles $\propto a^{-1}$, where a is the semi-major axis of the particle.

The power law used to generate this type of cloud is

$$a = \left[a_{min}^{p+1} + ({a_{max}}^{p+1} - {a_{min}}^{p+1})r\right]^{\frac{1}{(p+1)}} \quad (13)$$

where

a_{min} = minimum semi-major axis of cloud

a_{max} = maximum semi-major axis of cloud

r = a random variable [0,1]

p = the power law parameter [0,1]

So, for example, $p = 0$ results in $a = [a_{min}, a_{max}]$, i.e. a uniform distribution, and for $p = 1$, $a = \left[\sqrt{a_{min}}, \sqrt{a_{max}}\right]$.

However, in practice the test particles were, usually assigned semi-major axes from a uniform random distribution. In generating the test particle cloud, a minimum semi-major axis of 0.01 AU was used. This value must be larger than the distance at which a test particle was stopped as being too close to the central body, and this was set at 0.002 AU (see next section).

Test particle orbits with inclinations ranging from fully prograde to fully retrograde were used. In coplanar cases the test particle cloud was initially uniformly distributed, circular and of zero absolute inclination (i.e. an inclination of 0° for prograde particles and 180° for retrograde particles).

3.8.4 Test particle removals

The exoplanet orbiting closest to its central body (a pulsar) is PSR 1719 – 14 b, at 0. 0044 AU, while Kepler-42c has the closest orbit to a "normal" star, at 0.006 AU. The heliocentric distance at which a test particle is stopped, being considered too close to the central body, was therefore selected to be 0.002 AU.

The furthest planet from its host star yet discovered is HIP 77900 b, at 3 200 AU. The distance at which a test particle was assumed to have escaped from the central body was therefore set at 10 000 AU.

These two limits were occasionally varied depending on the type of planetary orbit considered.

The code checks for close approaches between test particles and other bodies, and if a test particle approaches within a certain distance of another body it is stopped. It is recommended that this distance is set at greater than a Hill sphere. This is calculated in the next section.

3.8.5 The Hill stability criterion

An astronomical body's Hill (or Roche) sphere approximates the gravitational sphere of influence of this body in the face of perturbations from a more massive body – it is the region in which it dominates the attraction of satellites.

In binary systems the integral of motion or Jacobi constant defines allowable regions of planetary motion. For a planet that begins with a circular orbit around one star, there is a critical value of the semi-major axis ratio. Below this value the zero-velocity curve with the same Jacobi constant is "closed" and the planet cannot escape, and vice versa.

The Hill radius R_{H} for a small body of mass m_2 orbiting a larger body of mass m_1 with a semi-major axis a and eccentricity e is

$$R_{\mathrm{H}} = a(1-e)\left[\frac{1}{3}\left(\frac{m_2}{m_1+m_2}\right)\right]^{\frac{1}{3}} = a(1-e)\left(\frac{\mu_1}{3}\right)^{\frac{1}{3}} \quad (14)$$

If $m_2 \ll m_1$,

$$R_{\mathrm{H}} \approx a(1-e)\left(\frac{m_2}{3m_1}\right)^{\frac{1}{3}} \quad (15)$$

Assuming that a typical exoplanet has $m_2 \sim 1\ M_J$ and $a \sim 1$ AU (as shown in Figure 3) and $e = 0$, and that a typical intermediate-mass star has $m_1 \sim 4\ M_S$, then $R_{\mathrm{H}} \sim 0.04$. The stopping distance was set at 0.1 AU.

3.9 Orbit Stability Bounds – Edge Detection Routine

It was necessary to automate a procedure for identifying the edges of the test particle cloud at the end of an integration. This routine is outlined below for P-type orbits, with the modifications required for S-type orbits discussed in the relevant sections in Chapter 4.

The procedure first extracts the data from the binary file produced by the HJS code. It then takes a cross-section through the centre of the system and test particle cloud and constructs a density function, being the surviving particles' frequency distribution.

The test particles are binned according to their semi-major axis, independent of any inclination of their orbit, i.e. this variable is *not* the projection of their orbits on the horizontal plane. This becomes pertinent when inclined orbits are considered. There are many heuristics for the optimal number of bins, with two popular ones being the square root rule and Rice's rule. If n is the number of observations (i.e. remaining test particles), the optimal number of bins k is given by $k = \sqrt{n}$ and $k = 2\sqrt[3]{n}$ respectively. We took the average of these:

$$k = \frac{\sqrt{n}}{2} + \sqrt[3]{n} \tag{16}$$

We then set a cutoff value for the particle density function (PDF) to define the edge of the test particle cloud and determine its semi-major axis. These cutoff values were determined by optimizing the algorithm using visual estimates of the edges of a wide range of integration outcomes.

One problem, for P-type orbits only, is the sparsity of the particle density function. For example, beginning with 1 000 test particles, at the end of a 10^5 year integration the number of remaining particles in the inner P1 orbits can be quite small. Determining the outer stability bound of the inner orbits (and occasionally the inner stability bound of the outer orbits) is then difficult, since the histogram can be quite discrete, as shown in Figure 14.

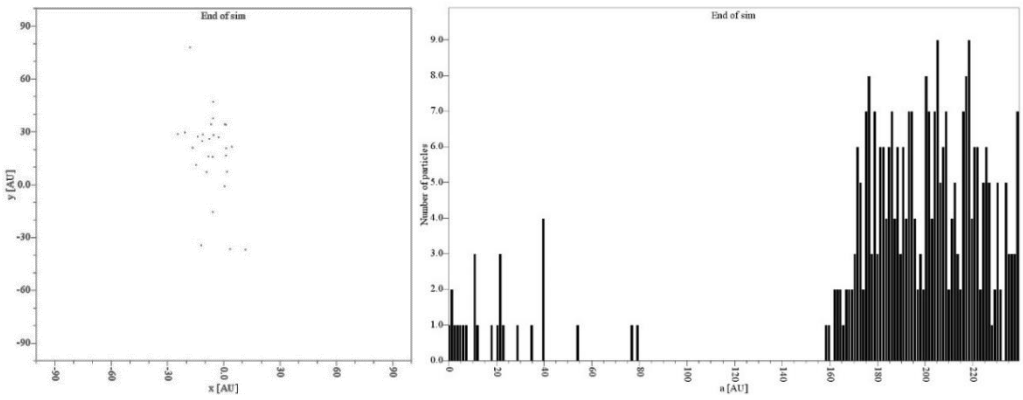

Figure 14. a) Cartesian plot of final particle positions, b) corresponding density function

The histogram's particle density function can be smoothed by using a final time period (f_t) for the integration instead of the final instant, say the last 10% of the integration time. The integrity of its profile should remain unaffected, as it is

unlikely that many particles will be ejected within this period, and even if a few are, this will not change the distribution materially. The use of a final time period leads to a much smoother particle density function, as shown in Figure 15.

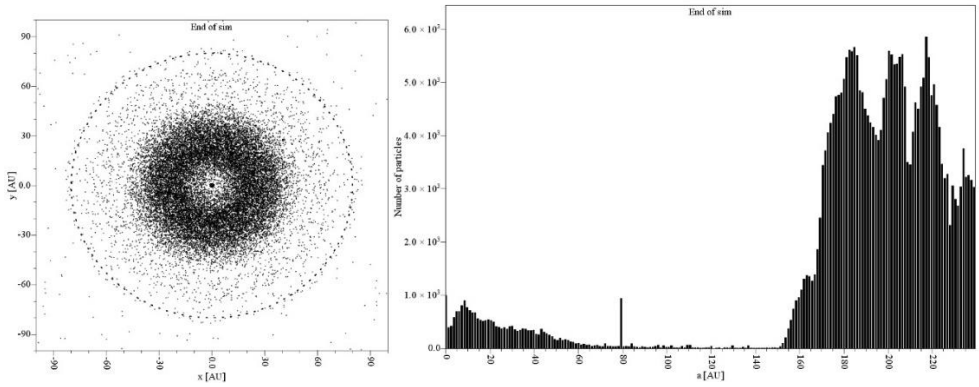

Figure 15. a) Cartesian plot of final particle positions over the last 5% of the integration time b) corresponding density function

The algorithm then begins at the origin of the particle density function and steps along the semi-major axis, as shown in Figure 16, until it locates the maximum (max_i) of the inner orbit's density function, i.e. between the binary, comprising Star 1 (at the origin) and Star 2 (very close to it), and Star 3.

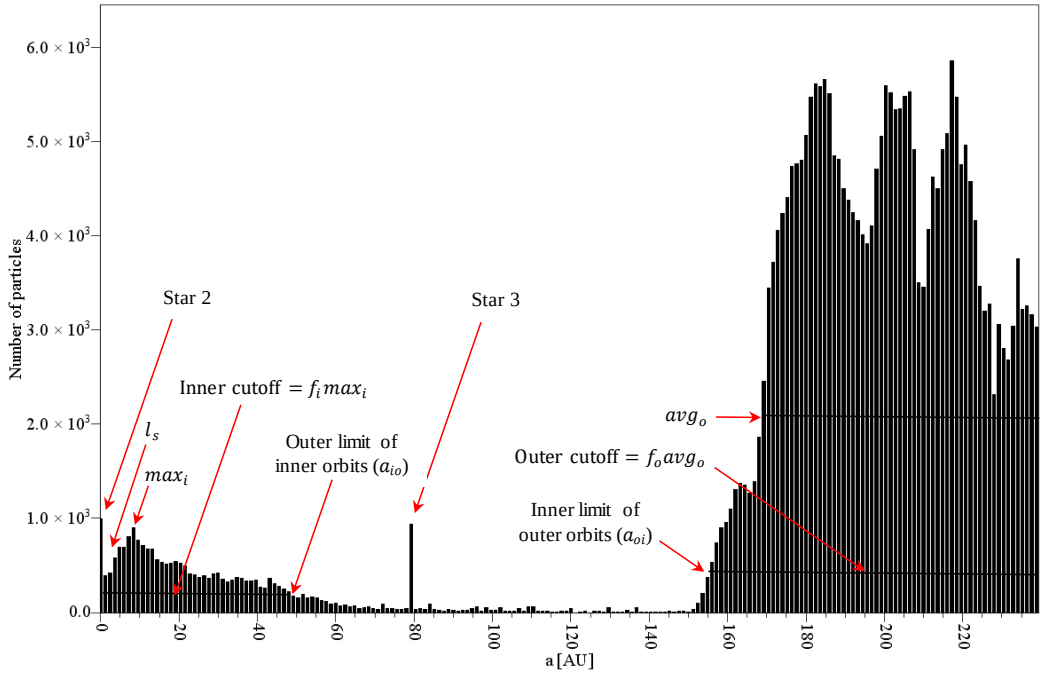

Figure 16. The particle density function and edge detection algorithm

The inner orbit's boundary can be quite diffuse, particularly for retrograde orbits, so one must first decide whether any well-defined edge for the inner orbit exists at all. To do this, the maximum inner orbit density (max_i) is divided by the mean density of the inner orbits (avg_i). If this "peakiness" falls below a certain empirical value (f_p), an orbit edge is deemed not to exist.

If it exceeds this value, the procedure continues and selects an empirically-determined fraction of the maximum density (f_i) as the density cutoff limit, i.e. the inner cutoff value is $f_i\ max_i$ for the inner orbits' edge. Moving along the horizontal axis until this value is reached, we then read off the corresponding value for the semi-major axis (a_{io}). Because the distribution can still be noisy, additional smoothing of the bin values is used. In determining the inner edge, to avoid the routine picking empty bins close to $a = 0$, a minimum inner orbit semi-major axis is set, as a fraction of the outer star's semi-major axis (l_s).

The algorithm then continues stepping along the semi-major axis, past Star 3. The inner edge of the outer test particle disc is then found by applying an outer density cutoff limit to the outer particle density function. This outer cutoff is found as a (different) empirically-determined fraction (f_o) of the mean density (avg_o) of the outer density function; when the density function reaches this value the inner limit of the outer orbits (a_{oi}) is established. Here the mean is used instead of the maximum because of the multi-modality of the outer distribution.

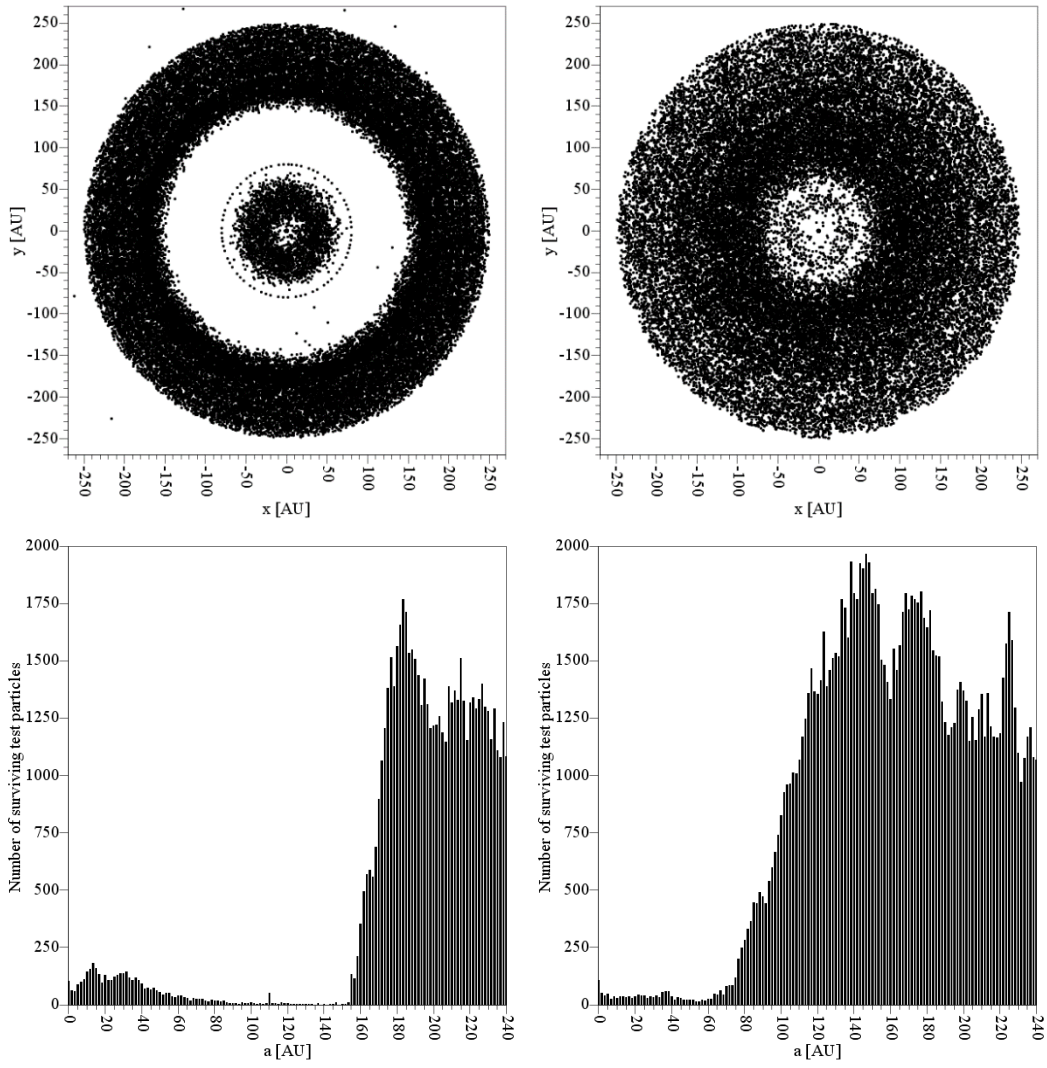

Figure 17. Test particle cloud and density function of: a) prograde planets b) retrograde planets, with all other parameters identical

The characteristic profile of the cross-sectional particle density function is quite different for prograde and retrograde orbits. For retrograde orbits the density of the inner orbits relative to the outer orbits is much lower than for prograde orbits. Also, since retrograde orbits are stabler than prograde ones, the region cleared by the outer star in this case is much narrower than for prograde orbits, as shown in Figure 17.

This necessitates an additional test for the existence of the inner edge. The ratio of the mean density of the inner orbits to the outer orbits is calculated (a_a). If this is below a certain threshold, the inner edge is too sparse to be defined. This criterion is independent of, and overrides, the "peakiness" test.

The six parameters (f_t, f_p, f_i, f_o, l_s and a_a) were then optimised by training against a wide range set of particle density functions. Because of the different characteristic profiles of prograde and retrograde orbits, the parameters had to be optimised separately for these two cases.

The optimised edge-detection parameters used for P1 and P2 orbits are shown in Table 8.

Parameter	Prograde orbits	Retrograde orbits
f_t	0.105	0.153
f_p	1.500	1.000
f_i	0.520	0.300
f_o	0.028	0.400
l_s	0.500	0.500
a_a	0.016	0.028

Table 8. Edge detection parameters for triple system P1 and P2 orbits

These parameters are for fully prograde and retrograde orbits. For orbit inclinations lying between these extreme values, the parameters were interpolated between these values according to the "degree of progradeness". We found this degree of progradeness to be approximately related to the ratio of the mean density of the inner and outer orbits, so this metric was used.

During early integration runs it became apparent that some results were implausible. These had one thing in common – there was a large outlier spike in the test particle density histogram that resulted in an incorrect result from the edge detection routine. In every case these spikes were caused by a single anomalous test particle; the reason for this remains unclear. The edge detection routine was therefore modified to identify and remove any anomalous spikes from the particle density function and this de-spiking routine solved the problem.

Chapter 4

Results

4.1 Orbit Types P1 And P2

4.1.1 Configuration

The configuration of P1-type circumbinary orbits and P2-type circumtriple orbits around the inner binary and whole triple respectively is shown in Figure 18.

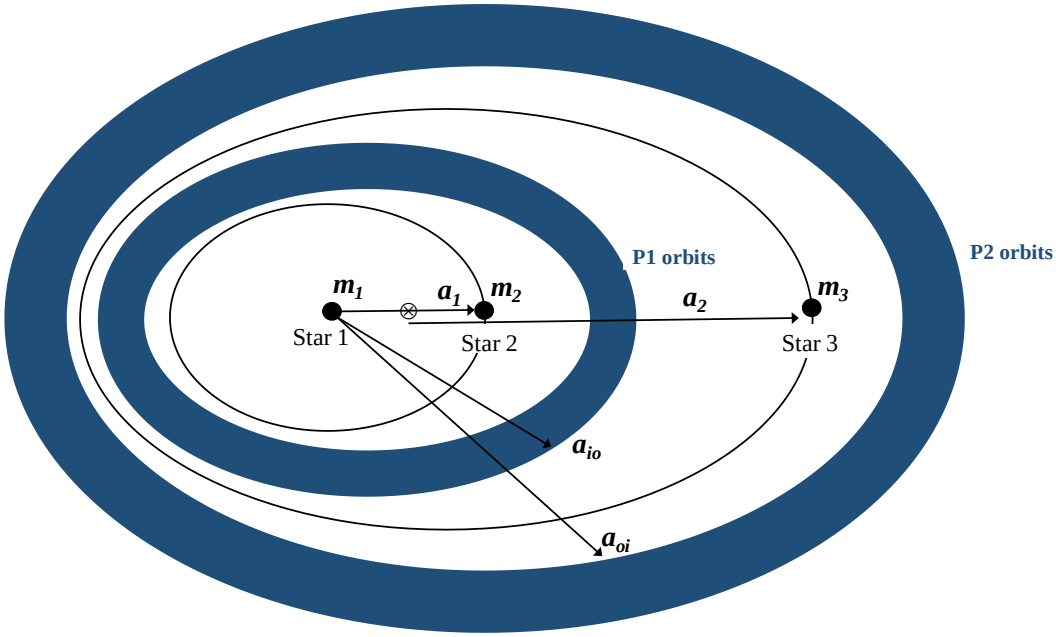

Figure 18. P1 and P2 orbits. Triple system configuration

Note that the inclination of Star 3, to either the orbital plane of Star 1 and Star 2 or to the invariable plane, is not indicated.

The initial test particle cloud is continuous, ranging from very close to Star 1 to well beyond Star 3 as discussed in the previous section; the orbits of Star 2 and Star 3 then clear this area as shown and create the stability bounds a_{io} and a_{oi}.

4.1.2 Parameter space

The parameter space used is shown in Table 9.

For the planets and outer star, prograde or retrograde orbits are indicated by 0 and 1 respectively. The lower limit of the semi-major axis ratio a_m represents the Mardling limit. The remaining parameters are as discussed in the previous chapter.

For most integrations, parameter values were randomly generated to be uniformly

Parameter ranges	Units	Orbit type P1 and P2	
Prograde (0) and retrograde (1) outer star	-	0	1
Prograde (0) and retrograde (1) planets	-	0	1
Geometry			
Semimajor axis ratio $a = a_2/a_1$	-	a_m	100
Inner mass ratio $\mu_1 = m_2/(m_1+m_2)$	-	0.1	0.5
Outer mass ratio $\mu_2 = m_3/(m_1+m_2)$	-	0.2	2.3
Star 2			
Eccentricity e_1	-	0	0.9
Inclination i_1	deg	0	-
Longitude of ascending node Ω_1	deg	0	-
Argument of periapsis ω_1	deg	0	-
True anomaly v_1	deg	0	-
Star 3			
Eccentricity e_2	-	0	0.9
Inclination i_2	deg	0-60	120-180
Longitude of ascending node Ω_2	deg	0	270
Argument of periapsis ω_2	deg	0	270

Table 9. P1 and P2 orbits – parameter space

distributed between the lower and upper limits of the ranges shown, except for the prograde/retrograde binary toggles. Combinations were checked for validity, e.g. if $e = 0$ then ω does not exist and if $i = 0$ then Ω does not exist.

4.1.3 Computational parameters

The computational parameters used are shown in Table 10.

Parameter		Units	Orbit type P1 and P2
Central star mass	m_1	M_S	1
Timestep	*dt*	yr	$T_{bin}/20$
Number of test particles		-	1000 - 3000
Test particle orbit centres		-	-1 -1 -1
Minimum semi-major axis (1)	*amin*	AU	0.01
Maximum semi-major axis	*amax*	AU	2x 5:1 MMR
Collision with central body	*rmin*	AU	0.005
Ejection from system	*rmax*	AU	10^4

(1) Must be > specified collision distance

Table 10. P1 and P2 orbits – computational parameters

The test particle orbit centres describe the system's hierarchy in Swift-HJS. The remaining parameters were discussed in the previous chapter.

The stellar and computational parameters used for the different orbit types are also tabled in Appendix A.

4.1.4 An example integration

An example integration is illustrated below. The parameters in this specific case included an intentionally large inverse outer mass ratio, and were: $a_1 = 1$ AU, $a_2 = 100$ AU, $m_1 = 1\ M_s$, $m_2 = 4\ M_s$ and $m_3 = 15\ M_s$, so $a = a_2/a_1 = 100$, $\mu_1 = 0.8$, $\mu_2 = 3.0$, and e, i, Ω, ω and M for stars 2 and 3 are all zero. A time step of 2.236×10^{-2} yr or around 8 d was used, with a full integration time of 10^5 yr. The test particle cloud consisted of a disc of uniform density initially containing 10 000 test particles with eccentricities of zero, and extended from the centre of the system to 300 AU, where it was truncated.

The clearing of the inner area over time is shown in Figure 19. The first graph in each pair shows the test particle disc in the cartesian plane and the second graph is of the corresponding cross-sectional particle density function.

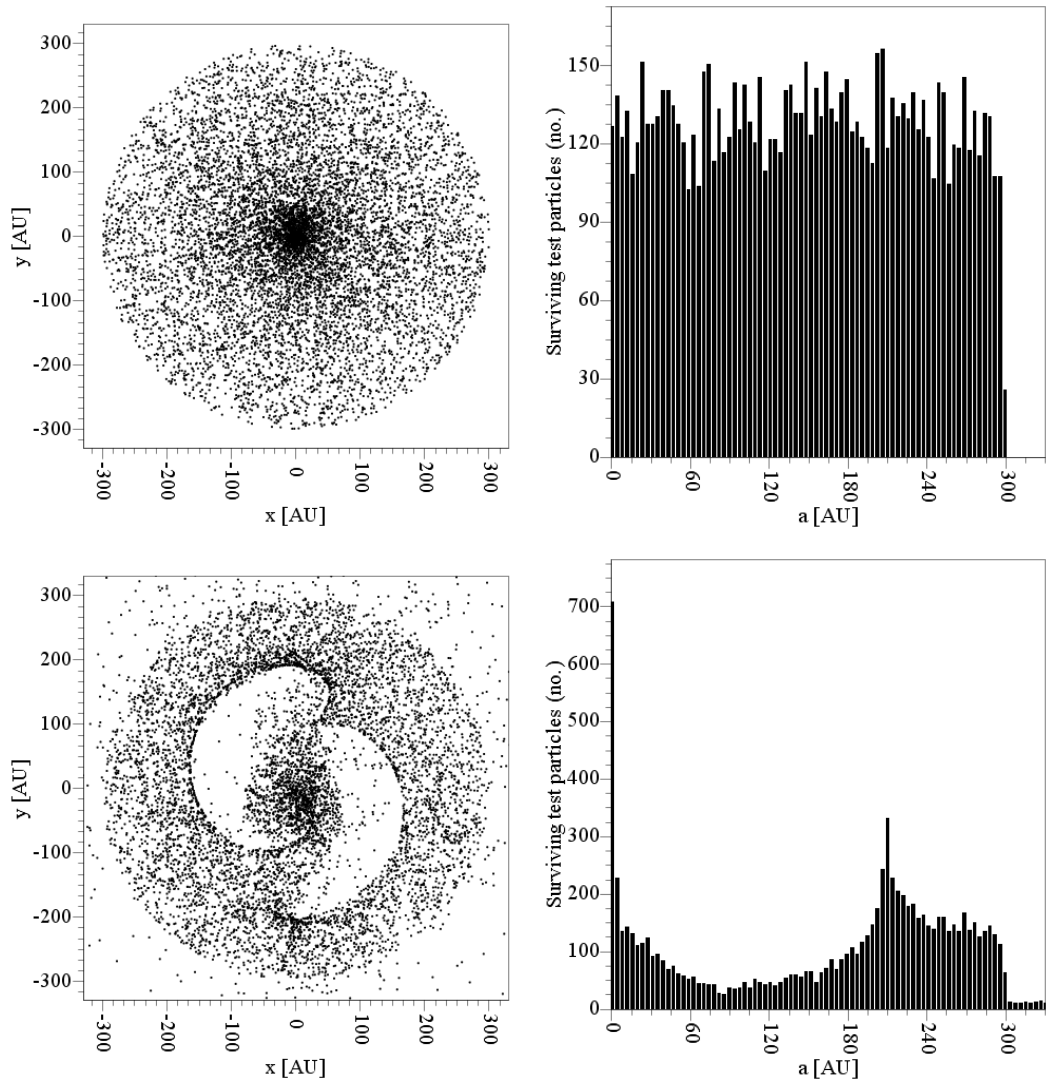

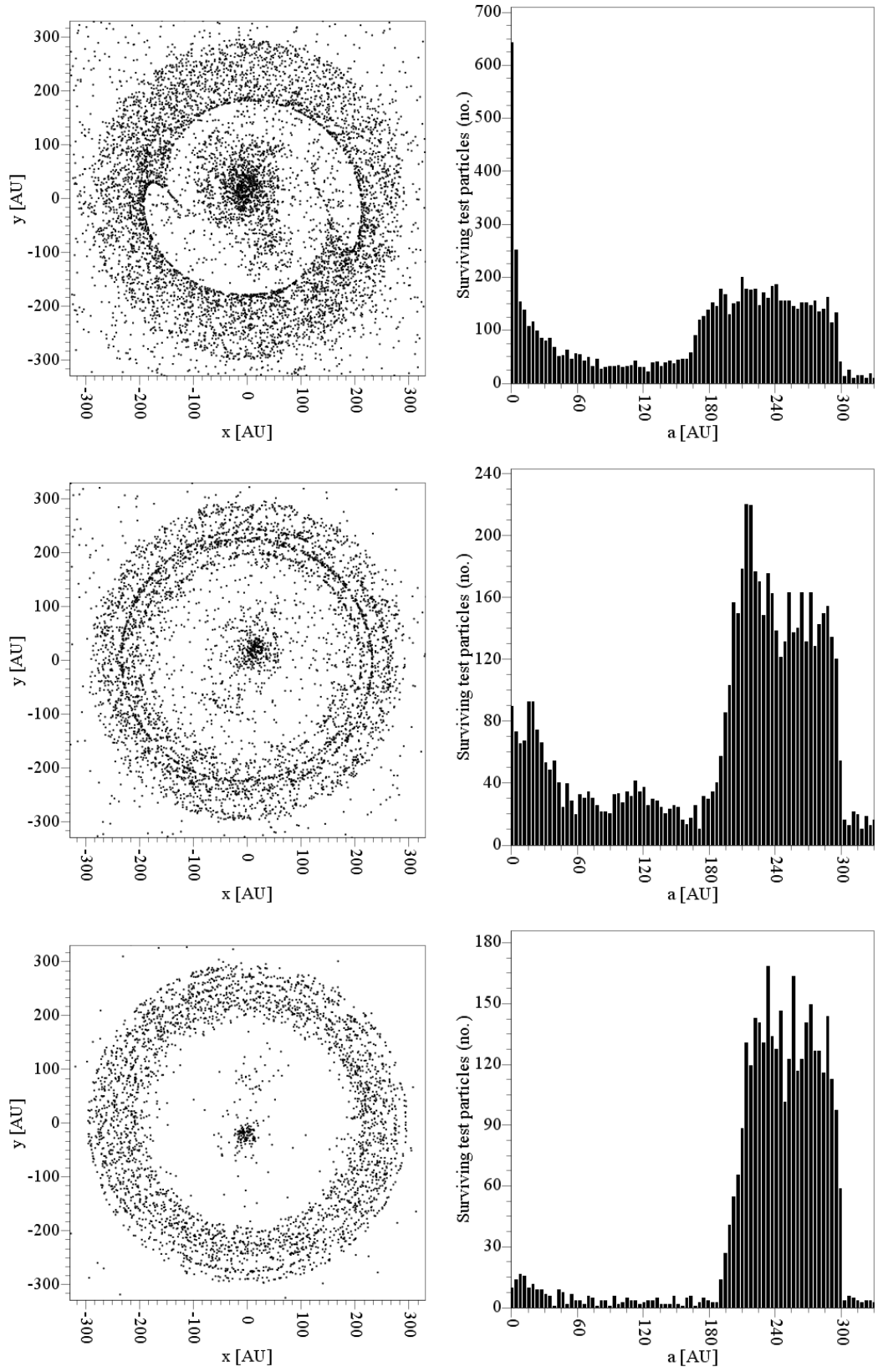

Figure 19. P1 and P2 orbits. Progression of the clearing of the inner area, at times $t = 0$ yr, 170 yr, 290 yr, 1 380 yr and 10 000 yr

The first pair shows the initial test particle distribution. The second pair shows an early stage of clearing. Here clearing proceeds most rapidly in the middle of the

test particle cloud and more slowly close to the centre and at the outer regions. In the last two pairs one can see the development of regions of relative stability and instability. After 10^4 yr, 48% of the original test particles remained.

The initial clearing by the outer Star 3 orbiting at 100 AU (not shown) is rapid, with most of the ejections occurring early in the integration. At the end of the integration at 10^5 yr there are some test particles remaining in P1 orbits around the inner binary, but the edge of this stable region (a_{io}) is not sufficiently well-defined, with only 67 particles remaining inside the orbit of Star 3. However, the inner edge of the P2 orbits (a_{oi}) has stabilised and this outer limit of the cleared region is estimated by the edge detection algorithm as 196 AU.

This is also shown in Figure 20, where the stable outer ring of test particles begins at around 190 AU, with final eccentricities mostly ranging from 0 to around 0.15, while a few bodies are orbiting the triple at under 90 AU, with a wide range of eccentricities from approximately 0.1 to almost one.

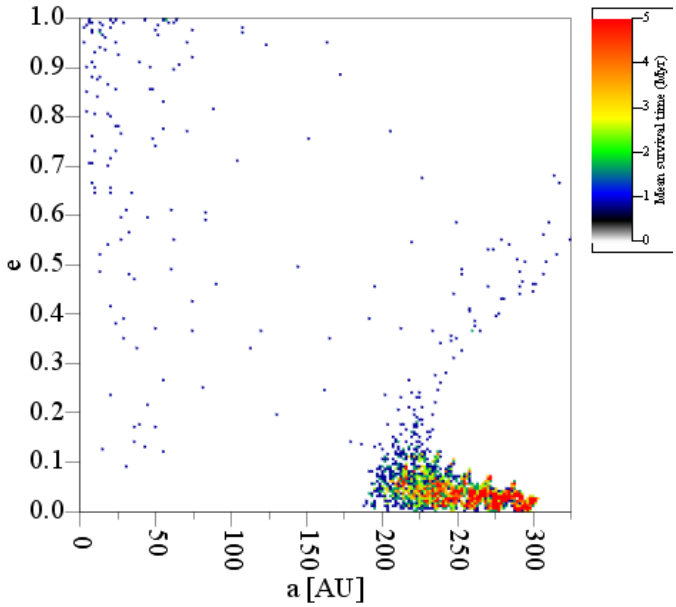

Figure 20. P1 and P2 orbits. Semi-major axes and eccentricities of test particles after 100 000 yr

An examination of these orbits shows that the outer P2 orbits are Keplerian and the inner P1 orbits are more chaotic as well as eccentric, as shown in Figure 21. These inner chaotic orbits are nevertheless stable (in the sense of being bounded) for their survival time of 10^5 yr.

The relevant stability criteria in an integration are the variation ranges of individual orbital elements, particularly semi-major axes. In the case of regular dynamics from mean-motion resonances, semi-major axes are secular invariants that are expected to undergo very small and rapid changes. So, any significant variation in semi-major axes is usually a sign of instability. The orbital parameters a, e *and* ω of a test particle at $a \cong 208$ AU, close to the inner edge of the outer test particle cloud, are shown in Figure 22.

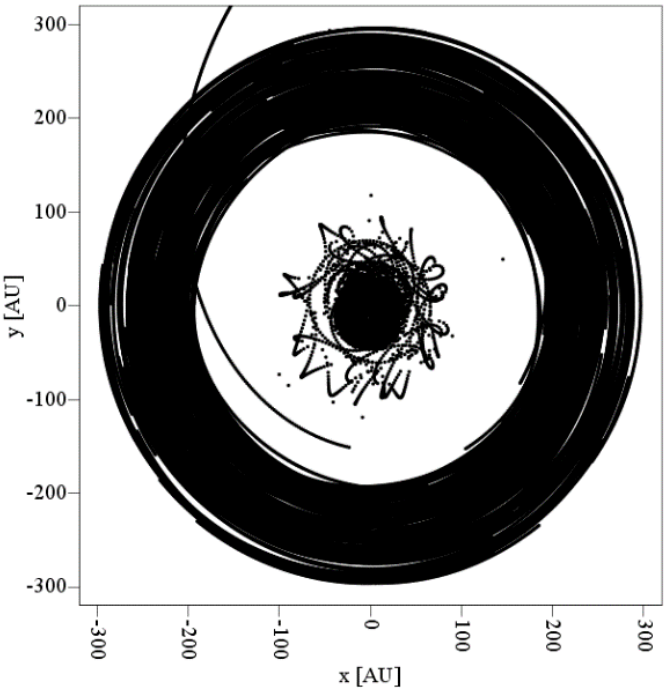

Figure 21. Keplerian outer P2 orbits and chaotic and eccentric inner P1 orbits

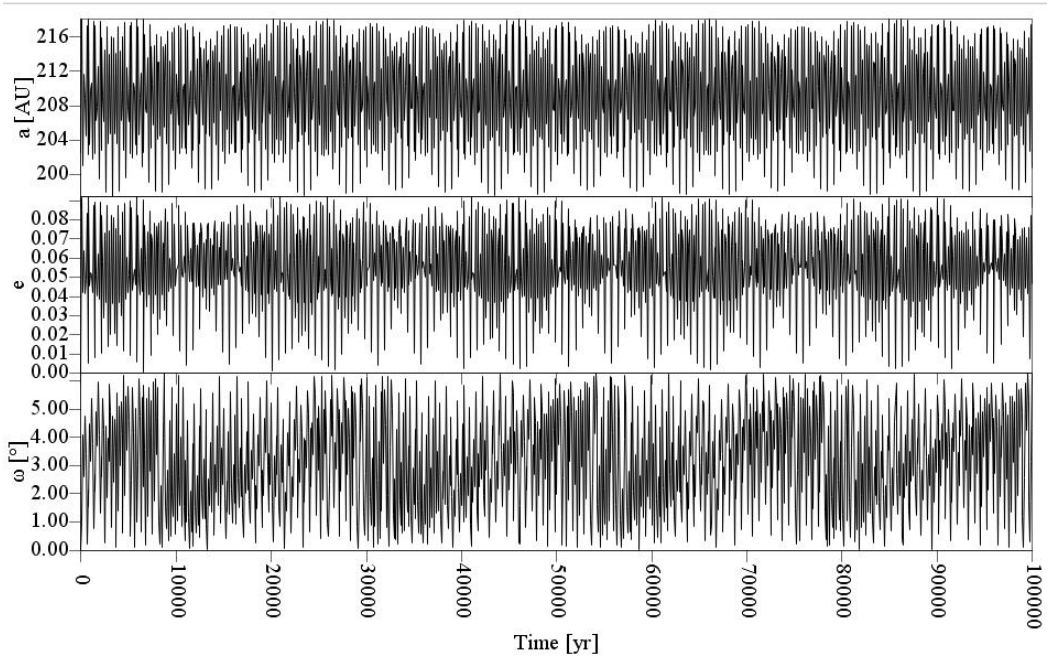

Figure 22. Selected orbital elements of test particle #942

Over the duration of the integration there is no secular trend in semi-major axis, which fluctuates on either side of 208 AU by around 4%, with the particle's orbital eccentricity also showing a small oscillation between zero and 0.09. The orbital precession is also small, with the argument of periapsis cycling between zero and 6°.

In contrast, the behaviour of some of the outermost and innermost particles from the inner test particle cloud are shown in Figure 23 and Figure 24.

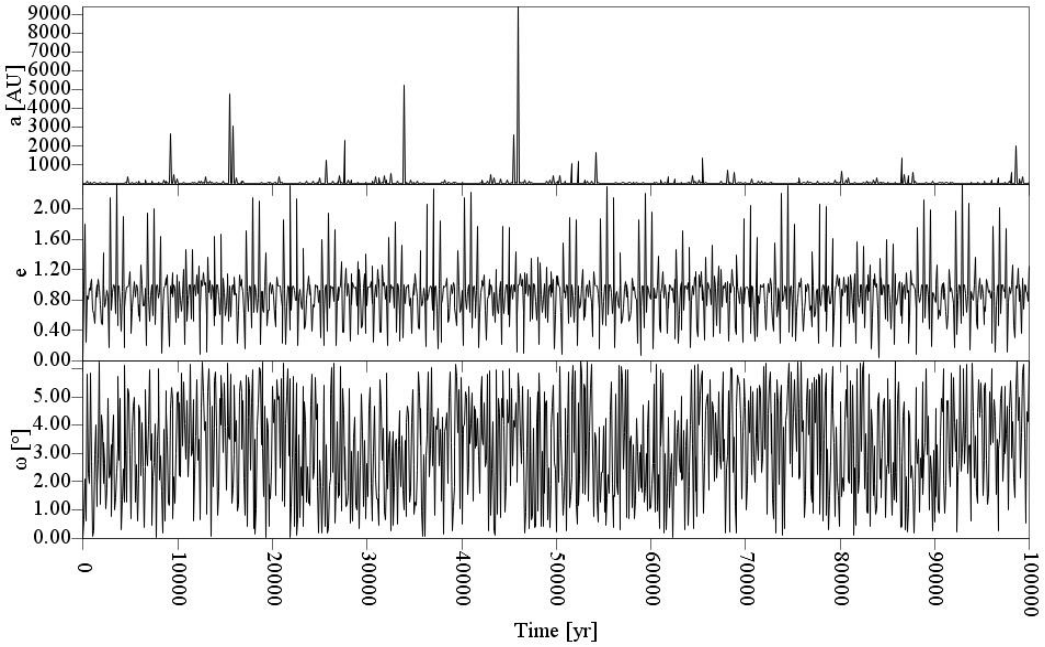

Figure 23. Selected orbital elements of test particle #902

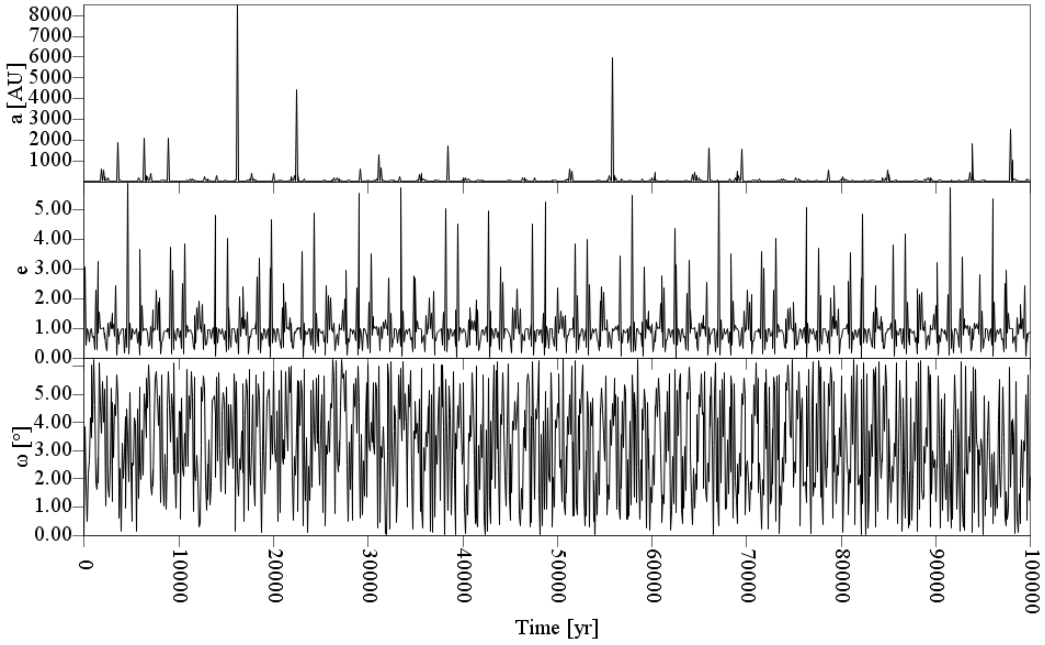

Figure 24. Selected orbital elements of test particle #727

These inner particles are clearly unstable, with their semi-major axes jumping by orders of magnitude at random times and with eccentricities regularly exceeding unity – many inner orbits were chaotic, albeit bounded. Also, some particles in

this region may not be in orbits around the inner binary but in very wide, elliptical orbits around the complete triple.

At the end of 10^5 yr, 333 of the 1 000 test particles remained in the outer stable orbits. The integration was then checked by re-running for 10^6 yr. At the end of this time only six more test particles had been ejected, with the last one being expelled relatively early at 0.75 Myr.

The fact that most ejections occur in the early stages of orbit clearing is illustrated in Figure 25.

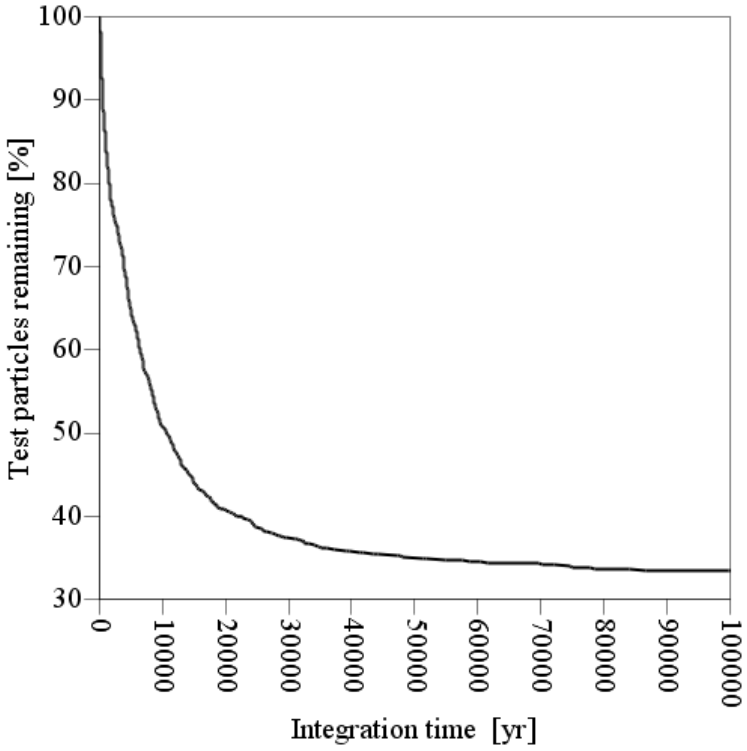

Figure 25. Decline in the number of surviving test particles over time

Over 90% of the ejections occurred in the first 24 000 years, and 99% by 85 000 years. Many configurations show even more precipitous declines.

Another integration of 10^6 yr was run to check the stability of the results. The output variables of interest are the semi-major axes of the inner and outer bounds a_{io} and a_{oi}, and these were stable. The outer bound is usually well defined, but the inner bound is often tenuous, so if the edge of a_{io} could not be measured with any certainty, it was excluded from the data.

Characteristics of prograde and retrograde planetary orbits

The results of another typical integration are shown in Figure 26. The upper charts show the orbits of the inner binary and the outer star, together with the test particle clouds after 10^5 yr, for prograde and retrograde test particles respectively. In each case $a = 10,\ \mu_1 = 0.5,\ \mu_2 = 0.5$ and all other parameters were zero. The last 10% of the integration time is shown, to increase the density of the test particles and their density functions in the lower graphs.

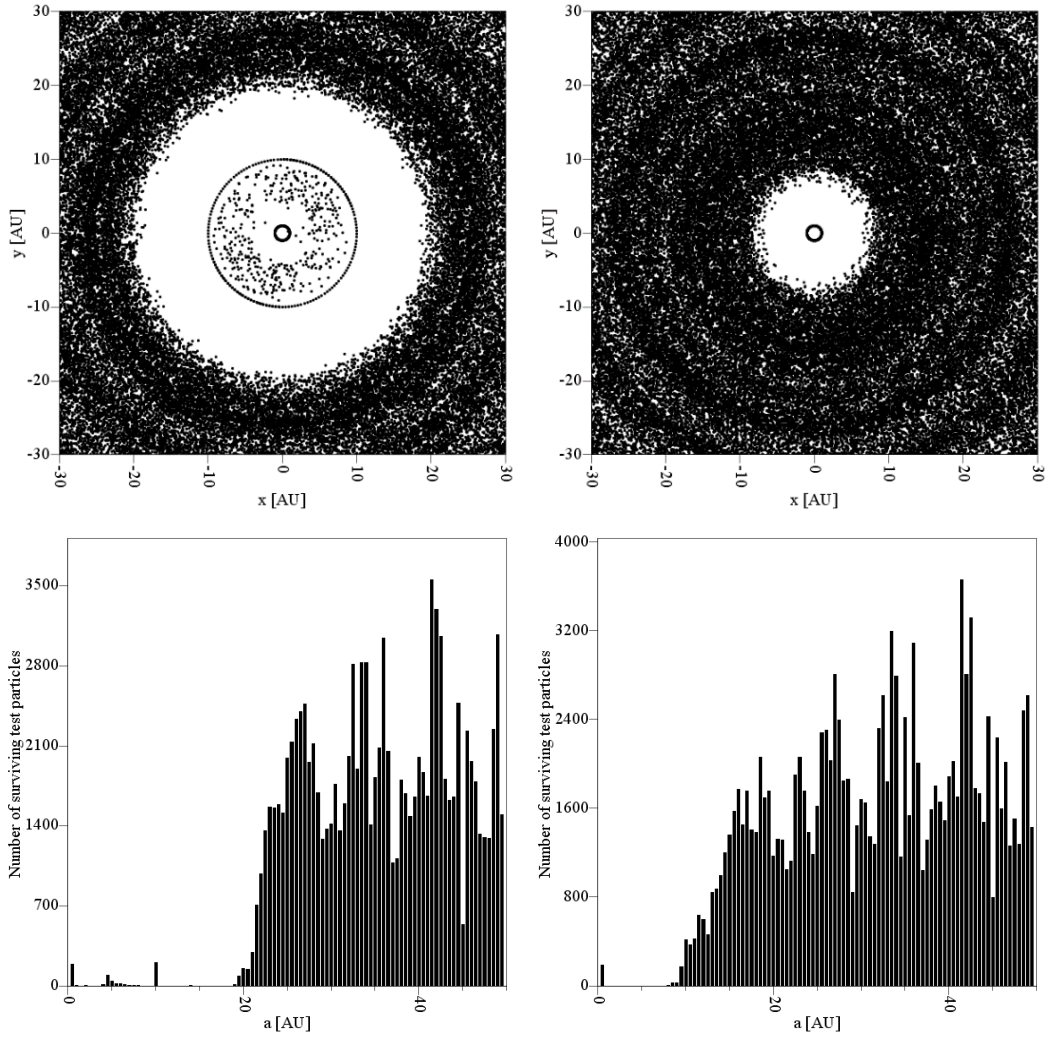

Figure 26. P1 and P2 orbits. a) prograde planetary orbits b) retrograde planetary orbits

In the prograde case the inner stable region is constrained between the orbit of the inner binary and that of the outer star, which also clears an outer region to about 20 AU. In the retrograde case the greater stability of these orbits allows this outer bound to shrink until it is almost coincident with the outer star's orbit. In this particular case a stable inner region does not exist.

Resonances

The varying density of the outer test particle cloud, which is also clearly reflected in the density histograms, may be attributed to n: 1 MMRs, which in this case lie at approximately 21, 25, 29, 33, 37, 40, 43 and 45 AU.

For mean motion resonances, the inner body's approximate nominal resonance location a_n, of the $(p+q)$: p resonance has a semi-major axis given by

$$a_n = \left(\frac{p}{p+q}\right)^{\frac{2}{3}} a' \tag{17}$$

where p and q are integers, q is the "order" of the resonance and a' is the perturber's semi-major axis, as given by equation 8.24 in Murray and Dermott (1999). For large n the n: 1 resonance is found at

$$a_n = n^{\frac{2}{3}} a' \tag{18}$$

Regressions

For P1 and P2 orbits, the respective inner and outer edges of the cleared area of the test particle cloud were standardised by taking them as ratios of the semi-major axis of the outer star, a_2. These standardised dependent variables a_{io}/a_2 and a_{oi}/a_2 are denoted the *critical* semi-major axis ratios delineating the bounds of the stable regions. They were then regressed against the parameters discussed in Section 4.1.2 using linear regression to extract semi-analytical relationships of the form

$$\frac{a_{io}}{a_2}, \frac{a_{oi}}{a_2} = f(a, \mu_1, \mu_2, e_1, e_2, i_2, \Omega_2, \omega_2)$$

Since the critical semimajor axis ratios scale with a, its regression coefficient is zero and the regression equations are the form

$$\frac{a_{io}}{a_2}, \frac{a_{oi}}{a_2} = C + a_1\mu_1 + a_2\mu_2 + a_3 e_1 + a_4 e_2 + a_5 i_2 + a_6\Omega_2 + a_7\omega_2 \tag{19}$$

Previous theoretical studies of the stable regions for S-type orbits and P-type orbits in binary and triple systems, summarised by e.g. Georgakarakos (2008) offer relationships in many different functional forms, some derived from theory and some empirically. Even the relatively simple empirical regression models provided by Holman and Wiegert (1999) use cross-terms up to quadratic order. However, 1) these cross terms have no obvious physical meaning, 2) the larger number of orbital parameters used in our analysis of triples compared with this binary case would lead to an unwieldy number of these terms, 3) in the regressions the univariate relationships between the dependent variables and these parameters turned out to be linear, with only one exception, and 4) a sample of (smaller) regression fits using cross terms was done and they provided no material improvement in fit.

Since our goal is to provide the simplest empirical formulation that is sufficiently descriptive, we limited the regressions to simple linear combinations of the configuration parameters. Of these terms, only those significant at the 95% level were retained.

Key output metrics

For all the triple configurations examined, two main metrics were extracted to indicate the regions of stability:

1. The mean critical semi-major axis ratio (MCSAR). The stable orbits remaining at the end of an integration have a distribution of semi-major axes. From this distribution one has a rough indication of the probability of a planet being in a stable orbit at any distance from its central star or stars. Unfortunately, these distributions are jagged because of resonances and cannot usefully be fitted with smooth functions. Our main metric was therefore the mean and range of this distribution. The mean represents an

average over all the combinations of variable values used in the variable space.

2. Using all these combinations of variables, we extracted regression equations in the form of equation (19), which provides a model for the most likely semi-major axis ratio for any specific set of variables. Our main metric here was the regression constant. This represents the most likely semi-major axis ratio for circular, coplanar orbits where both outer bodies are of negligible mass relative to the central body (and where the longitude of ascending node and argument of periapsis are zero).

These two measures will normally be different. Both were used as indicators of the stability boundary for planets.

4.1.5 Prograde outer star

A total of 10 756 integrations was run. An overview of the results for the inner and outer stability bounds for prograde and retrograde planetary orbits is shown in Figure 27 and Figure 28 respectively. Generally, most of the inner orbits lie well inside the orbit of the third star and all the outer orbits well outside it.

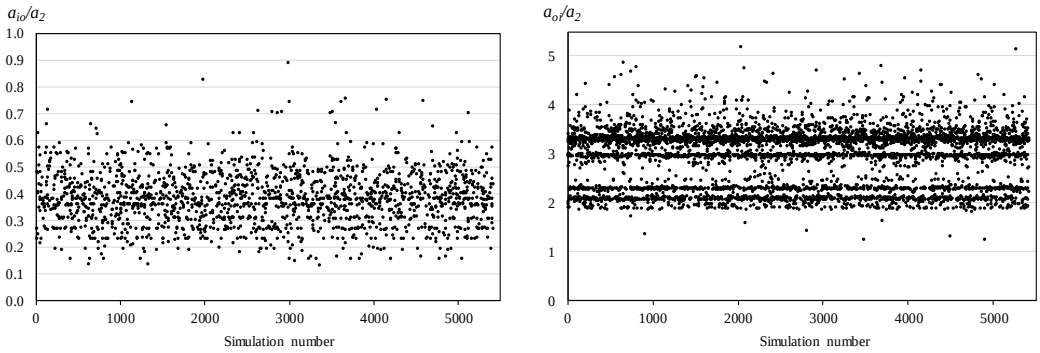

Figure 27. P1 and P2 orbits, prograde outer star, prograde planets. a) inner bounds b) outer bounds

For prograde planetary orbits, most of the inner bounds lie between 0.1 and 0.6 times the outer star's semi-major axis, averaging around 0.4 times, while the outer bounds range from a bit under 2 times to around 4 times, averaging approximately 3 times.

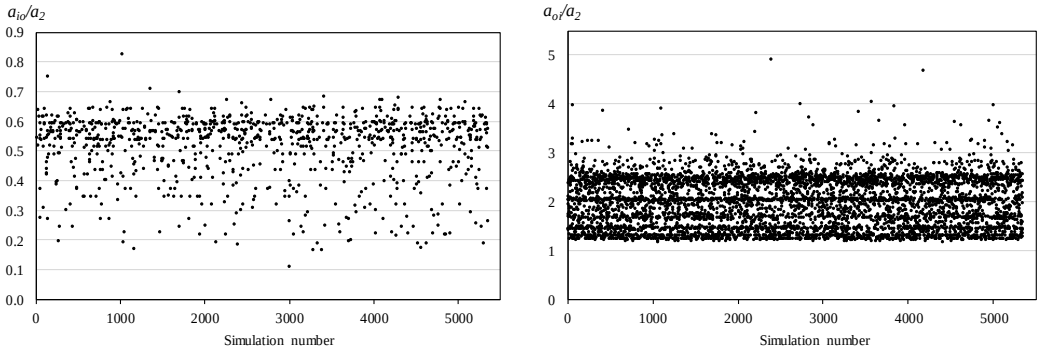

Figure 28. P1 and P2 orbits, prograde outer star, retrograde planets. a) inner bounds b) outer bounds

For retrograde planetary orbits, there is a clear migration of the orbital bounds towards the outer star. The semi-major axis of the inner bounds lies mostly between 0.1 and 0.8, averaging 0.5 times the outer star's semi-major axis, while the outer bounds lie mainly between 1 and 3 times this distance, averaging 2 times.

There are clear striations in the outer bounds, indicating variations of stability at different distances from the inner binary. This is particularly evident for prograde orbits, where, for example, a region of relative instability lies between 2.3 and 3.0. The fewer striations in the retrograde bounds is attributable to the fact that these orbits are generally more stable. There are some suggestions of striations in the inner region, but they are much weaker.

Others have also found striations of instability, especially for high eccentricities of the inner binary ($e_1 \geq 0.5$) and inclinations of the outer star of $i_2 \sim 0$ and $\pi/2$, and have hypothesized that these unstable regions are caused by orbital resonances between the test particles and the inner binary (Doolin & Blundell 2011).

The number of stable bounds found is shown in Table 11, where orbit type refers to planets.

Cases with well-defined orbit bounds							
Orbit type	Total simulations	a_{io}/a_2			a_{oi}/a_2		
		Bounds found (no.)	Success rate (%)	Distribution (%)	Bounds found (no.)	Success rate (%)	Distribution (%)
Prograde	5413	1782	33	65	5133	94.8	50
Retrograde	5343	976	18	35	5082	95.1	50
Total	10756	2758	26	100	10215	95.0	100

Table 11. P1 and P2 orbits, prograde outer star. Number of bounds found

Of the total of 10 756 integrations, outer bounds were found in 10 215 integrations or 95% of the cases, split evenly between prograde and retrograde cases.

Inner bounds were found in only 2 758 cases; a substantially smaller 26% of all integrations had inner stability bounds that were sufficiently well-defined to be measured. Of these, retrograde orbits accounted for only 35% – retrograde inner orbit bounds have particularly diffuse edges, which are difficult to determine.

The mean critical semi-major axis ratios and their ranges are shown in Table 12, where SD denotes standard deviation.

Orbit type	a_{io}/a_2				a_{oi}/a_2			
	Min	Avg	Max	SD	Min	Avg	Max	SD
Prograde planetary orbits	0.131	0.383	0.892	0.147	1.253	2.936	5.197	1.449
Retrograde planetary orbits	0.113	0.519	0.828	0.108	1.184	1.976	4.916	0.507
Difference (%)	-	35	-	-	-	-33	-	-

Table 12. P1 and P2 orbits, prograde outer star – mean critical semi-major axis ratios

There is a substantial difference in the stability bounds of prograde and retrograde orbits. For inner orbits the stability limit for retrograde orbits is 35% larger than

for prograde ones, while for outer orbits the stability limit for retrograde orbits is 33% smaller.

These mean critical semi-major axis ratios are *averages over all whole parameter space*. We next derived the regression equations for these ratios.

The signs of the coefficients in the regressions for the inner and outer bounds, a_{io}/a_2 and a_{oi}/a_2, are expected to be as shown in Table 13.

Coefficient	Inner orbits	Outer orbits
μ_1	+	+
μ_2	–	+
e_1	+	+
e_2	–	+
i_2	+	–
Ω_2	–	+
ω_2	–	+

Table 13. P1 and P2 orbits, prograde outer star – expected signs of regression coefficients

For the semi-major axis ratio a, if the outer star is further away from the binary, it should allow the inner stability bound to move outwards, implying a positive sign for this coefficient. This larger distance also reduces the influence of the inner binary on the outer bound, allowing it to be relatively closer to the outer star, here resulting in a negative coefficient (although the effect on the outer bound is likely to be minimal relative to that on the inner bound).

As the inner mass ratio μ_1 increases, the influence of the outer binary star becomes stronger, pushing the inner bound outwards, leading to a positive coefficient. The outer bound would feel the same effect, (although far less so), also giving its coefficient a positive sign.

A larger outer mass ratio μ_2 increases the influence of the outer star relative to the inner binary, which pushes the inner bound inwards and the outer bound outwards, which should result in negative and positive coefficients respectively.

As the eccentricity of the inner binary e_1 increases (with the semi-major axis constant) it will force the inner bound to move outward because of the effective increase in semi-minor axis, with a similar but far weaker effect on the outer bound, making both coefficients positive. However, the influence on the outer bound is expected to be so small that the sign is effectively indeterminate.

For the outer star a higher eccentricity e_2 results in a more elongated orbit. This results in it having a smaller perihelion distance from the centre of mass of the binary, leading to a contraction of the inner bound. As the outer star's orbit becomes more elongated it also clears an area that extends further out, pushing the outer bound outwards. Signs of the coefficients for inner and outer orbits should therefore be negative and positive respectively.

In our study of coplanar cases we change the inclination of the outer star by only small amounts, usually less than 30°. Higher-inclination configurations are discussed in Section 4.2. As the inclination of the outer star i_2 increases by a small

amount, its distance from both the inner and outer bounds increases compared with the coplanar case. Its diminished influence therefore allows the inner bound to extend further out and the outer bound to move further in, resulting in positive and negative coefficients, respectively, for these bounds. Inner and outer orbits that are inclined relative to each other should be more stable.

For inclined orbits, and an outer orbit that is noncircular, as the longitude of the ascending node Ω_2 increases from 0° to 90° it will push the outer bound outwards and the inner bound inwards – a similar effect to that of the outer star's eccentricity increasing and which results in the same signs.

Again, for a noncircular outer orbit, now not necessarily inclined, an increase in the argument of periapsis $\omega_2$will have the same effect and result in the same signs.

These coefficient signs apply to both prograde and retrograde stellar orbits.

We now performed the regressions on the inner and outer regions, for both prograde and retrograde planetary orbits. As expected, for retrograde orbits the outer stable region moves inwards compared with the prograde case, and the inner stable region moves outwards, i.e. both move closer to the outer star.

Note that while the critical semimajor axis ratio scales with a (except for very small separations) and its regression coefficient should be zero, it has nevertheless been included in all regressions as an additional indication of model error; it is of course excluded in the regression equations.

Outer region

Prograde planetary orbits

For the outer region the regression resulted in the following relationship, where the error terms are the average 95% confidence limits. Where coefficients are zero to three decimal places they are excluded.

$$a_{oi}/a_2 = (2.377 \pm 0.024) + (-0.003 \pm 0.000)a + (0.053 \pm 0.036)\mu_1 + (0.044 \pm 0.007)\mu_2 + (0.090 \pm 0.026)e_1 + (1.997 \pm 0.013)e_2 + (-0.002 \pm 0.000)\Omega_2 + (-0.002 \pm 0.000)\omega_2 \quad (20)$$

A typical partial regression plot, here of a_{oi}/a_2 against eccentricity e_2, is shown in Figure 29. A linear fit appears appropriate in this case.

Data on the above regression coefficients are listed in Table 14. In this and subsequent tables of regression results, the various parameters are defined as follows: σ-standard deviation; R^2-coefficient of determination, F- F statistic for overall significance, SE-standard error and MAPE-mean average percentage error, all being for the overall regression fit; t-t statistic for individual coefficients, N-number of points.

The model shows that for a dominant central star and coplanar, circular orbits the outer stability bound would be found at around 2.4 times the semi-major axis of the outer star.

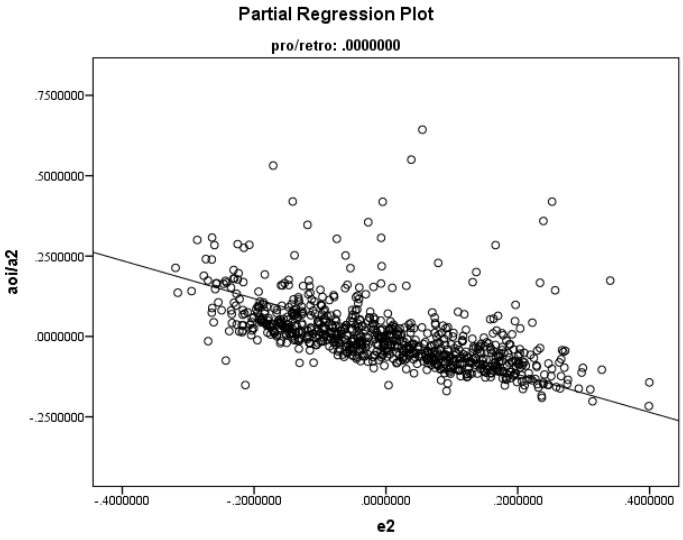

Figure 29. Regression plot of outer critical semi-major axis ratio against outer star eccentricity

Model	Unstandardized Coefficients		Standardised Coefficients	*t*	Sig.	95% Confidence	
	B	Std. Error	Beta			Lower Bound	Upper Bound
C	2.377	.012		194.6	0.000	2.353	2.401
a	-0.003	.000	-.143	-23.8	0.000	-0.003	-0.002
μ_1	0.053	.018	.017	2.9	0.004	0.017	0.089
μ_2	0.044	.004	.067	11.5	0.000	0.036	0.051
e_1	0.090	.013	.040	6.8	0.000	0.064	0.115
e_2	1.997	.013	.883	151.8	0.000	1.972	2.023
i_2	0.000	.000	.018	3.1	0.002	0.000	0.001
Ω_2	-0.002	.000	-.111	-15.9	0.000	-0.002	-0.002
ω_2	-0.002	.000	-.093	-13.4	0.000	-0.002	-0.002

Table 14. P1 and P2 orbits, prograde outer star. Regression coefficients – outer region, prograde planetary orbits

The only parameter that has a major influence on this distance is the eccentricity of the outer star's orbit. For very high eccentricities it could push this bound out as far as almost 4.4 times the semi-major axis of the outer star.

The outer bound's dependence on the remaining orbital parameters is very weak for the two mass ratios and the inner binary's eccentricity e_2 and is effectively zero for the remaining parameters. The configuration of the inner binary and the inclination of the outer star has no material effect on the outer bound.

The regression equation has an R^2 of 0.828, the F-statistic was 3 080 and the standard error of the regression was 0.239. The model has a low mean absolute percentage error (MAPE) of 6%.

Retrograde planetary orbits

The best fit to the data is given by

$$a_{oi}/a_2 = (1.483 \pm 0.019) + (0.131 \pm 0.028)\mu_1 + (-0.008 \pm 0.006)\mu_2 + (-0.036 \pm 0.020)e_1 + (1.725 \pm 0.020)e_2 + (0.002 \pm 0.000)i_2 + (0.001 \pm 0.000)\Omega_2 + (0.001 \pm 0.000)\omega_2 \quad (21)$$

The constant term is 38% smaller than that for the prograde case, confirming that retrograde orbits are substantially more stable than prograde ones. Data on the regression coefficients is listed in Table 15.

Model	Unstandardized Coefficients		Standardised Coefficients	*t*	Sig.	95% Confidence	
	B	Std. Error	Beta			Lower Bound	Upper Bound
C	1.483	.010		153.4	0.000	1.465	1.502
a	-0.004	.000	-.220	-40.4	0.000	-0.004	-0.003
μ_1	0.131	.014	.048	9.1	0.000	0.103	0.159
μ_2	-0.008	.003	-.015	-2.8	0.005	-0.014	-0.003
e_1	-0.036	.010	-.018	-3.5	0.000	-0.057	-0.016
e_2	1.725	.010	.876	166.1	0.000	1.705	1.745
i_2	0.002	.000	.103	19.6	0.000	0.002	0.002
Ω_2	0.001	.000	.054	8.5	0.000	0.001	0.001
ω_2	0.001	.000	.032	5.1	0.000	0.000	0.001

Table 15. P1 and P2 orbits, prograde outer star. Regression coefficients – outer region, retrograde planetary orbits

The coefficient of the eccentricity of the outer star is larger than the constant; an orbit with an eccentricity approaching one would add 1.7 to the critical semi-major axis of the outer bound, more than doubling it. This factor's influence is thus much stronger than in the case of a prograde planet. The inner mass ratio's influence is larger than for the prograde case, but it remains small, and the significance of the remaining variables is again minimal.

The regression equation has a slightly better fit than the prograde case, with an R^2 of 0.860, a F-statistic of 3 880 and a standard regression error of 0.190. The model's MAPE was again 6%.

Inner region

Prograde planetary orbits

The regression equation was as follows:

$$a_{io}/a_2 = (0.439 \pm 0.018) + (-0.005 \pm 0.025)\mu_1 + (-0.020 \pm 0.005)\mu_2 + (-0.004 \pm 0.018)e_1 + (-0.114 \pm 0.025)e_2 + (-0.001 \pm 0.000)\Omega_2 + (-0.001 \pm 0.000)\omega_2 \quad (22)$$

Data on the regression coefficients is listed in Table 16.

Model	Unstandardized Coefficients		Standardised Coefficients	*t*	Sig.	95% Confidence	
	B	Std. Error	Beta			Lower Bound	Upper Bound
C	0.439	.009		47.8	0.000	0.421	0.457
a	0.000	.000	.009	0.4	0.692	0.000	0.000
μ_1	-0.005	.013	-.009	-0.4	0.694	-0.029	0.020
μ_2	-0.020	.003	-.160	-7.1	0.000	-0.025	-0.014
e_1	-0.004	.009	-.011	-0.5	0.633	-0.022	0.013
e_2	-0.114	.013	-.213	-8.9	0.000	-0.139	-0.089
i_2	0.000	.000	.049	2.2	0.027	0.000	0.000
Ω_2	-0.001	.000	-.172	-6.1	0.000	-0.001	0.000
ω_2	-0.001	.000	-.174	-6.3	0.000	-0.001	0.000

Table 16. P1 and P2 orbits, prograde outer star. Regression coefficients – inner region, prograde planetary orbits

The constant indicates that the inner stability bound for a circular, coplanar triple should have a critical ratio of roughly 0.44. The largest influence on this bound is again the eccentricity of the outer star rather than the inner binary, but relative to the constant term its influence is three times weaker than for the outer stability bounds.

The sign of some of the coefficients are not as expected. However, in many of these cases, particularly for inner orbits, the errors in the coefficients are larger than the coefficients themselves. This has therefore been ignored.

This regression equation has an R^2 of only 0.132, the F-statistic was 34 and the standard error of the regression was 0.093. The model has a higher mean absolute percentage error (MAPE) of 19%. This again reflects the more indistinct nature of the inner bound's edge compared with that of the outer stability bound.

Retrograde planetary orbits

The best-fit equation for the critical ratio of this stability bound is

$$a_{io}/a_2 = (0.573 \pm 0.015) + (0.009 \pm 0.021)\mu_1 + (-0.043 \pm 0.004)\mu_2 + (-0.010 \pm 0.015)e_1 + (-0.469 \pm 0.029)e_2 \quad (23)$$

Data on the regression coefficients is listed in Table 17.

The constant is similar to that for the prograde case and the coefficient of the eccentricity of the outer star, while still small relative to the outer region cases, is three times larger than it was for the prograde case. The remaining variables are insignificant.

The regression's R^2 of 0.671, F-statistic of 246, standard error of 0.062 and MAPE of 10% are better than for the prograde case. The inner retrograde stability limits have better-defined edges than the prograde limits.

Model	Unstandardized Coefficients		Standardised Coefficients	*t*	Sig.	95% Confidence	
	B	Std. Error	Beta			Lower Bound	Upper Bound
C	0.573	.007		76.4	0.000	0.558	0.588
a	0.000	.000	.102	4.8	0.000	0.000	0.001
μ_1	0.009	.011	.016	0.8	0.398	-0.012	0.030
μ_2	-0.043	.002	-.386	-19.2	0.000	-0.047	-0.038
e_1	-0.010	.007	-.026	-1.4	0.166	-0.025	0.004
e_2	-0.469	.015	-.631	-31.8	0.000	-0.498	-0.440
i_2	0.000	.000	-.052	-2.8	0.005	0.000	0.000
Ω_2	0.000	.000	.022	1.0	0.324	0.000	0.000
ω_2	0.000	.000	.028	1.3	0.195	0.000	0.000

Table 17. P1 and P2 orbits, prograde outer star. Regression coefficients – inner region, retrograde planetary orbits

Summary – prograde outer star

For triple configurations with circular, coplanar outer stellar orbits, the inner (P1) and outer (P2) stability boundaries for prograde planetary orbits are found at around 0.4 times and 2.4 times the distance of the outer star respectively, and for retrograde planetary orbits at around 0.6 times and 1.5 times this distance respectively.

The configuration of the inner binary has little influence on either inner or outer orbits. This results from the fact that, as a consequence of the Mardling stability limit, the outer star is sufficiently far away that the inner binary effectively resembles a single point mass.

The outer star dominates the regions of stability in a triple system, with its eccentricity having by far the largest influence.

These conclusions hold for both prograde and retrograde planetary orbits. However, the greater stability of retrograde orbits results in outer bounds that are closer to the outer star and inner bounds that are further from the binary, compared with the prograde case.

The difference in these bounds can be significant, as shown in Table 18, which uses the regression equations to calculate the sensitivity of the critical semi-major axis ratio to the outer star's eccentricity, for prograde and retrograde planetary orbits.

For circular orbits of the outer star the absolute difference in critical ratio for prograde and retrograde orbits is 31%-38% while for highly eccentric stellar orbits it is 27%-68%.

For highly eccentric orbits of the outer star, the semi-major axis of the outer bound can expand 84% further out for prograde orbits and more than double (116%) for retrograde orbits, while the inner bound reduces by 26% for prograde planetary orbits and can contract by as much as 82% for retrograde planetary orbits.

Bound	a_{io}/a_2			a_{oi}/a_2		
e_2	0	1	Δ (%)	0	1	Δ (%)
Prograde	0.44	0.33	-26	2.38	4.37	84
Retrograde	0.57	0.10	-82	1.48	3.21	116
Δ (%)	31%	-68%	-	-38%	-27%	-

Table 18. P1 and P2 orbits, prograde outer star. Critical semi-major axis ratio versus direction of planetary motion and outer star eccentricity

The accuracy of the relationships derived to determine these bounds is good for the outer bound (~6%) but less so for the inner bound (~14%).

4.1.6 Retrograde outer star

To investigate this case, a set of 4 807 integrations was run. The parameter space used is shown in Table 9, with the range of i_2 changing from 0° – 60° to 120° – 180° and the semi-major axis ratio a_m now calculated from equation (9).

The test particle cloud was again an initially uniformly distributed circular disc of zero eccentricity, with its outer limit extending to the 5th MMR as previously described.

The results for prograde and retrograde planetary orbits are shown in Figure 30 and Figure 31 respectively. The inner orbits are quite sharply defined at their lower limit for prograde orbits and at their outer limit for retrograde orbits, with only a few outliers beyond these, while outer orbits display a sharp edge only for retrograde orbits.

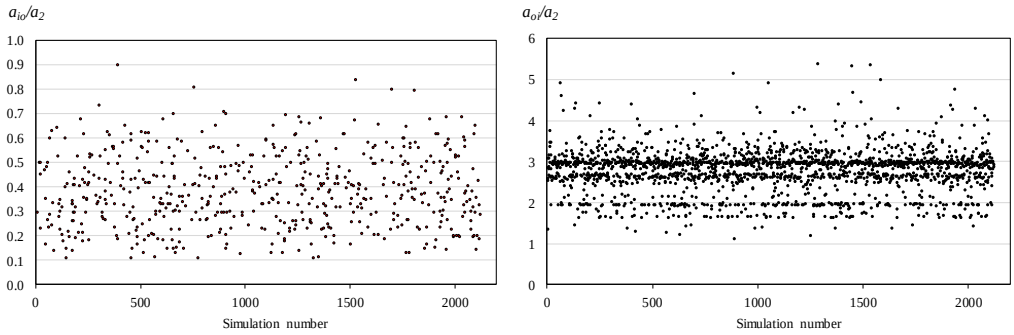

Figure 30. P1 and P2 orbits, retrograde outer star, prograde planets. a) inner bounds b) outer bounds

The prograde inner bounds are uniformly distributed and the critical ratio lies between 0.1 and a more diffuse limit around 0.7, averaging close to 0.4. The prograde outer critical ratio generally ranges from around 1.5 to around 3.5, averaging 2.7. The striations in the pattern again indicate resonances – for example, there is a region of relative instability between 2.0 and 2.6.

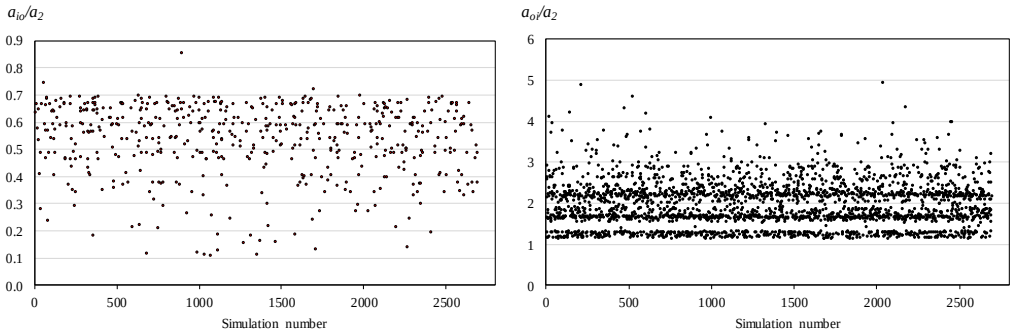

Figure 31. P1 and P2 orbits, retrograde outer star, retrograde planets. a) inner bounds b) outer bounds

For retrograde inner orbits the inner critical ratio is diffuse, but the outer limit is well-defined at around 0.7. For retrograde outer orbits the inner critical ratio lies at about 1.1, with a diffuse outer bound from about 3. A region of strong instability is visible between 1.3 and 1.5, with a second one between 1.7 and 2.1.

The number of bounds found is shown in Table 19.

Cases with well-defined orbit bounds							
Planet orbit type	Total simulations	a_{io}/a_2			a_{oi}/a_2		
		Bounds found (no.)	Success rate (%)	Distribution (%)	Bounds found (no.)	Success rate (%)	Distribution (%)
Prograde	2122	569	27	51	1895	89.3	44
Retrograde	2685	539	20	49	2455	91.4	56
Total	4807	1108	23	100	4350	90.5	100

Table 19. P1 and P2 orbits, retrograde outer star. Number of bounds found

Compared with the case of a prograde outer star, slightly fewer outer orbits were found and they were no longer evenly split between prograde and retrograde planetary orbits. Of the total of 4 807 integrations, outer orbit bounds were found in 4 350 integrations or 91% of cases compared with 95% previously, with a small preponderance of retrograde cases, as before.

Inner orbit bounds were found in only 1 108 or 23% of these cases, compared with 26% previously. Prograde and retrograde planetary orbits accounted for 27% and 20% of these respectively, compared to 33% and 18% previously, probably indicating less stability when the motions of the planets and outer star are in the same direction.

Orbit type	a_{io}/a_2				a_{oi}/a_2			
	Min	Avg	Max	SD	Min	Avg	Max	SD
Prograde planetary orbits	0.110	0.385	0.897	0.077	0.924	2.773	5.384	0.891
Retrograde planetary orbits	0.112	0.537	0.857	0.132	0.591	1.960	4.957	0.571
Difference (%)	-	39	-	-	-	-29	-	-

Table 20. P1 and P2 orbits, retrograde outer star. Mean critical semi-major axis ratios

The mean semi-major axis ratios and their ranges are shown in Table 20.

There are once again substantial differences in the critical ratio for prograde and retrograde planetary orbits, averaging 34% in absolute terms, with the differences for inner and outer orbits being quite similar to those found for the prograde stellar case.

Differences in critical ratios for prograde and retrograde stellar orbits

The mean semi-major axis ratios for prograde and retrograde outer stars are compared in Table 21.

Stability bound averages						
Orbit type	a_{io}/a_2			a_{oi}/a_2		
Stellar orbit:	Prograde	Retrograde	Δ%	Prograde	Retrograde	Δ%
Prograde planetary orbit	0.383	0.385	1	2.936	2.773	-6*
Retrograde planetary orbit	0.519	0.537	3*	1.976	1.960	-1
Δ%	35	39		-33	-29	

* significant at the 5% level

Table 21. P1 and P2 orbits. Difference in mean critical semi-major axis ratios for prograde and retrograde stellar orbits

It is worth briefly comparing the differences in our results for prograde and retrograde systems with other studies related to planetary stability.

Looking at an example of a single stellar case, in an analysis of the orbital stability of systems of closely-spaced planets, Smith and Lissauer (2009) set up stylised planetary systems of five planets in which every planet orbits in the opposite direction to its nearest neighbours. The resulting systems were dramatically more stable than an identical system of prograde planets, albeit with more scatter in the results. The five-planet retrograde systems could be packed more than twice as closely together as prograde systems. The data in their Table 3 shows that the outermost retrograde planets orbited 27% closer to the star, which is comparable to the 35% – 39% above.

More pertinently to our stellar configuration, Quarles and Lissauer (2016) examined the long-term stability of planets in the binary α Centauri AB system (i.e. ignoring Proxima Centauri). For P1 circumbinary orbits their data (Fig. 8) shows that retrograde test particles were stable 38% closer to the central star, identical to our result.

The difference that the orbital direction of the outer star makes, for both prograde and retrograde planetary orbits, is small but not insignificant. The differences, of a few percent, are statistically meaningful for inner retrograde planetary orbits and outer prograde planetary orbits.

For the case where the outer star moves in a retrograde orbit, compared with the case with the star moves in a prograde orbit, one would expect that:

1. For outer planetary orbits, those that are prograde would move inwards, towards the outer star and retrograde ones would move outwards, away from it. This occurred for prograde planets, which moved in by a statistically

significant 6%; the 1% that retrograde planets also moved in by was not statistically meaningful.

2. For inner planetary orbits, prograde ones would move outwards, towards the outer star and retrograde ones would move inwards, away from it. The prograde bounds did this, moving out by a statistically insignificant 1%, but the retrograde bounds moved in the wrong direction, by a statistically meaningful 3%. More investigation is required.

Outer region

Prograde planetary orbits

The regression equation is

$$a_{oi}/a_2 = (2.089 \pm 0.092) + (0.809 \pm 0.116)\mu_1 + (0.114 \pm 0.011)\mu_2 + (0.015 \pm 0.025)e_1 + (1.298 \pm 0.060)e_2 + (-0.001 \pm 0.000)i_2 \quad (24)$$

Again, where coefficients are zero to three decimal places they are excluded. Data on the regression coefficients is detailed in Table 22.

Model	Unstandardized Coefficients		Standardised Coefficients	*t*	Sig.	95% Confidence	
	B	Std. Error	Beta			Lower Bound	Upper Bound
C	2.089	.047		44.5	.000	1.997	2.181
a	-.004	.000	-.278	-17.5	.000	-.004	-.004
μ_1	.809	.059	.229	13.7	.000	.693	.925
μ_2	.114	.011	.172	10.8	.000	.093	.134
e_1	.015	.025	.010	0.6	.551	-.034	.064
e_2	1.298	.030	.668	42.7	.000	1.238	1.358
i_2	-.001	.000	-.058	-3.6	.000	-.001	.000
Ω_2	.000	.000	.031	2.0	.049	.000	.001
ω_2	.000	.000	.001	0.1	.930	.000	.000

Table 22. P1 and P2 orbits, retrograde outer star. Regression coefficients – outer region, prograde orbits

The constant is 12% smaller than in the case where the outer star is prograde. The major change is that the dependence on both mass ratios has increased, by an order of magnitude for the inner ratio and by 2.6 times for the outer ratio. The influence of the inner binary's eccentricity remains negligible while that of the outer star is again dominant, although less so than for the case where this star is prograde. The inclination of the outer star (over the limited range used in this case) again has no effect on the planetary stability bounds.

The most significant feature of the retrograde stellar case is therefore that, in addition to the outer eccentricity, the inner mass ratio is a significant determinant of the critical semimajor axis ratio.

The fit was poorer than for the prograde stellar case. The regression equation has an R^2 of 0.271, the F-statistic was 26 and the standard error of the regression was 0.126. The model has a high mean absolute percentage error (MAPE) of 31%.

Retrograde planetary orbits

The best fit to the data was given by

$$a_{oi}/a_2 = (1.708 \pm 0.070) + (0.182 \pm 0.083)\mu_1 + (0.023 \pm 0.014)\mu_2 + (0.018 \pm 0.035)e_1 + (1.693 \pm 0.041)e_2 + (-0.001 \pm 0.000)i_2 \quad (25)$$

Here the constant term is 15% larger than for a prograde outer star. The coefficients for the two mass ratios have also risen but remain small – the increased influence of the inner mass ratio seen for prograde planetary orbits does not hold for retrograde planetary orbits. The coefficient of the eccentricity of the outer star is slightly smaller but remains comparable in magnitude to the constant. Data on the regression coefficients is listed in Table 23.

Model	Unstandardized Coefficients		Standardised Coefficients	*t*	Sig.	95% Confidence	
	B	Std. Error	Beta			Lower Bound	Upper Bound
C	1.708	.036		47.6	.000	1.638	1.778
a	-.006	.000	-.320	-32.7	.000	-.006	-.005
μ_1	.182	.042	.045	4.3	.000	.100	.265
μ_2	.023	.007	.032	3.2	.001	.009	.037
e_1	.018	.018	.010	1.0	.325	-.018	.053
e_2	1.693	.021	.795	80.4	.000	1.652	1.734
i_2	-.001	.000	-.068	-7.0	.000	-.001	-.001
Ω_2	.000	.000	.012	1.2	.212	.000	.000
ω_2	.000	.000	.011	1.1	.264	.000	.000

Table 23. P1 and P2 orbits, retrograde outer star. Regression coefficients – outer region, retrograde orbits

The regression equation has a much better fit than for the prograde case, with an R^2 of 0.773, a F-statistic of 1 039 and a standard regression error of 0.269. The model's MAPE is also much better, at 8%.

Inner region

Prograde planetary orbits

The model was as follows:

$$a_{io}/a_2 = (0.463 \pm 0.058) + (0.190 \pm 0.071)\mu_1 + (-0.037 \pm 0.013)\mu_2 + (-0.021 \pm 0.031)e_1 + (-0.187 \pm 0.053)e_2 + (-0.001 \pm 0.000)i_2 \quad (26)$$

Data on the regression coefficients is listed in Table 24.

Model	Unstandardized Coefficients		Standardised Coefficients	*t*	Sig.	95% Confidence	
	B	Std. Error	Beta			Lower Bound	Upper Bound
C	.463	.030		15.6	.000	.405	.521
a	.000	.000	.066	1.8	.073	.000	.001
μ_1	.190	.036	.203	5.3	.000	.120	.261
μ_2	-.037	.006	-.212	-5.8	.000	-.050	-.024
e_1	-.021	.016	-.049	-1.3	.191	-.052	.010
e_2	-.187	.027	-.262	-7.0	.000	-.240	-.134
i_2	-.001	.000	-.187	-4.9	.000	-.001	.000
Ω_2	.000	.000	-.066	-1.8	.073	.000	.000
ω_2	.000	.000	-.051	-1.4	.171	.000	.000

Table 24. P1 and P2 orbits, retrograde outer star. Regression coefficients – inner region, prograde orbits

Compared with the prograde stellar case the constant is larger, as expected, albeit marginally. For the mass ratios, the coefficient of the inner one has increased by nearly forty times, and that for the outer one by less than twice. The coefficient for the eccentricity of the outer star is materially larger than for a prograde outer star.

The key difference is that the influence of the inner mass ratio has become significant and comparable to that of the outer eccentricity.

This regression equation has an R^2 of 0.547, the F-statistic was 285 and the standard error of the regression was 0.358. The model has a mean absolute percentage error (MAPE) of 9%.

Retrograde planetary orbits

The best-fit equation for the critical ratio of this stability bound is

$$a_{io}/a_2 = (0.656 \pm 0.041) + (-0.056 \pm 0.044)\mu_1 + (-0.022 \pm 0.01)\mu_2 + (0.005 \pm 0.020)e_1 + (-0.510 \pm 0.029)e_2 \quad (27)$$

Data on the regression coefficients is listed in Table 25.

Compared with the prograde stellar case the constant has increased as expected, but the other coefficients are largely unchanged, with only that for the inner mass ratio increasing appreciably. However, it remains an uninfluential determinant of the critical semimajor axis ratio.

The regression's R^2 of 0.710, F-statistic of 162, standard error of 0.071 and MAPE of 12% are similar to the prograde case.

Model	Unstandardized Coefficients		Standardised Coefficients	*t*	Sig.	95% Confidence	
	B	Std. Error	Beta			Lower Bound	Upper Bound
C	.656	.021		31.6	.000	.615	.697
a	.000	.000	-.033	-1.4	.172	.000	.000
μ_1	-.056	.022	-.065	-2.5	.012	-.100	-.012
μ_2	-.022	.005	-.108	-4.4	.000	-.032	-.012
e_1	.005	.010	.011	0.5	.640	-.016	.025
e_2	-.510	.015	-.882	-34.1	.000	-.539	-.480
i_2	.000	.000	.032	1.3	.184	.000	.000
Ω_2	.000	.000	-.057	-2.4	.015	.000	.000
ω_2	.000	.000	-.009	-0.4	.708	.000	.000

Table 25. P1 and P2 orbits, retrograde outer star. Regression coefficients – inner region, retrograde orbits

Comparisons

The mean critical semi-major axis ratio data for inner and outer orbits, for the previous eight combinations of orbital motion, are shown in Table 26. These are the *average* ratios found over all the combinations used in the parameter space.

Orbit type	Critical ratio	Motions[1] Star 3	Planet	Mean critical semi-major axis ratio Min	**Mean**	σ	Max
P1	a_{io}/a_2	P	P	0.131	**0.383**	0.147	0.892
			R	0.113	**0.519**	0.108	0.828
		R	P	0.110	**0.385**	0.077	0.897
			R	0.112	**0.537**	0.132	0.857
P2	a_{oi}/a_2	P	P	1.253	**2.936**	1.449	5.197
			R	1.184	**1.976**	0.507	4.916
		R	P	0.924	**2.773**	0.891	5.384
			R	0.591	**1.960**	0.571	4.957

1. P - prograde, R - retrograde

Table 26. P1 and P2 orbits. Mean critical semi-major axis ratios for various combinations of orbital motions

For P1 planetary orbits the mean critical ratio is materially (36%) different for prograde and retrograde planetary orbits, being 0.383 and 0.519 respectively. Both these ratios are slightly (~2%) larger for retrograde stellar orbits.

For P2 orbits the mean critical ratio is similarly (-33%) different for prograde and retrograde planetary motions, being 2.94 and 1.98 respectively. For retrograde stellar orbits these ratios are slightly (~3%) smaller.

Summary graphs of the corresponding regressions are presented in Figure 32.

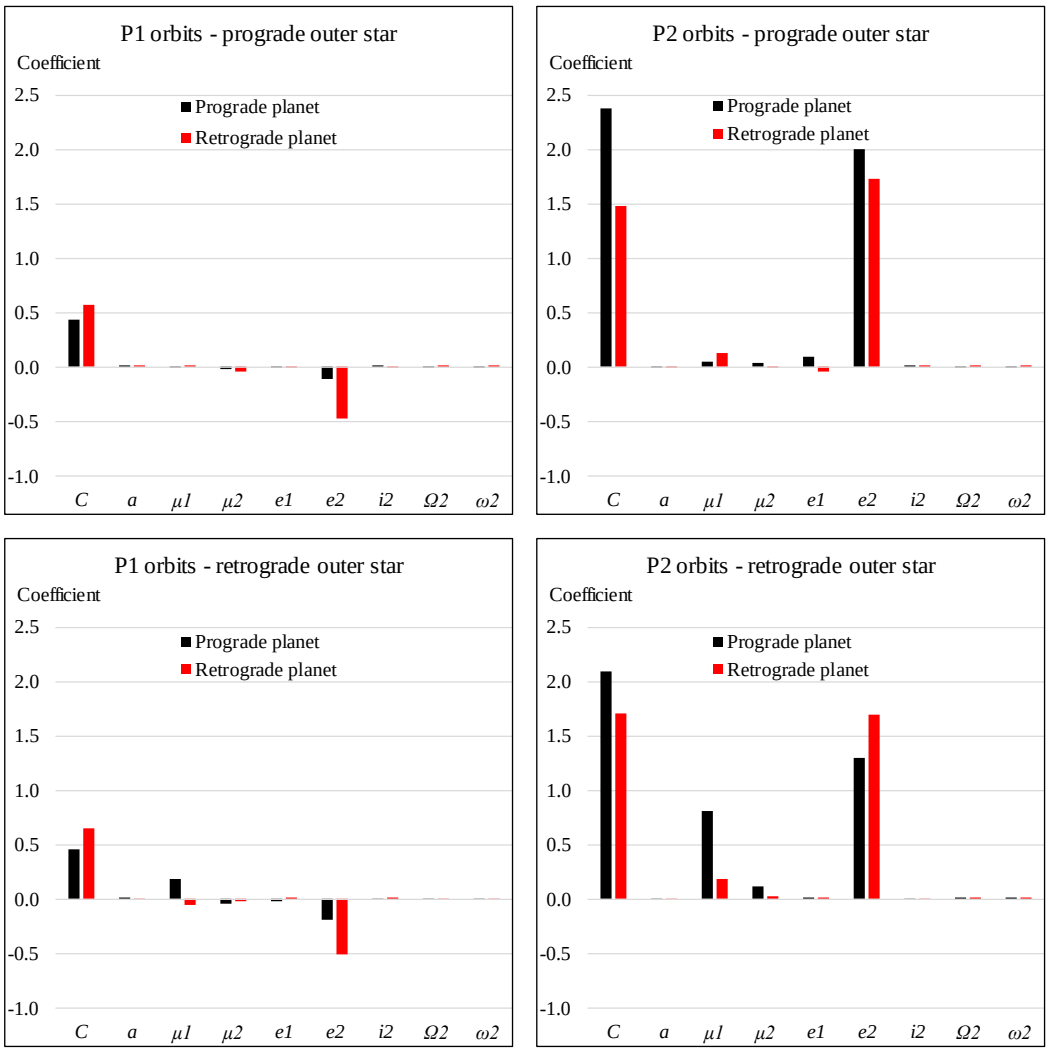

Figure 32. P1 and P2 orbits. Regression coefficients for various combinations of orbital motions. Upper panel a) prograde outer star, lower panel b) retrograde outer star

For P1 orbits the dominant influence on the critical ratio is only the outer star's eccentricity, particularly for retrograde planetary orbits. For P2 orbits this effect is even stronger, for both planetary motions. In the case of a retrograde outer star these influences are largely unchanged for P1 orbits, but for P2 orbits the inner mass ratio becomes important for a prograde planet.

The differences between the regression coefficients for prograde and retrograde stellar orbits are summarised in Table 27. Where the signs of coefficients are different for very weak terms, this is ignored.

In summary, a retrograde outer star results in a greater influence from the two mass ratios, particularly the inner one, with this effect being greater for prograde planetary orbits than for retrograde ones. The effect of the inner binary's eccentricity remains insignificant. The effect of the outer star's eccentricity remains large but is lower for outer bounds (for both prograde and retrograde planetary orbits) but is largely unchanged for inner bounds, for both these planetary motions.

		Outer bounds			Inner bounds		
		Coefficient		Ratio	Coefficient		Ratio
		Prograde stellar orbit	Retrograde stellar orbit	(abs.)	Prograde stellar orbit	Retrograde stellar orbit	(abs.)
C	Prograde planetary orbits	**2.377**	**2.089**	0.88	**0.439**	**0.463**	1.06
a		-0.003	-0.004	-	0.000	0.000	9.75
μ_1		0.053	0.809	15.16	-0.005	0.190	38.68
μ_2		0.044	0.114	2.61	-0.020	-0.037	1.86
e_1		0.090	0.015	0.17	-0.004	-0.021	4.79
e_2		1.997	1.298	0.65	-0.114	-0.187	1.65
C	Retrograde planetary orbits	**1.483**	**1.708**	1.15	**0.573**	**0.656**	1.15
a		-0.004	-0.006	1.58	0.000	0.000	0.47
μ_1		0.131	0.182	1.39	0.009	-0.056	6.22
μ_2		-0.008	0.023	2.75	-0.043	-0.022	0.51
e_1		-0.036	0.018	0.49	-0.010	0.005	0.47
e_2		1.725	1.693	0.98	-0.469	-0.510	1.09

Table 27. P1 and P2 orbits. Differences in regression coefficients for prograde and retrograde motions of the outer star

The directional movements of the stability bounds for planetary orbits are as expected for three of the four cases. However, for retrograde inner planetary orbits the bound increases instead of shrinking. This may be attributable to the small sample, since very few retrograde star/retrograde planet combinations were stable.

Relationship between stability bounds and the outer star's eccentricity

Since the eccentricity of the outer star is by far the most influential variable on both the inner and outer planetary stability bounds, a series of integrations was run to examine the relationship between these two variables.

Outer bounds

The relationship between the two variables is shown in Figure 33, where the values of the other variables were: $a = 100$ AU, $\mu_1 = \mu_2 = 0.5$, $e_1 = i_1 = \Omega_2 = \omega_2 = 0$ and $i_2 = 0°$ and $180°$.

For the outer bound the critical ratio should be an increasing function of outer eccentricity e_2. This is true for all four cases shown, although for the two retrograde planet cases the critical ratio flattens out from e_2~0.6. There are discontinuities in the critical ratio in each case. This is most visible in the prograde star/prograde planet case, with gaps occurring at eccentricities of 0.10, where the critical ratio jumps from 2.37 to 2.70; and at 0.39, with the ratio undergoing a step change from 2.82 to 3.05. These instabilities are less pronounced in the two retrograde planet cases.

A retrograde outer body allows the outer bound to move substantially closer to it, with a critical ratio at $e_2 = 0$ of 1.3, compared with 2.1 for a prograde outer star. However, this difference diminishes with increasing outer eccentricity, with both critical ratios converging towards 3.2 as this eccentricity approaches unity.

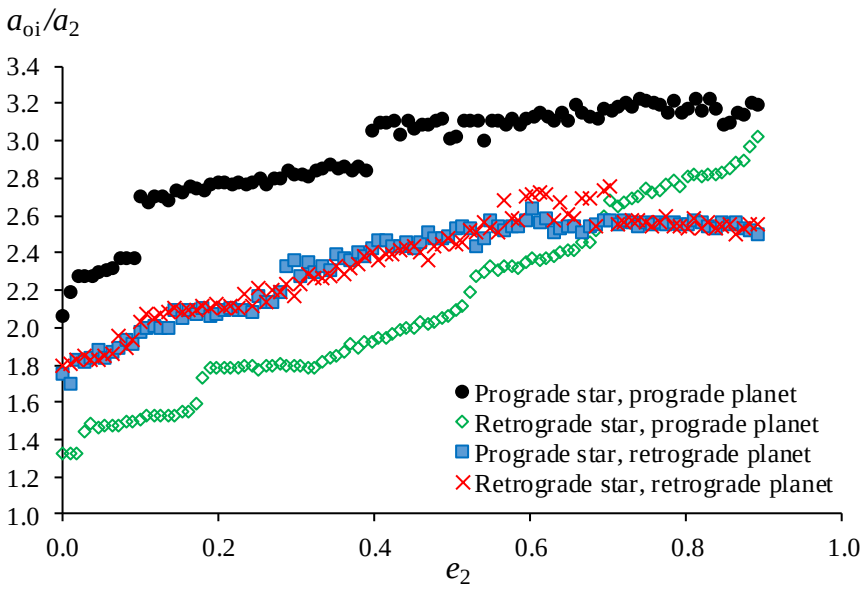

Figure 33. P2 orbits. Outer stability bound as a function of outer star eccentricity

Inner bounds

The original series of integrations did not result in sufficient data points because of the small number of inner bounds that are defined well enough for their edges to be established. Fewer bounds are found when

1. stellar and planetary orbits are in the same direction, i.e. both are prograde or both are retrograde, as these are less stable situations, and
2. stellar eccentricity increases.

Running more integrations resulted in Figure 34.

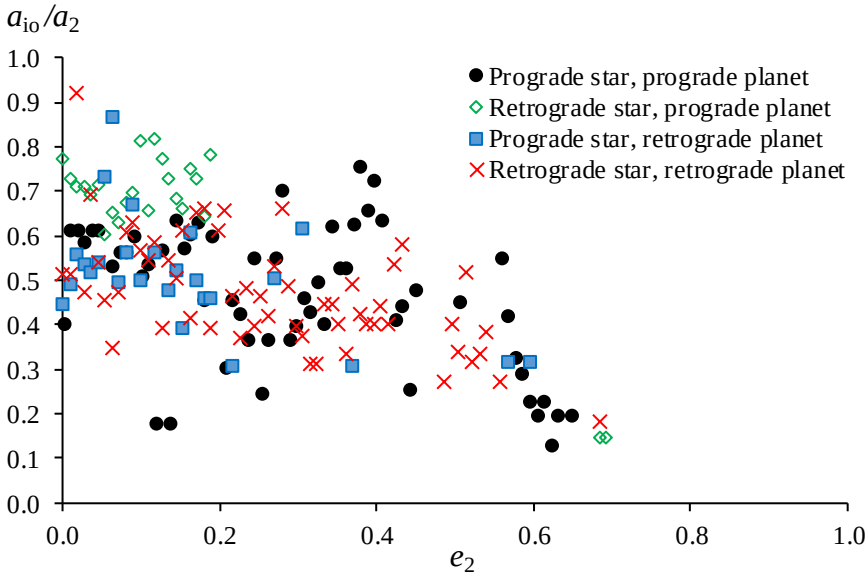

Figure 34. P1 orbits. Inner stability bound as a function of outer star eccentricity

For the inner bound the critical ratio is expected to be a decreasing function of outer eccentricity. This was the general trend in each case, albeit with the high

scatter that reflects the diffuse nature of inner orbit bounds, which in turn results from the greater sparsity of surviving test particles compared with outer orbits. Interestingly, no stable inner orbits were found for outer eccentricities above 0.7.

4.1.7 Comparison with previous work on P1 and P2 bounds

The regression constant for the prograde and retrograde inner orbits corresponds approximately with those for binaries, as published by Morais and Giuppone (2012) and those for the outer orbits are similar to those originally found by Holman and Wiegert (1999) for binaries and later by Verrier and Evans (2007) for triples. (In the Holman and Wiegert paper, their equation (3) appears not to depend on a_b at all, unlike their equation (1); this is probably a misprint.)

Holman and Wiegert found that for P-type orbits around binaries, the regression constant for the inner critical ratio (our a_{oi}/a_2) was 1.6, with an average model error of 4%, while for S-type orbits, the equivalent to our a_{io}/a_2 was 0.464, with an average model error of 3%.

The results from Verrier and Evans for the critical ratios a_{oi}/a_2 and a_{io}/a_2 were 2.92 and 0.466 respectively, and no model accuracies were provided. (Note that in their regressions, their definition of mass ratios differs from Holman and Wiegert's and from ours.)

A more comprehensive comparison of our results with previous empirical work is provided in Section 4.7.

Pertinent to our results, Doolin and Blundell (2011) also found striations of instability, probably a result of resonances between the binary and the planet, and that there were "pinnacles and peninsulas of unstable regions for the non-librating and librating regions respectively, except when the stellar masses are equal". They also found that at high mutual inclinations, planetary systems are more stable.

Also regarding inclination, Li, Holman and Tao (2016) noted that of ten circumbinary systems they sampled, nine had inner planets quite close to the stability bound and all were effectively coplanar with the stellar orbits. They suggest the dearth of circumbinary systems around short-period solar-type main-sequence binaries is because it is hard to form planets around short period binaries, which could be exacerbated by the Kozai mechanism, which contributes to the formation of these binaries. Hamers, Perets and Portegies Zwart (2015) suggest that this lack of circumbinary systems, which is the opposite to what may be expected from observational biases, is because many of the short-period Kepler eclipsing binaries are actually triples and is a result of the secular gravitational influence of the circumbinary planet, within an hierarchical triple system, on the binary.

4.1.8 Some observational examples of P1 and P2 orbits

The only P1 orbit found in a triple system to date is in HW Virginis, which is not a classical triple as it consists of an inner binary of aggregate mass 0.63 M_S, a planet of 14.3 M_J and an outer body whose mass of 30 – 120 M_J classifies it as brown dwarf. The semi-major axes of these two bodies are estimated at 4.69 AU and 12.8 AU (Beuermann et al. 2012), giving a semi-major axis ratio of 3.13. No circumtriple P2 orbits have been discovered to date.

The smallest exoplanet orbit found in a P1 orbit around a binary, in terms of *absolute* semi-major axis, is Kepler 47b, at 0.296 AU (Orosz et al. 2012). The semi-major axis of the close binary is 0.0836 AU, giving a semi-major axis ratio (relative to the binary) of $a_{io}/a_1 = 3.54$.

However, the smallest semi-major axis *ratio* of a planet's orbit is for Kepler 16b, with the semi-major axis of the planet being 0.705 AU and that of the binary 0.224 AU, giving a ratio of $a_{io}/a_1 = 3.14$ (Doyle et al. 2011).

Both of these lie outside the smallest mean critical semi-major axis ratios found in the simulations of ~0.1, so the possibility exists of finding planets in even smaller orbits.

4.1.9 Triples compared with binaries

Effects of a mass-dominant outer star on the inner binary region

To highlight how the P1 and P2 planetary stability bounds in a triple differ from those in a binary, one needs to remove the disturbing influence of the inner binary and then compare the results with those from the previous section. This is because when the outer star of a triple is mass-dominant, as in our integrations for inverted mass ratios, it will it will tend to induce a wobble in the orbit of the inner binary, which will then affect the planetary orbits around it, particularly the P1 orbits. One can isolate this effect by merging the inner binary into a single mass.

An example of the influence of a massive outer star on the orbit of the inner binary is shown in Figure 35, where the top two graphs show the outer and inner stellar orbits respectively for a low-mass outer star of $0.001\ M_s$ and the bottom two graphs for a high-mass outer star of $6\ M_s$. The other parameters are $a_1 = 1,\ a_2 = 50,\ m_1 = m_2 = 1,\ e_1 = e_2 = 0.5,\ \Omega_2 = 45°,\ t = 1$ Myr

For the low-mass outer star the inner orbit in b) is effectively unperturbed, but a high-mass outer star induces eccentricity and precession effects in the inner orbit, as shown in d). The consequent effect on planetary orbits is shown by the test particle clouds in Figure 36. The upper panel shows the test particle cloud for the low-mass outer star case, and the bottom panel for the high-mass outer star case.

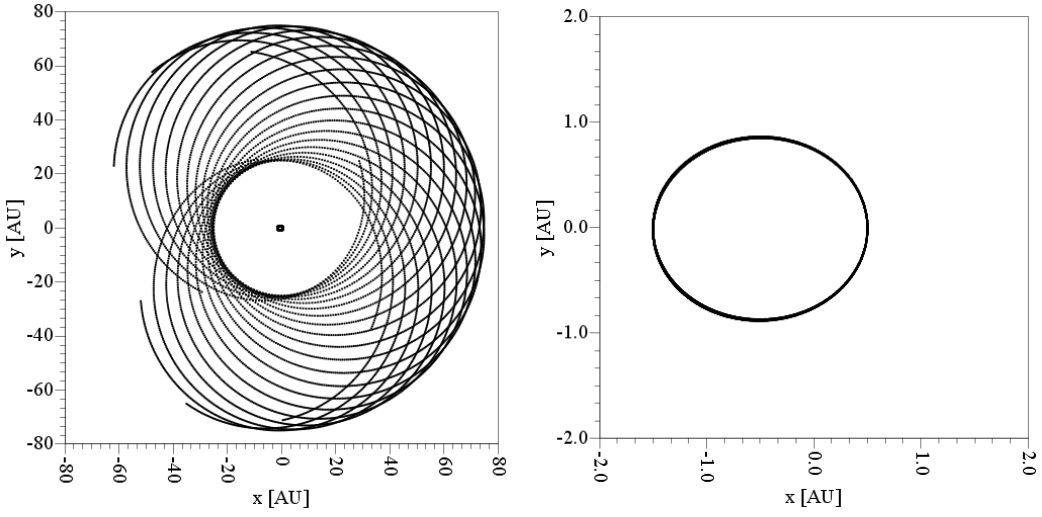

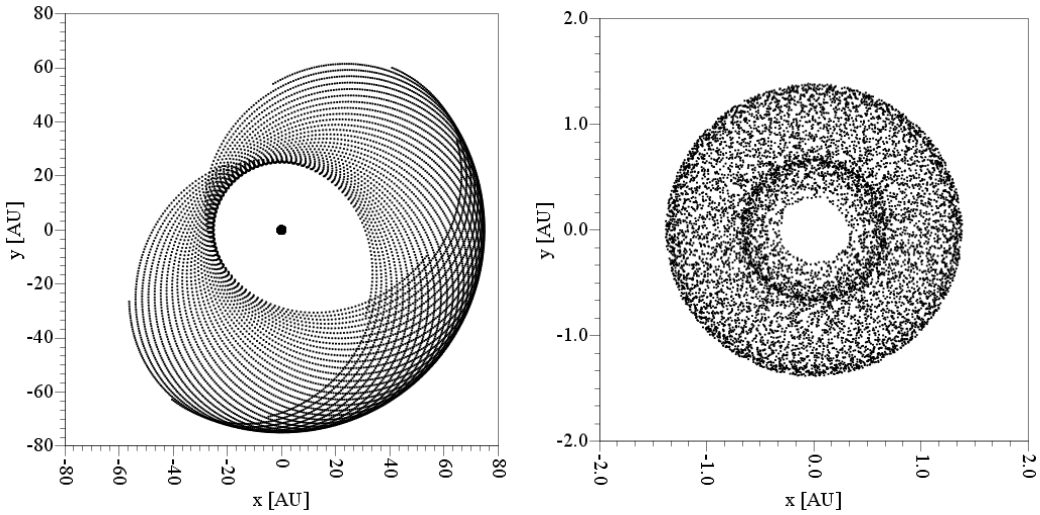

Figure 35. For $m_3 = 0.001\ M_s$ (upper panel) a) outer orbit b) inner orbit. For $m_3 = 6\ M_s$ (lower panel) c) outer orbit d) inner orbit

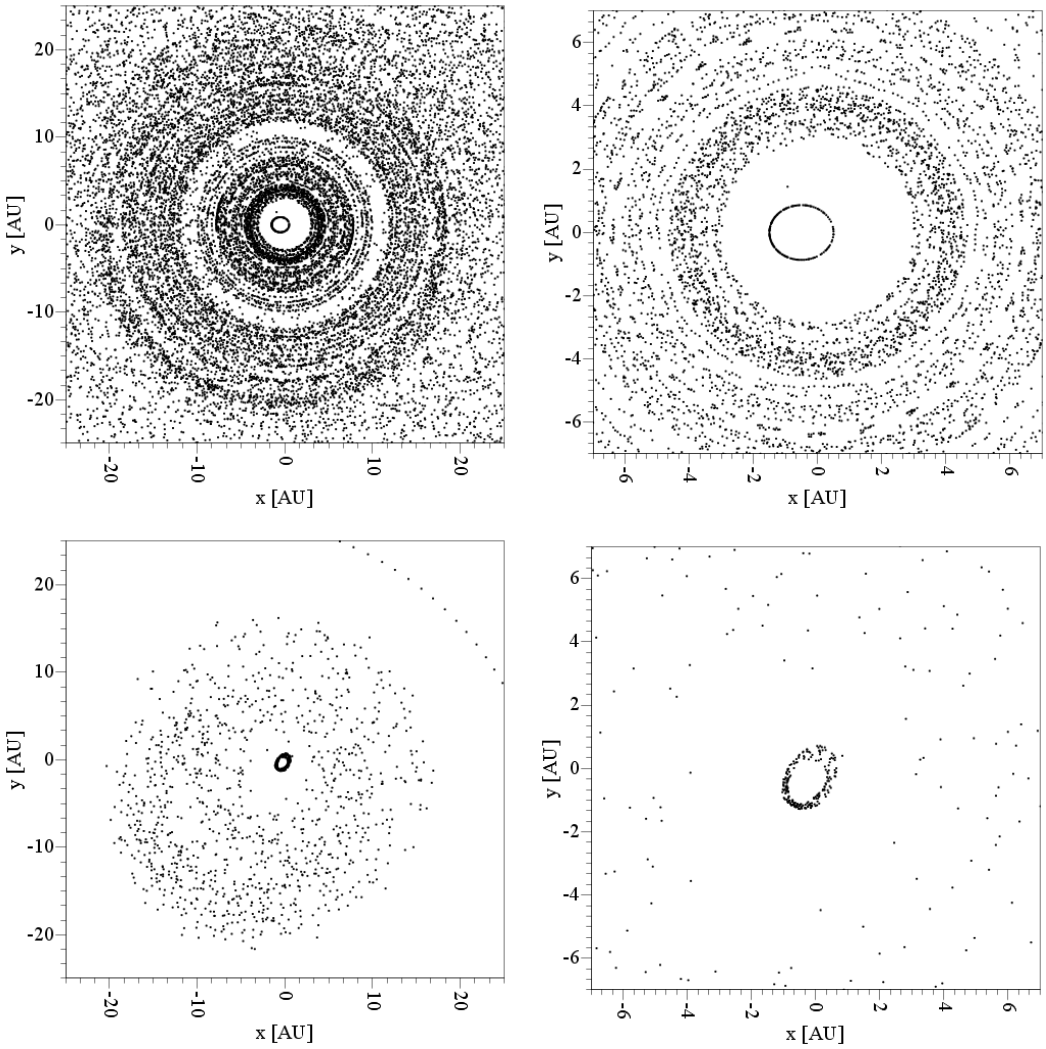

Figure 36. For $m_3 = 0.001\ M_s$ (upper panel) a) test particle cloud b) zoomed in. For $m_3 = 6\ M_s$ (lower panel) c) test particle cloud d) zoomed in

An outer star of very low mass relative to the inner binary, i.e. a low μ_2, has a negligible effect on the planetary orbits and there is no outer stability bound to the test particle cloud. However, as this star's mass increases, to a high μ_2, there are two effects:

1. First, the outer star, whose orbit is visible in the upper right of graph c), clears a much larger region around its orbit, resulting in an outer bound (a_{oi}, outside the graph's range) and an inner bound (a_{io}, here shown at ~17 AU).
2. Second, the clearing of the region around the inner binary increases because of the induced precession of this binary by the outer star. This effect can be significant – in Figure 36 the semi-major axis of this cleared region almost doubles, from ~2.8 AU in b) to ~5.5 AU in d).

Configuring a binary case

To highlight these effects, the previous P-type integrations were repeated for the case of a binary stellar system to isolate the characteristics specifically attributable to a triple configuration. This was done for prograde planetary orbits only. Rather than creating a new configuration and algorithms specific to binaries, to preserve as much consistency as possible, particularly should the triple/binary differences be small, the existing framework for triples was used, and as much of the procedure as possible was kept unchanged.

The inner binary was reduced to a single star by allocating effectively all the binary's mass to the central star and placing the second star, now of inconsequential mass, at a negligible distance from the central star. If the total mass of the binary is $M = m_1 + m_2$, $0.999M$ was given to the central star and only $0.001M$ to the second star, whose orbital distance was also reduced from $a_1 = 1$ AU to 0.01 AU with zero eccentricity.

The semi-major axis of Star 3 was varied over the same range as the previous integrations, i.e. from the smallest Mardling stability limit of 3.3 AU up to 100 AU. The inner mass ratio now needed to be selected in the range 0 – 1 instead of 0 – 0.5, since the inner binary was no longer symmetrical.

Since the time step of the integrations is based on the period of the inner binary, this required changing to the base of the new "binary", i.e. what was previously the outer binary. The new formula also required an adjustment to ensure the time step was in no case larger than in the previous integrations. This was done by identifying the configurations that gave the smallest time step for the original binary and for the new "binary", and equalising these time steps by calculating the new factor required to replace the 1/20 used in the original binary. The resulting formula was as follows:

Original triple: $$\Delta t = \frac{1}{20}\left(\frac{a_1^3}{m_1+m_2}\right)^{\frac{1}{2}} \quad (28)$$

New "binary": $$\Delta t = \frac{1}{38}\left(\frac{a_2^3}{m_1+m_2+m_3}\right)^{\frac{1}{2}} \quad (29)$$

The time step for the first set of integrations ranged from 0.035 yr-0.047 yr, averaging 0.042 yr, while the new time step averaged 0.030 yr.

The effect on a typical particle density function of minimising the second star of the inner binary is illustrated in Figure 37, where the heavily inverted outer mass configuration moves from the inner binary having stars of equal mass, to the central star having 99.98% of the binary mass and the secondary orbiting the central star at a very close 0.01 AU, i.e. the inner binary effectively approximates a single point mass. In both cases $a_2 = 100$ AU, $m_3 = 15\ M_s$ and i, e, Ω, and ω for stars 2 and 3 are zero. Integrations were for 10^5 yr.

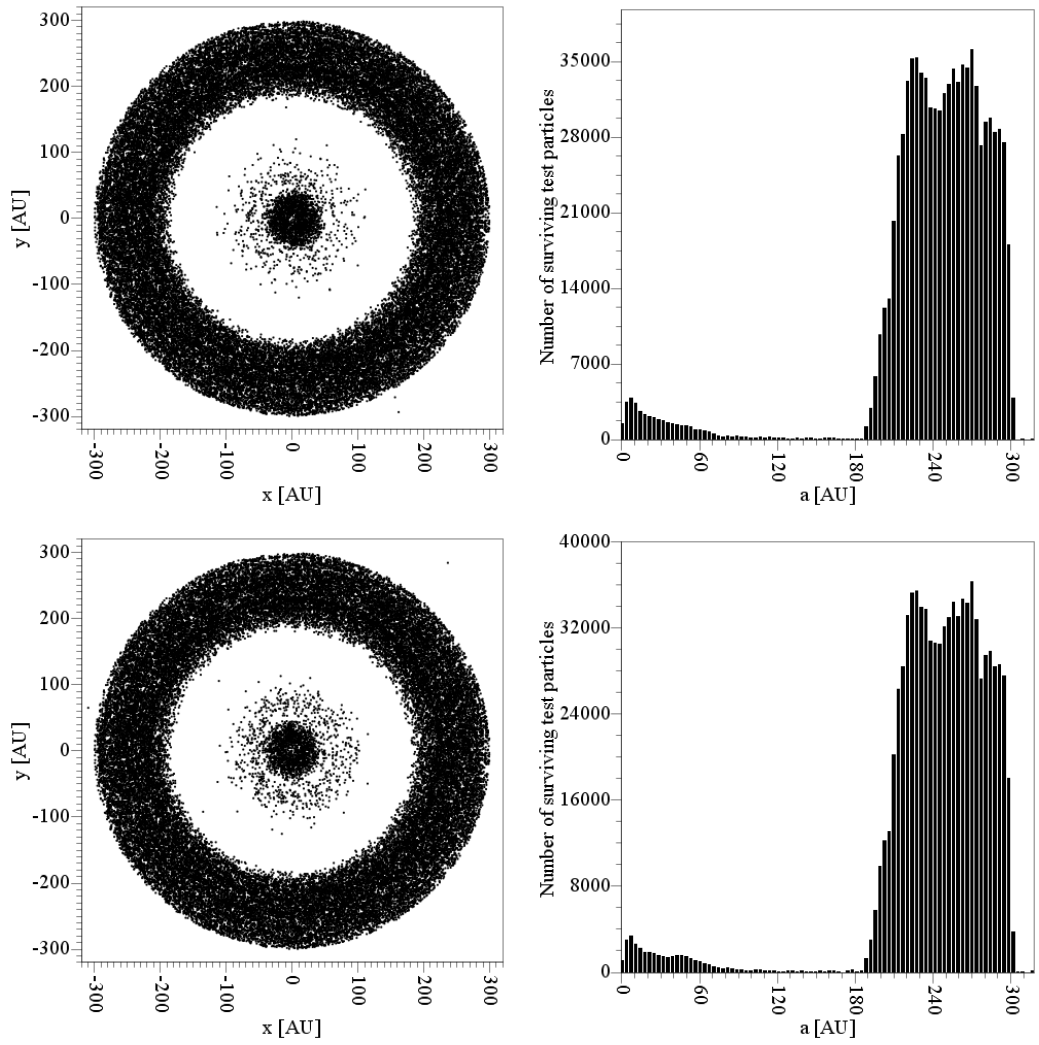

Figure 37. Reducing the inner binary. a) upper panel: $m_1 = 2.5\ M_s$, $m_2 = 2.5\ M_s, a_1 = 1\ AU$ b) lower panel: $m_1 = 4.999\ M_s$, $m_2 = 0.001\ M_s, a_1 = 0.01\ AU$

The differences appear subtle, being visible mainly in the changed density profile of the inner test particle cloud. Nevertheless, when the inner binary is merged, the inner stability bound reduces as expected, from 46 AU to 36 AU, a contraction of over 20%. The inner test particle cloud is diffuse, as always, with some arbitrary judgement involved in determining its edge (via the selection of parameters in the edge detection algorithm). Since the test particle density profile is different to the triple case, these parameters required re-optimization. However, a consistent procedure that changes as few parameters as possible will minimise the

introduction of any structural bias into the determination of the orbital stability bounds.

The outer bound is sharply defined and is unaffected by the merging of the inner binary. The parameters used are shown in Table 28; the only parameters that required modification were f_i and f_o.

Parameter	Prograde orbits	Retrograde orbits
f_t	0.105	0.153
f_p	1.500	1.000
f_i	0.250	0.400
f_o	0.028	0.170
l_s	0.500	0.500
a_a	0.016	0.028

Table 28. P1 and P2 orbits. Edge detection parameters for reduced binary system

Results for the binary case

In the reduced binary configuration, the case of a retrograde outer star falls away. For comparison with the triple star analysis done for a prograde outer star in Section 4.1.5, 5 865 integrations of the reduced binary model were run. The resulting smallest sample, for retrograde inner orbits, provided 859 stability bounds, which was a sufficiently large sample. The inner and outer stability limits for prograde and retrograde planetary orbits are shown in Figure 38 and Figure 39.

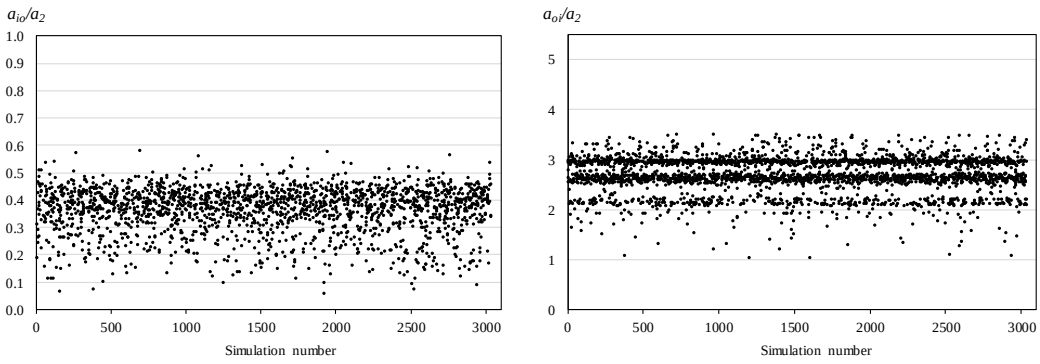

Figure 38. Binary P1 and P2 orbits, prograde outer star, prograde planets: a) inner bounds b) outer bounds

Comparison with Figure 27 shows that in the binary case the inner stable orbits are on average closer to the central star, but with a more asymmetrical distribution of critical ratios, with a more well-defined upper limit at around 0.5.

The outer stable orbits are slightly closer to the outer star on average, with some orbits very close to it. There are fewer orbits beyond a critical ratio of around 3.5 compared with the triple case.

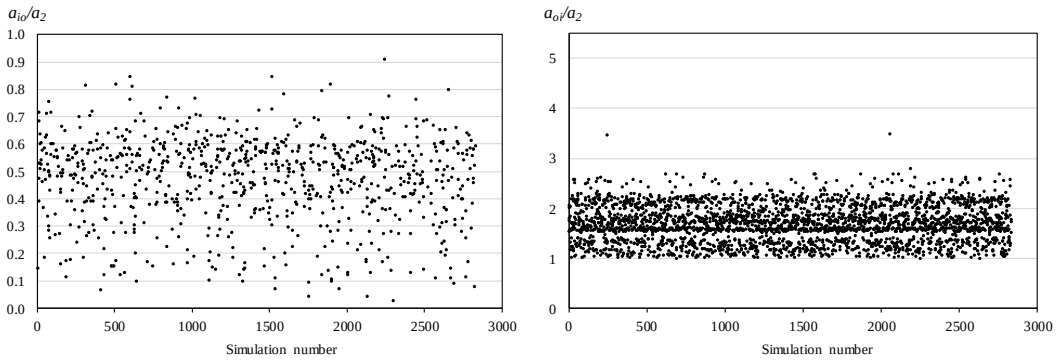

Figure 39. Binary P1 and P2 orbits, prograde outer star, retrograde planets: a) inner bounds b) outer bounds

For retrograde planetary orbits the range of critical ratios has a more symmetrical and uniform distribution than for triples as shown in Figure 28. The outer orbits' critical ratios lie closer to the central star and have a tighter range compared with those for triples.

The number of stable bounds found for the binary integrations is shown in Table 29.

Cases with well-defined orbit bounds							
Orbit type	Total simulations	a_{io}/a_2			a_{oi}/a_2		
		Bounds found (no.)	Success rate (%)	Distribution (%)	Bounds found (no.)	Success rate (%)	Distribution (%)
Prograde	3034	1972	65	70	2994	99	51
Retrograde	2831	859	30	30	2831	100	49
Total	5865	2831	48	100	5825	99	100

Table 29. Binary P1 and P2 orbits, prograde outer star. Number of bounds found

For the inner orbits the success rate in identifying stability bounds was almost double that for the triple case, while the relative proportion of prograde to retrograde bounds was broadly the same. In the simpler binary system the edges of bounds were generally better defined.

For the outer orbits, the success rate compared with triples was slightly higher at almost 100%, and the relative proportions of prograde and retrograde orbits remained the same.

The mean critical semi-major axis ratio ranges of these bounds are shown in Table 30.

Orbit type	a_{io}/a_2					a_{oi}/a_2				
	N	Min	Avg	Max	SD	N	Min	Avg	Max	SD
Prograde planetary orbits	1972	0.058	0.364	0.581	0.143	2994	1.030	2.703	3.501	1.176
Retrograde planetary orbits	859	0.026	0.471	0.911	0.153	2831	1.001	1.691	3.478	0.365
Difference (%)	-	-	29	-	-	-	-	-37	-	-

Table 30. Binary P1 and P2 orbits, prograde outer star – mean critical semi-major axis ratios

Comparison with the triple case

Comparing triple and binary stellar systems with the outer star having the same semi-major axis, if the inner binary merges into a single star, all orbit bounds may be expected to move towards the central star.

The results for the binary case in Table 30 are compared with the triple case in Table 31.

Difference in average bounds	a_{io}/a_2			a_{oi}/a_2		
Orbit type	Triple	Binary	Δ%	Triple	Binary	Δ%
Prograde planetary orbits	0.383	0.364	-5*	2.936	2.703	-8*
Retrograde planetary orbits	0.519	0.471	-9*	1.976	1.691	-14*
Δ%	35	29	-	-33	-37	-

* significant at the 5% level

Table 31. Binary P1 and P2 orbits. Difference between mean critical semi-major axis ratios in triples and binaries

The data show that, as expected, both the inner and outer mean critical semi-major axis ratios move towards the central star, for both prograde and retrograde planetary orbits. While these movements are statistically significant, they are nevertheless small, suggesting that the influence of the outer star is dominant.

The regressions for the binary case can also be compared with those shown previously for the triple case, as shown in Table 32.

Table 87 in Section 4.6 shows the results of previous studies of binaries. For P-type orbits (equivalent to our outer orbits, reduced from the P2 orbits of the triple) the regression constants have varied widely, from 1.6 to 3.9, averaging 2.6. These were for prograde orbits. Our value above of 2.4 is consistent with these results. Only one result for retrograde planetary orbits has been reported, by Doolin and Blundell (2011), with a constant of 1.3 – 2.7, averaging 2.0. This study's 1.5 falls in the lower end of this range.

For S-type prograde orbits (equivalent to our inner orbits, reduced from the P1 orbits of the triple) the constants ranged from 0.22 to 0.80, averaging 0.43. Our result of 0.44 is almost identical to this average. Again, there was only one previous study for retrograde orbits, by Morais and Giuppone (2012), which gave 0.60 – 0.94. Our 0.57 is lower than their range.

For binaries, as for triples, the stability bounds for outer orbits have better-defined edges than for inner orbits, resulting in higher model R^2s and lower model errors (measured by MAPEs). The regression coefficients are illustrated in Figure 40.

Inner, prograde	Triple		Binary	
	B	*t*	B	*t*
C	0.439	47.8	0.195	19.1
a	0.000	0.4	0.000	47.9
μ_1	-0.005	-0.4	-	-
μ_2	-0.020	-7.1	-0.006	-1.8
e_1	-0.004	-0.5	-	-
e_2	-0.114	-8.9	-0.435	-39.4
i_2	0.000	2.2	-	-
Ω_2	-0.001	-6.1	-	-
ω_2	-0.001	-6.3	-	-
R^2	0.132		0.563	
Model error (%)	19		11	

Outer, prograde	Triple		Binary	
	B	*t*	B	*t*
C	2.377	194.6	2.719	84.2
a	-0.003	-23.8	0.000	-25.8
μ_1	0.053	2.9	-	
μ_2	0.044	11.5	-0.017	-1.4
e_1	0.090	6.8	-	
e_2	1.997	151.8	0.884	25.4
i_2	0.000	3.1	-	
Ω_2	-0.002	-15.9	-	
ω_2	-0.002	-13.4	-	
R^2	0.828		0.893	
Model error (%)	6		3	

Inner, retrograde	Triple		Binary	
	B	*t*	B	*t*
C	0.573	76.4	0.211	14.3
a	0.000	4.8	0.000	31.6
μ_1	0.009	0.8	-	
μ_2	-0.043	-19.2	-0.026	-4.9
e_1	-0.010	-1.4	-	
e_2	-0.469	-31.8	-0.567	-34.9
i_2	0.000	-2.8	-	
Ω_2	0.000	1.0	-	
ω_2	0.000	1.3	-	
R^2	0.671		0.444	
Model error (%)	10		13	

Outer, retrograde	Triple		Binary	
	B	*t*	B	*t*
C	1.483	153.4	1.235	141.9
a	-0.004	-40.4	0.000	-45.7
μ_1	0.131	9.1	-	
μ_2	-0.008	-2.8	0.023	7.3
e_1	-0.036	-3.5	-	
e_2	1.725	166.1	1.681	175.0
i_2	0.002	19.6	-	
Ω_2	0.001	8.5	-	
ω_2	0.001	5.1	-	
R^2	0.860		0.921	
Model error (%)	6		4	

Table 32. Binary P1 and P2 orbits. Regression coefficients and model fits, triples compared with binaries

In all cases, aside from the constant the only variable of any influence is the eccentricity of the outer star, e_2. Generally, the effect of the outer star's eccentricity is far larger on the outer stability bounds than on the inner stability bounds. For inner orbits its influence is larger in binaries than in triples, for both prograde and retrograde planetary orbits. For outer orbits, its effect in binaries and triples is essentially the same for retrograde orbits, but for prograde orbits it has a larger influence in triples than in binaries.

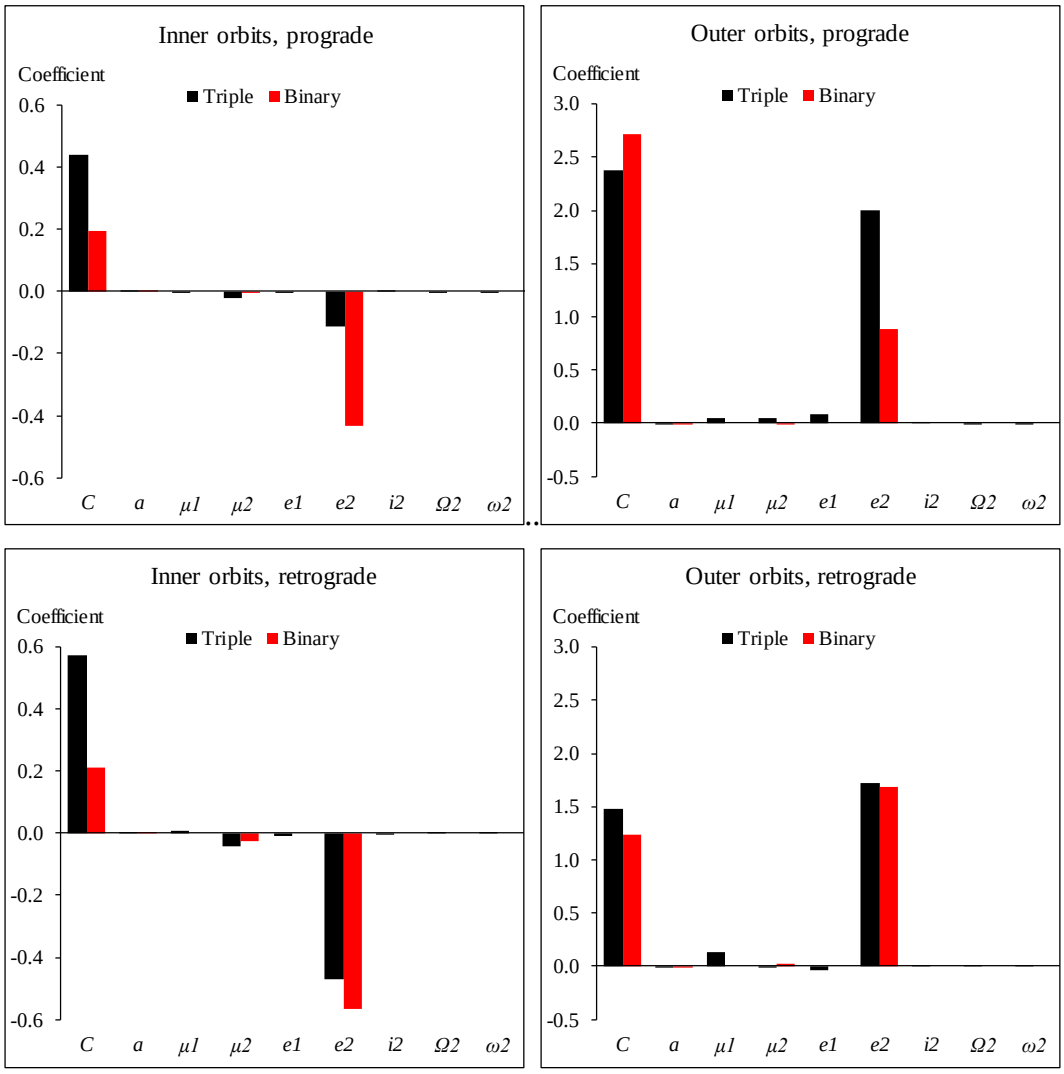

Figure 40. Binary P1 and P2 orbits. Regression coefficients, triples compared with binaries

4.1.10 Conclusions – P1 and P2 orbits

Comparing the stable regions of triples with binaries to highlight their differences shows that the inner and outer critical semi-major axis ratios of binaries are closer to the central star for both prograde and retrograde planetary orbits. While statistically significant, the difference is small, ranging from 5%-14%, indicating the dominant influence of the outer star over the inner binary. Compared with binaries the influence of the outer star's eccentricity is significantly smaller for inner prograde orbits and materially larger for outer prograde orbits; there are no similar differences for retrograde orbits. The relatively small differences between triples and binaries results from the Mardling stability limit for triples, which precludes them from becoming too compact.

For triple configurations with prograde, circular, coplanar outer stellar orbits and a wide range of mass ratios, the inner and outer stability boundaries as measured by the critical semi-major axis ratio, are found at around 0.36 times and 2.7 times the distance of the outer star respectively for prograde planetary orbits, and at around 0.47 times and 1.7 times this distance respectively for retrograde planetary orbits.

The configuration of the inner binary has little influence, as the stability limit of the outer star is sufficiently far away that the inner binary effectively resembles a single point mass, so the outer star's influence is dominant, with its eccentricity having the strongest effect. The greater stability of retrograde planetary orbits results in both inner and outer bounds moving closer to the outer star compared with the prograde case. The difference in critical ratios for prograde and retrograde planetary orbits is significant, ranging from ~30%-70% depending on the eccentricity of the outer star. For highly eccentric orbits of the outer star, the semi-major axis of the outer stability bound can expand by over 80% for prograde orbits and more than double for retrograde orbits, while the inner bound shrinks by a quarter for prograde planetary orbits and by over 80% for retrograde planetary orbits.

For a retrograde outer star the two mass ratios have a greater influence, particularly the inner one, with this effect being greater for prograde planetary orbits than for retrograde ones. The effect of the inner binary's eccentricity remains insignificant. The eccentricity of the outer star remains the largest influence; it is essentially unchanged for inner bounds but is lower for outer bounds.

The outer stability bound increases approximately linearly with increasing outer star eccentricity, with the critical semi-major axis ratios of prograde and retrograde planetary orbits converging to the same value of around 3.1. The inner critical ratio shows only very weak dependence on the outer eccentricity. Prograde star/prograde planet orbits are the least stable; combinations with one or more retrograde orbits are more stable.

These results are consistent with the few observational examples of P1 and P2 orbits found to date.

4.2 Orbit Types P1 And P2 In Highly Inclined Triple Systems

4.2.1 Vertical characteristics of the stability region

Only prograde planetary orbits were considered. The previous analyses, which have been largely coplanar in that they have used only reasonably small variations in the outer star's inclination, have been relative to the plane of the inner binary. In this section, which deals with large inclinations of the outer star, the analysis needs to be relative to the invariable plane of the triple system.

The invariable plane is the plane passing through the system's barycentre and perpendicular to its total angular momentum vector. For example, in Figure 41 the invariable plane is orthogonal to the total angular momentum vector $L = L_1 + L_2$, where L_1 and L_2 are the angular momentum vectors of the inner and outer binary orbits respectively.

The inclinations i_1 and i_2 of Stars 1 and 2 respectively are now also measured relative to the invariable plane.

For the orbital configurations used in the analysis of Kozai effects in this section, the angular momentum of the outer star contributes most of the total angular momentum of the system. This is because the angular momentum of one body

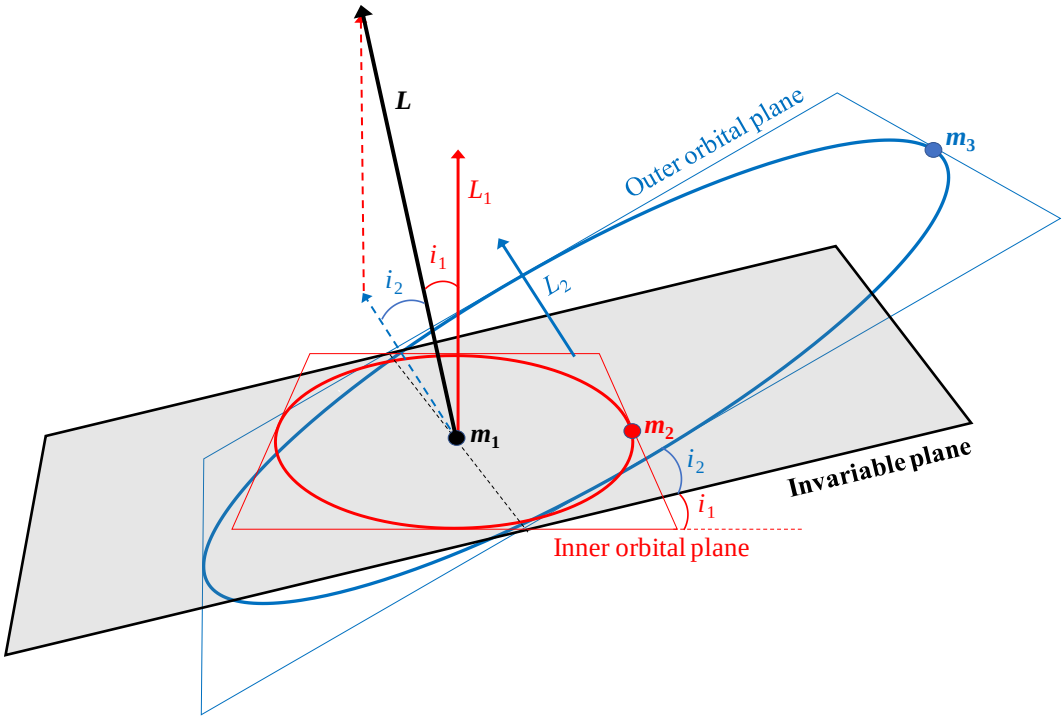

Figure 41. The invariable plane in a triple system

orbiting another is given by

$$L = \mu\sqrt{GMa(1-e^2)} \tag{30}$$

where

$\mu = \frac{m_a m_b}{m_a+m_b}$ is the reduced mass of the system, comprising masses m_a, m_b

G = the gravitational constant

$M = \sum_{i=1}^{n} m_i$ is the total mass of the system

a = the semi-major axis of the body

e = the eccentricity of the body's orbit

Since for the outer binary in a triple both M and a are larger than for the inner binary, the outer angular momentum would usually tend to dominate the inner angular momentum. This can be better quantified by writing the ratio of the angular momenta of Star 3 and Star 2, from equation (30), i.e.

$$\frac{L_3}{L_2} = \left[\frac{m_2(m_0+m_1)^2}{m_0 m_1(m_0+m_1+m_2)}\right]\sqrt{1+\left(\frac{m_2}{m_0+m_1}\right)}\sqrt{\frac{a_2}{a_1}}\sqrt{\frac{1-e_2^2}{1-e_1^2}} \tag{31}$$

In this analysis we used relatively large masses for the outer star to highlight significant Kozai resonances. Since the first term is ≳1 for stars of broadly comparable mass, the second term is always >1 (e.g. 1.5 for stars of equal mass), a_2/a_1>~3 – 5 from the Mardling limit and the last term is > 0.7 for the eccentricities used, a momentum ratio larger than one is assured, and is in most cases significantly larger because of the higher values of a_2/a_1used.

This is shown in Table 33, which shows the highest and lowest contributions of the outer star for the stellar configurations used later in this section.

Range	Body	Semi-major axis	Mass	Angular momentum		
		a	m	L	Ratio	Contribution
		(AU)	(M_s)	(kg m^2/sec)	(x)	(% of total)
	Star1	-	1.00	-	-	-
Maximum	Star2	1	0.01	8.9E+43	1	-
	Star3	100	2.02	1.8E+47	2030	99.95
Minimum	Star2	1	1.00	8.9E+45	1	-
	Star3	40	0.20	1.6E+46	1.8	64.14

Table 33. Highest and lowest contributions to system angular momentum for high-inclination integrations

The highest is effectively 100% and the lowest 64%. More importantly, the mean contribution is 92%, with over 70% of the contributions lying between 90% and 100%.

The dominant angular momentum of the outer star results in the invariable plane lying close to the orbital plane of the outer star. Aligning the test particle disc with the outer orbital plane instead of the invariable plane is therefore an acceptable approximation.

As an example, the next two figures show the initial and final states of the test particle cloud for the integration of a triple system consisting of three equal-mass stars of $1M_S$ with an outer star inclination of 65°. The test particle disc has also been set at an inclination of 65° to be coplanar with the outer orbital plane (and to have the same longitude of ascending node).

Figure 42 shows the test particle cloud in the coordinate system of the inner orbital plane, and Figure 43 shows the same data using the coordinate system of the outer orbital plane, which lies close to the invariable plane. The configuration is: prograde test particle cloud, $a = 20$ AU, $e_1 = e_2 = 0$, $\mu_1 = \mu_2 = 0.5$, $i_1 = 0$, $i_2 = 65°, \Omega = 0, \omega = 0$.

In the coordinate system of the inner orbital plane the initial test particle cloud is a flat disc. It is also a flat disc in the second case, but this is less obvious because it is inclined at the same 65° of the outer orbital plane, so it appears as an ellipse in both the *x*-*y* plane and (to a lesser extent) in the *x*-*z* plane. The final shape of the test particle cloud is identical in both cases, but because of its inclination in the second case, its projections on the *x*-*y* and *x*-*z* plane appear more complex. At the end of the integration the symmetry around the 65° inclination in the *x*-*z* plane is clear.

A numerical simulation of the debris disc around HD 98800 by Verrier and Evans (2008) showed a similarly warped coplanar disc, inclined at almost 50°, around the inner binary, with a small inner ring and high-inclination outer halo. Similar dynamics have been explored more generally by Farago and Laskar (2010) and Doolin and Blundell (2011) and stable high-inclination particles were also reported in simulations of GGTau (Beust & Dutrey 2005, 2006). As pointed out by Ford, Kozinsky and Rasio (2000), as the orbits of Star 2 and Star 3 exchange

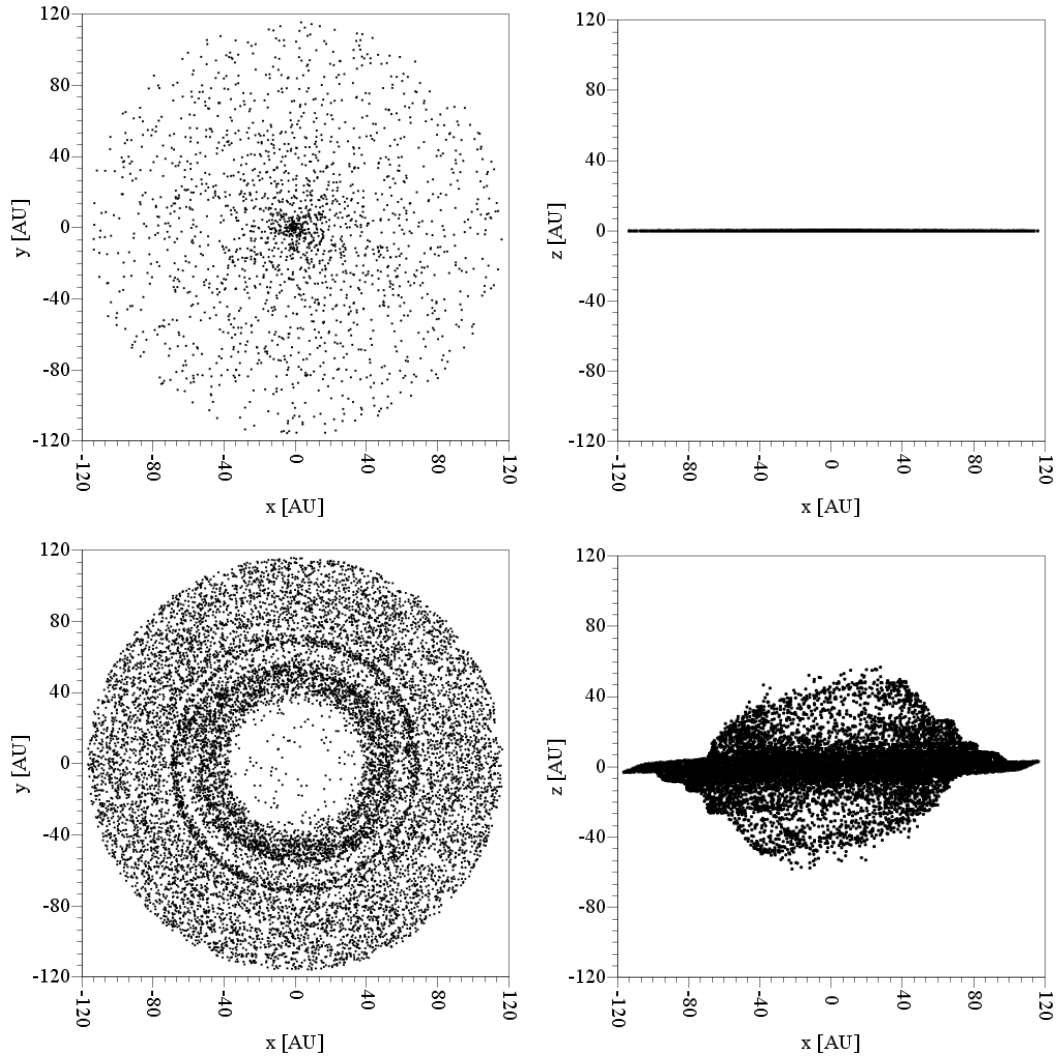

Figure 42. P1 and P2 orbits, using coordinate system of the inner orbital plane. a) upper panel: $t = 0\ yr$ b) lower panel: $t = 100\ kyr$

angular momentum, their eccentricities will display periodic oscillations over secular timescales that are long compared to their orbital periods. For non-coplanar systems these oscillations also occur in orbital inclinations.

Once the orbit of the outer star is no longer coplanar with the orbit of the inner binary, i.e. the mutual inclination of the two orbits is no longer zero, the stable planetary region will also no longer be coplanar but will extend vertically above this plane, with its shape being sculpted primarily by the outer star.

An example is illustrated in Figure 44, where the *x-y* plane is aligned with the invariable plane, approximated by the outer orbital plane. The parameters are $a = 40\ \text{AU}, e_1 = 0, e_2 = 0, i_1 = 0, \mu_1 = 0.5, \mu_2 = 2.0, i_2 = 65°$.

Note that the outer limit of the test particle cloud is of no relevance, since this is simply where it has been truncated.

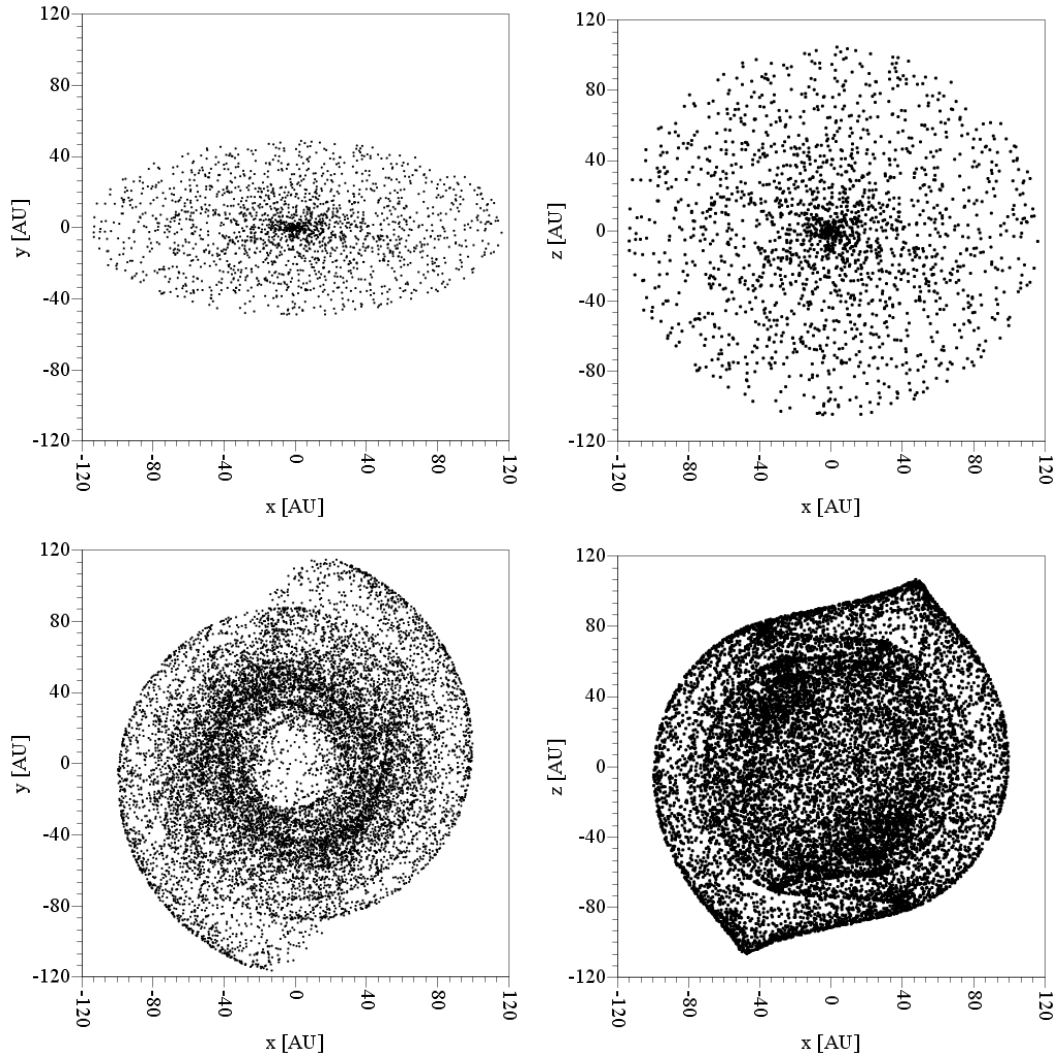

Figure 43. P1 and P2 orbits, using coordinate system of the outer orbital plane. a) upper panel: $t = 0\ yr$ b) lower panel: $t = 100\ ky$

The test particle orbits are initially coplanar with the invariable plane and circular, with the result that the horizontal cross-section, projected onto this plane, is circular. However, for different configurations of the triple there is great variation in the vertical cross-sectional profiles of the stable region, as shown by the vertical projection in Figure 44.

Examining the paths of individual test particles over time yields the following observations:

1. Their orbits librate, with the argument of periapsis ω oscillating.
2. The semi-major axis of their orbits, a, remains effectively constant.
3. Their orbits remain circular, i.e. their eccentricity remains very close to zero.
4. These orbits vary in inclination. They are initially coplanar with the inner binary and then become more inclined over time, eventually oscillating around a final non-zero inclination.
5. Some test particles develop Kozai resonance and some of these eventually undergo orbit flipping into retrograde motion.

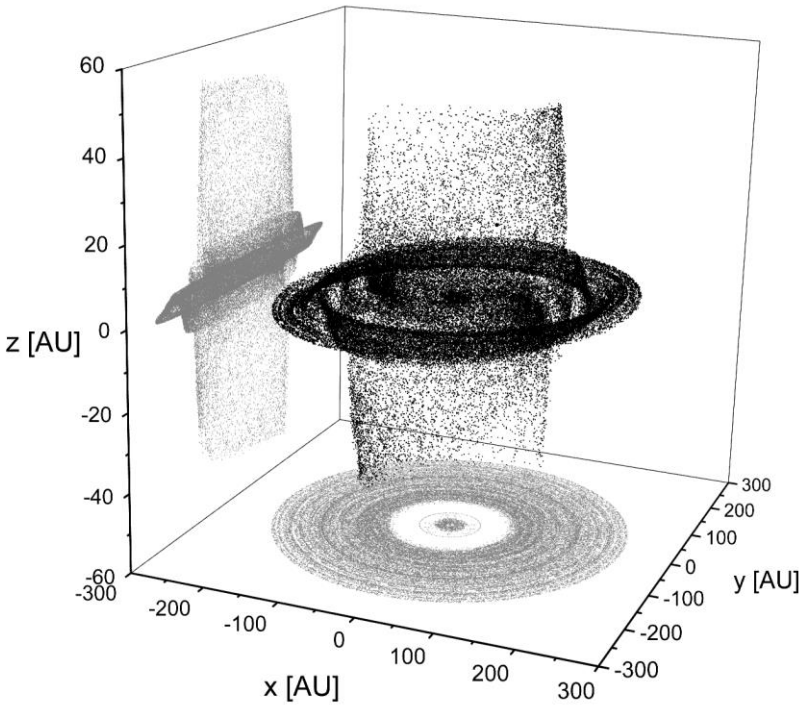

Figure 44. Position in space of surviving test particles after 100 kyr. P1 and P2 prograde orbits

The annular vertical "chimney" shown in Figure 44 therefore consists of test particles in circular orbits of constant semi-major axis but varying inclination. This may be more clearly illustrated by tracking a specific single test particle over time, as shown in Figure 45. The cross-sections show the positions of this particle over the last 0.1% of the integration time.

The projection of the test particle's position on the horizontal plane is annular, with changes in semi-major axis, eccentricity and inclination, as well as precession, contributing to this in varying degrees. The period of oscillations in inclination is much longer than those in the other orbital elements. This particle's orbit reaches a maximum inclination of 34°.

There is a limit to the maximum inclination of planetary orbits. The number of stable orbital bounds falls exponentially with increasing inclination, as shown in Figure 46, where the legend refers to the triple configurations discussed later in Table 34.

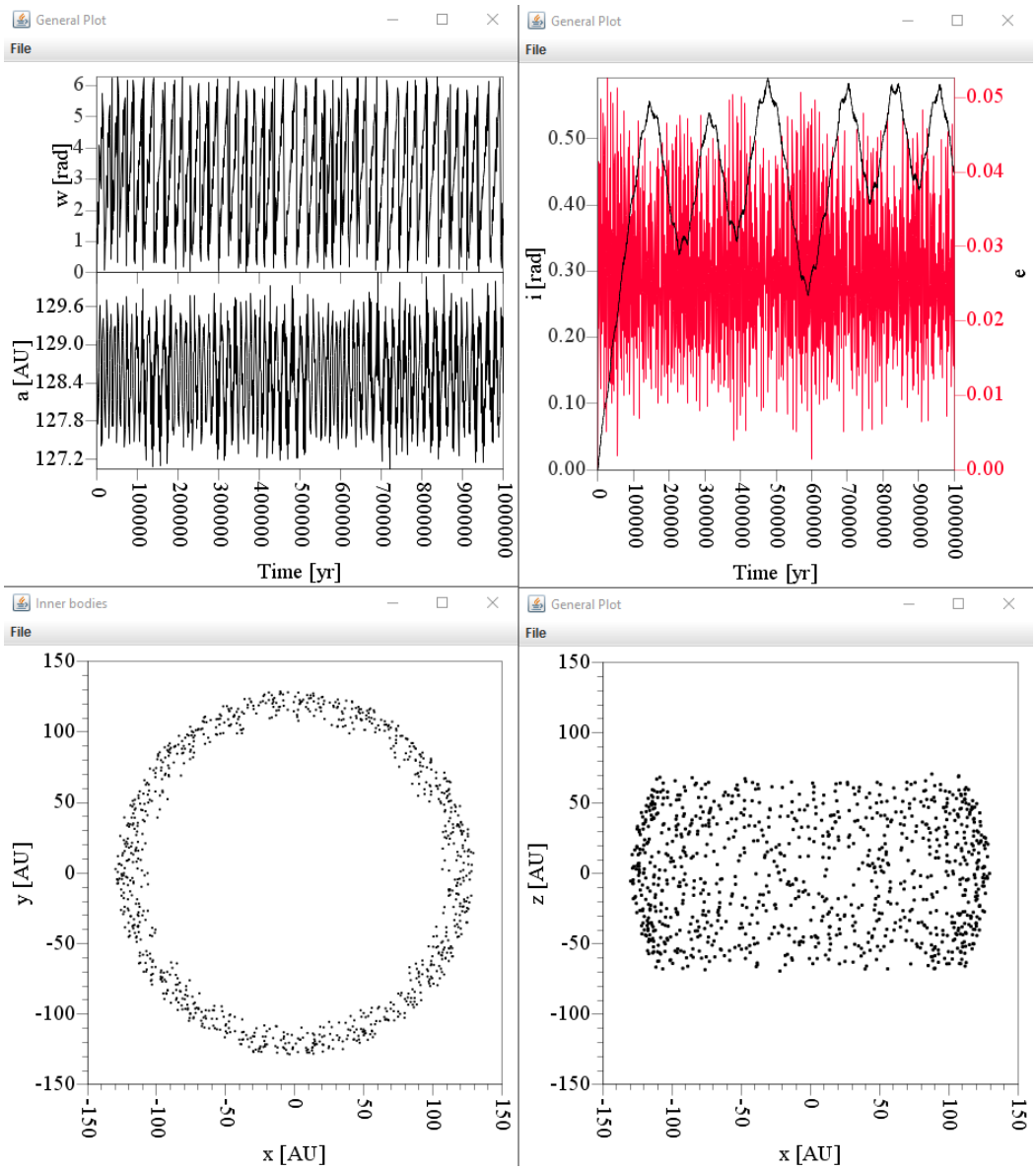

Figure 45. P1 and P2 orbits. Single prograde test particle cloud after $1\ Myr$, $a = 40\ AU, e_1 = e_2 = 0, i_1 = 0, \mu_1 = 0.5, \mu_2 = 2.0, i_2 = 65°$

The lines end when there are no more stable prograde bounds. (However, the number of remaining bounds is not zero, as there are usually a few left with inclinations greater than 90° – these are planetary orbits that have flipped and become retrograde, and are ignored.)

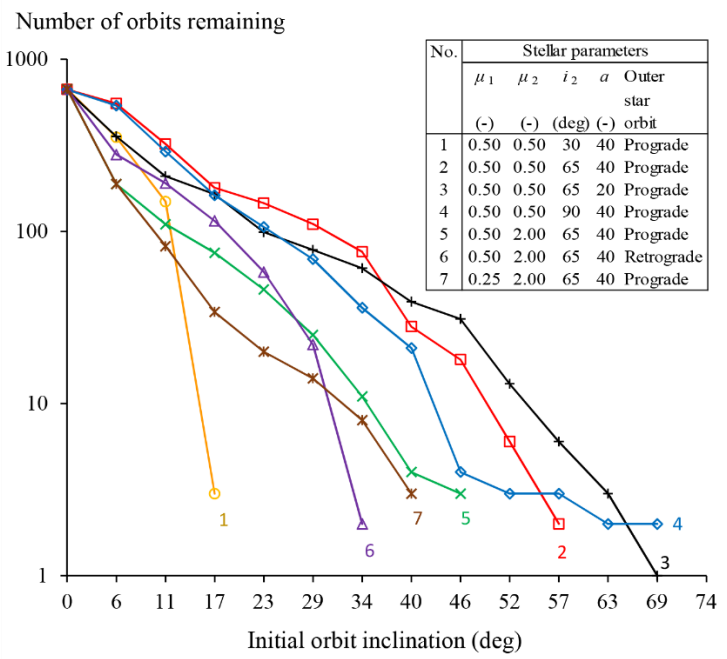

No.	Stellar parameters				
	μ_1	μ_2	i_2	a	Outer star orbit
	(-)	(-)	(deg)	(-)	
1	0.50	0.50	30	40	Prograde
2	0.50	0.50	65	40	Prograde
3	0.50	0.50	65	20	Prograde
4	0.50	0.50	90	40	Prograde
5	0.50	2.00	65	40	Prograde
6	0.50	2.00	65	40	Retrograde
7	0.25	2.00	65	40	Prograde

Figure 46. Number of stable P1 and P2 prograde orbits remaining after 1 Myr as a function of initial planetary inclination, for various triple configurations

4.2.2 Stellar Kozai resonances in the triple

This section illustrates visually some of the manifestations of the stellar Kozai mechanism for different configurations of triple systems, i.e. the shape of the test particle clouds relative to the outer orbital plane. The results are then analysed in the following section.

For all configurations, the initial eccentricities of both stellar orbits were zero. The initial inclination of the inner orbit was always zero, so the mutual inclination between the two orbits was the inclination of the outer star, i_2. The same cloud of test particles, all in prograde orbits, was used in all configurations and the integration time was usually 10^6 yr. The longitude of ascending node Ω and argument of periapsis ω for both stellar orbits were zero. The parameters that were varied are shown under the figures.

The non-resonant case is shown in Figure 47. The third graph shows the linearised relationship between the inclination and eccentricity of the inner binary's orbit. The square root of the slope of this line is the conserved quantity L_z in the Kozai relationship

$$L_z = \cos i_2 \sqrt{1 - e_2^2} \tag{32}$$

The three stars are of equal mass. At the 30° inclination of the outer star, no Kozai resonance appears. The inner binary's semi-major axis, inclination and eccentricity all remain constant, although there is libration. (Libration occurs when ω oscillates between fixed limits, while for circulation ω increases or decreases without reversing.) The third graph indicates that there is no Kozai effect.

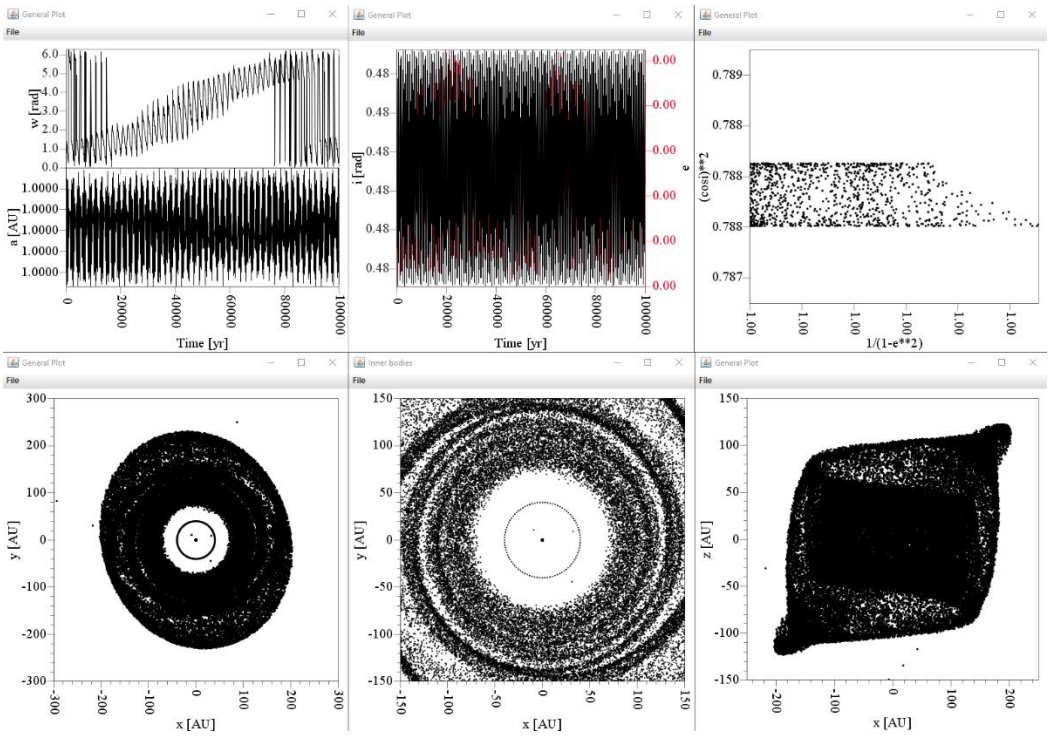

Figure 47. P1 and P2 orbits, base case, no Kozai resonance, $\mu_1 = \mu_2 = 0.5, i_2 = 30°, a = 40\ AU$

However, the test particle cloud is no longer coplanar with the inner binary and extends materially in the *z*-direction, up to 125 AU. The *x*-*y* projection appears oval because of the tilt of the invariable plane, and the general inclination of the test particle cloud of close to 30° is visible in the *x*-*z* projection. While the shape of the outer boundary of the test particle cloud will be referred to, it must be remembered that its extent in the *x*-*y* plane is arbitrarily truncated, which will also constrain its extent in the *z*-direction to some extent; the shape of the inner region is usually of more importance.

In the next case, shown in Figure 48, the inclination of the outer star is increased to 65°, well above the 39.2° (and 140.8°) theoretical critical inclinations for Kozai resonance in small bodies.

Here Kozai resonance develops. Libration begins at around 100 kyr, with a period of 122 yr and oscillates between 45° and 135°, a range of 90°. The interchange between the inclination and eccentricity of the inner binary's orbit is shown in the second graph, with the period of the Kozai resonance being 114 kyr. The range of inclination is 60° and that of eccentricity is 0.80. The third graph confirms that strong Kozai resonance is indeed occurring.

Note that the critical inclinations and equation (32) apply to the standard Kozai mechanism, where the test particle's orbit is circular and vertical angular momentum is conserved. However, when the test particle's orbit is eccentric, then vertical angular momentum varies, the dynamics can no longer be solved analytically, the Kozai oscillations are modulated on longer timescales and can exhibit behavior completely different to that of the standard Kozai mechanism.

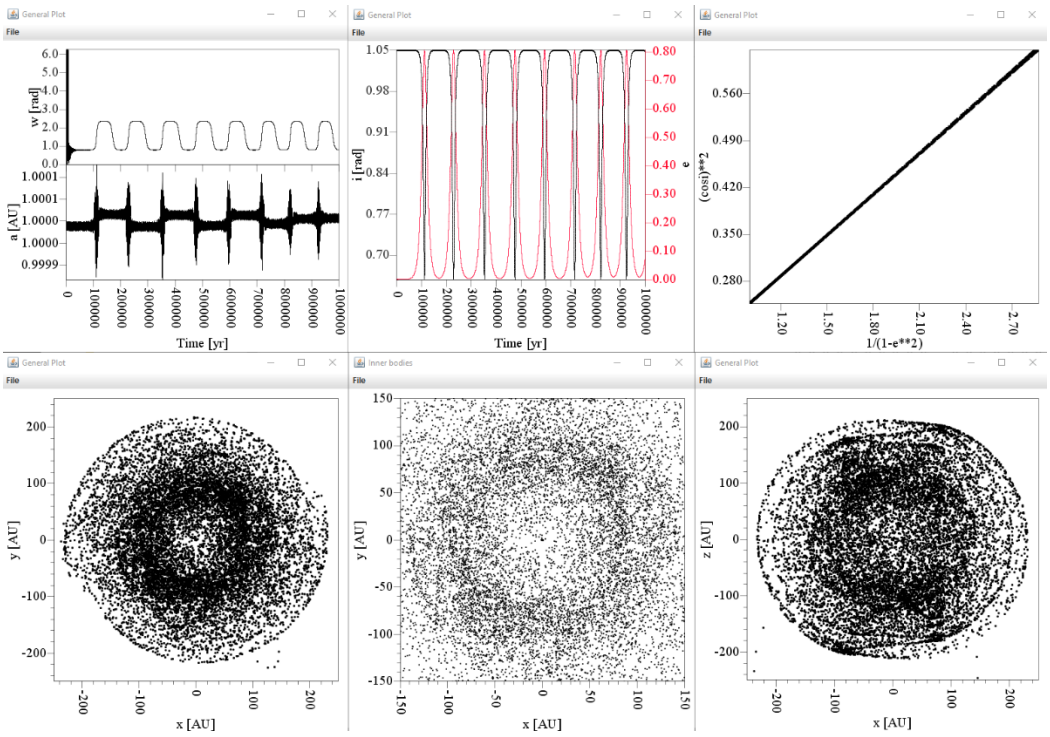

Figure 48. P1 and P2 orbits, higher outer star inclination, $\mu_1 = \mu_2 = 0.5, i_2 = 65°, a = 40\ AU$

This so-called eccentric Kozai mechanism (EKM) has been analysed by e.g. Lithwick and Naoz (2011).

Note that in this integration, as well as all the others, the semi-major axis ratio (i.e. the semi-major axis of the outer star, since we set the semi-major axis of the inner star to one) remained effectively constant; the largest variation was 0.1%.

The next integration, shown in Figure 49, shows the effect when the outer star is brought closer to the inner binary.

In this case the resonance begins much earlier, at 10 kyr. Here we have circulation rather than libration, with a period of 36 kyr. The period of the Kozai resonance is much shorter at 11.3 kyr, the range of mutual inclination is a lower 19° and the range of eccentricity is approximately the same at 0.79.

In Figure 50 the inclination of the outer star has been increased to 90°, compared with the 65° in the case illustrated in Figure 48.

The higher inclination results in the Kozai resonance developing earlier, at around 95 kyr. Circulation has a period of 150 kyr, the period of the Kozai resonance is a shorter 76 kyr, the range of relative inclination is lower at 45° and the range of eccentricity is very high at 0.98.

The effect of increasing μ_2, i.e. increasing the mass of the outer star, is shown in Figure 51 (to be compared with Figure 48).

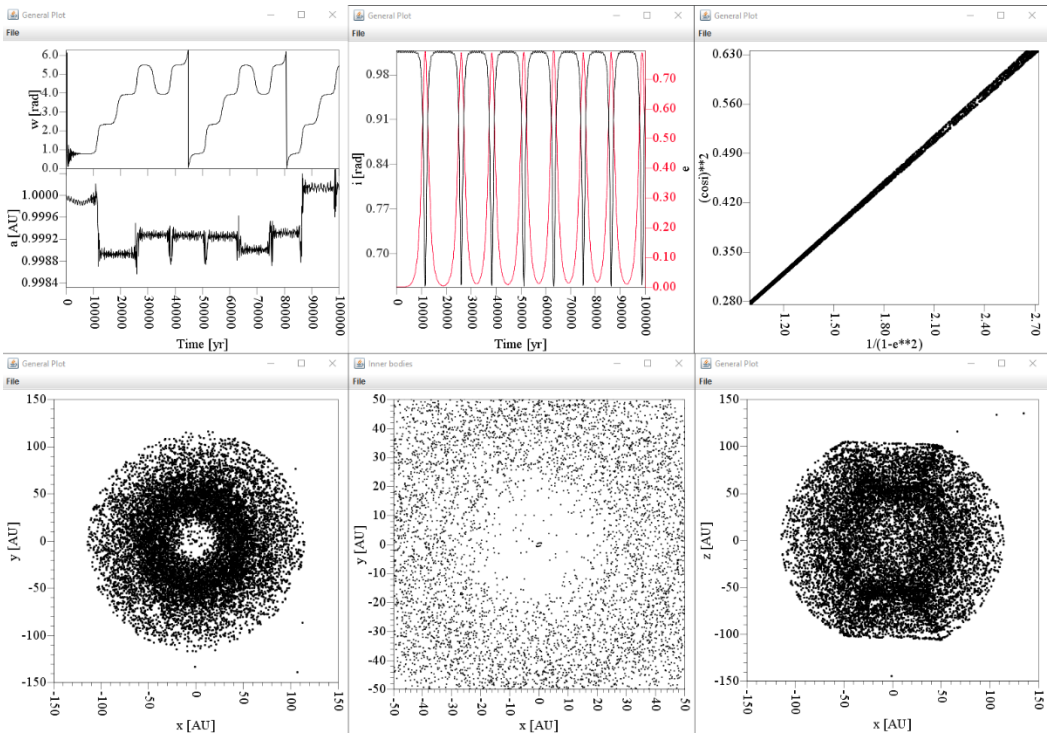

Figure 49. P1 and P2 orbits, closer outer star,
$\mu_1 = \mu_2 = 0.5, i_2 = 65°, a = 20\ AU$

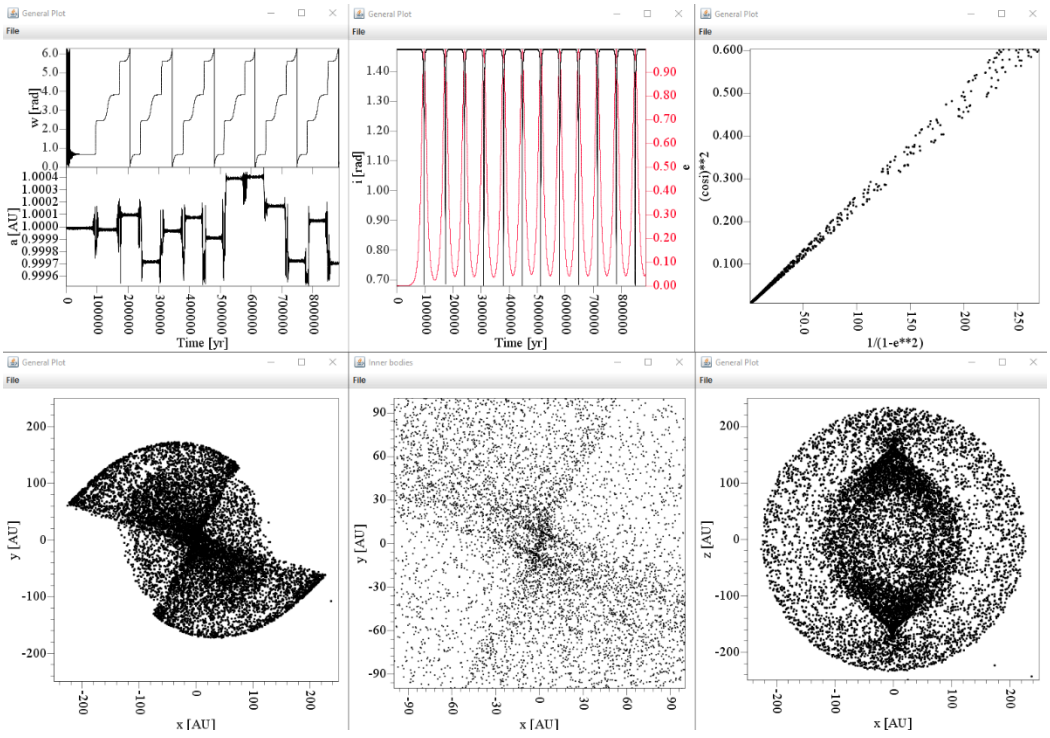

Figure 50. P1 and P2 orbits, higher outer star inclination,
$\mu_1 = 0.5, \mu_2 = 0.5, i_2 = 90°, a = 40\ AU$

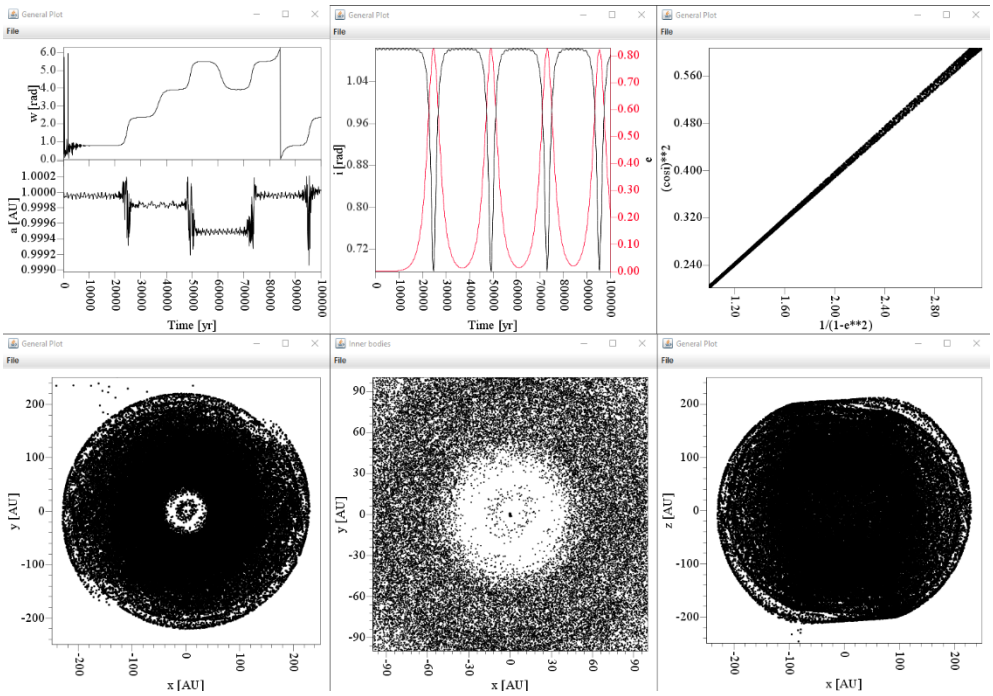

Figure 51. P1 and P2 orbits, higher outer star mass,
$\mu_1 = 0.5, \mu_2 = 2.0, i_2 = 65°, a = 40\ AU$

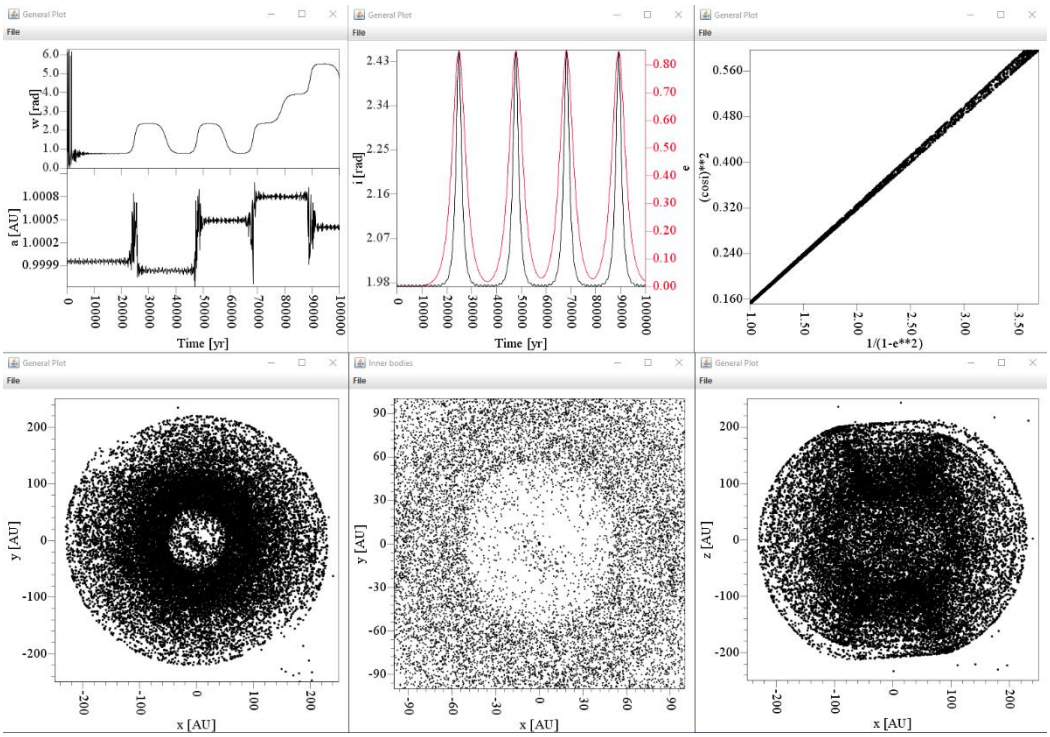

Figure 52. P1 and P2 orbits, retrograde outer star,
$\mu_1 = 0.5, \mu_2 = 2.0, i_2 = 115°, a = 40\ AU$

Compared with the equal-mass case, resonance begins earlier, at 22.3 kyr. The circulation period is 710 kyr, the period of the Kozai resonance is again much shorter at 19 kyr, the range of relative inclination is a lower 24° and the range of eccentricity is similar at 0.83.

Keeping the same mass ratios but putting the outer star into a retrograde 65° orbit (i.e. 115°) now results in the behaviour shown in Figure 52.

In the second graph of the figure the inclination is now greater than 90°, ranging between 113° and 140° or 27°. Resonance begins at a similar 20 kyr, the period of the Kozai resonance is also similar at 23 kyr, circulation has a much shorter period of 46 kyr, the range of eccentricity is essentially unchanged at 0.85 but the range of inclination of 28° is slightly higher.

The effect of changing the mass of one of the inner binary stars is shown in Figure 53 (to be compared with Figure 51).

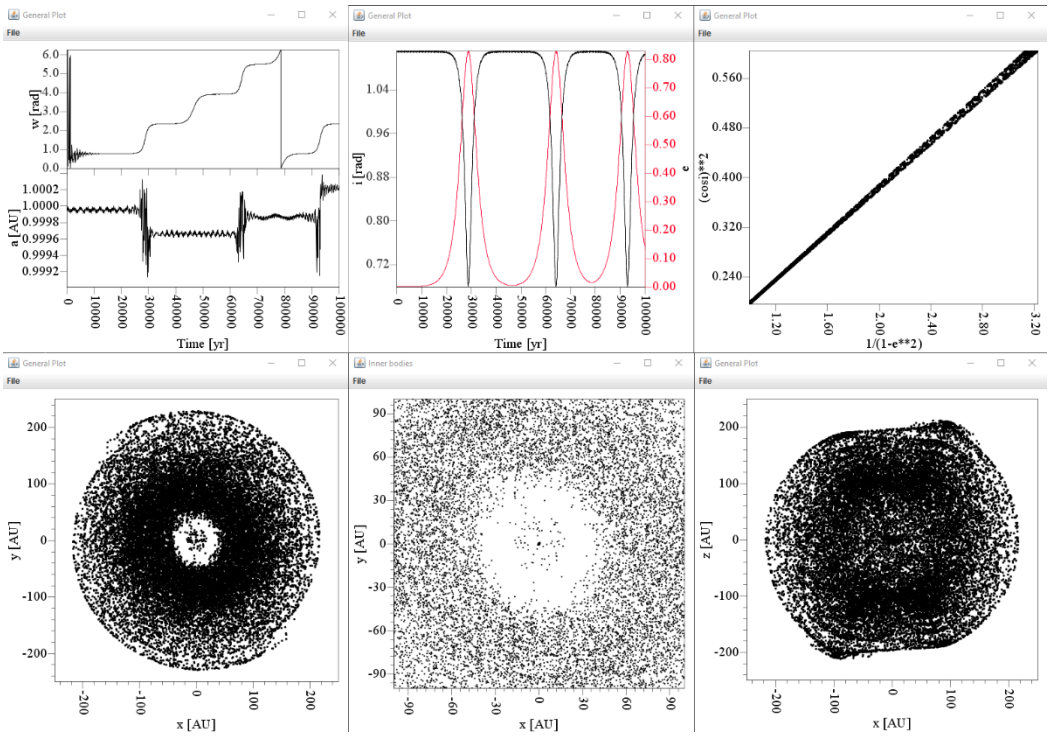

Figure 53. P1 and P2 orbits, higher outer star mass and lower inner star mass, $\mu_1 = 0.25, \mu_2 = 2.0, i_2 = 65°, a = 40\ AU$

As the mass of one of the inner stars decreases relative to the other one, resonance begins later at 27 kyr and has a longer period of 27 kyr. The circulation period of 625 kyr has shortened, the range of relative inclination is unchanged at 25° and the range of eccentricity is also the same at 0.83.

4.2.3 Analysis of stellar Kozai resonances

The data from the previous integrations are summarised in Table 34, where P and R represent prograde and retrograde orbits and KR denotes Kozai resonance. These have been extracted graphically and are approximate.

No.	Stellar parameters					Kozai parameters																
	μ_1	μ_2	i_2	a	Outer star	KR	Libration								KR	Inclination			Eccentricity			Lz
						begins	Period	Min	Max	Range	Min	Avg	Max	Range	period	Low	High	Range	Low	High	Range	
	(-)	(-)	(deg)	(-)	orbit	(kyr)	(kyr)	(rad)	(rad)	(rad)	(deg)	(deg)	(deg)	(deg)	(kyr)	(deg)	(deg)	(deg)	(-)	(-)	(-)	(-)
1	0.50	0.50	30	40	P	-	-	0.00	6.28	6.28	0	180	360	360	-	27	27	0	0.00	0.00	0.00	-
2	0.50	0.50	65	40	P	100.0	122	0.79	2.35	1.56	45	90	135	89	122.0	38	60	22	0.00	0.83	0.83	0.45
3	0.50	0.50	65	20	P	10.0	36	0.00	6.28	6.28	0	180	360	360	11.3	39	58	19	0.00	0.79	0.79	0.46
4	0.50	0.50	90	40	P	95.0	150	0.00	6.28	6.28	0	180	360	360	76.0	39	84	45	0.01	0.99	0.98	0.05
5	0.50	2.00	65	40	P	22.3	69	0.79	2.34	1.55	45	90	134	89	19.0	39	64	25	0.02	0.85	0.83	0.44
6	0.50	2.00	65	40	R	20.0	46	0.20	6.00	5.80	11	178	344	332	23.0	113	140	27	0.04	0.85	0.81	0.40
7	0.25	2.00	65	40	P	26.5	650	0.00	6.27	6.27	0	180	359	359	27.0	39	64	25	0.00	0.83	0.83	0.43

Table 34. P1 and P2 orbits. Summary of Kozai characteristics

A further 102 integrations were run with various other parameter combinations. From a qualitative examination of this larger sample the conclusions were:

1. For larger a, μ_1, μ_2 and i_2, the period of Kozai resonance is shorter and resonance begins earlier.
2. The influence of μ_1 on Kozai resonance period is the largest, followed by μ_2 and then i_2, while that of a is small.
3. Of the two Kozai resonance orbital elements, the range for inclinations is between the critical value of 39° to over 80°. The influence of i_2 on this range is strong. The change in eccentricities is large, ranging from zero to very close to one. This range does not vary much with the different configurations, but the strongest influence was again from i_2. The value of the Kozai conserved quantity L_z appeared to be reasonably constant for the same values of i_2, as shown in Table 34, but it was very different for different values of i_2.
4. The period of libration also tends to be much shorter for higher a, μ_1 and μ_2, but longer for higher i_2. Libration occurs with centering around 90° and a range of 90°. The outer star's inclination i_2 has a strong influence on this range. As previously noted, ω can either librate (oscillate around 90° or 270°) or circulate (increase or decrease continuously), and the cases with an average ω of 180° and range 360° correspond to circulation.
5. When the outer star is in a retrograde instead of prograde orbit, the resonance period and inclination range increase, but only modestly, and the eccentricity range almost not at all. However, the libration period more than doubles and the libration range also widens considerably. As usual, the edges of the stability bounds for retrograde orbits are less well defined because of the greater stability of these orbits.

The above numerical values of maximum eccentricity, Kozai resonance period and libration period can be compared with equations (3), (4) and (7) discussed in Section 3.4.3 and rewritten using our notation here, i.e.

$$e_{in,max} \cong \left[1 - \left(\frac{5}{3}\right)\cos^2(i_{initial})\right]^{\frac{1}{2}} \text{ for } i_{initial} > i_c \tag{33}$$

$$P_e \cong P_{in}\left(\frac{m_1+m_2}{m_3}\right)\left(\frac{a_2}{a_1}\right)^3 (1-e_2^2)^{\frac{3}{2}} \tag{34}$$

$$P_{lib} = \frac{4}{3\sqrt{30}} \frac{P_{out}^2}{P_{in}} \frac{\left(1-e_{out}^2\right)^{\frac{3}{2}}\left[\frac{m_1+m_2+m_3}{m_3}\right]}{\left[1-\left(\frac{5}{3}\right)\cos^2 i_{fix}\right]^{\frac{1}{2}}\sin i_{fix}} \quad (35)$$

These are compared in Table 35. The point around which libration occurs is denoted by i_{fix} and where $i_{fix} = 180°$ there is circulation rather than libration.

No.	Stellar parameters					Resonance parameters						
	μ_1	μ_2	i_2	a	Outer star orbit	i_{fix}	Libration period	Equation (35)	Kozai period	Equation (34)	e_{max}	Equation (33)
	(-)	(-)	(deg)	(-)		(deg)	(kyr)	(kyr)	(kyr)	(kyr)	(-)	(-)
2	0.50	0.50	65	40	Prograde	90	122	46.7	122	128	0.83	0.84
3	0.50	0.50	65	20	Prograde	180	36	-	11	16	0.79	0.84
4	0.50	0.50	90	40	Prograde	180	150	-	76	128	0.99	1.00
5	0.50	2.00	65	40	Prograde	90	69	23.4	19	32	0.85	0.84
6	0.50	2.00	65	40	Retrograde	178	46	-	23	32	0.85	0.84
7	0.25	2.00	65	40	Prograde	180	650	-	27	32	0.83	0.84

Table 35. P1 and P2 orbits. Comparison of libration periods, Kozai resonance periods and maximum eccentricity

For the libration periods and Kozai resonance periods the correspondence is somewhat better than order-of-magnitude, with absolute errors averaging ~40%. The performance of $e_{in,max}$ is much better, with an average absolute error of only ~2%.

While this limited overview of stellar Kozai effects is interesting, the intention is not to map their characteristics in triple systems *per se*; we are more interested in their influence on the stability of the P-type planetary orbits. These two strong influences on planetary stability, i.e. the simple inclination of the outer star and of the Kozai motion, cannot be separated as they are interlinked (for inclinations greater than the critical inclination).

4.2.4 Planetary stability bounds and the outer star's inclination

In this section we examine the effect of stellar Kozai resonance on the sculpting of the shape of the stable region, as manifested by the test particle cloud. We do not address Kozai resonance of the individual planets, i.e. test particles, themselves.

Characteristics of the stellar configurations used

For the relatively small values of inclination for the outer star used in the previous quasi-coplanar regressions, there was no significant relationship between inclination and the inner and outer bounds. A series of integrations was now run to examine any relationship between these variables for higher inclinations. Both prograde and retrograde stellar orbits were used, but only prograde planetary motions were considered.

As the Kozai critical angle of 39° is theoretical and applicable to test particles only, whereas we are using a relatively massive outer star, this critical angle may

no longer be applicable as a criterion for Kozai resonance, so the integrations were instead split into what were experimentally determined to be non-Kozai and Kozai regimes, i.e. those of relatively low inclination whose nodes circulate and those of high inclination where the nodes librate about 90° or 270°. In practical terms, we know that for real bodies, as opposed to test particles:

1. The critical inclination is larger than the theoretical 39°, e.g. Grishin et al. (2017).
2. If the ratio of initial angular momentum of the outer orbit to that of the inner orbit is $\gtrsim$4 then significant Kozai resonance usually occurs, e.g. Beust et al. (2012).

In the integrations, the orbital parameters of the triple were selected to display Kozai resonance. They are shown in the table inside Figure 54, together with the resulting distribution of angular momentum ratios.

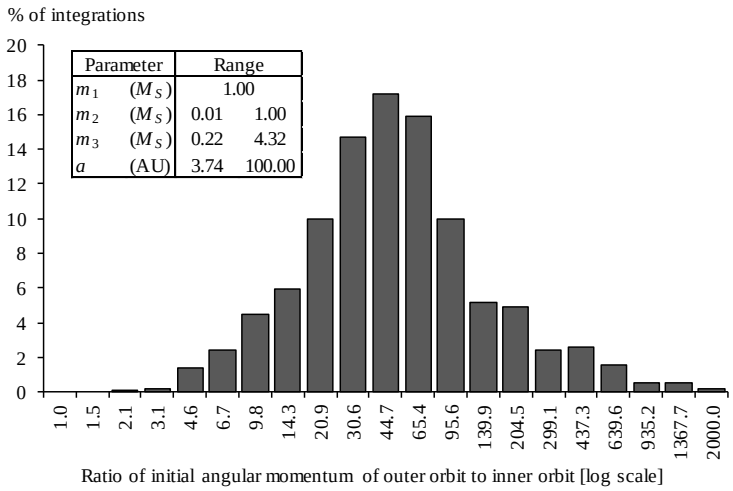

Figure 54. Angular momentum ratio distribution for Kozai integrations

The number of instances where the angular momentum ratio was not $\gtrsim$ 4 was negligible, so the sole determinant of whether Kozai resonance would occur in our sample of configurations was the outer star's inclination i_2.

For the integrations the sample was first split into the prograde and retrograde stellar cases. Each case was then split into the subsets where Kozai resonance did or did not occur.

Results of the integrations

Figure 55 shows the critical semi-major axis ratios for the inner and outer planetary orbits against the "absolute" inclination i_2 (i.e. i_2 for prograde orbits and $180° - i_2$ for retrograde orbits), for both Kozai and non-Kozai regimes. As usual, there is more scatter for inner orbits than outer orbits.

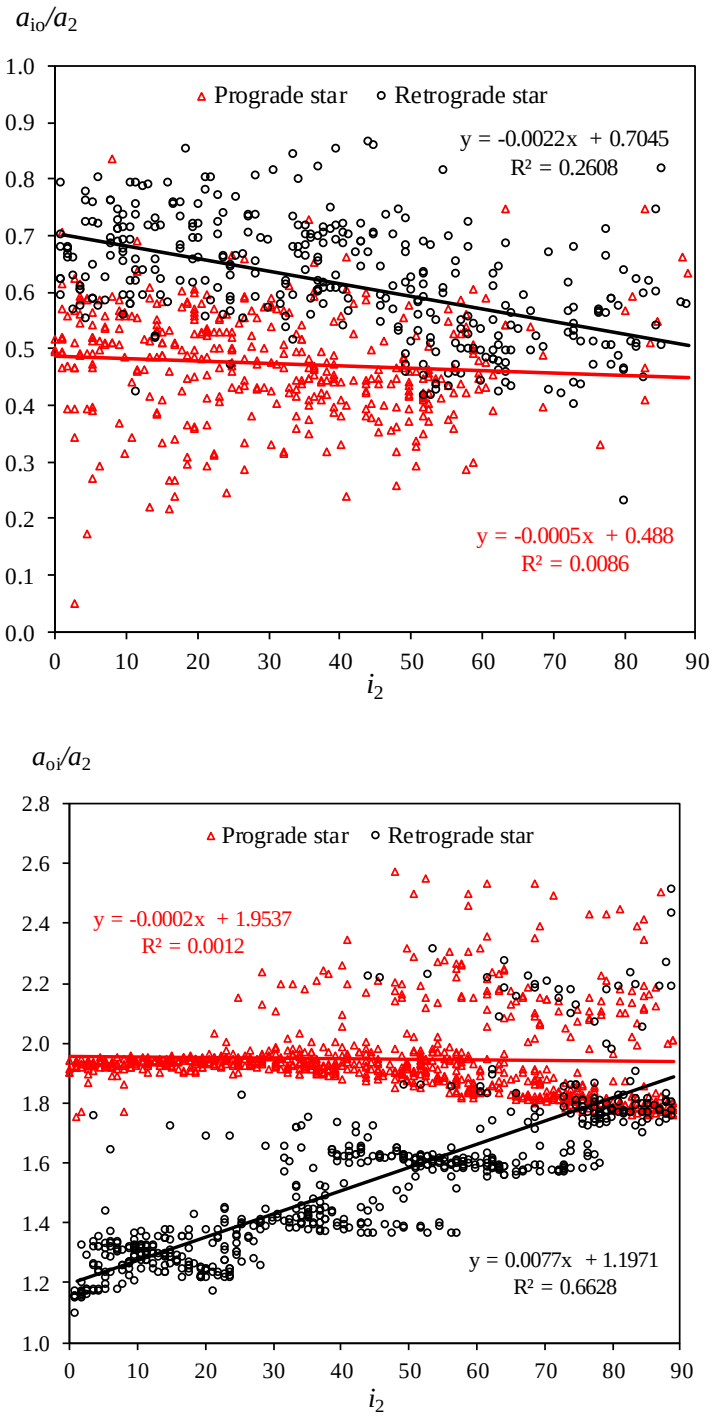

Figure 55. P1 and P2 orbits. Critical semi-major axis ratios versus outer star inclination a) inner stability bound b) outer stability bound

For inner orbits, the critical semi-major axis ratio has almost no dependence on the outer star's inclination for prograde stellar orbits, and only a weak one for retrograde orbits. Retrograde stellar orbits allow the stable planetary region to extend further out because of greater dynamic stability (with a regression constant representing a semi-major axis ratio of 0.70 versus 0.49), but as inclination approaches 90°, this benefit decreases. (The regression lines should, theoretically, coincide at 90°, for both inner and outer orbits.)

For outer orbits, the critical ratio also has no dependence on inclination for prograde stellar orbits. However, it can be seen in Figure 55 b) that this low average dependence is made up of two parts. For low inclinations the critical ratio is constant at 1.92, but as inclinations increase the critical ratio begins to decline, i.e. the orbital stability bound begins to move inwards. This makes intuitive sense because once Kozai resonance begins, as the outer star's inclination increases, the eccentricity of the inner binary decreases, which allows this to occur.

This divergence begins at around 45° and is probably a manifestation of the start of Kozai resonance. This suggests that for real bodies that may also be relatively large, Kozai resonance is more likely to begin when $i_2 \gtrsim 45°$ than for $i_2 > 39°$.

Interestingly, for retrograde stellar orbits dependence on i_2 is much stronger. In this case planetary orbits can again approach much closer to the outer star (with a regression constant representing a semi-major axis ratio of 1.2 versus 1.9), but this increased stability declines as inclination rises to 90°. Also of interest are the regions of stability interspersed with gaps of instability, which is similar to that seen in Figure 33. This characteristic was not seen in any of the other orbits types.

The mean semi-major axis ratios for the non-Kozai and Kozai cases are shown in Table 36.

Orbit type	Regime	N	Mean stable critical ratio	Δ (%)	SD	Min	Max
Prograde outer star							
Inner	Non-Kozai	256	0.484		0.099	0.049	0.837
a_{io}/a_2	Kozai	47	0.495	2.2	0.100	0.288	0.748
Outer	Non-Kozai	341	1.941		0.051	1.755	2.242
a_{oi}/a_2	Kozai	317	1.933	-0.4	0.176	1.759	2.532
Retrograde outer star							
Inner	Non-Kozai	177	0.666		0.078	0.423	0.853
a_{io}/a_2	Kozai	101	0.531	-20.4 *	0.096	0.105	0.818
Outer	Non-Kozai	272	1.335		0.126	1.095	1.820
a_{oi}/a_2	Kozai	204	1.753	31.3 *	0.195	1.363	2.510

* Differences significant at the 5% level

Table 36. Non-Kozai and Kozai cases, mean critical semi-major axis ratios for prograde and retrograde stellar orbits

Two points may be made from the table:

1. Generally, with a retrograde outer star the inner orbits move outwards towards this star and the outer orbits move inwards; both these motions are towards the star and reflect the greater stability of retrograde orbits, as previously found.
2. For a prograde outer star, the existence of Kozai resonance makes no difference to the critical ratios of either the inner or outer bounds, which remain virtually identical. For a retrograde outer star, however, the bounds are very different. When Kozai resonance occurs the inner bound contracts

inwards, while the outer bound moves outwards, and by a larger proportional amount.

For both inner and outer orbits these movements are in a direction opposite to that usually induced by a retrograde stellar orbit. This suggests that Kozai resonance increases planetary instability, which should not be surprising.

At the 5% level of significance, the critical semi-major axis ratios for planetary orbits under non-Kozai and Kozai regimes do not differ for a prograde outer body, but for the retrograde case they are substantially different, by an absolute 20%-30%. The number of inner orbits that could be found under Kozai resonance with a prograde outer star was very small.

The regression data for the four cases may be found in Appendix C and in Table 85, and are summarised visually in Figure 56.

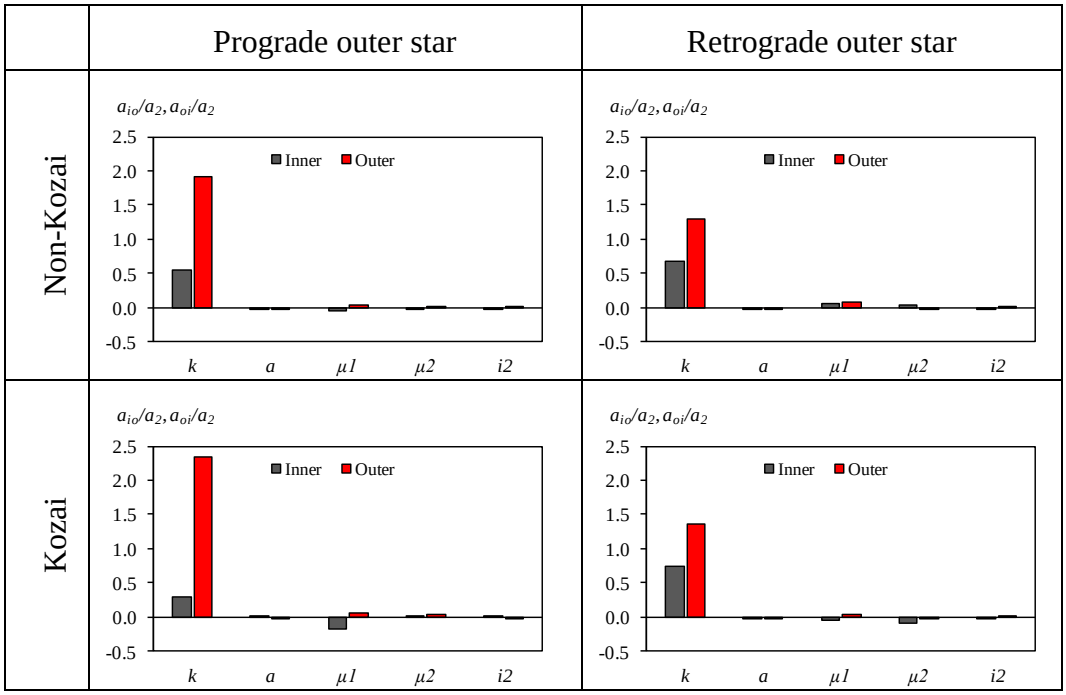

Figure 56. P1 and P2 orbits. Regression results for non-Kozai and Kozai regimes

None of the orbital parameters have any significant influence on the critical semi-major axis ratio, with the possible exception of μ_1 in the prograde star/Kozai case. This stability bound is therefore effectively represented by the constant, which also reflects the two points made previously.

The data for the constant in the four cases is summarised in Table 37.

For a prograde outer star, Kozai resonance results in the constant being 44% smaller for inner orbits and 22% larger for outer orbits, while a retrograde outer body does not cause a significant difference in either constant. Note that Table 36 and Table 37 are not inconsistent – the large differences in mean critical ratio are in the retrograde stellar case whereas the large differences in the constant are found for the prograde case.

Orbit type	Regime	N	Unstandardized			*t*	95%	
			Constant	Δ (%)	Std. Error		Lower Bound	Upper Bound
Prograde outer star								
Inner	Non-Kozai	256	.545		.032	17.2	.483	.607
a_{io}/a_2	Kozai	47	.303	-44	.130	2.3	.041	.566
Outer	Non-Kozai	341	1.92		0.01	207.6	1.90	1.94
a_{oi}/a_2	Kozai	317	2.35	22	.049	47.7	2.25	2.44
Retrograde outer star								
Inner	Non-Kozai	177	.685		.024	28.0	.637	.733
a_{io}/a_2	Kozai	101	.738	8	.086	8.6	.567	.908
Outer	Non-Kozai	272	1.29		0.02	67.4	1.25	1.33
a_{oi}/a_2	Kozai	204	1.36	5	0.07	18.3	1.21	1.50

Table 37. P1 and P2 orbits. Regression constants for non-Kozai and Kozai regimes

The Kozai bulge

The next question is whether there exists any relationship between the vertical extent of the stable region for planets and the outer star's inclination.

The scatter plots in Figure 55 do not reveal some details of the dependence of the orbit bounds on the outer star's inclination. Using the same data as in Figure 55 b), Figure 57 shows the relationship for four outer orbits, where $e_1 = e_2 = i_1 = \Omega_2 = \omega_2 = 0$ and the remaining configuration parameters are as shown in the legend. These latter parameters were selected to show Kozai resonances increasing from weak to strong. Here the full range of inclinations is shown, i.e. the actual value of i_2, from 0° to 180°, is used instead of the "absolute" inclination in the scatter plot. The outer star and planets were in prograde orbits and the integration time was 10^5 yr.

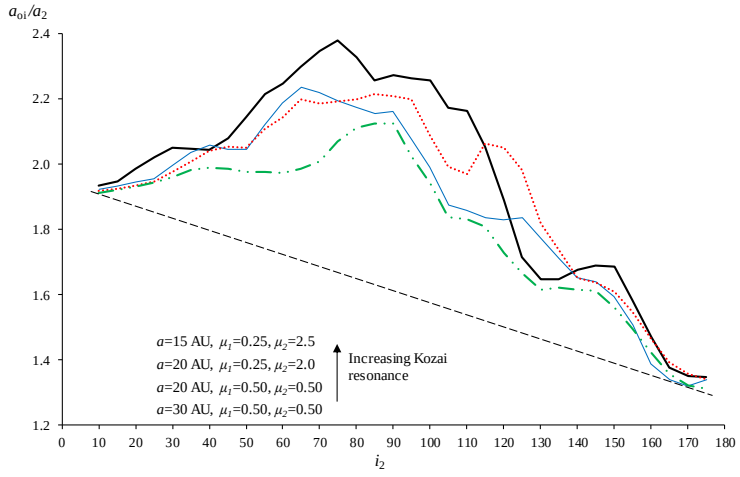

Figure 57. P1 and P2 orbits. Outer critical semi-major axis ratio versus outer star inclination (smoothed)

The general contraction of the outer bound as i_2 increases from zero to 180° remains the same as shown in Figure 55 b). However, what becomes visible is that for stellar inclinations between $\sim 45° - 135°$ (i.e. in the range where Kozai resonance occurs) there is a large shift outwards of this bound of up to ~20%, with this bulge being in the direction opposite to the general trend.

This increase in the critical semi-major axis ratio appears to be related to the strength of the Kozai resonance. Examining the underlying data, as the strength of the Kozai resonance increases,

1. The periods of libration and of the resonance shorten;
2. The Kozai *i-e* relationship weakens; and
3. The z-range of the P-orbit stability bound decreases strongly.

The last point may be seen from Figure 58 to Figure 60, which show the stable regions, identically scaled, for three of the cases shown in Figure 57, in order of increasing strength of Kozai resonance. The integrations were all at $i_2 = 70°$ and were run for 10^5 yr.

The vertical extent of stable planetary orbits more than halves, from 170 AU to 80 AU (although the absolute values are irrelevant as they are largely determined by where the test particle cloud is truncated in the *x-y* plane).

The stellar Kozai resonance increases as the outer star comes closer to the binary and as its inclination increases. In the first case this causes the planetary orbits to become less highly-inclined and to contract in the *z*-direction, while in the second case this results in a larger variation in the eccentricity of the inner binary, causing a larger clearing of the inner region, evidenced by the central "hole" in the horizontal projections becoming more visible in the previous three figures.

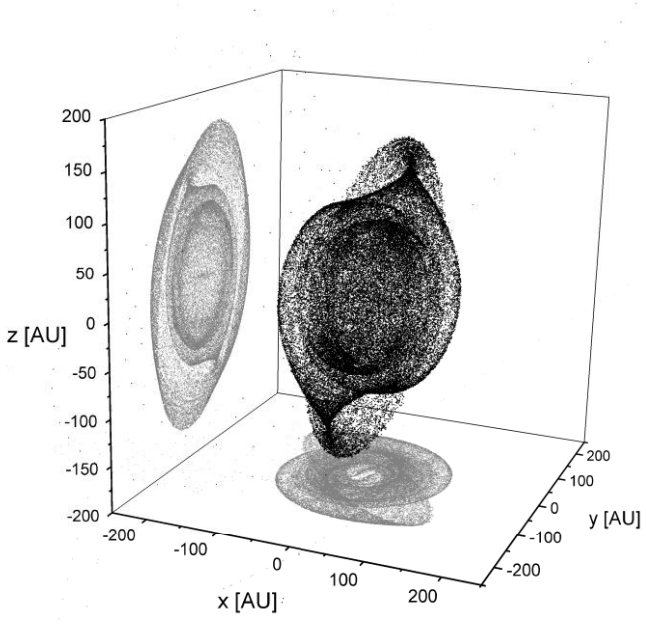

Figure 58. P1 and P2 orbits under Kozai resonance, $a = 30\ AU,\ \mu_1 = 0.5,\ \mu_2 = 0.5$

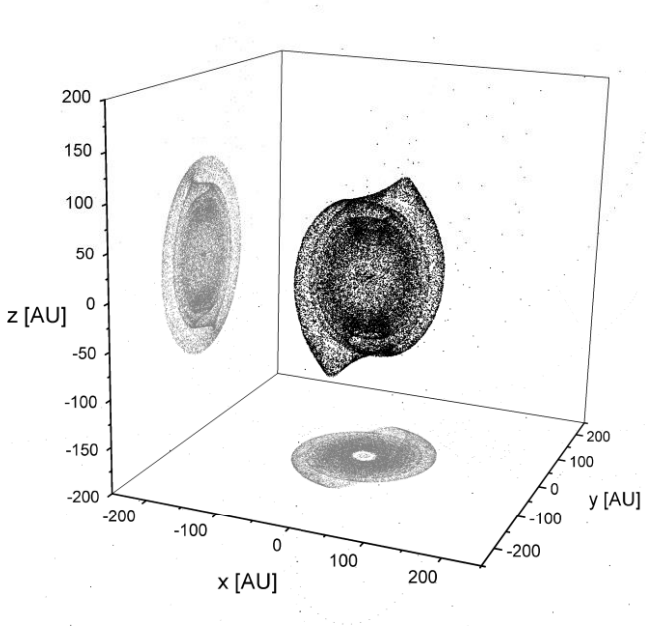

Figure 59. P1 and P2 orbits under Kozai resonance, $a = 20\ AU,\ \mu_1 = 0.5,\ \mu_2 = 0.5$

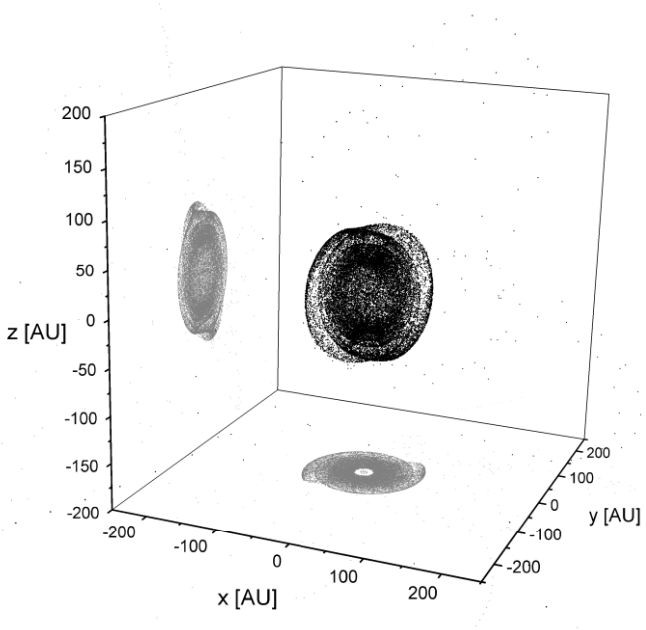

Figure 60. P1 and P2 orbits under Kozai resonance, $a = 15\ AU,\ \mu_1 = 0.25,\ \mu_2 = 2.5$

There is no similar analysis for the inner orbits, because when there are strong Kozai effects there are also usually no well-defined inner orbit bounds.

In summary:

1. For real bodies that may also be relatively large, Kozai resonance tends to occur when $45° < i_2 < 135°$.
2. The dependence of the planetary orbital stability bounds on inclination is much stronger for retrograde stellar orbits than prograde ones. In the

retrograde case, when Kozai resonance occurs the inner bound contracts inwards, while the outer bound moves outwards, by a larger proportional amount.

3. For inner planetary orbits, the critical semi-major axis ratio has almost no dependence on the outer star's inclination. While a retrograde outer stellar orbit allows the stable planetary region to extend further out, this benefit decreases as inclination approaches 90°.
4. For outer planetary orbits, at low stellar inclinations the critical ratio is constant, but as inclinations increase from zero to 180° the orbital stability bound begins to move inwards. However, in the region of inclinations where Kozai resonance occurs, there is a significant contrary outward shift which exceeds this general trend.

4.2.5 Comparison with previous work on non-coplanar orbits

There are a few studies that are of tangential interest to the work in this section.

A study of binaries with inclined circumbinary planetary orbits by Doolin and Blundell (2011) found three distinct modes of orbital behaviour for non-coplanar orbits. These were 1) close-to-coplanar prograde ($i \sim 0$); 2) close-to-coplanar retrograde ($i \sim 180°$), where these orbits precess in the longitude of the ascending node; and 3) close-to-polar orbits ($i \sim 90°$ and $\omega \sim \pm 90°$), which have their longitude of ascending node and inclination coupled to precess about the centre of an island of libration.

As mentioned in Section 1.4, Verrier and Evans (2009) examined the dynamics of planetesimals in the specific quadruple star system HD 98800, where test particles in circumbinary polar orbits about the inner binary appeared to evade Kozai instability. They concluded that high mutual planet-star inclinations are very likely, and that if regions of stability exist, planetary systems may be found in them.

Kennedy et al. (2012) suggest that the misaligned circumbinary debris disc around 99 Herculis can be explained by a ring of polar orbits that move in a plane perpendicular to the binary pericentre direction and discuss possible shapes of test particle clouds, which were also generated by the Swift-HJS code.

Hamers et al. (2015) studied the evolution of short-period main sequence binaries within triple systems, where circumbinary planets can change this evolution significantly, by either shielding the inner binary from Kozai cycles induced by the tertiary or undergoing Kozai resonance itself and either being ejected or surviving in an inclined and eccentric orbit.

Pejcha et al. (2013) focused mainly on stellar, rather than planetary, Kozai effects in quadruple systems, comparing them to triple stellar systems. However, they touch on the interesting case where the inner “binary” consists of a star and a planet in orbit around a distant binary (equivalent to our S3-type orbit in a later section), suggesting that the planet can experience the eccentric Kozai mechanism, resulting in both high eccentricity and the frequent occurrence of orbital flips, which could explain the abundance of retrograde hot Jupiters.

4.2.6 Observational examples of stellar Kozai resonance in triples

As a stellar example, HD 109648 is a triple comprising three stars with approximately equal masses of around 1 M_s, with a compact inner binary of period ~5 days and relative orbital inclination of $6° \leq i \leq 54°$. The significantly non-zero eccentricity of 0.0119 of the inner orbit has been attributed to perturbation by the outer companion. A similar situation applies to HD 284163, consisting of an inner pair of masses 0.72 M_s and 0.33 M_s in a 2.4-day orbit, with a smaller outer star of 0.5 M_s at 7.4 AU, where the inner binary has an eccentricity of 0.057. Another triple, β Per, consists of an inner binary of masses 1.7 M_s and 3.7 M_s and period 2.87 days and an outer body of 1.7 M_s with a 1.86 yr period; it has an inner eccentricity of 0.0653. In all these cases, discussed by Ford, Kozinsky and Rasio (2000), tidal dissipation should have led to circularised inner orbits, so their significantly different eccentricities point to Kozai resonance as a possible cause.

Another example is TY Coronae Australis (TY Cra), mentioned by Beust (2003), made up of a close binary of masses 3.1 $M_s$and 1.6 M_s and period 2. 88 days orbited by an outer star of 1.26 M_s at ~1.5 AU, with a very high mutual orbital inclination of around 85° (using updated observations).

4.2.7 The limitations of a theoretical approach

Section 2.1 briefly mentioned the inadequacy in many situations of theoretical approaches to the analysis of stability. We are now better able to substantiate this statement with an illustration of the limits of theoretical approximations and how they break down. We do this by comparing the theoretical analysis of a high-inclination triple with the numerical results from integrations.

The configuration of this triple is an equal-stellar mass, high-inclination case with both orbits eccentric and a 90° longitude of ascending node. The parameters used were: $a = 20$ AU, $\mu_1 = 0.5$, $\mu_2 = 0.5, e_1 = 0.5$, $e_2 = 0.5$, $i_1 = 0°$, $i_2 = 60°, \Omega_2 = 90°$ and $\omega_2 = 0°$.

In their paper on the secular three-body problem Farago and Laskar (2010) address two limiting cases, the inner restricted problem, where the inner body (i.e. our Star 2) has no mass, and the outer restricted problem, where the outer body (Star 3) has negligible mass. They used the latter approximation to explain the finding that small bodies with very high inclinations around one of the binaries of the double binary HD 98800 remain stable despite the perturbation of the other binary (Verrier & Evans 2008; Verrier & Evans 2009). We developed the approximation for the outer restricted model and compared its results with the output of a numerical integration.

In this model there are no restrictions on the negligible-mass particle (i.e. planet) regarding its inclination or eccentricity. The Hamiltonian is given by

$$\langle H \rangle = -k[2\cos^2 i_2 - e_1^2 \sin^2 i_2 (3 - 5\cos 2\Omega_2)] \quad (36)$$

where

$$k = -\frac{\alpha G_2}{4}$$

$$\alpha = \frac{3}{4} n_1 \left(\frac{a_1}{a_2}\right)^{\frac{7}{2}} \frac{\beta_1}{M_{01}} \frac{1}{(1-e_2^2)^2}$$

$n_1 = \sqrt{\frac{GM_{01}}{a_1^3}}$ is the mean motion of the binary

$\beta_1 = \frac{m_0 m_1}{m_0 + m_1}$ is the reduced mass

$M_{01} = m_0 + m_1$ is the mass of the system

$G_2 = \sqrt{GM_{01}a_2(1-e_2^2)}$ is the angular momentum of the particle

$G =$ the gravitational constant

$m_0 =$ mass of Star 1

$m_1 =$ mass of Star 2

$a_1 =$ semi-major axis of the inner binary

$a_2 =$ semi-major axis of a particle

$e_1 =$ eccentricity of the binary

$e_2 =$ eccentricity of the particle

$i_2 =$ inclination of the particle

Transforming equation (36) with new variables $p = i_2 \cos\Omega_2$, $q = i_2 \sin\Omega_2$ results in

$$\langle H \rangle = k\left(\frac{1.25p^2 + (0.75p^2 + 2q^2)\cos[2\sqrt{p^2+q^2}]}{p^2+q^2}\right) \tag{37}$$

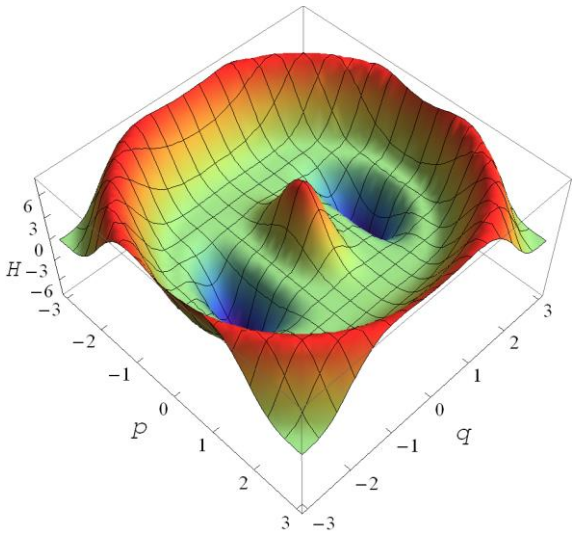

Figure 61. Outer restricted approximation, Hamiltonian surface

For the example configuration used, the general form of the three-dimensional surface defined by the Hamiltonian is shown in Figure 61, for $k = 1$.

The contours for the Hamiltonian for different values of k are shown in Figure 62. (This configuration is, coincidentally, essentially the same as that illustrated by Doolin and Blundell (2011)).

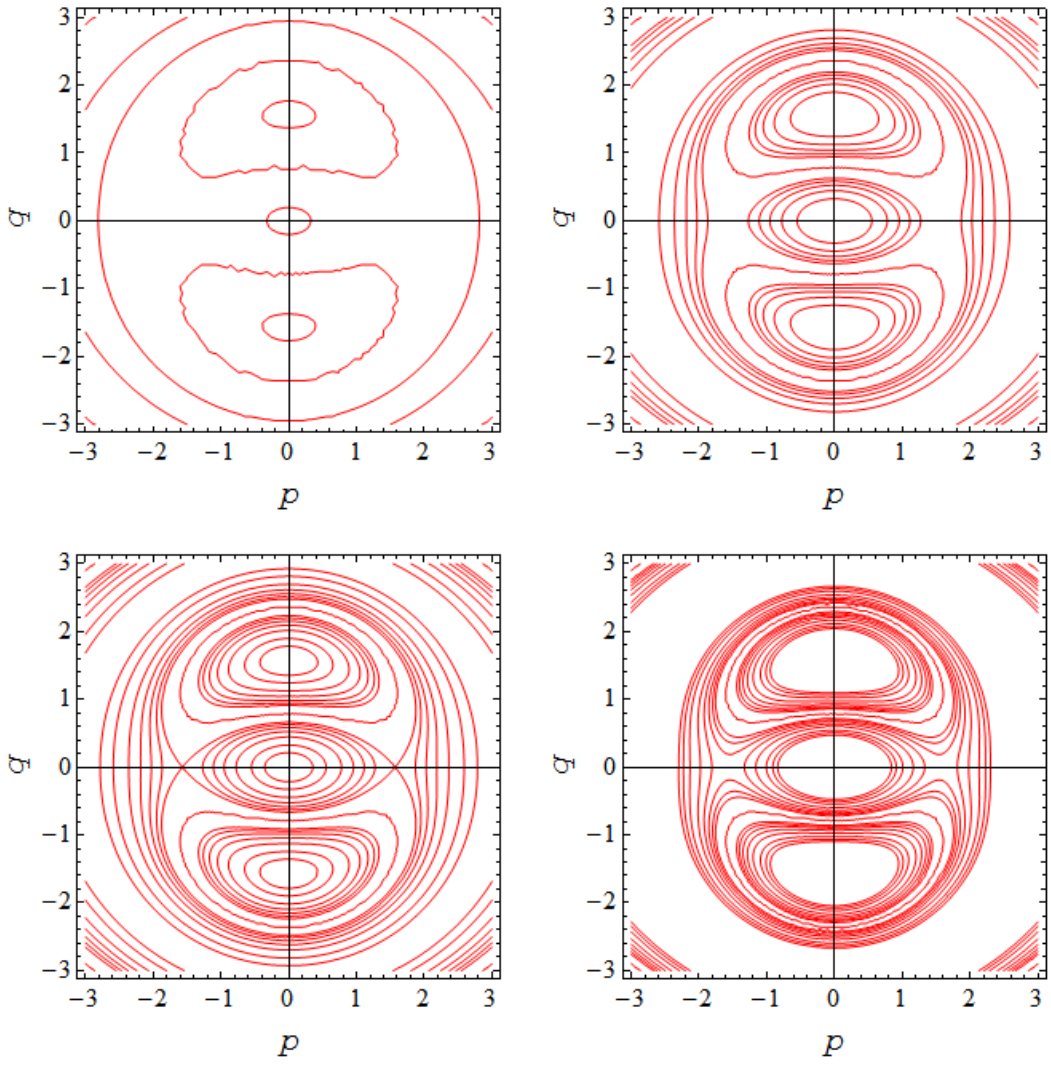

Figure 62. Outer restricted approximation, curves of constant Hamiltonian for values of k of a) 0.02 b) 0.5 c) 1.0 d) 5.0. Contours cover the range $H = [-8, 8]$

We then compared this approximation with the numerical integration of this case where the outer body has a non-negligible mass that is comparable to the stars in the inner binary, using $m_0 = m_1 = m_2 = 1\ M_S$. The integration was run using an initial 10 000 test particles that left 3 637 survivors after 10^6 yr. The initial inclination of the test particles ranged between 0° and 90°, resulting in an initially spherical cloud. The cloud at the end of the integration is shown in Figure 63; it remains spherical, with a higher-density internal shell.

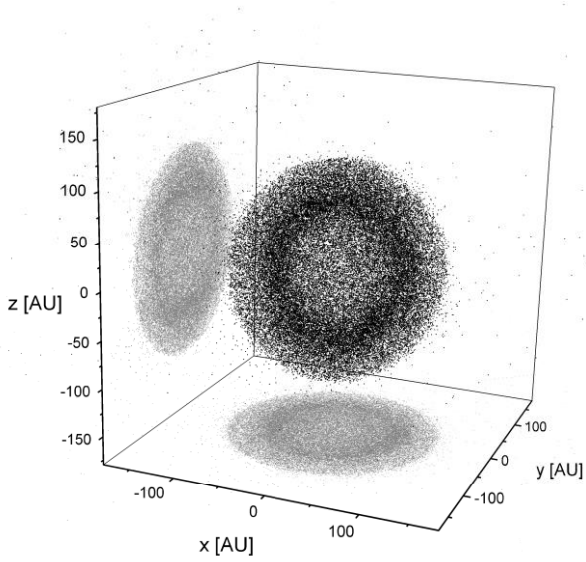

Figure 63. P1 and P2 orbits. High-inclination example, $a = 20\ AU,\ \mu_1 = 0.5,\ \mu_2 = 0.5, e_1 = 0.5,\ e_2 = 0.5,\ i_1 = 0°,\ i_2 = 60°, \Omega_2 = 90°,\ \omega_2 = 0°$

The surviving test particles were then plotted on the (p, q) plane using the *p-q* transformations used previously. The results are shown in Figure 64 a). In Figure 64 b) this test particle distribution is then overlaid on the contour plot from Figure 62 c).

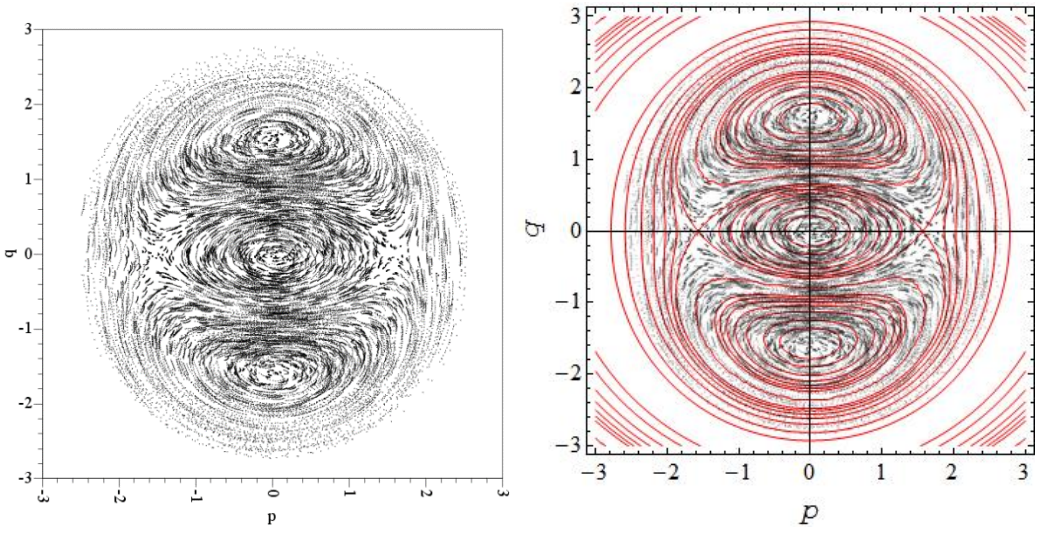

Figure 64. P1 and P2 orbits. a) final distribution in the p-q plane of test particles from an initial spherical cloud b) test particle distribution overlaid with curves of constant Hamiltonian

The correspondence between the model and the test particle distribution is very good, with no discernible differences. The model appears to perform well, given that the outer star's mass is far from negligible. Similar transformed test particle distributions result from a wide combination of outer mass ratios and outer star inclinations in the ranges $\mu_2 = [0.05, 2.5]$ and $i_2 = [20°, 80°]$ respectively.

However, a more appropriate starting configuration may be a tilted disc, on the basis that most planets will form in a circumstellar disc whose plane will be close to the invariable plane (as opposed to random capture). Beginning with an initial test particle cloud in the form of a disc aligned with the invariable plane instead of a spherical cloud then results in a very different distribution, as shown in Figure 65.

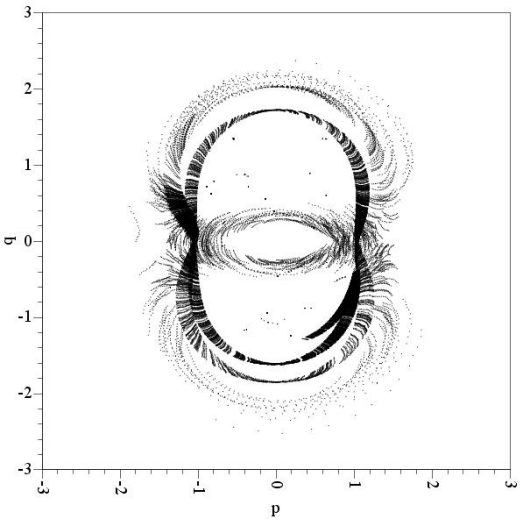

Figure 65. P1 and P2 orbits. Final distribution in the p-q plane of test particles from an initial disc aligned with the invariable plane

A further 24 integrations were performed, for outer mass ratios ranging from 0.01 to 2.5 (an outer mass ratio as high as 2.5 is not implausible, as discussed in Section 3.6.5.) and outer star inclinations from 30° to 80°. The remaining parameters were unchanged and all integrations were for 10^6 yr. These are collected in Appendix B, with some selected cases shown in Figure 66.

The distributions most resembling that in Figure 64 a), although the resemblance is weak, are a) and d), i.e. for outer mass ratios between 0.25 and 1.0 and outer inclinations around 40°. The characteristic features of the theoretical distribution generally erode for higher outer inclinations and, interestingly, for *lower* outer mass ratios, irrespective of inclination (see Appendix B). As the outer mass ratio increases beyond 1.0 and inclinations increase past 40°, the characteristic structure of the outer lobes first breaks down, after which the inner lobe disappears, with the accuracy of the approximation declining rapidly

This illustrates that theoretical approximations can be unsuitable for studies that encompass the full range of possible configurations of real triples.

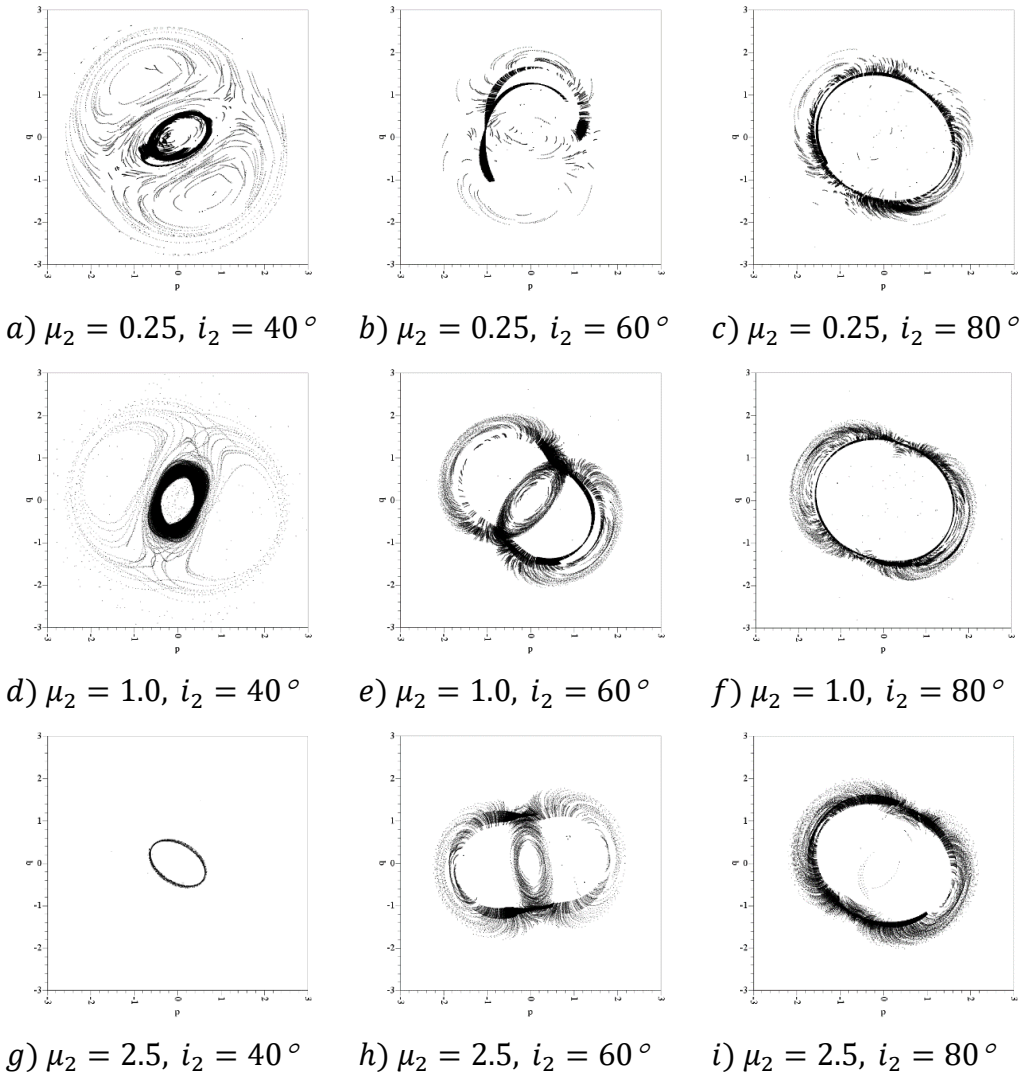

$a)\ \mu_2 = 0.25,\ i_2 = 40^\circ$ $b)\ \mu_2 = 0.25,\ i_2 = 60^\circ$ $c)\ \mu_2 = 0.25,\ i_2 = 80^\circ$

$d)\ \mu_2 = 1.0,\ i_2 = 40^\circ$ $e)\ \mu_2 = 1.0,\ i_2 = 60^\circ$ $f)\ \mu_2 = 1.0,\ i_2 = 80^\circ$

$g)\ \mu_2 = 2.5,\ i_2 = 40^\circ$ $h)\ \mu_2 = 2.5,\ i_2 = 60^\circ$ $i)\ \mu_2 = 2.5,\ i_2 = 80^\circ$

Figure 66. P1 and P2 orbits. Final distribution in the p-q plane of test particles from initial discs aligned with the invariable plane, for various outer mass ratios and inclinations

4.2.8 Conclusions – highly inclined triple systems

In highly inclined triples, test particle with circular orbits initially coplanar with the invariable plane evolve with semi-major axes that remain constant and orbits that remain circular, librate and become more inclined over time, eventually oscillating around a final inclination, with some developing Kozai resonance or undergoing orbit flipping into retrograde motion. The number of stable orbital bounds falls exponentially with increasing inclination.

Analysis of a limited sample of stellar Kozai resonances in triples showed that for larger a, μ_1, μ_2 and i_2, the period of the Kozai resonance is shorter and resonance begins earlier, with the influence of μ_1 on the Kozai resonance period being the largest, followed by μ_2 and i_2, and that of a being small. Of the two Kozai resonance orbital elements, the range for inclination was between the critical value of 39° to over 80°, with a strong influence from i_2. The change in eccentricities was large, ranging from zero to very close to one. The period of

libration was much shorter for higher a, μ_1 and μ_2, but longer for higher i_2. Libration occurs with a centering around 90° and a range of 90°, again strongly influenced by i_2. For retrograde stellar orbits the resonance period and inclination range increased modestly, but the libration period more than doubled and the libration range widened considerably. Comparing the numerical results with the theoretical equations, the libration periods and Kozai resonance periods differed by ~40% while maximum eccentricity was within ~2%.

Extracting and comparing the critical semi-major axis ratios under Kozai and non-Kozai regimes and analysing the effect of stellar Kozai resonance on the sculpting of the shape of the stable region showed that for the inner stability bound, the critical semi-major axis ratio had little dependence on the outer star's inclination. For the outer stability bound, there is no dependence at low inclinations, but as the stellar inclination increases the critical semi-major axis ratio begins to decline, since the eccentricity of the inner binary decreases, causing this. This divergence begins at around 45° as a result of stellar Kozai resonance beginning. For retrograde stellar orbits dependence on i_2 is generally much stronger. For a prograde outer star, stellar Kozai resonance has no effect on the critical ratios of the inner or outer bounds. For a retrograde outer star, however, when Kozai resonance occurs the inner bound contracts inwards, while the outer bound moves outwards, by a larger proportional amount. These movements are in the opposite direction to the general effect of a retrograde stellar orbit, indicating that Kozai resonance increases planetary instability. While the semi-major axis ratio of the outer bound shows an overall decrease as i_2 increases from zero to 180°, between $\sim 45° - 135°$, where Kozai resonance occurs, there is an increase of up to ~20%, which appears to be related to the strength of the Kozai resonance.

A comparison of the theoretical and numerical results for the analysis of a high-outer mass, high-inclination triple confirms that theoretical approximations are inadequate for the analysis of realistic triple systems and a numerical approach is necessary.

4.3 Orbit Type S1/S2

4.3.1 Configuration

The investigation of S-type orbits in triples has a direct application to searches for extrasolar planets, since radial velocity variations are easier to measure for planets close to their host stars.

Some early stability studies of S-type and P-type orbits in binaries included Harrington (1977), Szebehely (1980), Dvorak (1984), Dvorak, Froeschle and Froeschle (1986), Rabl and Dvorak (1988), Dvorak, Froeschle and Froeschle (1989), Holman and Wiegert (1999) and Musielak et al. (2005). These largely circular, coplanar models were extended to other eccentricities by Pilat-Lohinger and Dvorak (2002) and inclined P-type orbits for equal-mass binaries by Pilat-Lohinger, Funk and Dvorak (2003).

The stellar configuration for the triple and the region of interest containing S1 planetary orbits is shown in Figure 67.

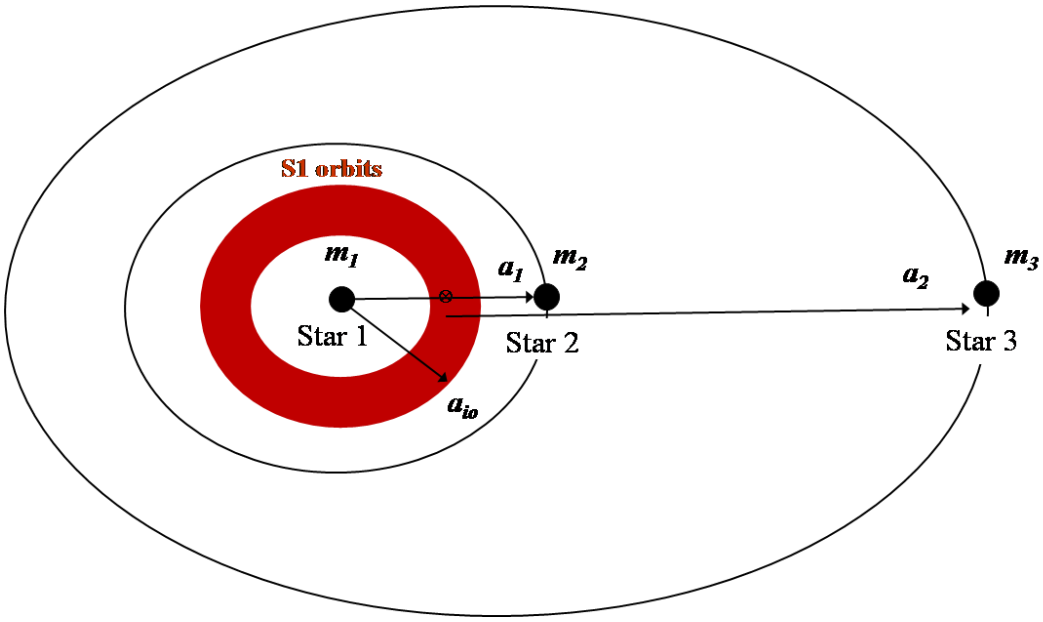

Figure 67. S1/S2 orbits, triple system configuration

The S1 and S2 orbits around Star 1 and Star 2 respectively (shown in Figure 8) are interchangeable, so only one case needs to be examined. These will henceforth be referred to simply as S1 orbits, to distinguish them from S3 orbits, which are centred on Star 3.

4.3.2 Parameter space

It is helpful to scale the masses of the stars in the triple differently to those in the previous analysis of P-type orbits. Table 38 shows the values used in some relevant studies for the total mass and semi-major axis of the inner binary, for both S-type orbits and P-type orbits. Verrier and Evans (2007) is the only study pertinent to a triple.

For binaries the distribution of the mass ratio is quite flat, as discussed in an earlier section – there is a relative scarcity of low-mass companions and a preponderance of like-mass pairs, and this also applies to binary pairs in triples. These like-mass pairs tend to have short periods, with most being well below 10^3 yr (equivalent to ~126 AU), and most short-period binaries are found in triples (Raghavan et al. 2010).

We retained the binary semi-major axis of 1 AU, but used a mass for the central star of 0.01 M_s, resulting in a minimum binary period of 7 yr, close to the median and the studies by Morais and Giuppone (2012), Musielak et al. (2005) and Verrier and Evans (2007). The average binary period used in the integrations was 8.5 yr.

The mass ratio μ_1 was varied in the range 0.001 – 0.5 and μ_2 in the range 0.001 – 2.2, essentially the same as for the P-type orbits previously considered. Note that in Verrier and Evans (2007) the ratio of the masses of the inner binary stars (in our notation) m_1/m_2 is varied from 1 to 2, and the ratio of the outer binary m_3/m_2 from 0.1 to 2. This equates to our μ_1 ranging from 0.333 to 0.500 and μ_2 possibly in the range 0.0333 to 0.25 – our parameter range is much wider.

The parameter space used is shown in Table 39.

Reference	Binary semimajor axis a_1 (AU)	Maximum binary mass m_1+m_2 (Ms)	Minimum binary period P (yr)
Holman & Wiegert (1999)	1.00	?	?
Verrier & Evans (2007)	1.00	2.00	0.71
	5.00	2.00	7.91
David et al (2003)	1.00	1.00	1.00
	1.00	1.50	0.82
Musielak et al (2005)	15.00	1.33	50.37
	5.00	1.60	8.84
Morais & Giuppone (2012)*	1.00	0.03	6.28
Gould et al (2014)**	12.50	0.28	83.97
Median			7.09
Our S1 and S3 type selected (avg)	1.00	0.02	8.53
Our P-type selected (avg)	1.00	2.00	0.85

* mass adjusted for units used.

** OGLE-2013-BLG-0341L

Table 38. S1 orbits. Scaling of inner binaries

Parameter ranges	Units	Orbit type S1	
Prograde (0) and retrograde (1) outer star	-	0	1
Prograde (0) and retrograde (1) planets	-	0	1
Geometry			
Semimajor axis ratio $a = a_2/a_1$	-	a_m	100
Inner mass ratio $\mu_1 = m_2/(m_1+m_2)$	-	0.001	0.5
Outer mass ratio $\mu_2 = m_3/(m_1+m_2)$	-	0.001	2.2
Star 2			
Eccentricity e_1	-	0	0.7
Inclination i_1	deg	0	-
Longitude of ascending node Ω_1	deg	0	-
Argument of periapsis ω_1	deg	0	-
True anomaly v_1	deg	0	-
Star 3			
Eccentricity e_2	-	0	0.7
Inclination i_2	deg	0-60	120-180
Longitude of ascending node Ω_2	deg	0	270
Argument of periapsis ω_2	deg	0	270

Table 39. S1 orbits. Parameter space used

4.3.3 Computational parameters

Some changes to the computational parameters were necessary. For broadly similar parameter ranges there were more ejections in S-type integrations than there were for P-type integrations, and a larger number of initial test particles was therefore used to compensate for this. Nevertheless, for extreme configurations where most test particles are ejected, the edge-detection algorithm can produce poor results if there are too few test particles left at the end of the integration, i.e. if the density histogram is too sparse. An error trap for this situation was thus also required. Experimentally it was found that results became unreliable when the number of test particles per bin in the density histogram was below ~20. As described previously, the number of bins used, k, is given by equation (16),

$$k = \frac{\sqrt{n}}{2} + \sqrt[3]{n} \tag{16}$$

so the mean number of test particles, n, per bin is

$$\overline{\left(\frac{n}{k}\right)} = \frac{n}{\left\lfloor \frac{\sqrt{n}}{2} + \sqrt[3]{n} \right\rfloor} = \frac{2n^{\frac{2}{3}}}{n^{\frac{1}{6}} + 2} \tag{38}$$

For any required number of test particles per bin, one can calculate the minimum required number of remaining test particles from the above relationship. For 20 test particles per bin, this minimum number of test particles is ~300. A condition was therefore imposed that, if at the end of any integration the number of test particles was below this number, the results were discarded.

One also needs to specify the heliocentric distance at which a test particle is stopped, being considered too close to the star. We set this distance at 0.005 AU, equal to one solar radius.

Compared with P-type orbits we can also justify a lower escape distance for a test particle, since if it moves well beyond the semi-major axis of the binary it is highly likely to be ejected within a short time. We used a distance of 100 AU.

In terms of setting the initial semi-major axis of the test particle cloud, previous work on binaries e.g. Holman and Wiegert (1999) used the range 0.02 – 0.50 times the semi-major axis of the binary, a_1, and found the critical semi-major axis ratio at around $0.46a_1$, while our work on P1 orbits found a range of $0.38a_1 - 0.54a_1$. The range selected was much wider, at $0.02a_1 - 0.90a_1$. The choice of the lower limit was found to be important, in that choosing it to be zero resulted in nearly all test particles being ejected. The reason for this is unknown.

The default integration time was again 10^5 yr, with sample checks of 10^6 yr. Because most test particles are swiftly ejected in this configuration, a higher initial number of 3 000 was used to ensure that enough survived for a sufficiently smooth particle density function.

The edge-detection algorithm also required modification. The extraction of a_{oi} falls away and the de-spiking routine could be removed, as could the determination of the "peakiness" of the inner particle density function that determines whether inner orbits exist. The cutoff density level was then re-optimized from calibration runs. The S1 orbit bound was defined as the semi-

major axis of the last bin that contains test particles above this density level, *if* the next 15 consecutive bins are also below this cutoff (and are also below the limit l_s). The characteristic shapes of the particle density functions of prograde and retrograde particle clouds were the same, unlike those found for P1 orbits, while the retrograde distributions extended further out, as expected.

The relevant bound-determination parameters after re-optimisation are shown in Table 40.

Parameter	Prograde	Retrograde
f_t	0.020	0.020
f_p	1.500	1.000
f_i	0.020	0.020
f_o	0.028	0.400
l_s	0.010	0.010
a_a	0.016	0.028

Table 40. S1 orbits. Edge detection algorithm parameters

Since S1 orbits have sharper edges than P-type orbits, a very small number can be used for f_i, and a small value was also used for l_s. The other computational parameters are shown in Table 41.

Parameter		Units	Orbit type S1
Central star mass	m_1	M_S	0.01
Timestep	*dt*	yr	$T_{bin}/20$
Number of test particles		-	3 000
Test particle orbit centres		-	-1 0 0
Minimum semi-major axis (1)	*amin*	AU	0.02
Maximum semi-major axis	*amax*	AU	$0.9a_1$
Collision with central body	*rmin*	AU	0.005
Ejection from system	*rmax*	AU	10^2

(1) Must be > specified collision distance

Table 41. S1 orbits. Computational parameters

4.3.4 Prograde outer star

For S1 orbits the stability bound is defined in terms of the inner orbit's semi-major axis, i.e. a_{io}/a_1. A set of 5 406 integrations was run. The survival rates of the test particles are shown in Figure 68.

In these S1 orbits a complete range of stability was exhibited, evidenced by the number of test particles remaining at the end of the integrations, which varied from 100%, i.e. complete stability (up to 10^5 yr) to 0%, i.e. all particles being ejected, usually quite early in the integration. The average survival rate was a low

10%, indicating that within the parameter space used only a relatively narrow range of configurations was stable.

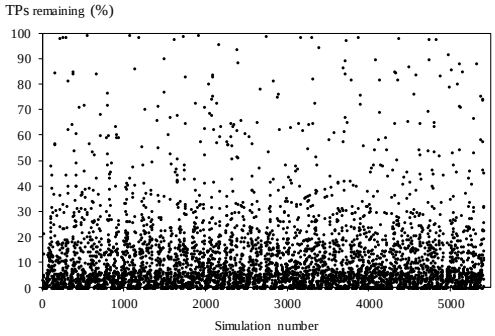

Figure 68. S1 orbits, prograde outer star, test particle survival rates

The critical semi-major axis ratios for prograde and retrograde orbits are shown in Figure 69.

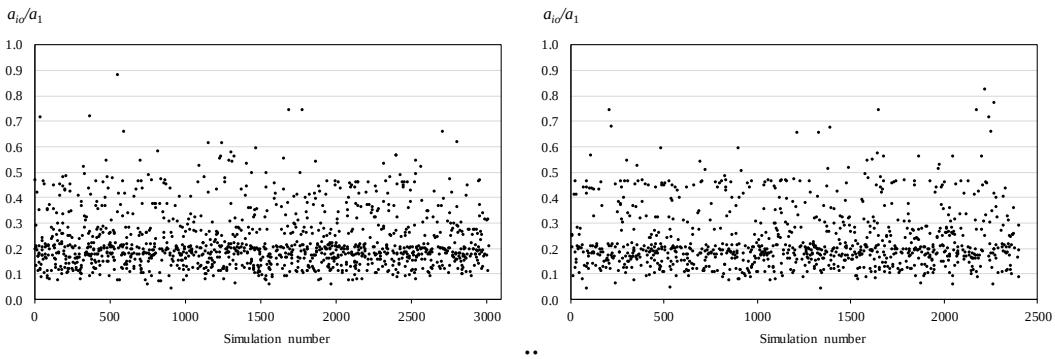

Figure 69. S1 orbits, prograde outer star. a) prograde bounds b) retrograde bounds

The semi-major axes of the stability bounds span a wide range, from very close to the central star (0.046 AU) to almost nine tenths of the distance to the second star (0.885 AU). This maximum is well above the ranges used in the previous studies mentioned earlier, but lies below the selected maximum size of the test particle cloud of $0.9a_1$ so this selection was sufficiently large. In most of the integrations, though, the test particle cloud underwent a very large contraction in semi-major axis (averaging 71%) from this initial value.

The stability bounds found are analysed in Table 42.

Well-defined bounds were found for 40% of the integrations, well ahead of the 26% found for P1 orbits. There was no distinction between prograde and retrograde bounds, whereas for P1 orbits there was a clear preponderance of prograde bounds (33% versus 18%). This is because the edges of the S1 retrograde stability bounds are far less diffuse than those for P1 retrograde bounds. The mean critical semi-major axis ratios and their ranges are shown in Table 43.

Cases with well-defined orbit bounds				
Planet orbit type	Total simulations	a_{io}/a_1		
		Bounds found (no.)	Success rate (%)	Distribution (%)
Prograde	3009	1232	41	56
Retrograde	2397	949	40	44
Total	5406	2181	40	100

Table 42. S1 orbits, prograde outer star. Number of bounds found

Orbit type	a_{io}/a_1			
	Min	Avg	Max	SD
Prograde planetary orbits	0.015	0.180	0.760	0.049
Retrograde planetary orbits	0.015	0.185	0.771	0.122
Difference (%)	-	2	-	-

Table 43. S1 orbits, prograde outer star. Mean critical semi-major axis ratios

The difference in mean critical semi-major axis ratios between prograde and retrograde planetary orbits of 2% is not statistically significant at the 5% level.

The expected signs of the coefficients in regressions of the orbit bounds a_{io}/a_1 are shown in Table 44.

Coefficient	S1 orbits
μ_1	−
μ_2	−
e_1	−
e_2	−
i_2	−
Ω_2	+
ω_2	+

Table 44. S1 orbits, prograde outer star, expected signs of regression coefficients

The expected signs of the regression coefficients for S1 bounds differ from those for P1 bounds as the P1 bounds are outside the inner binary while the S1 orbits are within it. A larger semi-major axis ratio a may be expected to allow the semi-major axis of the bound to increase. A more massive Star 2, i.e. larger μ_1, would push the bound inwards, with a similar effect (although much weaker) from μ_2. A higher eccentricity e_1 for Star 2 will also reduce the bound, with a similar (but again much weaker) effect from e_2. A higher inclination of the outer star i_2, which brings it closer to the inner stars and planets, will also tend to reduce the planets' critical semimajor axis. An increase in either the longitude of ascending node or argument of periapsis of the outer star should, however, move it further away from the inner stars and planets (assuming a non-zero inclination and eccentricity), allowing the stability bound to increase.

The regression equations for both types of planetary orbit are discussed in the following sections.

Prograde planetary orbits

The regression resulted in the following relationship, where the error terms are the average 95% confidence limits:

$$a_{io}/a_1 = (0.390 \pm 0.027) + (-0.746 \pm 0.045)\mu_1 + (0.005 \pm 0.009)\mu_2 + (-0.398 \pm 0.040)e_1 + (-0.006 \pm 0.027)e_2 \quad (39)$$

Where coefficients are zero to three decimal places they are excluded. Data on the regression coefficients are listed in Table 45.

Model	Unstandardized Coefficients		Standardised Coefficients	*t*	Sig.	95% Confidence	
	B	Std. Error	Beta			Lower Bound	Upper Bound
C	.390	.014		28.4	.000	.363	.416
a	.000	.000	.056	2.4	.016	.000	.001
μ_1	-.746	.023	-.804	-32.4	.000	-.792	-.701
μ_2	.005	.004	.024	1.1	.284	-.004	.013
e_1	-.398	.020	-.484	-19.7	.000	-.437	-.358
e_2	-.006	.014	-.010	-0.5	.647	-.034	.021
i_2	.000	.000	.036	1.6	.116	.000	.001
Ω_2	.000	.000	.033	1.4	.154	.000	.000
ω_2	.000	.000	.021	0.9	.352	.000	.000

Table 45. S1 orbits, prograde outer star. Regression coefficients – prograde planetary orbits

The variable with by far the greatest influence on S1 orbits is the inner mass ratio, with a coefficient almost twice that of the regression constant, followed by the eccentricity of the inner orbit, with a coefficient comparable to the constant. The signs of these large coefficients are as expected. In comparison, the outer star has a negligible effect on the planetary orbits. The mass ratio and eccentricity of its orbit have very weak influences, with the standard error of the coefficient of the latter being larger than the (absolute) coefficient itself. In cases like this, the fact that the sign of the coefficient appears to be wrong is simply ignored. The inclination i_2 and elements Ω_2 and ω_2 do not enter the regression equation.

The regression equation has an R^2 of 0.583, much higher than that found for P1 orbits, the F-statistic was 142 and the standard error was 0.081. The model, however, has a poor mean absolute percentage error (MAPE) of 35%.

Retrograde planetary orbits

The best-fit equation for the critical semi-major axis ratio is

$$a_{io}/a_1 = (0.393 \pm 0.028) + (-0.667 \pm 0.044)\mu_1 + (0.003 \pm 0.009)\mu_2 + (-0.383 \pm 0.040)e_1 + (0.002 \pm 0.027)e_2 \quad (40)$$

Data on the regression coefficients is listed in Table 46.

Model	Unstandardized Coefficients		Standardised Coefficients	*t*	Sig.	95% Confidence	
	B	Std. Error	Beta			Lower Bound	Upper Bound
C	.393	.014		27.9	.000	.365	.421
a	.000	.000	.066	2.8	.006	.000	.001
μ_1	-.667	.022	-.760	-29.8	.000	-.711	-.623
μ_2	.003	.005	.015	0.6	.519	-.006	.012
e_1	-.383	.020	-.476	-18.7	.000	-.424	-.343
e_2	.002	.014	.004	0.2	.880	-.025	.029
i_2	.000	.000	-.005	-0.2	.832	.000	.000
Ω_2	.000	.000	-.008	-0.4	.725	.000	.000
ω_2	.000	.000	-.001	0.0	.970	.000	.000

Table 46. S1 orbits, prograde outer star. Regression coefficients – retrograde planetary orbits

The regression coefficients are virtually identical to those for the prograde case, with the previous conclusions remaining unchanged.

The retrograde regression equation has a R^2 of 0.561, the F-statistic is 124 and the standard error of the regression was 0.081. The model has a mean absolute percentage error (MAPE) of 37%

4.3.5 Retrograde outer star

For this case a set of 3 041 integrations was run.

The parameter space used was the same as in Table 39, with the outer star's inclination now ranging from $120° - 180°$ instead of $0° - 60°$ for the prograde case. The results are shown in Figure 70 and Figure 71. (The periodic pattern displayed in Figure 70 is an artefact of some of the integrations being run in batches of 128.)

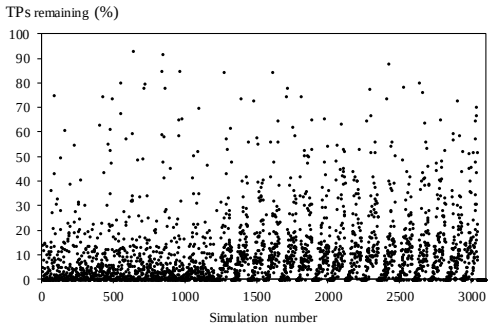

Figure 70. S1 orbits, retrograde outer star, test particle survival rates

The range of test particle survivorship was slightly less than for a prograde outer star; the maximum number of test particles remaining was 93% and the average survival rate was 10%.

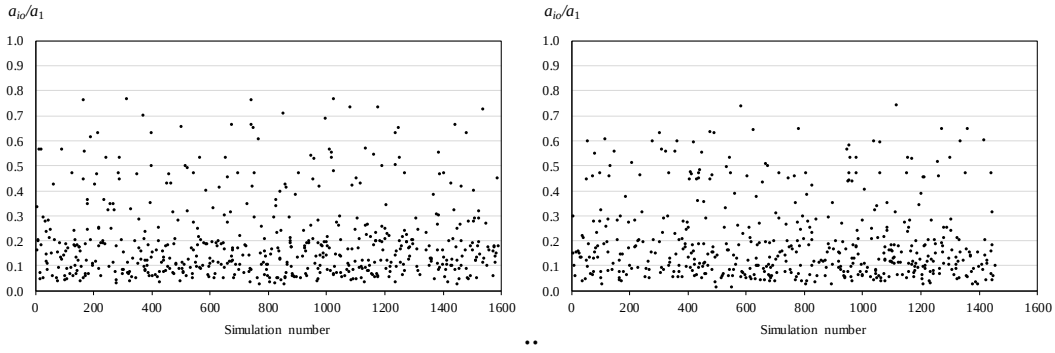

Figure 71. S1 orbits, retrograde outer star. a) prograde bounds b) retrograde bounds

The stability bounds are generally closer to the central star than for the prograde stellar case, with a minimum ratio of 0.028 and a maximum of 0.772. In the integrations the test particle cloud's average contraction was slightly less, at 75%. There is no visible difference between the prograde and retrograde critical semimajor axis ratios. The stability bounds found are analysed in Table 47.

Cases with well-defined orbit bounds				
Planet orbit type	Total simulations	a_{io}/a_1		
		Bounds found (no.)	Success rate (%)	Distribution (%)
Prograde	1586	957	60	55
Retrograde	1455	791	54	45
Total	3041	1748	57	100

Table 47. S1 orbits, retrograde outer star. Number of bounds found

The overall success rate was 57% compared with 53% for a prograde outer star, attributable mostly from the higher number of prograde planetary bounds (60% versus 53% previously). This hints that prograde planetary orbits may be more stable if the outer star is in a retrograde orbit.

The mean critical semi-major axis ratios and their ranges are shown in Table 48.

Orbit type	a_{io}/a_1			
	Min	Avg	Max	SD
Prograde planetary orbits	0.015	0.197	0.772	0.059
Retrograde planetary orbits	0.028	0.196	0.772	0.157
Difference (%)	-	-1	-	-

Table 48. S1 orbits, retrograde outer star. Mean critical semi-major axis ratios

The mean critical ratio of 0.196 is 8% higher than the average 0.183 for prograde stellar orbits. Although the -1% difference shown is not significant at the 5% level, the sign would be correct in that the critical ratio for retrograde planetary orbits should be smaller than for prograde orbits (opposite to the situation for prograde stellar orbits) since the retrograde direction of motion of the outer star should have some small influence on planets within the inner binary, conferring additional stability to prograde planets and less stability to retrograde planets. The effect would be small, as the mean period of the outer binary star is ~10 times larger than that of the planet.

The expected signs of the regression coefficients remain unchanged. The regression equations for both types of orbit are discussed in the following sections.

Prograde planetary orbits

The regression resulted in the following relationship, where the error terms are the average 95% confidence limits:

$$a_{io}/a_1 = (0.277 \pm 0.097) + (-0.387 \pm 0.067)\mu_1 + (-0.005 \pm 0.014)\mu_2 + (-0.125 \pm 0.055)e_1 + (-0.005 \pm 0.043)e_2 \quad (41)$$

Where coefficients are zero to three decimal places the variable is excluded. Data on the regression coefficients are listed in Table 49.

Model	Unstandardized Coefficients		Standardised Coefficients	*t*	Sig.	95% Confidence	
	B	Std. Error	Beta			Lower Bound	Upper Bound
C	.277	.049		5.6	.000	.180	.374
a	.000	.000	.003	0.1	.929	.000	.000
μ_1	-.387	.034	-.360	-11.4	.000	-.453	-.320
μ_2	-.005	.007	-.023	-0.7	.461	-.019	.009
e_1	-.125	.028	-.141	-4.4	.000	-.180	-.070
e_2	-.005	.022	-.007	-0.2	.816	-.048	.038
i_2	.000	.000	.034	1.1	.273	.000	.001
Ω_2	.000	.000	-.005	-0.2	.876	.000	.000
ω_2	.000	.000	-.009	-0.3	.759	.000	.000

Table 49. S1 orbits, retrograde outer star. Regression coefficients – prograde planetary orbits

As in the prograde stellar case, the dominant variables are again the inner mass ratio and the eccentricity of the inner orbit. However, their influence is substantially weaker, with their respective coefficients being 48% and 69% smaller respectively.

This regression equation has a R^2 of only 0.126, the F-statistic was 17 and the standard error of the regression was 0.139. The model has a very large mean absolute percentage error (MAPE) of 67%.

Retrograde planetary orbits

The best-fit equation for the critical semi-major axis ratio is

$$a_{io}/a_1 = (0.423 \pm 0.106) + (-0.451 \pm 0.072)\mu_1 + (-0.006 \pm 0.016)\mu_2 + (-0.056 \pm 0.061)e_1 + (-0.048 \pm 0.048)e_2 \quad (42)$$

Data on the regression coefficients is listed in Table 50.

Model	Unstandardized Coefficients		Standardised Coefficients	*t*	Sig.	95% Confidence	
	B	Std. Error	Beta			Lower Bound	Upper Bound
C	.423	.054		7.8	.000	.317	.529
a	.000	.000	-.063	-1.9	.054	-.001	.000
μ_1	-.451	.037	-.416	-12.3	.000	-.523	-.379
μ_2	-.006	.008	-.023	-0.7	.481	-.022	.011
e_1	-.056	.031	-.061	-1.8	.074	-.117	.005
e_2	-.048	.025	-.064	-2.0	.051	-.097	.000
i_2	.000	.000	-.040	-1.2	.223	-.001	.000
Ω_2	.000	.000	-.036	-1.1	.269	-.001	.000
ω_2	.000	.000	.011	0.3	.734	.000	.000

Table 50. S1 orbits, retrograde outer star. Regression coefficients – retrograde planetary orbits

The regression coefficients are again much weaker than for the prograde stellar case, with the coefficients for $\mu_1$and e_1 being 32% and 85% smaller respectively.

However, the coefficient of e_2 has increased, approaching that of e_1, so the outer star now has a small influence, unlike in the prograde stellar case.

The regression equation has a poor fit like the prograde planetary case, with an R^2 of 0.176, F-statistic of 20 and a standard error of regression of 0.143. The model has a mean absolute percentage error (MAPE) of 74%

Comparisons

The mean critical semi-major axis ratios for the four combinations of orbital motion are summarised in Table 51 and graphs of the corresponding regressions are presented in Figure 72.

S1 planetary orbits on average extend ~8% further out when the outer star is in a retrograde orbit. For prograde stellar orbits, retrograde planetary orbits extend slightly (3%) further out while for retrograde stellar orbits they are virtually the same.

In the study of the long-term stability of planets in the binary α Centauri AB system mentioned in Section 4.1.6 (Quarles & Lissauer 2016) the data for S1 orbits (Fig. 7) shows that retrograde test particles were stable 9% closer to the outer companion, larger but still comparable to our 3%.

Orbit type	Critical ratio	Motions[1] Star 3	Planet	Mean critical semi-major axis ratio Min	**Mean**	σ	Max
S1	a_{io}/a_1	P	P	0.015	**0.180**	0.049	0.760
			R	0.015	**0.185**	0.122	0.771
		R	P	0.015	**0.197**	0.059	0.772
			R	0.028	**0.196**	0.157	0.772

1. P - prograde, R - retrograde

Table 51. S1 orbits. Mean critical semi-major axis ratios for various combinations of orbital motions

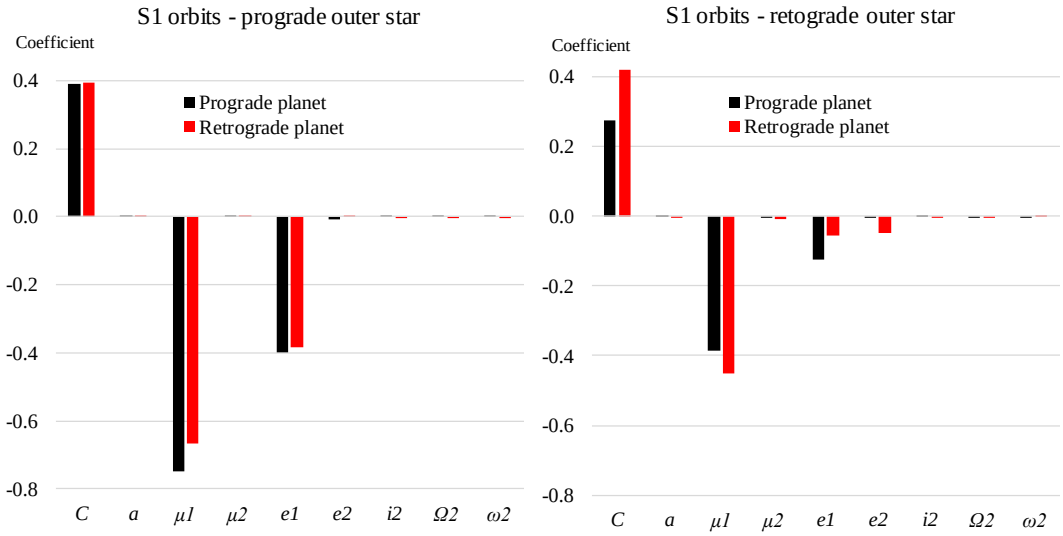

Figure 72. S1 orbits. Regression coefficients for various combinations of orbital motions a) prograde outer star, b) retrograde outer star

In summary, the determinants of the critical semi-major axis ratio for planetary orbits in S1 orbits are the inner binary's mass ratio and eccentricity only; for a retrograde outer star the influence of the eccentricity is much weaker.

Differences between prograde and retrograde stellar orbits

The S1 regression equations are shown below excluding error terms, where the first subscript refers to a prograde or retrograde outer stellar orbit and the second subscript to a prograde or retrograde planetary orbit.

$$\left(\frac{a_{io}}{a_1}\right)_{pp} = 0.390 - 0.746\mu_1 + 0.005\mu_2 - 0.398e_1 - 0.006e_2 \quad (43)$$

$$\left(\frac{a_{io}}{a_1}\right)_{pr} = 0.393 - 0.667\mu_1 + 0.003\mu_2 - 0.383e_1 + 0.002e_2 \quad (44)$$

$$\left(\frac{a_{io}}{a_1}\right)_{rp} = 0.277 - 0.387\mu_1 - 0.005\mu_2 - 0.125e_1 - 0.005e_2 \quad (45)$$

$$\left(\frac{a_{io}}{a_1}\right)_{rr} = 0.423 - 0.451\mu_1 - 0.006\mu_2 - 0.056e_1 - 0.048e_2 \quad (46)$$

Comparing the two stellar directions, for the retrograde case the coefficients concerning the binary have become weaker, with the coefficients for the outer star becoming (relatively) stronger. This is particularly true for the coefficient of e_2 relative to e_1. So a retrograde outer star has an increased influence on the planetary stability bounds, albeit small.

Also, using the above nomenclature we would expect the planetary stability of these configurations to be ranked $pp < pr < rp < rr$. To test this, the previous four equations were evaluated for 10^4 different combinations of μ_1, e_1, μ_2 and e_2, using the ranges $\mu_1 = [0,1],\ e_1 = e_2 = [0, 0.7]$ and $\mu_2 = [0, 2.3]$.

The normalised average critical semi-major axis ratio for each configuration is shown in Table 52, which confirms the expected ranking and reveals the effect of the outer star, where its retrograde motion appears to strongly stabilise both prograde and retrograde planetary orbits.

Outer star and planet motion	Average a_{io}/a_1
pp	0.010
pr	0.147
rp	0.456
rr	0.770

Table 52. S1 orbits. Relative stability of combinations of stellar and planetary orbital motions

In the equations above, the prograde stellar case the constant is effectively the same for prograde and retrograde planetary orbits, but in the retrograde stellar case they are quite different. Also, in the first case the coefficient of μ_1 for retrograde planets was smaller than for prograde planets, while the opposite holds in the second case.

As a result, by looking at the equations one can see that in the prograde stellar case, since the intercept for prograde and retrograde planetary orbits is almost the same (as is the coefficient of e_1), the retrograde orbits bound will always be further from the inner star, since the coefficient of $\mu_1$is smaller i.e.

$$\left(\frac{a_{io}}{a_1}\right)^{ps}_{pp} \approx 0.390 - 0.746\mu_1 - 0.398e_1 \quad (47)$$

$$\left(\frac{a_{io}}{a_1}\right)^{ps}_{rp} \approx 0.393 - 0.667\mu_1 - 0.383e_1 \quad (48)$$

Where superscript ps refers to the prograde outer stellar orbit and subscripts pp and rp refer to the prograde and retrograde planetary orbit bounds respectively.

However, in the retrograde stellar case the equations for the critical semi-major axis ratios are

$$\left(\frac{a_{io}}{a_1}\right)_{pp}^{rs} \approx 0.277 - 0.387\mu_1 - 0.125e_1 \quad (49)$$

$$\left(\frac{a_{io}}{a_1}\right)_{rp}^{rs} \approx 0.423 - 0.451\mu_1 - 0.056e_1 \quad (50)$$

In this case the retrograde orbit bound will be further from the inner star only for $\mu_1 \lesssim 2.28 - 3.36$ (obtained by equalising the two expressions and setting $e_1 = 0$ and 1); for larger values of $\mu_1$the opposite would hold. Although this value of μ_1 is meaningless in this instance, one can see that the direction of rotation of the outer star influences the retrograde planetary orbits, even though they are generally more stable.

4.3.6 Comparison with the Hill stability criterion

As mentioned in Section 2.1, theoretical approaches to stability are often imperfect. Another good example is to compare the numerical results for S1 orbits with the Hill stability criterion, which has been used extensively in dynamical studies (although not completely without criticism, e.g. Cuntz and Yeager (2009)).

If the critical semi-major axis ratio is equal to one third of the Hill radius, i.e. $R_{\mathrm{H}}/3$ (Mudryk & Wu 2006), then from equation (14) we get

$$\frac{a_{io}}{a_1} = \frac{R_{\mathrm{H}}}{3a} = (1-e)\left(\frac{1-\mu_1}{81}\right)^{\frac{1}{3}} \quad (51)$$

A log-log plot of a_{io}/a_1 against $1-\mu_1$ should have a slope of $1/3$ and intercept $(1-e)/\sqrt[3]{81}$. For circular orbits this intercept would be 0.231.

Various integrations were run using a range of mass ratios μ_1 and semi-major axis ratios a, for circular, coplanar, prograde planetary (and outer star) orbits and with μ_2 fixed at 0.5. A typical result is shown in Figure 73, for $a = 50, \mu_2 = 0.5, e_1 = 0, e_2 = 0, i_2 = 0, \Omega_2 = 0$ and $\omega_2 = 0$.

For $\mu_1 \ll 1$ and $\mu_1 \to 1$, one would expect the critical semi-major axis to follow the one-third power relationship. As shown in the figure, this is indeed true, but there are two distinct regimes. For $1-\mu_1 \lesssim 0.645$ (or $\mu_1 \gtrsim 0.355$) the critical semi-major axis ratio lies close to, and below, the Hill relationship and converges towards it for small values of μ_1. For $\mu_1 \lesssim 0.355$ there is an abrupt change in regime to a different and equally good relationship, with much higher critical semi-major axis ratios.

For different stellar semi-major axis ratios a (in the range $10-100$) this regime-switching point for μ_1 remains approximately the same. The $\mu_1 \to 1$ relationship also does not change much, but the exponent of the $\mu_1 \ll 1$ relationship varies strongly.

This suggests that the use of the Hill criterion as a determinant of planetary stability in a triple would be overly simplistic, and again highlights the inadequacy of theoretical approaches in the analysis of this situation.

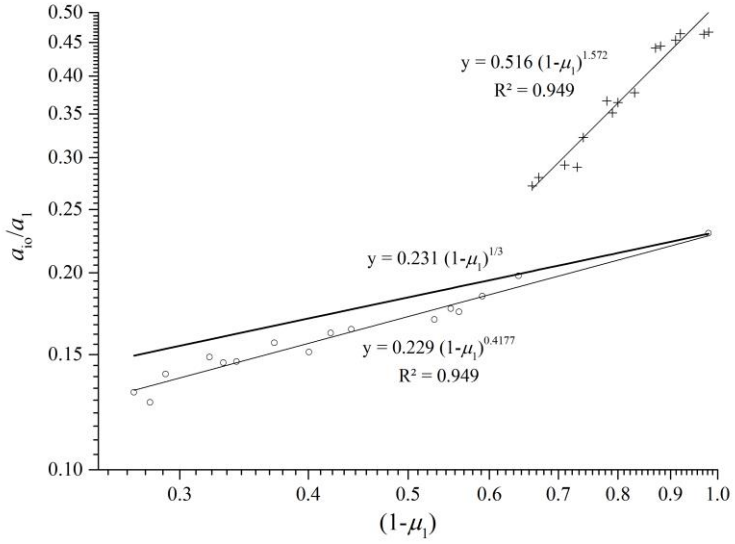

Figure 73. S1 orbits. Critical semi-major axis ratios versus (1-μ_1)

In fact, even its use in binaries is not straightforward. For example, it was pointed out in the semi-analytic study by Mudryk and Wu (2006), in which the numerical work also used the Hierarchical Jacobi Symplectic integrator by Beust (2003), that even if a planet is allowed to escape according to the Hill criterion, it will only do so if its orbit is chaotic as a result of overlapping resonances, implying that the Hill criterion is a necessary but not sufficient condition for instability – this criterion describes the energy condition for instability while resonance overlap provides the proximate cause. However, they found that *for practical purposes* the criterion was a sufficient condition.

The original Hill derivation for coplanar, circular orbits was later split into prograde and retrograde cases. For example, Innanen (1979) incorporated the Coriolis force to find stability limits at $0.69R_{\mathrm{H}}$ and $1.44R_{\mathrm{H}}$ for prograde and retrograde orbits respectively. This was later corrected to $0.80R_{\mathrm{H}}$ and $2.60R_{\mathrm{H}}$ by Hamilton and Burns (1991), who then found very different limits of $0.49R_{\mathrm{H}}$ for prograde orbits and $1R_{\mathrm{H}}$for retrograde ones.

The Hill criterion was recently generalised to the three-body problem with an outer body of arbitrary inclination by Grishin et al. (2017). A mass hierarchy of "star" ≫ "planet" ≫ "satellite" was used. However, even if we could reduce our four-body problem to three by ignoring the outer body, this mass assumption would severely restrict the mass ratios of the inner binary, so it would be of little help in our investigation.

4.3.7 Comparison with previous work on S1 bounds

Few empirical studies have been done on S1 orbits, even in binaries.

Holman and Wiegert (1999) found a critical semi-major axis ratio (our a_{io}/a_1) of 0.464, while Musielak et al. (2005) found critical ratios in the range $0.22 - 0.46$.

The stability of prograde versus retrograde planets in circular binary systems has been investigated by e.g. Morais and Giuppone (2012), who used numerical

integrations of S-type systems to produce detailed a-μ_1 maps of the stability boundary and showed that retrograde planets are stable at distances up to 0.66 times closer to the perturber than prograde planets (compared with the 0.5 times found in this study). They found a range beginning at $0.4 - 0.5$ for prograde planetary orbits and 0.6 for retrograde planetary orbits, although data for the latter case was much sparser.

The only previous work done on S1 orbits in triples was by Verrier and Evans (2007). Their regression equation is not comparable to ours as it uses cross-terms and a differently-defined mass ratio. The outer star does not appear in the regression and they concluded that "the addition of a stable third star does not distort the original binary stability boundaries". Retrograde orbits were not considered, for either the planet or the outer star.

A more comprehensive comparison of these numerical results with previous work is provided in Section 4.7.

4.3.8 Some observational examples of S1 orbits.

Among the closest S1 orbits found in a binary are: 0.7 AU for OGLE-2013-BLG-0341L b, with a binary separation of ~12 AU-17 AU, resulting in a semi-major axis ratio a_{io}/a_1 of 0.058 – 0.041 (Gould et al. 2014); 1.09 AU with a binary separation of 13.6 AU for HD59686 b, yielding $a_{io}/a_1 \sim 0.080$ (Trifonov et al. 2018); and 0.382 AU and 5.3 AU respectively for KOI-1257 b, giving $a_{io}/a_1 \sim 0.072$ (Santerne et al. 2014).

No radial-velocity or transit surveys have found S-type planets in any binary systems with a separation less than ~10 AU (Lissauer, Dawson & Tremaine 2014).

Only three S1 orbits in triple systems have been found to date, and are shown in Table 53. Again, there is some uncertainty whether Fomalhaut b is a planet or a dust cloud or disc.

Planet	Mass (M_j)	a_{io} (AU)	P (d)	e	a_1 (AU)	a_2 (AU)	a_{io}/a_1
Fomalhaut b	-	177±68	3.201×10^5	0.80±0.10	58000	159000	0.00305
HD 126614 A b	0.38±0.04	2.35±0.02	1244±17	0.41±0.10	36.2	≳1000	0.0649
HD 2638 b	0.48	0.0440	3.4442 ± 0.0002	0	25.6 ± 1.9	-	0.00172

Table 53. S1 orbits of planets discovered in triple-star systems

The generally low values for the semi-major axis ratios are a manifestation of observational bias. Although some of our integrations showed stable bounds with semi-major axis ratios as low as 0.015, they also extended to almost 0.8, with the greatest concentration in a "sweet spot" of $0.03 - 0.25$, so there appears to be significant scope for planets to be found much further out from their host stars.

4.3.9 Triples compared with binaries

Configuring a binary case

To highlight how the S1 planetary stability bounds in a triple differ from those in a binary, one needs to remove the disturbing influence of the outer star of the triple and compare the results with those from the previous section. Only one case of stellar orbit direction need be considered, as the removal of the outer star means the stellar prograde/retrograde distinction falls away.

As discussed previously, changes to the experimental procedure should be minimised to extract what may be subtle differences. This was done by repeating identically the S1 integrations, with the only change being that the outer star's mass was simply reduced to a negligible value. Unlike the case for P1/P2 orbits, no other changes were needed; in particular, the edge-extraction routine did not require re-optimization.

The mass of the outer star was selected to be one thousandth of the central star's (Star 1's) mass, i.e. $10^{-5}\ M_S$. In the integrations for triples the range used for μ_2 resulted in the outer star's mass varying from zero to 0.043 M_S. As shown by the coefficient of μ_2 in Table 45, the dependence on the outer star's mass is weak. However, it is not negligible, as shown by plotting the critical semi-major axis ratio directly against the outer star's mass m_3, shown in Figure 74.

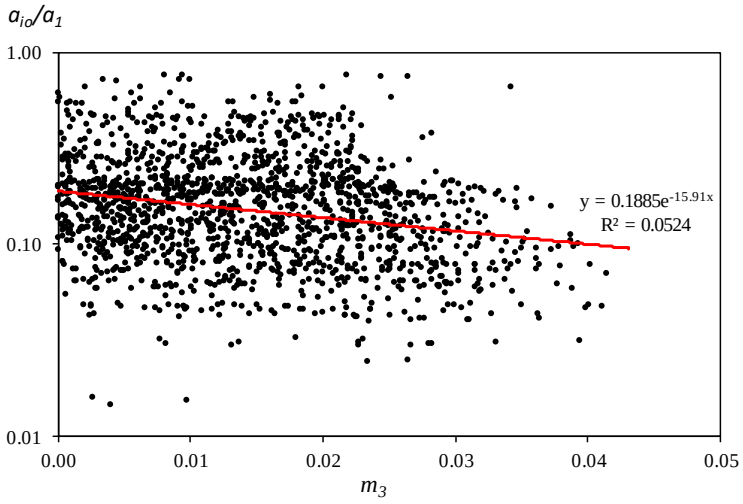

Figure 74. S1 orbits. Critical semi-major axis ratio versus mass of outer star

Although the scatter in this univariate plot is large, the dependence on mass is exponential – a reduction in mass from the maximum of 0.043 M_S to the proposed $10^{-5}\ M_S$ would result in a doubling of the critical ratio from approximately 0.095 to 0.188.

Results for the binary case

For comparison with the triple star analysis (for a prograde outer star) in Section 4.3.4, 5 121 integrations of this binary model were run. The stability limit a_{io}/a_1 for all orbits is shown in Figure 75 a). The graph is not separated into prograde and retrograde planetary cases as there is no visible difference between them. This is compared in Figure 75 b) with the combined graph of prograde and retrograde bounds, from Figure 69.

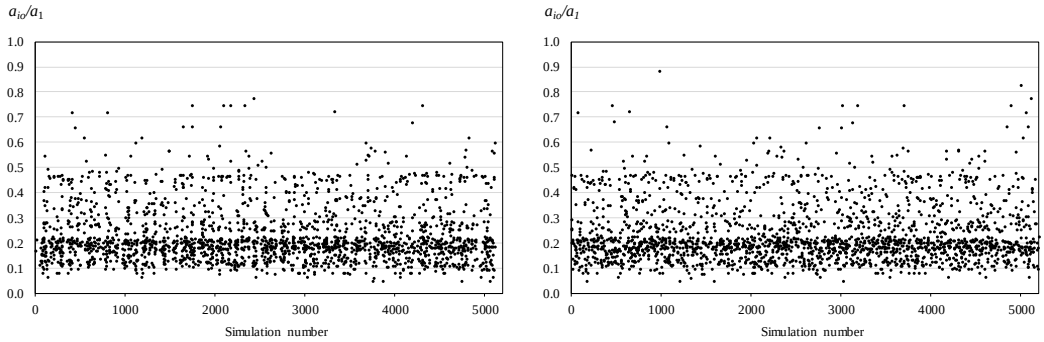

Figure 75. S1 orbits. All stability bounds a) binary bounds b) triple bounds

The binary bounds show a similar distribution of critical semi-major axis ratios, but with the smallest ones being further away from the central star. There are two ranges of differing density (i.e. regions of differing stability) – at critical ratios from a bit under 0.1 up to 0.22 and then from 0.22 to 0.48. These also existed in the triple case. A plot of the distribution of critical semi-major axis ratios, shown in Figure 76, highlights the two regions.

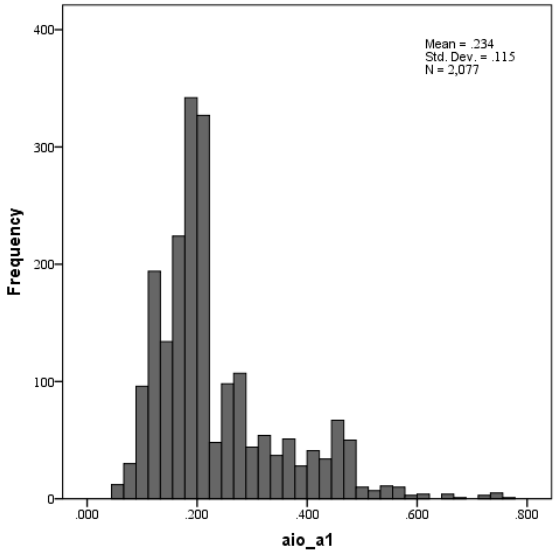

Figure 76. Binary S1 orbits. Distribution of critical semi-major axis ratios

The region from 0 – 0.22 has the highest stability, followed by lower stability in the range 0.24 – 0.48 and a largely unstable region from 0.50 outwards. The proportions of stable orbits falling into these three regions are 64:33:3 respectively. The average contraction of the initial test particle cloud was 71%, slightly less than the 77% for the triple case. This relative expansion of the test particle cloud is expected, given the removal of the influence of the outer star.

The stability bounds found are analysed in Table 54.

As for the triple case, there was no distinction between the success rate of prograde and retrograde bounds found, as both types of orbits had equally sharply-defined stability bounds, where they existed. The overall success rate of 41% was, however, lower than the 53% for the triple case. The ranges of the mean critical semi-major axis ratio for these bounds are shown in Table 55.

Cases with well-defined orbit bounds				
Planet orbit type	Total simulations	a_{io}/a_1		
		Bounds found (no.)	Success rate (%)	Distribution (%)
Prograde	2856	1169	41	56
Retrograde	2265	908	40	44
Total	5121	2077	41	100

Table 54. Binary S1 orbits. Number of bounds found

Orbit type	a_{io}/a_1			
	Min	Avg	Max	SD
Prograde planetary orbits	0.046	0.257	0.885	0.066
Retrograde planetary orbits	0.047	0.289	0.775	0.120
Difference (%)	-	12	-	-

Table 55. Binary S1 orbits. Mean critical semi-major axis ratios

Comparing Table 55 with Table 43 shows that the closest orbits lie substantially further from the central star, with critical ratios of around 0.046 compared with 0.015 for the triple case. The mean critical ratio of 0.270 is 48% higher than the 0.183 for triples. The largest critical ratios are also slightly higher than in the triple case.

In the binary case retrograde planetary orbits again extend further out relative to prograde orbits, by 12% compared with 2% in triples.

Comparison with the triple case

The results for the binary case shown in Table 55 are compared with the triple case in Table 56.

Difference in average bounds	a_{io}/a_1		
Orbit type	Triple	Binary	Δ%
Prograde planetary orbits	0.180	0.257	43*
Retrograde planetary orbits	0.185	0.289	57*
Δ%	2	12	-

* significant at the 5% level

Table 56. Binary S1 orbits. Difference between average planetary bounds in triples and binaries

Although smaller than measured by the univariate relationship in Figure 74, the difference in critical ratios averaged 50%. (Although this is much larger than the absolute ~9% difference between the triple and binary cases for P1 and P2 orbits, this is simply because the critical semi-major axis ratio is measured relative to a_1 rather than the larger a_2.)

The regressions for the binary case can also be compared with those found for the triple case, as shown in Table 57.

S1 orbits	Triple		Binary		Δ (%)
prograde planet	B	*t*	B	*t*	B
C	.390	28.4	.360	54.4	-8
a	.000	2.4	.000	1.3	-77
μ_1	-.746	-32.4	-.497	-50.7	-33
μ_2	.005	1.1	.000	0.0	-
e_1	-.398	-19.7	-.396	-58.8	0
e_2	-.006	-0.5	-.011	-1.6	67
i_2	.000	1.6	.000	-0.3	-
Ω_2	.000	1.4	.000	-0.9	-
ω_2	.000	0.9	.000	0.8	-
R^2	0.58		0.68		-
Model error (%)	34.9		40.6		-

S1 orbits	Triple		Binary		Δ (%)
retrograde planet	B	*t*	B	*t*	B
C	.393	27.9	.378	44.5	-4
a	.000	2.8	.000	-1.7	-136
μ_1	-.667	-29.8	-.491	-39.6	-26
μ_2	.003	0.6	.000	0.0	-
e_1	-.383	-18.7	-.411	-47.9	7
e_2	.002	0.2	.000	0.1	-77
i_2	.000	-0.2	.000	1.9	-
Ω_2	.000	-0.4	.000	-0.1	-
ω_2	.000	0.0	.000	-0.2	-
R^2	0.56		0.64		-
Model error (%)	36.7		41.8		-

Table 57. S1 orbits. Regression coefficients and model fits, triples versus binaries

The results of previous studies of S-type orbits in binaries are shown in Table 87 in Section 4.6. The binary case has modestly higher model R^2s and lower model errors (MAPEs) than for the triple case.

For S-type prograde orbits the regression constants ranged from 0.22 to 0.464, averaging 0.38. Our result (for a prograde planet) of 0.36 is very close to this average. The single study addressing retrograde orbits, by Morais and Giuppone (2012), gave ~0.6 and our 0.38 is well below this.

The regression coefficients for triples and binaries are illustrated in Figure 77.

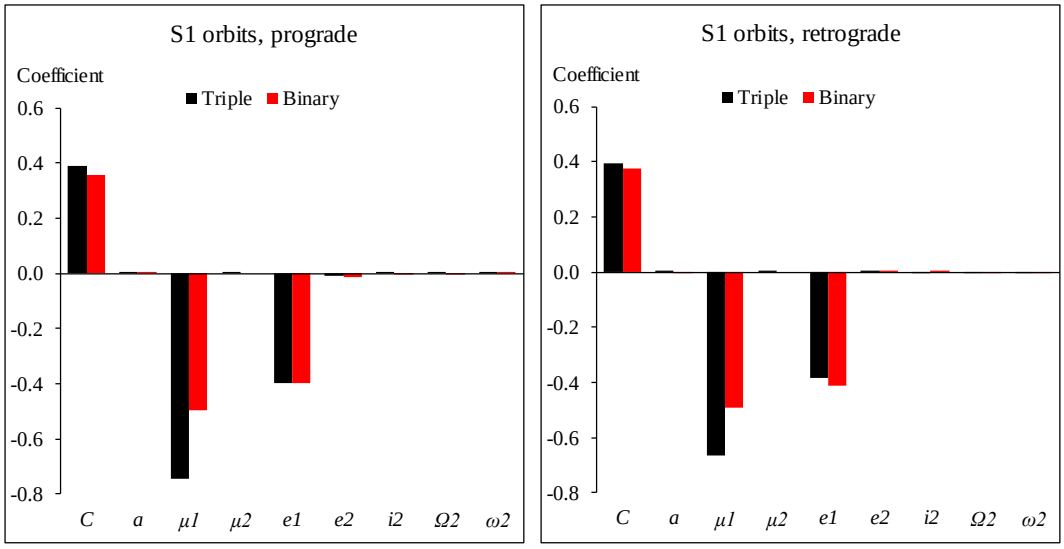

Figure 77. S1 orbits. Regression coefficients, triples versus binaries – a) prograde planets b) retrograde planets

The results for prograde and retrograde planetary orbits in triples and binaries are qualitatively similar, in that the only variables of influence are the inner mass ratio μ_1 and eccentricity e_1. However, the influence of the mass ratio is significantly larger in triples than in binaries, while that of eccentricity (and the constant) are effectively the same.

4.3.10 Conclusions – S1/S2 orbits

On average the outer star of a triple has a significant constraining influence on S1-type orbits compared with the binary case. In triples the added influence of the outer star makes S1 orbits move inwards, with the mean critical semi-major axis ratio reducing substantially from 0.270 to 0.183 or over 30%, with the difference in critical ratio between prograde and retrograde planetary orbits also shrinking by around 10%. The mass ratio has a larger influence in triples than in binaries, while the effect of eccentricity is the same.

For S1 planetary orbits in triples, the critical semi-major axis ratio is in the range $\sim 0.180 - 0.196$. The sole significant determinants of this ratio are the inner binary's mass ratio and eccentricity, in approximately equal measure, as reported by other researchers, although we found the influence of eccentricity declines sharply for a retrograde outer star. The critical ratio is generally ~7% greater for retrograde stellar orbits. Retrograde planetary orbits extend slightly further out (by 3%) for prograde stellar orbits, but for retrograde stellar orbits they are essentially the same.

4.4 Orbit Type S3

4.4.1 Configuration

As mentioned in the introduction, we are not aware of any previous empirical work on this configuration in triples.

The region of S3 orbits is illustrated in Figure 78. The nomenclature of all the variables remain the same as in the previous configurations discussed. However, for computational convenience the origin of the coordinate system was moved from Star 1 to Star 3, to leave, for example, the edge detection routine, used here to determine a_{io}, unchanged. The "outer star" is now the inner binary, which will be called the "outer binary".

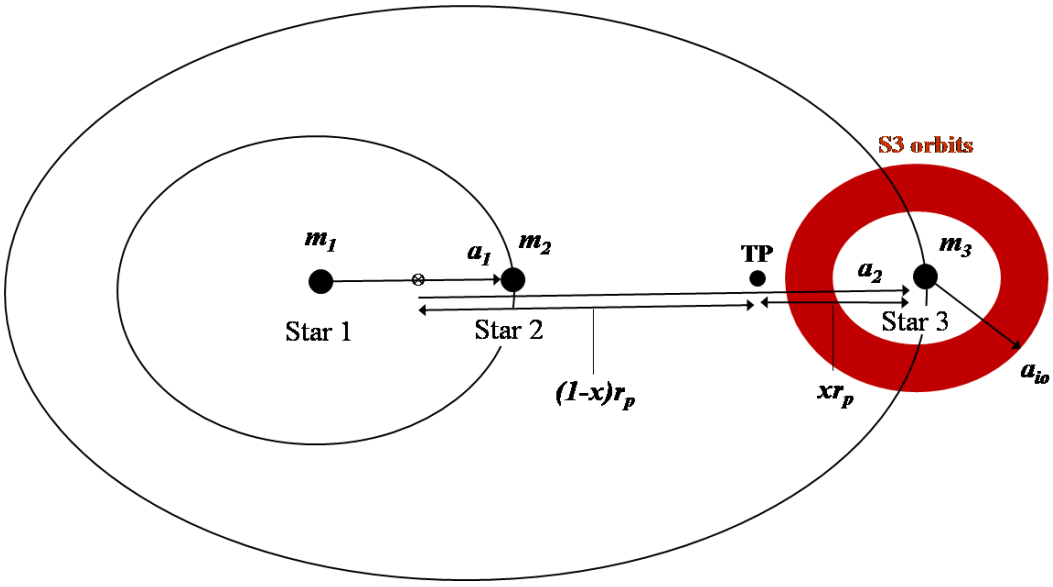

Figure 78. Triple system configuration – S3 orbits

4.4.2 Parameter space

The parameter space used is shown in Table 58. It is identical to that used for S1 orbits.

Parameter ranges	Units	Orbit type S3	
Prograde (0) and retrograde (1) outer star	-	0	1
Prograde (0) and retrograde (1) planets	-	0	1
Geometry			
Semimajor axis ratio $a = a_2/a_1$	-	a_m	100
Inner mass ratio $\mu_1 = m_2/(m_1+m_2)$	-	0.001	0.5
Outer mass ratio $\mu_2 = m_3/(m_1+m_2)$	-	0.001	2.2
Star 2			
Eccentricity e_1	-	0	0.7
Inclination i_1	deg	0	-
Longitude of ascending node Ω_1	deg	0	-
Argument of periapsis ω_1	deg	0	-
True anomaly v_1	deg	0	-
Star 3			
Eccentricity e_2	-	0	0.7
Inclination i_2	deg	0-60	120-180
Longitude of ascending node Ω_2	deg	0	270
Argument of periapsis ω_2	deg	0	270

Table 58. S3 orbits. Parameter space used

4.4.3 Computational parameters

The initial size of the test particle cloud around Star 3 was first set at half the distance to the centre of mass of the inner binary, or $a_2/2$. However, it became apparent that the size of the test particle cloud needed to be chosen with more care, particularly for large values of the inner mass ratio μ_1 or a high eccentricity e_2 for the outer star.

For example, Figure 79 shows the orbit of the outer binary, consisting of Star 1 and Star 2, and its eccentric orbit relative to Star 3 in an integration. Note that per the new coordinate system, the outer orbit now consists of the close binary pair.

With an initial test particle cloud semi-major axis of $a_2/2$ or 31 AU in this example, which extends to the perihelion of the outer binary's orbit, some test particles are attracted to, and become associated with, this binary. When this sub-cloud of captured particles is at aphelion, the test particle density histogram nevertheless appears normal, as shown in Figure 80.

The edge detection routine for the test particle cloud correctly picks the edge at 5 AU. However, at perihelion the histogram has a completely different profile, making correct edge identification impossible, as shown in Figure 81.

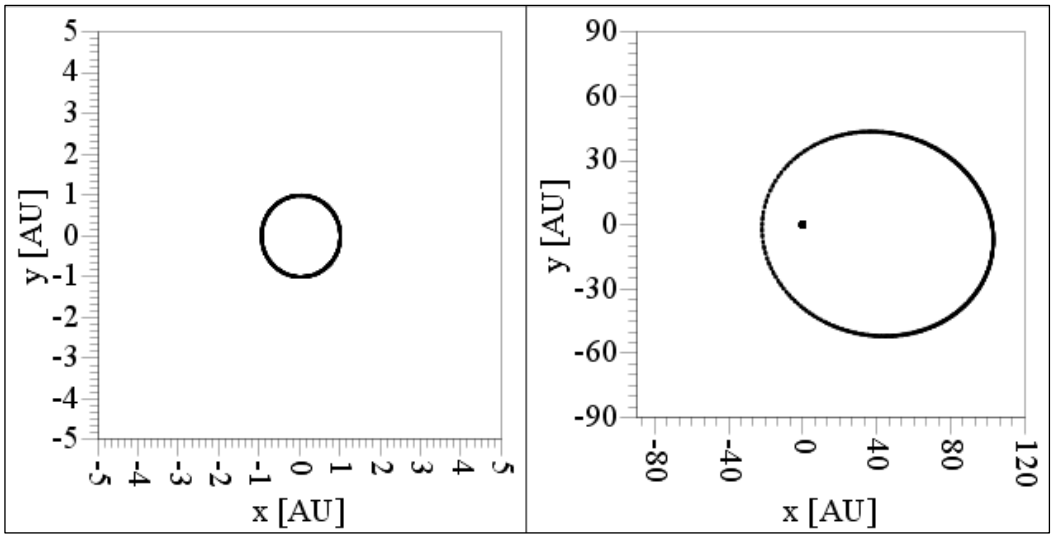

Figure 79. S3 orbits. a) orbit of close binary pair Star 1 and Star 2 b) orbit of binary pair around Star 3. Parameters $a_1 = 1\ AU, a_2 = 62\ AU,$ $\mu_1 = 0.176, \mu_2 = 0.375, e_1 = 0.042, e_2 = 0.651, \Omega_2 = 32°$

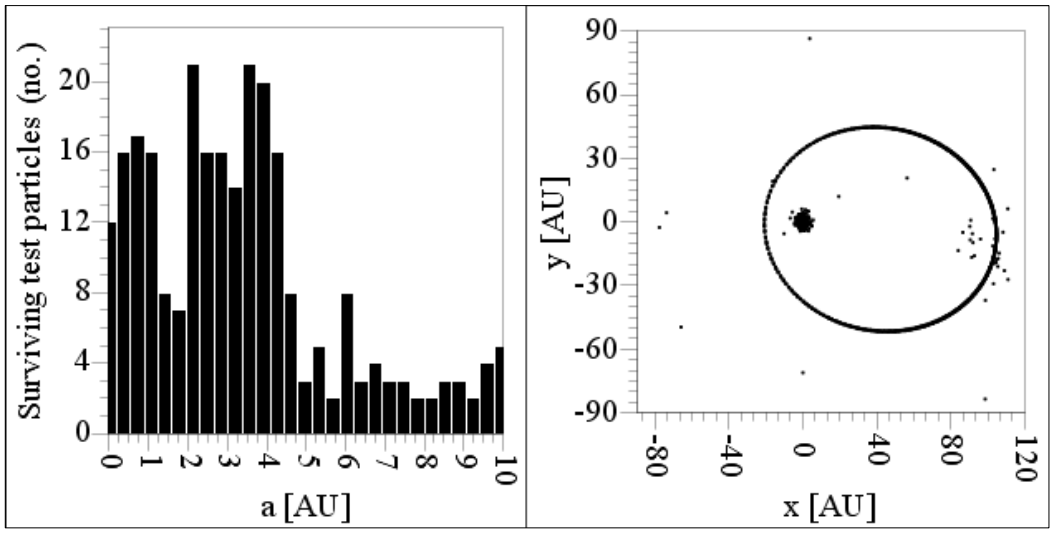

Figure 80. S3 orbits. a) test particle density function at aphelion b) test particle cloud at centre with captured sub-cloud at aphelion

The test particle cloud therefore must be small enough that particles are not lost from Star 3 to the binary at its perihelion. As a rough approximation let this distance r_p be defined as the point at stellar perihelion where the gravitational attraction of Star 3 on a particle is the same as that of the outer binary. Assuming that $a_2 >> a_1$, this can be calculated without regard to the orientation of the outer binary by considering this binary to be a point mass of $m_1 + m_2$ located at its centre of mass. At stellar perihelion, $r_p = a_2(1 - e_2)$. At this separation, the point of equal gravitational attraction from Star 3 and the binary then depends only on the masses of the three stars. Assuming that Figure 78 represents the orbits at perihelion rather than aphelion, at the point of equal gravitational attraction on a test particle (labelled TP) we have

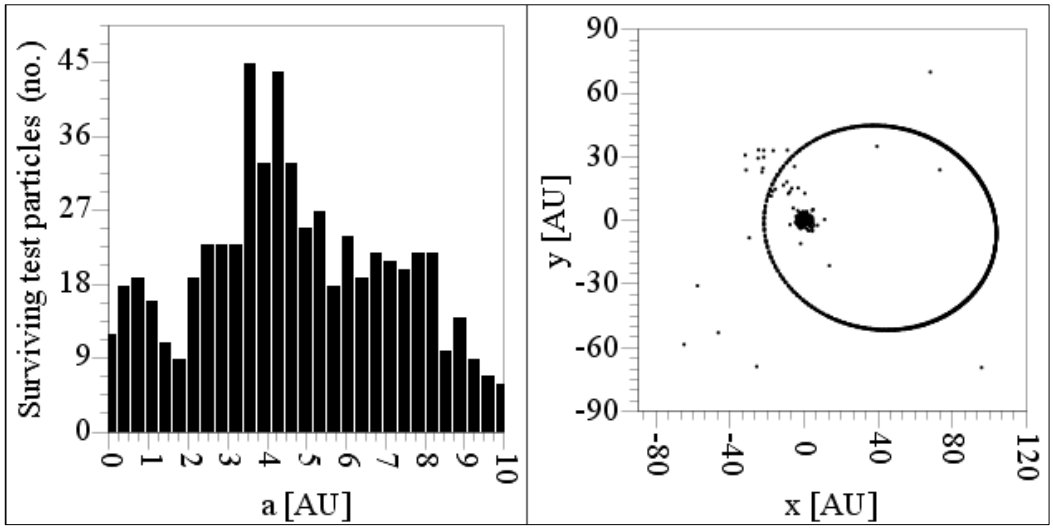

Figure 81. S3 orbits. a) test particle density function at perihelion b) test particle cloud at centre with captured sub-cloud at perihelion

$$\frac{m_1+m_2}{[(1-x)r_p]^2} = \frac{m_3}{[xr_p]^2} \tag{52}$$

with solutions for x of

$$x_+ = \frac{\sqrt{(m_1+m_2)m_3}-m_3}{(m_1+m_2)-m_3} \text{ and } x_- = \frac{-\sqrt{(m_1+m_2)m_3}-m_3}{(m_1+m_2)-m_3} \tag{53}$$

Only the positive root needs evaluating, since the only meaningful cases are when x_- is positive, and in these cases it is always larger than x_+.

The maximum semi-major axis a_{max} of the test particle cloud should therefore be

$$a_{max} = xr_p = a_2(1-e_2)\left(\frac{\sqrt{(m_1+m_2)m_3}-m_3}{(m_1+m_2)-m_3}\right) \tag{54}$$

A few test particles are still captured by the binary when using this value, but use of this approximation essentially solved the problem.

As for S1 orbits, the integration time was again 10^5 yr with test integrations of 10^6 yr. The initial number of test particles was reduced from 3 000 to 2 000 and the system ejection limit was increased from 10^2 AU to 10^4 AU. The other computational parameters are shown in Table 59.

Since the S3 orbits are conceptually the same as S1 orbits, the edge detection routine is unchanged, and the parameters used for S3 orbits, as shown in Table 60, are the same as for S1 orbits.

Parameter		Units	Orbit type S3
Central star mass	m_1	M_S	0.01
Timestep	*dt*	yr	$T_{bin}/20$
Number of test particles		-	2 000
Test particle orbit centres		-	-1 0 0
Minimum semi-major axis (1)	*amin*	AU	0.02
Maximum semi-major axis	*amax*	AU	Eqn. (54)
Collision with central body	*rmin*	AU	0.005
Ejection from system	*rmax*	AU	10^4

(1) Must be > specified collision distance

Table 59. S3 orbits. Computational parameters

Parameter	Prograde orbits	Retrograde orbits
f_t	0.020	0.020
f_p	1.500	1.000
f_i	0.020	0.020
f_o	0.028	0.400
l_s	0.010	0.010
a_a	0.016	0.028

Table 60. S3 orbits. Edge detection algorithm parameters

4.4.4 Prograde outer star

For S3 orbits the stability bound is defined in terms of the outer orbit's semi-major axis, i.e. a_{io}/a_2. A set of 3 166 integrations was run. The survival rates of the test particles are shown in Figure 82.

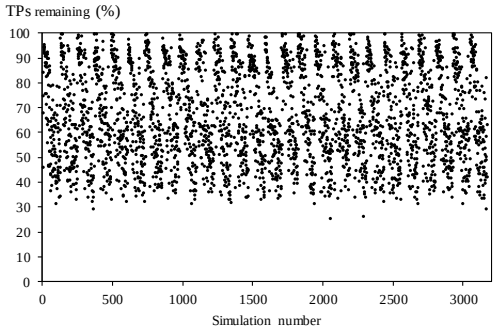

Figure 82. S3 orbits, prograde outer star, test particle survival rates

Again, the periodicity is an artefact of the batch-wise running of integrations. The number of test particles remaining after 10^5 years ranges widely, from 100% down to around 30%. The pattern is inverse to that for S1 orbits in that there were no integrations where all test particles were ejected, a consequence of the fact that

$a_2 >> a_1$. The number of stable orbits found is far higher for S3 orbits than S1 orbits.

The critical semi-major axis ratios for prograde and retrograde orbits are shown in Figure 83.

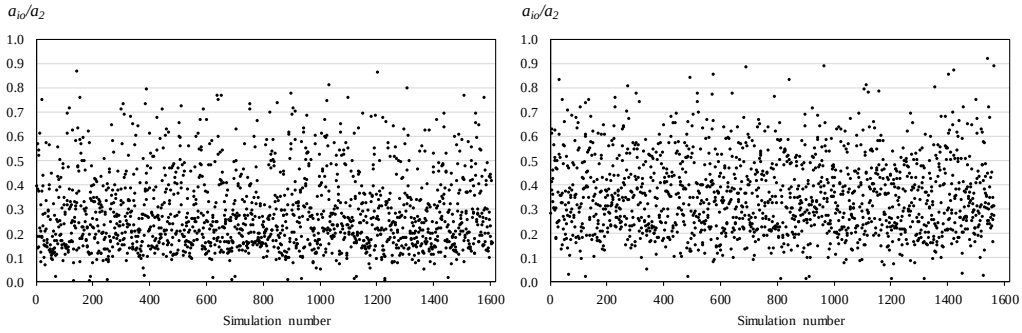

Figure 83. S3 orbits, prograde outer star a) prograde bounds b) retrograde bounds

In the integrations the test particle cloud always shrank from the initial a_{max}, by a minimum of 2% and maximum of 89%, with an average contraction of 35%.

The critical semi-major axis ratio a_{io}/a_2 varied widely with the orbital configurations used, ranging from less than 0.01 to over 0.9 and averaging around 0.3. Prograde planetary orbits are seen to be concentrated closer to the parent star, while retrograde orbits lay further away on average, as expected, and were more uniformly dispersed. The distribution of critical semi-major axis ratios for both orbital motions was generally more uniform than for S1 orbits.

The orbital stability bounds found for each case are shown in Table 61.

Cases with well-defined orbit bounds				
Planet orbit type	Total simulations	a_{io}/a_2		
		Bounds found (no.)	Success rate (%)	Distribution (%)
Prograde	1604	1599	100	52
Retrograde	1562	1501	96	48
Total	3166	3100	98	100

Table 61. S3 orbits, prograde outer star. Number of bounds found

A similar number of integrations were carried out for each type of planetary motion and well-defined bounds were found for almost all of them (compared with only 53% for S1 orbits), with little difference in success rate between prograde and retrograde planetary orbits. The mean critical semi-major axis ratios and their ranges are shown in Table 62.

The mean critical ratios for S3 bounds are not comparable with those for S1 orbits as they have different denominators. As expected, retrograde planetary orbits are more stable than prograde, with their mean critical ratio being 25% larger than for prograde orbits.

Orbit type	a_{io}/a_2			
	Min	Avg	Max	SD
Prograde planetary orbits	0.009	0.289	0.893	0.098
Retrograde planetary orbits	0.010	0.361	0.920	0.158
Difference (%)	-	25	-	-

Table 62. S3 orbits, prograde outer star. Mean critical semi-major axis ratios

The expected signs of the coefficients in the regressions for the orbit bounds a_{io}/a_2 are shown in Table 63.

Coefficient	S3 orbits
μ_1	−
μ_2	+
e_1	−
e_2	−
i_2	−
Ω_2	+
ω_2	+

Table 63. S3 orbits, prograde outer star. Expected signs of regression coefficients

The only change in coefficients compared with S1 orbits is for μ_2. Since the small bodies are now orbiting Star 3, as μ_2 increases, the mass and hence influence of the binary declines relative to this body, allowing the stability bound to move outwards from Star 3 and the critical ratio to increase. The regression equations for both types of planetary orbit are discussed in the following sections.

Prograde planetary orbits

The regression resulted in the following relationship, where the error terms are the average 95% confidence limits:

$$a_{io}/a_2 = (0.392 \pm 0.022) + (-0.075 \pm 0.028)\mu_1 + (0.037 \pm 0.007)\mu_2 + (-0.020 \pm 0.021)e_1 + (-0.602 \pm 0.021)e_2 \quad (55)$$

Where coefficients are zero to three decimal places they are ignored. Data on the regression coefficients is listed in Table 64.

The value of the constant is quite similar to the mean critical ratio of 0.384 found by other investigators for prograde S1 orbits in binaries. The notable feature of the regression is the very strong dependence only on the eccentricity of the outer star, with a coefficient for this variable that is 50% larger than the constant. The sign for this coefficient, and for the other variables, is correct, but the influence of the other variables is largely irrelevant. This reflects the behavior discussed in Section 4.4.3 and the variable outer limit used for the test particle cloud.

The regression equation has an R^2 of 0.71, the F-statistic was 478 and the standard error of the regression was 0.084. The model has a mean absolute percentage error (MAPE) of 25%.

Model	Unstandardized Coefficients		Standardised Coefficients	*t*	Sig.	95% Confidence	
	B	Std. Error	Beta			Lower Bound	Upper Bound
C	.392	.011		35.6	.000	.370	.413
a	.002	.000	.277	20.2	.000	.001	.002
μ_1	-.075	.014	-.071	-5.2	.000	-.103	-.046
μ_2	.037	.003	.151	11.0	.000	.030	.043
e_1	-.020	.011	-.026	-1.9	.053	-.041	.000
e_2	-.602	.010	-.798	-58.3	.000	-.622	-.582
i_2	.000	.000	.000	0.0	.998	.000	.000
Ω_2	.000	.000	.005	0.3	.733	.000	.000
ω_2	.000	.000	.012	0.9	.387	.000	.000

Table 64. S3 orbits, prograde outer star. Regression coefficients – prograde planetary orbits

In all the regressions of P-type and S-type orbits so far, the univariate relationships between the critical ratios and the independent variables were linear. Interestingly, in S3 orbits a nonlinear relationship appeared for the first time, between a_{io}/a_2 and μ_2. This is shown in Figure 84, with a power law regression line fitted. The slope of the regression line is positive, as expected.

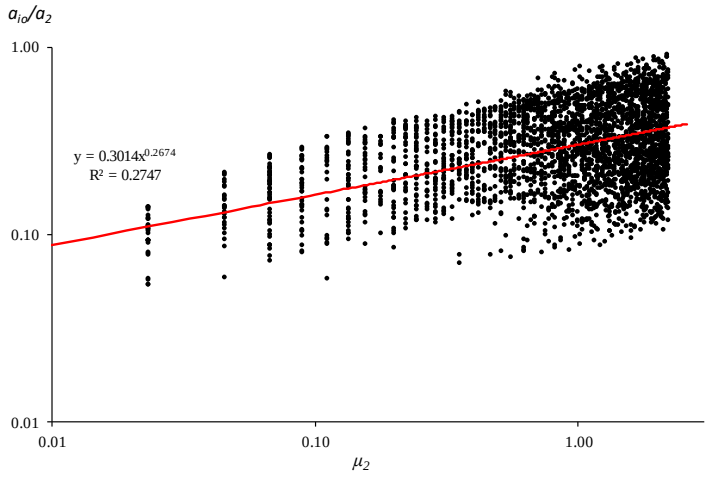

Figure 84. S3 orbits, prograde outer star. Relationship between critical semimajor axis ratio and μ_2, linearised

The regression equation was not changed to incorporate this as a nonlinear term, for comparability and since a linear fit was not too dissimilar ($R^2 = 0.14$).

Retrograde planetary orbits

The regression equation for this case is given by

$$a_{io}/a_2 = (0.441 \pm 0.018) + (0.001 \pm 0.025)\mu_1 + (0.113 \pm 0.006)\mu_2 + (-0.012 \pm 0.018)e_1 + (-0.584 \pm 0.018)e_2 \quad (56)$$

Data on the regression coefficients is listed in Table 65.

Model	Unstandardized Coefficients		Standardised Coefficients	*t*	Sig.	95% Confidence	
	B	Std. Error	Beta			Lower Bound	Upper Bound
C	.441	.009		47.0	.000	.423	.459
a	.001	.000	.107	9.1	.000	.000	.001
μ_1	.001	.013	.001	0.1	.920	-.023	.026
μ_2	.113	.003	.460	39.0	.000	.108	.119
e_1	-.012	.009	-.016	-1.4	.173	-.030	.005
e_2	-.584	.009	-.759	-64.3	.000	-.602	-.567
i_2	.000	.000	-.006	-0.5	.604	.000	.000
Ω_2	.000	.000	-.040	-3.4	.001	.000	.000
ω_2	.000	.000	-.051	-4.3	.000	.000	.000

Table 65. S3 orbits, prograde outer star. Regression coefficients – retrograde planetary orbits

The outer eccentricity again has by far the largest influence, followed by the constant and then, to a much lesser degree, μ_2. The signs of all the non-zero coefficients except for (the very weak) μ_1 are all correct.

The regression has an R^2 of 0.796, the F-statistic was 722 and the standard error of the regression was 0.071. The model's mean absolute percentage error (MAPE) of 17% is much better than for the prograde case.

4.4.5 Retrograde outer star

The integrations were now repeated with all parameters remaining as shown in Table 58 except for the inclination of the outer orbit, which changed from the range $0° - 60°$ to $120° - 180°$. A total of 3 133 integrations were run. The results are shown in Figure 85 and Figure 86.

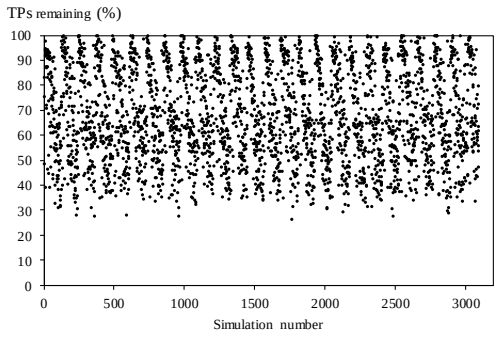

Figure 85. S3 orbits, retrograde outer star, test particle survival rates

The distribution of the critical stability ratio is not visibly different to that for the system with a prograde outer star. The orbital stability bounds found for each planetary motion are shown in Table 66.

Again, well-defined bounds were detected in nearly all cases. The mean critical semi-major axis ratio ranges of these bounds are shown in Table 67.

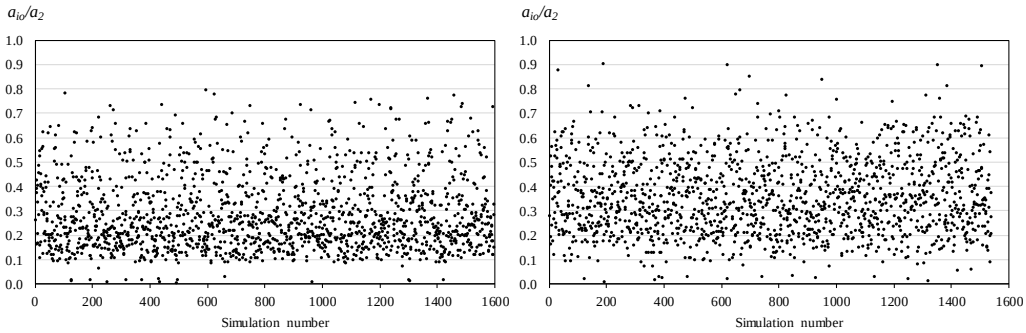

Figure 86. S3 orbits, retrograde outer star. a) prograde bounds b) retrograde bounds

Cases with well-defined orbit bounds				
Planet orbit type	Total simulations	a_{io}/a_2		
		Bounds found (no.)	Success rate (%)	Distribution (%)
Prograde	1596	1591	100	52
Retrograde	1537	1489	97	48
Total	3133	3080	98	100

Table 66. S3 orbits, retrograde outer star. Number of bounds found

Orbit type	a_{io}/a_2			
	Min	Avg	Max	SD
Prograde planetary orbits	0.007	0.287	0.853	0.096
Retrograde planetary orbits	0.009	0.360	0.908	0.156
Difference (%)	-	25	-	-

Table 67. S3 orbits, retrograde outer star. Mean critical semi-major axis ratio

The mean stability bounds are effectively identical to those for the prograde stellar case.

Prograde planetary orbits

The regression equation is

$$a_{io}/a_2 = (0.391 \pm 0.037) + (-0.071 \pm 0.027)\mu_1 + (0.033 \pm 0.006)\mu_2 + (-0.001 \pm 0.019)e_1 + (-0.597 \pm 0.019)e_2 \quad (57)$$

Data on the regression coefficients are listed in Table 68.

The regression coefficients are virtually identical to those for the prograde stellar case, with the greatest influence by far remaining the outer eccentricity. The only coefficient to change materially is that for e_1, which is weaker by a factor of nearly 30 compared with the prograde case. The signs of all the significant regression coefficients are correct.

Model	Unstandardized Coefficients		Standardised Coefficients	*t*	Sig.	95% Confidence	
	B	Std. Error	Beta			Lower Bound	Upper Bound
C	.391	.019		20.5	.000	.353	.428
a	.002	.000	.316	23.7	.000	.002	.002
μ_1	-.071	.014	-.069	-5.2	.000	-.097	-.044
μ_2	.033	.003	.144	10.9	.000	.027	.039
e_1	-.001	.010	-.001	-0.1	.937	-.019	.018
e_2	-.597	.010	-.817	-61.4	.000	-.616	-.578
i_2	.000	.000	.002	0.1	.894	.000	.000
Ω_2	.000	.000	-.002	-0.2	.873	.000	.000
ω_2	.000	.000	-.010	-0.8	.447	.000	.000

Table 68. S3 orbits, retrograde outer star. Regression coefficients – prograde planetary orbits

The regression has an R^2 of 0.727, the F-statistic was 522 and the standard error of the regression was 0.077. The model has a mean absolute percentage error (MAPE) of 23%.

Retrograde planetary orbits

The regression equation for retrograde planetary orbits is given by

$$a_{io}/a_2 = (0.425 \pm 0.037) + (-0.002 \pm 0.025)\mu_1 + (0.114 \pm 0.006)\mu_2 + (-0.002 \pm 0.018)e_1 + (-0.580 \pm 0.018)e_2 \quad (58)$$

Data on the regression coefficients is listed in Table 69.

Model	Unstandardized Coefficients		Standardised Coefficients	*t*	Sig.	95% Confidence	
	B	Std. Error	Beta			Lower Bound	Upper Bound
C	.425	.019		22.7	.000	.388	.461
a	.000	.000	.074	6.2	.000	.000	.001
μ_1	-.002	.013	-.002	-0.1	.887	-.027	.023
μ_2	.114	.003	.480	40.0	.000	.108	.119
e_1	-.002	.009	-.002	-0.2	.861	-.019	.016
e_2	-.580	.009	-.765	-63.5	.000	-.598	-.562
i_2	.000	.000	.009	0.8	.436	.000	.000
Ω_2	.000	.000	-.049	-4.1	.000	.000	.000
ω_2	.000	.000	-.020	-1.6	.100	.000	.000

Table 69. S3 orbits, retrograde outer star. Regression coefficients – retrograde planetary orbits

Again, the regression equation is almost the same as for the prograde stellar case, with all signs as expected except for μ_1. The largest difference is again for e_1, which is smaller than in the prograde stellar case by a factor of 8.

The regression has an R^2 of 0.790, the F-statistic was 688 and the standard error of the regression was 0.071. The model has a mean absolute percentage error (MAPE) of 17%.

Comparisons

The mean critical semi-major axis ratio data for the four orbital motions are summarised in Table 70 and graphs of the corresponding regressions are presented in Figure 87.

Orbit type	Critical ratio	Motions[1] Star 3	Motions[1] Planet	Mean critical semi-major axis ratio Min	**Mean**	σ	Max
S3	a_{io}/a_2	P	P	0.009	**0.289**	0.098	0.893
			R	0.010	**0.361**	0.158	0.920
		R	P	0.007	**0.287**	0.096	0.853
			R	0.009	**0.360**	0.156	0.908

1. P - prograde, R - retrograde

Table 70. Mean critical semi-major axis ratios for S3-type orbits

The averages of the mean critical semi-major axis ratios for prograde and retrograde planetary orbits are 0.288 and 0.360 respectively, with wide ranges around these values depending on the parameters of the triple. These ratios are independent of the direction of motion of the outer star.

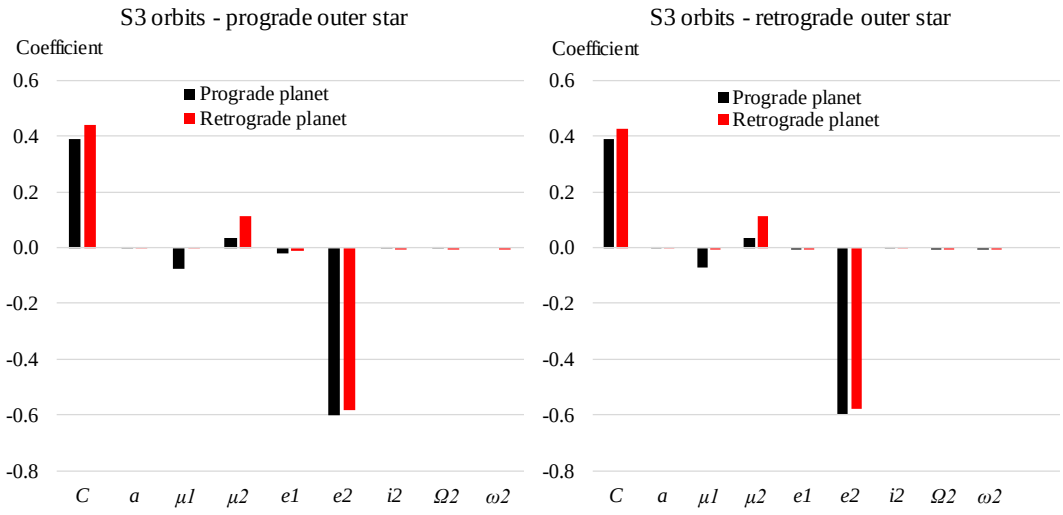

Figure 87. S3 orbits. Regression coefficients for various combinations of orbital motions a) prograde outer star, b) retrograde outer star

For non-circular orbits the eccentricity of the outer star has the dominant influence on the critical ratio, while its inclination has an insignificant effect. The inner and

outer mass ratios have weak but non-zero influences. These effects are virtually identical for prograde and retrograde motions of the outer star.

4.4.6 Comparison with previous work on S3 bounds

Although the major portion of S-type orbits discovered in triples are S3 (31 out of 36), we are not aware of any empirical work on S3 orbits *per se*.

4.4.7 Some observational examples of S3 orbits.

A listing of all the known S3 orbits is given in Table 5. The semi-major axes of some host stars and for the planets in S3 orbits around them, providing their semi-major axis ratios, are shown in Table 71, based on data in Wagner et al. (2016). For systems lacking an orbital model, projected separations are given instead of semi-major axes.

Planet	a_{io} [AU]	a_2 [AU]	a_{io}/a_2 [-]	Orbital model?	Orbit type
16 Cyg Bb	1.72	700	0.00246	No	S3
51 Eri b	13	1960	0.00663	Yes	S3
HD 196050Ab	2.47	501	0.00493	No	S3
HD 41004Ab	1.64	22	0.07450	Yes	S3
Kepler 444Ae	0.07	66	0.00106	Yes	S3
Kepler-444Ab	0.04	66	0.00061	Yes	S3
Kepler-444Ad	0.06	66	0.00091	Yes	S3
Kepler-444Af	0.08	66	0.00121	Yes	S3
Kepler-44AAc	0.05	66	0.00076	Yes	S3

Table 71. S3 orbits. Selected planets found in these orbits in triple-star systems

The semi-major axis of the planet closest to its parent star of 0.04 AU still lies well outside our inner limit of $a_{min} = 0.005$. The smallest and largest values of a_{io}/a_2 are 0.000606 and 0.265. As for S1 orbits, the discovered S3 orbits suffer from observational bias. Although the integrations found some stable bounds with semi-major axis ratios as close as 0.009 to the host star for a few stellar configurations, there were very few critical ratios lying below ~0.1 and most stable bounds ranged from 0.1 – 0.6, with some as far out as 0.9. There are probably many planets at much greater distances from their host stars than discovered to date.

The most recent discovery is KELT-4 Ab, an inflated hot Jupiter in an S3 orbit around the bright component of a hierarchical triple. The semi-major axis of KELT-4 B and KELT-4 C (our a_1) is 10 AU and that between the binary and KELT-4 A (our a_2) is 328 AU. The planet's semi-major axis is 0.0432 AU, giving it an extremely small a_{io}/a_2 of 0.000132. It is likely that BC is currently undergoing Kozai–Lidov cycles and is therefore highly eccentric (Eastman et al. 2016).

4.4.8 Triples compared with binaries

Configuring a binary case

As in the case of P1/P2 and S1 orbits, the characteristics of planetary orbits specific to triples are highlighted by repeating the previous integrations for a binary, in this case by merging the inner binary into a single star. An unchanged experimental procedure was used, and the merging of the inner binary was done exactly as described for the P1/P2 case in Section 4.1.9, i.e. of the total inner binary mass, $0.999M$ was allocated to the central star and $0.001M$ to the second star, whose orbital distance was also reduced from $a_1 = 1$ AU to $a_1 = 0.01$ AU and whose eccentricity was set at zero, while the semi-major axis of outer Star 3 was varied from 3.8 AU (the smallest Mardling limit found for S3 stellar orbits) up to 100 AU. The inner mass ratio varied from 0 to 1 and the integration time step used was calculated from equation (29), averaging ~0.030 yr or ~11 d. No other changes were necessary and the edge-detection routine did not require re-optimization. As for the S1 case, the merging of the inner binary into one star means the stellar prograde/retrograde distinction falls away.

Results for the binary case

For comparison with the triple star analysis (for a prograde outer star only) in Section 4.4.4, 6 310 integrations of this binary model were run. The critical semi-major axis ratio a_{io}/a_2 for all orbits and the test particle survival rates are shown in Figure 88. The prograde and retrograde planetary cases are not shown separately as there are no visible differences between them.

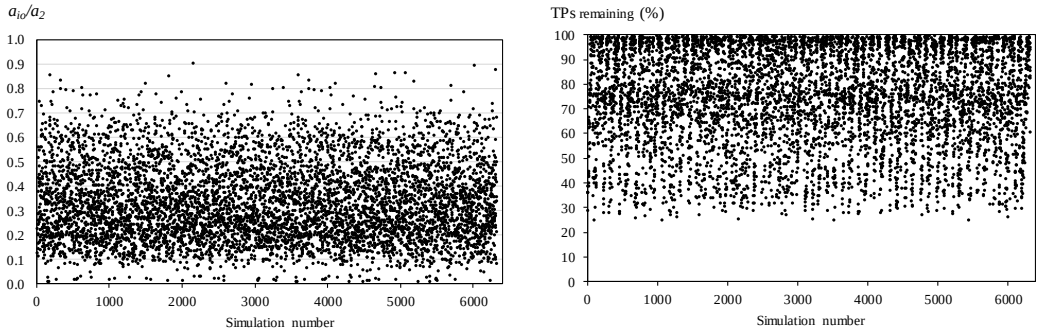

Figure 88. Binary S3 orbits. a) all stability bounds b) test particle survival rates

Compared with Figure 82 this shows a similar distribution of critical semi-major axis ratios. The average contraction of the initial test particle cloud was 32%, a bit less than the 34% for the triple case, with this smaller shrinkage being consistent with the slightly reduced influence of the inner binary because of its mergence into a single star.

The number of stability bounds found are shown in Table 72.

Bounds were found in 6 235 cases or almost all the integrations. As for the triple case, there was no meaningful difference between the number of prograde and retrograde bounds found, meaning that they were equally well-defined in the binary S3 case. The ranges of the mean critical semi-major axis ratio for these bounds are shown in Table 73.

Cases with well-defined orbit bounds				
Planet orbit type	Total simulations	a_{io}/a_2		
		Bounds found (no.)	Success rate (%)	Distribution (%)
Prograde	3218	3195	99	51
Retrograde	3092	3040	98	49
Total	6310	6235	99	100

Table 72. Binary S3 orbits. Number of bounds found

Orbit type	a_{io}/a_2			
	Min	Avg	Max	SD
Prograde planetary orbits	0.011	0.309	0.907	0.181
Retrograde planetary orbits	0.015	0.368	0.880	0.160
Difference (%)	-	19	-	-

Table 73. Binary S3 orbits. Mean critical semi-major axis ratios

The merging of the inner binary has allowed the mean critical ratio to move outwards, for both prograde and retrograde planetary orbits, and the smallest and largest orbits found have also generally increased. This is because the semi-major axis a_2 is measured to the centre of mass of the outer binary, so these two stars orbit closer at a distance closer than a_2, compared with a single star at that distance. The perturbing influence of a binary is larger than that of a single star of the same mass located at the centre of mass of the binary.

As may be expected from appropriate scaling, the difference between the mean critical ratios for the S1 and S3 binary cases is small, despite their being relative to semi-major axes a_1 and a_2 respectively, which differ by two orders of magnitude. This ratio is only 20% larger for prograde S3 binary orbits and 27% larger for retrograde orbits. As mentioned later in Section 4.5.1, S3 orbits as a fraction of a_2 extend proportionally further out than S1 orbits as a fraction of a_1.

As always, retrograde orbits are stabler, allowing the planet to approach closer to the binary companion. However, the difference in average ratio between these two types of planetary orbit of 19% for the binary case is smaller than the 25% found for the triple system from which it was reduced.

Comparison with the triple case

These results for the binary case, as shown in Table 73, are compared with the triple case in Table 74.

The average difference in S3 orbits for binaries and triples is around 5%, which is much smaller than the average 50% difference found for S1 orbits and is comparable with the average (absolute) 9% difference for P1/P2 orbits. This difference is 7% for prograde orbits, while for retrograde orbits it is a statistically insignificant 2%.

Difference in average bounds	a_{io}/a_2		
Orbit type	Triple	Binary	Δ%
Prograde planetary orbits	0.289	0.309	7*
Retrograde planetary orbits	0.361	0.368	2
Δ%	25	19	-

* significant at the 5% level

Table 74. Binary S3 orbits. Difference between mean planetary bounds in triples and binaries

The regressions for the binary case are compared with those for the triple case in Table 75.

S3 orbits	Triple		Binary		Δ (%)	S3 orbits	Triple		Binary		Δ (%)
prograde planets	B	*t*	B	*t*	B	retrograde planets	B	*t*	B	*t*	B
C	.392	35.6	.385	67.5	-2	*C*	.441	47.0	.446	88.8	1
a	.002	20.2	.000	26.6	-99	*a*	.001	9.1	.000	6.1	-100
μ_1	-.075	-5.2	-	-	-	μ_1	.001	0.1	-	-	-
μ_2	.037	11.0	.062	28.1	-	μ_2	.113	39.0	.114	58.3	-
e_1	-.020	-1.9	-	-	-	e_1	-.012	-1.4	-	-	-
e_2	-.602	-58.3	-.585	-83.1	-3	e_2	-.584	-64.3	-.599	-96.7	2
i_2	.000	0.0	-	-	-	i_2	.000	-0.5	-	-	-
Ω_2	.000	0.3	.000	-2.8	-	Ω_2	.000	-3.4	.000	-1.7	-
ω_2	.000	0.9	.000	-0.6	-	ω_2	.000	-4.3	.000	-3.1	-
R^2	0.71		0.72		-	R^2	0.8		0.81		-
Model error (%)	24.7		30.9		-	Model error (%)	16.8		22.4		-

Table 75. S3 orbits. Regression coefficients and model fits, triples versus binaries

The regression coefficients, coefficients of determination (R^2) and model errors (MAPEs) are similar for both planetary orbital motions, confirming that the effect of the binary on S3 orbits in a triple is relatively weak.

The constant for the binary case of 0.39 for prograde orbits is 18% higher than the average value of 0.33 found in previous studies (as discussed for S1 orbits). No previous regression constants are available for retrograde planets.

The regression coefficients for triples and binaries are illustrated in Figure 89.

Aside from the constant, the only parameter of importance is e_2, the eccentricity of the outer star containing the S3 orbit. The next most important influence, the mass of the binary relative to the mass of the host star (i.e. μ_2^{-1}), is far smaller. The mass ratio μ_1 is smaller still, unlike in the S1 case, where it was of equal quantitative importance to e_2.

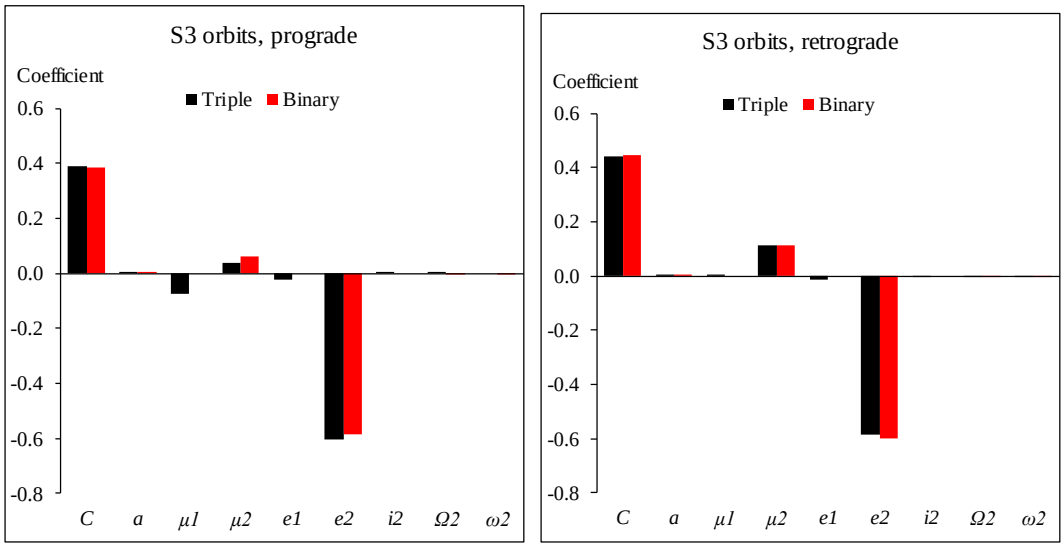

Figure 89. S3 orbits. Regression coefficients, triples versus binaries – a) prograde planets b) retrograde planets

4.4.9 Conclusions – S3 orbits

For S3 orbits a triple has a smaller mean critical semi-major axis ratio than a binary, since the outer binary has a larger effect on it than a single body of equal mass at the same distance. However, this difference is small, at around 5%. This is less than the average 7% and 11% differences for P1 and P2 orbits respectively and much smaller than the average 50% difference found for S1 orbits.

For S3 planetary orbits in triples, the critical semi-major axis ratio is in the range ~0.289 – 0.361 (compared with ~0.180 – 0.196 for S1 orbits) and is essentially independent of the direction of motion of the outer star. The critical semi-major axis ratio is ~25% larger for retrograde planetary orbits than for prograde orbits, significantly larger than the 7% difference found for S1 orbits.

The sole significant determinant of the critical ratio is the eccentricity of the outer star, with very minor contributions from the inner and outer mass ratios. These coefficients are virtually identical for prograde and retrograde planetary motions as well as the direction of motion of the outer star.

4.5 Orbit Types S1 And S3 In Triples Compared

S1 and S3 planetary orbits in triples are similar in that they both orbit a single star. They differ in that S1 orbits are in turn orbited by a close companion star and a much more distant outer star, while S3 orbits are orbited by a much more distant binary. S1 planetary orbits are therefore constrained to a relatively small size by the orbit of the close companion, whereas S3 orbits, being bounded by the more distant bodies, will have much larger critical semi-major axes. However, these semi-major axes need to be scaled by the distance of their respective perturbing bodies in order to compare the effect of the outer body being a single star or a binary. The S1 and S3 critical semimajor axis ratios for both types of planetary motion are now compared, for prograde motion of the outer body or bodies.

4.5.1 Prograde stellar orbits

In Table 76 the mean stability bounds for S1 orbits are shown as a ratio of the semi-major axis a_1 of the binary companion and those for S3 orbits as a ratio of the semi-major axis a_2 of the outer binary.

Orbit	S1	S3	
Stability bound	a_{io}/a_1	a_{io}/a_2	Δ%
All orbits	0.183	0.324	77
Prograde planetary orbits	0.180	0.289	60
Retrograde planetary orbits	0.185	0.361	95
Δ%	2	25	-

Table 76. S1 and S3 orbits compared. Mean critical semi-major axis ratios, prograde outer star/s

The S3 orbits extend proportionally further out, to around one third of a_2 while S1 orbits reach only one fifth of a_1. The scaled perturbing influence of the inner binary companion on the central star and its planets is far larger than the influence of the binary on the distant outer companion and its planets. The magnitude of this effect is large, with the critical ratio for S3 orbits being nearly 80% larger than that for S1 orbits. This difference is larger for retrograde planetary orbits than prograde orbits.

The individual components making up these average results, expressed by the regression coefficients, are shown together with their differences in Table 77.

Orbit	**Prograde**			**Retrograde**		
	S1	S3		S1	S3	
	Coefficient		Δ	Coefficient		Δ
C	.390	.392	0.002	.393	.441	0.048
a	.000	.002	0.001	.000	.001	0.000
μ_1	-.746	-.075	0.672	-.667	.001	0.668
μ_2	.005	.037	0.032	.003	.113	0.110
e_1	-.398	-.020	0.377	-.383	-.012	0.371
e_2	-.006	-.602	-0.595	.002	-.584	-0.586
i_2	.000	.000	0.000	.000	.000	0.000
Ω_2	.000	.000	0.000	.000	.000	0.000
ω_2	.000	.000	0.000	.000	.000	0.000

Table 77. S1 and S3 orbits compared. Difference in regression coefficients, prograde outer star/s

The differences for prograde and retrograde planetary orbits are very similar and the largest ones are concentrated in μ_1, e_1 and e_2. This is not surprising, as in S1 orbits the parameters of the inner binary are the dominant determinant, i.e. μ_1 and

e_1, while for S3 orbits the eccentricity of the outer star around the inner binary's orbit is the major influence (rather than the eccentricity of this distant binary itself). The outer mass ratio μ_2 has only a very small effect.

4.5.2 Retrograde stellar orbits

The mean stability bounds for S1 and S3 planetary orbits in systems where the outer stellar body or bodies are in retrograde motion are shown in Table 78.

Orbit	S1	S3	
Stability bound	a_{io}/a_1	a_{io}/a_2	Δ%
All orbits	0.196	0.322	64
Prograde planetary orbits	0.197	0.287	46
Retrograde planetary orbits	0.196	0.360	84
Δ%	-1	25	-

Table 78. S1 and S3 orbits compared. Mean critical semi-major axis ratios, retrograde outer star/s

The differences between S1 and S3 orbits are qualitatively like the prograde stellar case but smaller on average by 13%. The differences are larger for prograde planetary orbits (14% smaller) than for retrograde planetary orbits (11% smaller). Looking at the differences in regression coefficients, shown in Table 79, the general pattern is the same as for the prograde stellar case.

Orbit	Prograde			Retrograde		
	S1	S3		S1	S3	
	Coefficient		Δ	Coefficient		Δ
C	.277	.391	0.114	.423	.425	0.002
a	.000	.002	0.002	.000	.000	0.001
μ_1	-.387	-.071	0.316	-.451	-.002	0.449
μ_2	-.005	.033	0.038	-.006	.114	0.120
e_1	-.125	-.001	0.124	-.056	-.002	0.054
e_2	-.005	-.597	-0.592	-.048	-.580	-0.532
i_2	.000	.000	0.000	.000	.000	0.000
Ω_2	.000	.000	0.000	.000	.000	0.000
ω_2	.000	.000	0.000	.000	.000	0.000

Table 79. S1 and S3 orbits compared. Difference in regression coefficients, prograde outer star/s

However, the differences in influence of μ_1 and, to an even larger extent, e_1, are smaller, although the difference in e_2 remains the same. This is shown in the comparison in Figure 90. Also, the differences between prograde and retrograde planetary orbits are larger.

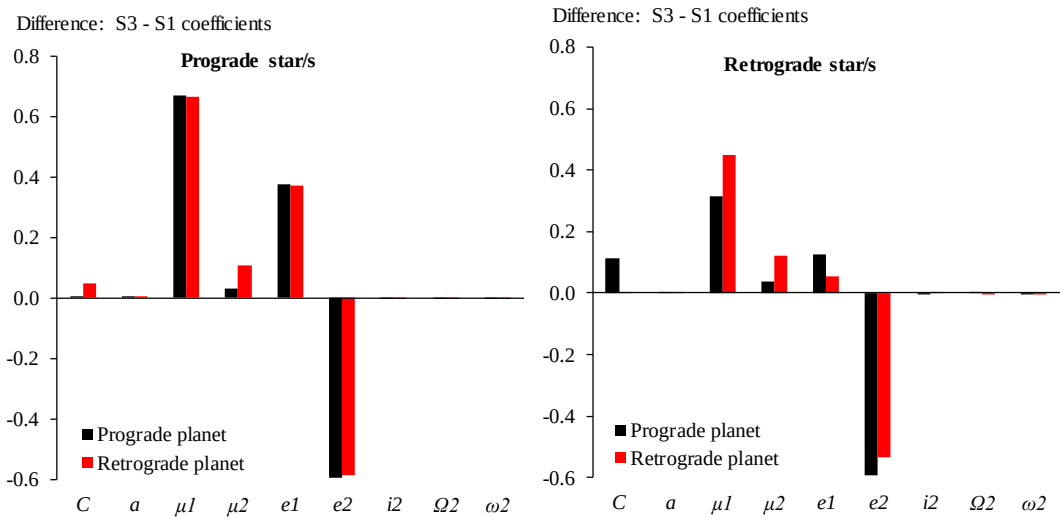

Figure 90. S1 and S3 orbits compared. Regression coefficients for a) prograde and b) retrograde outer star/s

4.5.3 Conclusions

The greater perturbing influence of a binary compared with a single star at the same distance has a correspondingly larger effect on the critical semi-major axis ratio of S3 orbits compared with S1 orbits. This difference is more muted for retrograde orbits of the outer stellar bodies.

Comparing S1 and S3 orbits, the largest differences in influence are for the inner mass ratio and the inner and outer eccentricities. However, for retrograde stellar orbits the influence of the inner eccentricity largely disappears. These effects are generally the same for prograde and retrograde planetary orbits.

4.6 Summary Of Results

4.6.1 Summary of differences between triples and binaries

The way in which the stability bounds in triples differ from those of binaries is summarised by their respective mean critical semi-major axis ratios in Table 80. The binary configurations are reduced from those of the triples by: 1) for P1 and P2 orbits, merging the inner close binary into a single star of equivalent mass, 2) for S1 orbits, reducing the outer star to one of negligible mass, and 3) for S3 orbits, again merging the close binary into a single star. All cases were for prograde motion of the outer star. The differences shown were statistically significant in all but one of the cases.

The differences in critical semi-major axis ratios were comparable for P1, P2 and S3 orbits, averaging an absolute ~8%, with this (relatively small) difference reflecting

1. the dominant influence of the outer body over the inner close binary for P-type orbits, and
2. the small semi-major axis of the close binary relative to its distance from the outer star (a consequence of the Mardling stability limit) for S3 orbits.

Orbit type	Planetary orbit	Difference in average bounds		
		Triple	Binary	Δ%
P1		a_{io}/a_2		
	Prograde	0.383	0.364	-5*
	Retrograde	0.519	0.471	-9*
	Δ%	35	29	-
P2		a_{oi}/a_2		
	Prograde	2.936	2.703	-8*
	Retrograde	1.976	1.691	-14*
	Δ%	-33	-37	-
S1		a_{io}/a_1		
	Prograde	0.180	0.257	43*
	Retrograde	0.185	0.289	57*
	Δ%	2	12	-
S3		a_{io}/a_2		
	Prograde	0.289	0.309	7*
	Retrograde	0.361	0.368	2
	Δ%	25	19	-

* significant at the 5% level

Table 80. Summary of differences between mean critical semi-major axis ratios in triples and binaries – all orbit types

The absolute differences in mean critical semi-major axis ratios for prograde and retrograde planetary orbits, of $\sim 20\% - 40\%$, are broadly comparable for triples and binaries.

For S1 orbits the differences in mean critical semi-major axis ratios are much larger at ~50%, because this ratio is measured relative to a_1 rather than the larger a_2. The differences between prograde and retrograde orbits are also more marked.

For the P-type orbits in triples the expansion of the inner body from a single star into a binary pushes planetary orbits outwards. The regressions in Table 32 show that compared with binaries, for triples the influence of the outer star's eccentricity is significantly smaller for inner prograde orbits and materially larger for outer prograde orbits, with no difference for retrograde orbits.

For S1 orbits in triples the additional influence of the outer star makes the planetary orbits move inwards, with the mean critical semi-major axis ratio reducing by around 30%; the difference in critical ratio between prograde and retrograde planetary orbits also shrinks proportionally more than for the other orbit types. The stability of S1 planetary orbits is determined only by the inner mass ratio and inner eccentricity of the binary, in approximately equal measure, and we find that the inner mass ratio has a larger effect in triples than in binaries, while the influence of inner eccentricity is the same.

For S3 orbits in triples, the presence of the outer close binary also pushes planetary orbits inwards, but the mean critical semi-major axis ratio in a triple is on average only 5% smaller than for a binary, since the enhanced effect of the second "body" being a binary rather than a single star is diminished because of its distance. For both binaries and triples the dominant determinant of the critical

ratio is the eccentricity of the outer body's orbit, with the outer mass ratio being of minor importance.

4.6.2 Summary of results for triples

The mean critical semi-major axis ratios and their ranges for the various orbital configurations are summarised in Table 81 and shown in Figure 91 and Figure 92. These are the average ratios over all the combinations of parameters used in the parameter space of the integration. The minimum and maximum critical ratios found in the integrations are of interest as a guide to the limits of possible orbits and in relation to observational discoveries.

Orbit type	Critical ratio		Motions[1]		Critical semi-major axis ratio			
			Star 3	Planet	Min	**Mean**	σ	Max
P1	a_{io}/a_2		P	P	0.131	**0.383**	0.147	0.892
				R	0.113	**0.519**	0.108	0.828
			R	P	0.110	**0.385**	0.077	0.897
				R	0.112	**0.537**	0.132	0.857
		Non-Kozai	P	P	0.049	**0.484**	0.099	0.837
		Kozai		P	0.288	**0.495**	0.100	0.748
		Non-Kozai	R	P	0.423	**0.666**	0.078	0.853
		Kozai		P	0.105	**0.531**	0.096	0.818
P2	a_{oi}/a_2		P	P	1.253	**2.936**	1.449	5.197
				R	1.184	**1.976**	0.507	4.916
			R	P	0.924	**2.773**	0.891	5.384
				R	0.591	**1.960**	0.571	4.957
		Non-Kozai	P	P	1.755	**1.941**	0.051	2.242
		Kozai		P	1.759	**1.933**	0.176	2.532
		Non-Kozai	R	P	1.095	**1.335**	0.127	1.820
		Kozai		P	1.363	**1.753**	0.195	2.510
S1	a_{io}/a_1		P	P	0.015	**0.180**	0.049	0.760
				R	0.015	**0.185**	0.122	0.771
			R	P	0.015	**0.197**	0.059	0.772
				R	0.028	**0.196**	0.157	0.772
S3	a_{io}/a_2		P	P	0.009	**0.289**	0.098	0.893
				R	0.010	**0.361**	0.158	0.920
			R	P	0.007	**0.287**	0.096	0.853
				R	0.009	**0.360**	0.156	0.908

1. P - prograde, R - retrograde

Table 81. Summary of mean critical semi-major axis ratios for various orbital configurations

The mean critical ratios for the various configurations were discussed in the relevant sections. There are only very small differences in the mean critical ratios of similar-motion (i.e. prograde or retrograde) planetary orbits for different orbital motions of the outer star.

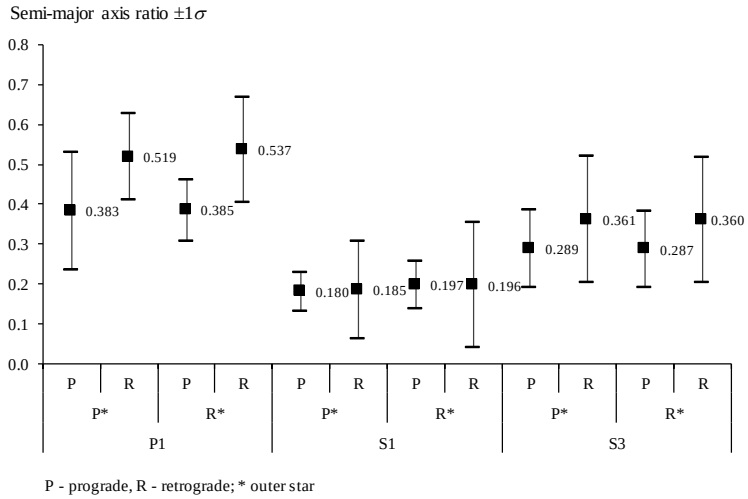

Figure 91. Summary of mean and standard deviation of critical semi-major axis ratios for P1, S1 and S3 orbits

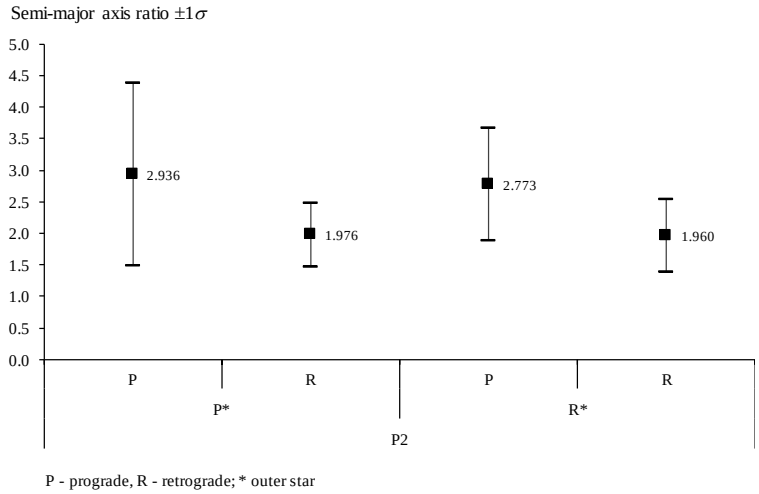

Figure 92. Summary of mean and standard deviation of critical semi-major axis ratios for P2 orbits

There are, however, large differences between the stable bounds for prograde and retrograde planetary orbits, with retrograde orbits being stabler and thus closer to the perturbing body. This means further away from the central binary for P1 orbits, closer to the central binary for P2 orbits and further away from the outer star for S3 orbits. This difference is, however, quite muted for S1 orbits.

This also manifests itself in the ranges, for the same reasons, reflecting the greater stability of retrograde orbits, which leads to better-defined stability boundary edges. It is noticeable that for P1 orbits the error range for P*/R and R*/P motions is smaller than for P*/P and R*/R combinations, where * refers to the outer star. A prograde orbit of the planet orbiting the outer star will be retrograde to the "outer" star of the binary and therefore more stable and vice versa.

S3 orbits generally have larger critical semimajor axis ratio than S1 orbits.

The effect on the planetary stability bounds of the outer star being retrograde is shown in Table 82. The table shows the percentage difference in the mean critical semi-major axis ratio for the various orbital configurations, where the directions of the planetary motions are the same in each case and the only difference is the direction of motion of the outer star. The significance level is shown for the mean critical ratio; differences in the regression constant are shown for comparison only.

Orbit type	Ratio	Planet motion	Difference in mean stable ratio (%)	Difference in regression constant (%)
P1	a_{io}/a_2	P	1	6
		R	3 *	15
P2	a_{oi}/a_2	P	-6 *	-12
		R	-1	15
S1	a_{io}/a_1	P	9 *	-29
		R	6 *	8
S3	a_{io}/a_2	P	-1	0
		R	0	-4
Average (abs.)		-	3	11

* significant at the 5% level

Table 82. Summary of differences in mean critical semi-major axis ratios and regression constants, for retrograde relative to prograde stellar motion, with the same planetary motion

Although the absolute differences in critical ratio are quite small, with an absolute average of 3%, half are statistically significant.

The effect on the planetary stability bounds of the direction of motion of the planets is shown in Table 83. The table again shows the percentage difference in the mean critical semi-major axis ratio and the regression constant, for a retrograde planet compared with a prograde one, with the direction of motion of the outer star being the same.

Here the absolute differences are significant and large, averaging 37% for P1 orbits, 31% for P2 orbits and 25% for S3 orbits, with the signs being consistent with the greater stability of retrograde orbits. S1 orbits are, as expected, unaffected.

The differences in the critical semimajor axis ratios between S1 and S3 orbits is summarised in Table 84.

For prograde stellar orbits the mean critical ratio for S3 orbits is on average nearly 80% larger than that for S1 orbits, as the perturbing effect of the inner binary companion on the central star and its planets is far larger than the influence of this inner binary on the distant outer companion and its planets. This difference is much larger for retrograde planetary orbits than prograde orbits. These differences are smaller for a retrograde outer star.

Orbit type	Ratio	Star 3 motion	Difference in mean stable ratio (%)	Difference in regression constant (%)
P1	a_{io}/a_2	P	36 *	31
		R	39 *	42
P2	a_{oi}/a_2	P	-33 *	-38
		R	-29 *	-18
S1	a_{io}/a_1	P	2	1
		R	-1	53
S3	a_{io}/a_2	P	25 *	13
		R	25 *	9
Average (abs.)		-	24	25

* significant at the 5% level

Table 83. Summary of differences in mean critical semi-major axis ratios and regression constants for retrograde relative to prograde planetary motion, with the same stellar motion

Stellar orbit	Planetary orbit	Orbit type S1 a_{io}/a_1	Orbit type S3 a_{io}/a_2	Δ%
P	All orbits	0.183	0.324	77
	P	0.180	0.289	60
	R	0.185	0.361	95
	Δ%	2	25	-
R	All orbits	0.196	0.322	64
	P	0.197	0.287	46
	R	0.196	0.360	84
	Δ%	-1	25	-

Table 84. Summary of differences in S1 and S3 mean critical semi-major axis ratios

For prograde stellar orbits, in S1 orbits the inner binary (μ_1 and e_1) is the dominant determinant of the stable region, while for S3 orbits e_2 has the major influence. For retrograde stellar orbits the influences of μ_1 and e_1, are smaller, while the effect of e_2 is unchanged.

The mean critical semi-major axis ratios and their ranges for non-Kozai and Kozai regimes are summarised in Figure 93, for prograde planetary orbits.

For a prograde outer body, the mean critical ratios for both inner and outer planetary orbits are essentially unaffected by the Kozai regime, but for a retrograde outer star they are substantially different, with the ratio for inner orbits shrinking by 20% and that for outer orbits expanding by over 30%.

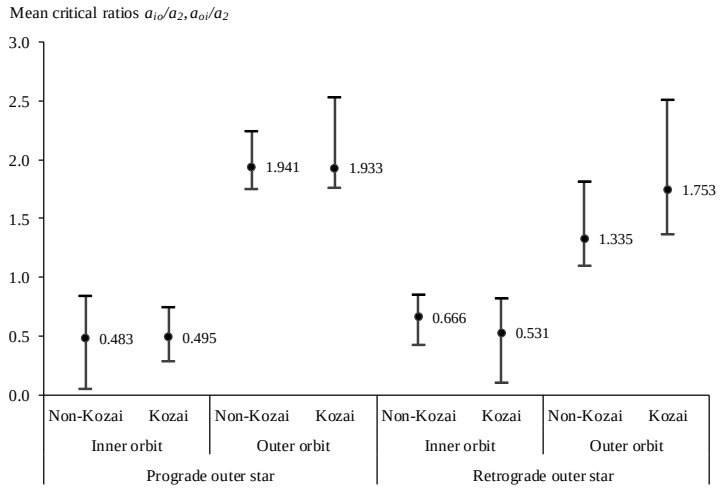

Figure 93. Summary of mean and range of critical semi-major axis ratios for non-Kozai and Kozai cases, for both stellar motions

For a prograde outer star, Kozai resonance results in a 44% smaller constant for inner orbits and one 22% larger for outer orbits, while a retrograde outer body does not result in a significant difference in either constant.

Statistics on the semi-analytical regression equations for each type of orbital configuration, 24 in all, are summarised in Table 85. The semi-major axis ratio a was included solely as an error check.

The following general conclusions may be drawn from Table 85:

1. Over 45 000 integrations were run, from which nearly 30 000 stability bounds were found, a success rate of 65%. One third of the integrations did not result in stability bounds with edges that were sufficiently well-defined. The success rate was 96%for P2 orbits, but only around 38% for P1 orbits due to their more diffuse nature. S3 orbits had success rates approaching 100%, while those for S1 orbits were approximately 55%, again because of their more tenuous boundaries.
2. The various regressions resulted in 24 regression constants and 192 coefficients. Ignoring those smaller than 0.01, only four were of the "wrong" sign and these were all small ($< |0.06|$).
3. Looking at the average of the absolute values of the coefficients, it is clear that i_2, Ω_2 and ω_2 have a negligible influence on the stability bounds.
4. The critical semimajor axis ratio scales with the semi-major axis ratio a and its coefficient should be zero, so its average absolute value of 0.001 provides an indication of the intrinsic error of the methodology.
5. The only influences (for relatively small inclinations) were therefore from the mass ratios and eccentricities, with those from μ_1 and e_2 being an order of magnitude larger than those from μ_2 and e_1.
6. For the mass ratios, on average the inner ratio μ_1 had far more influence on the stability bounds than the outer ratio μ_2, by a factor of six. The mass ratios' largest impact was on S1 orbits, with a much weaker but non-negligible effect on P2 orbits.
7. The configuration where μ_2 had the greatest effect was, unsurprisingly, on S3 and P2 orbits, but its effect was nevertheless negligible.

8. For the eccentricities, e_2 had an average effect of over eight times that of e_1. Its influence was pervasive over all orbital configurations except S1, with its strongest impact being on P2 orbits. The only configuration where e_1 had a significant influence was for S1 orbits; again, this was not surprising.
9. The average R^2 of the regressions was 0.49, ranging from a very poor 0.02 to a high 0.86. The mean average percentage error (MAPE) of the regression models generally correlated with R^2, ranging from a best case of 3% to a worst case of 74%, with an average of 20%.
10. P2 orbits generally had the best fits, followed by S3 orbits. The poorest fits were for S1 orbits with a retrograde star, followed by S1 orbits with a prograde star.

4.7 Comparison With Previous Work

Since the results for triples are largely new work, there is little existing empirical research against which our conclusions can be compared. The one area of overlap is between our "triple-reduced-to-binary" cases and previous work on binaries. Although the amount of data here is also very sparse, this comparison is included in this section as a check of our methodology.

Only results that correspond with previous comparable data are shown. Our results on S3 orbits are thus excluded, as are our results pertinent to retrograde stellar motion and high-inclination triples.

4.7.1 Comparison of scope

The ranges of the orbital parameters and test particle clouds used in this study are shown in Table 86, together with those used in the single triple study by Verrier and Evans (2007), which examined P1 and P2 orbits. The table excludes all the additional orbital parameters with which we extended previous studies. For interest, the parameters of prior studies of binaries are also shown, as well those of our triple-to-binary reductions.

Our semi-major axis ratio range a is slightly wider than used by Verrier & Evans, since the Mardling limit can extend as low as ~3. Our inner mass ratio range was also broader, with a smaller lower limit, while the range for the outer mass ratio was also larger and focused on higher mass ratios that included heavily inverted configurations. The range of inner and outer eccentricities we used was also larger.

Comparing binary studies, our integrations of S1 orbits covered a wider range of mass ratios and broadly the same eccentricities as previous studies. Mass ratios for our P1 orbits were the same (for technical reasons an upper limit of 1.0 was used, but this was actually equivalent to 0.5 in that specific case) and eccentricities were generally similar.

Retrograde planetary orbits were considered in only two of the eight prior studies, one for S1 orbits and one for P1 orbits, while our analyses examined prograde and retrograde planetary motions for all orbit types. The inner and outer limits of the test particle clouds we used were much more extended than in the two studies for which this data was shown.

Orbit type	Critical ratio	High-inclination	Motions[1]		Critical semi-major axis ratio				Regression coefficients[2]										Integrations			Model fit			
			Star 3	Planet	Min	Avg	σ	Max	C	a	μ_1	μ_2	e_1	e_2	i_2	Ω_2	ω_2	Done	Bounds found	Rate (%)	R^2	F	SE	MAPE (%)
P1	a_{i0}/a_2	-	P	P	0.131	0.383	0.147	0.892	0.439	0.000	-0.005	-0.020	-0.004	-0.114	0.000	-0.001	-0.001	5 413	1 782	32.9	0.132	34	0.093	19
		-		R	0.113	0.519	0.108	0.828	0.573	0.000	0.009	-0.043	*-0.010*	-0.469	0.000	0.000	0.000	5 343	976	18.3	0.671	246	0.062	10
		-	R	P	0.110	0.385	0.077	0.897	0.463	0.000	0.190	-0.037	*-0.021*	-0.187	-0.001	0.000	0.000	2 122	569	26.8	0.547	285	0.358	9
		-		R	0.112	0.537	0.132	0.857	0.656	0.000	*-0.056*	-0.022	0.005	-0.510	0.000	0.000	0.000	2 685	539	20.1	0.710	162	0.071	12
		Non-Kozai	P	P	0.049	0.484	0.099	0.837	0.545	0.000	-0.044	-0.018	0.000	0.000	-0.001	0.000	0.000	342	256	74.9	0.024	2	0.099	18
		Kozai		P	0.288	0.495	0.100	0.748	0.303	0.000	-0.170	0.016	0.000	0.000	0.003	0.000	0.000	319	47	14.7	0.173	2	0.095	19
		Non-Kozai	R	P	0.423	0.666	0.078	0.853	0.685	-0.001	0.066	0.029	0.000	0.000	-0.001	0.000	0.000	273	178	65.2	0.202	4	0.024	13
		Kozai		P	0.105	0.531	0.096	0.818	0.738	0.000	-0.038	-0.083	0.000	0.000	-0.001	0.000	0.000	207	102	49.3	0.194	6	0.088	12
P2	a_{o1}/a_2	-	P	P	1.253	2.936	1.449	5.197	2.377	-0.003	0.053	0.044	0.090	1.997	0.000	-0.002	-0.002	5 413	5 133	94.8	0.828	3 080	0.239	6
		-		R	1.184	1.976	0.507	4.916	1.483	-0.004	0.131	-0.008	*-0.036*	1.725	0.002	0.001	0.001	5 343	5 082	95.1	0.860	3 880	0.190	6
		-	R	P	0.924	2.773	0.891	5.384	2.089	-0.004	0.809	0.114	0.015	1.298	-0.001	0.000	0.000	2 122	1 895	89.3	0.271	26	0.126	31
		-		R	0.591	1.960	0.571	4.957	1.708	-0.006	0.182	0.023	0.018	1.693	-0.001	0.000	0.000	2 685	2 455	91.4	0.773	1 039	0.269	8
		Non-Kozai	P	P	1.755	1.941	0.051	2.242	1.921	-0.001	0.048	0.016	0.000	0.000	0.001	0.000	0.000	342	341	99.7	0.267	31	0.044	4
		Kozai		P	1.759	1.933	0.176	2.532	2.346	-0.004	0.066	0.044	0.000	0.000	-0.003	0.000	0.000	319	319	100.0	0.579	107	0.115	3
		Non-Kozai	R	P	1.095	1.335	0.127	1.820	1.288	-0.002	0.085	-0.004	0.000	0.000	0.007	0.000	0.000	273	273	100.0	0.555	83	0.085	4
		Kozai		P	1.363	1.753	0.195	2.510	1.357	-0.004	0.033	-0.016	0.000	0.000	0.009	0.000	0.000	207	204	98.6	0.574	67	0.129	5
S1	a_{i0}/a_1	-	P	P	0.015	0.180	0.049	0.760	0.390	0.000	-0.746	0.005	-0.398	-0.006	0.000	0.000	0.000	1 532	819	53.5	0.583	142	0.081	35
		-		R	0.015	0.185	0.122	0.771	0.393	0.000	-0.667	0.003	-0.383	0.002	0.000	0.000	0.000	1 480	785	53.0	0.561	124	0.081	37
		-	R	P	0.015	0.197	0.059	0.772	0.277	0.000	-0.387	-0.005	-0.125	-0.005	0.000	0.000	0.000	1 586	957	60.3	0.126	17	0.139	67
		-		R	0.028	0.196	0.157	0.772	0.423	0.000	-0.451	-0.006	-0.056	-0.048	0.000	0.000	0.000	1 455	791	54.4	0.176	20	0.143	74
S3	a_{i0}/a_2	-	P	P	0.009	0.289	0.098	0.893	0.392	0.002	-0.075	0.037	-0.020	-0.602	0.000	0.000	0.000	1 604	1 599	99.7	0.710	478	0.084	25
		-		R	0.010	0.361	0.158	0.920	0.441	0.001	0.001	0.113	-0.012	-0.584	0.000	0.000	0.000	1 562	1 501	96.1	0.796	722	0.071	17
		-	R	P	0.007	0.287	0.096	0.853	0.391	0.002	-0.071	0.033	-0.001	-0.597	0.000	0.000	0.000	1 596	1 591	99.7	0.727	522	0.077	23
		-		R	0.009	0.360	0.156	0.908	0.425	0.000	-0.002	0.114	-0.002	-0.580	0.000	0.000	0.000	1 537	1 489	96.9	0.790	688	0.071	17
Average[3]/total[4]		-	-	-	-	-	-	-	-	0.001	0.183	0.036	0.050	0.434	0.001	0.000	0.000	45 760	29 683	64.9	0.493	490	0.118	20

1. P - prograde, R - retrograde
2. Italics indicate wrong sign, except for Kozai data
3. Of absolute values for regression coefficients
4. Of integrations and bounds

Table 85. Summary of regression statistics for all triple orbital configurations

System	Orbit type	Reference	Integration time [yr]	Orbital parameter ranges							Test particle cloud parameters					
				a_1 [AU]	a_2 [AU]	$a=a_2/a_1$	u_1	u_2	e_1	e_2	$i_2^{(1)}$ [°]	TP e	TP i [°]	TP Ω_2 [°]	TP ω_2 [°]	TP *amin* [AU]	TP *amax* [AU]
Previous work																	
Triple	**P1**	**Verrier (2007)**	$\mathbf{10^7}$	**2 - 5**	**20 - 100**	**4 - 100**	**0.33 - 0.51**	**0.05 - 1.1**	**0 - 0.6**	**0 - 0.6**	**0**						
Triple	**P2**	**Verrier (2007)**	$\mathbf{10^6}$	**1 - 5**	**20 - 100**	**4 - 100**	**0.33 - 0.50**	**0.05 - 1.0**	**0 - 0.6**	**0 - 0.6**	**0**						
Binary	S1	Holman (1999)	10^4 T_{bin}	1	-	-	0.1 - .9	-	0 - 0.8	-	-	0	0			.02a_1	0.5a_1
Binary	P1	Holman (1999)	10^4 T_{bin}	1	-	-	0.1 - 0.5	-	0 - 0.7	-	-	0	0			1a_1	5a_1
Binary	P1	Pilat-Lohinger (2003)	$5x10^4$ T_{bin}	1	-	-	0.5	-	0 - 0.5	-	-	0	0 - 50				
Binary	P1	Musielak (2005)	10^3 - $4x10^4$ T_{planet}	5 - 15	-	-	0.091 - 474	-	0	-	-	0	0				
Binary	S1	Musielak (2005)	10^3 - $1.5x10^5$ T_{planet}	5 - 15	-	-	0.25 - 0.75	-	0	-	-	0	0				
Binary	S1	Mudryk (2006)	$3x10^3$ T_{bin}	1	-	-	0.1 - 0.5	-	0 - 0.6	-	-	0	0				
Binary	P1	Doolin (2011)	$5x10^4$ T_{bin}	-	-	-	0.1 - 0.5	-	0 - 0.6	-	-	0	0 - 180	0 - 180	90	1.5a_1	5a_1
Binary	S1	Morais (2012)	$1.2x10^4T_{bin}$	1	-	-	0 - 0.4	-	0	-	-	0	0, 180				
This work																	
Triple	**S1**	-	$\mathbf{10^5}$ - $\mathbf{10^6}$	**0.01**	**0.01a_m - 1**	**a_m - 100**	**0.001 - 0.5**	**0.001 - 2.2**	**0 -0.7**	**0 -0.7**	**0-60/120-180**	**0**	**0 -180**	**0**	**0**	**0.005**	**0.9a_1**
Triple	**P1**	-	$\mathbf{10^5}$ - $\mathbf{10^6}$	**1**	**a_m - 100**	**a_m - 100**	**0.1 - 0.5**	**0.2 - 2.3**	**0 -0.9**	**0 -0.9**	**0-60/120-180**	**0**	**0 -180**	**0**	**0**	**0.005**	**2x 5:1 MMR**
Triple	**P2**	-	$\mathbf{10^5}$ - $\mathbf{10^6}$	**1**	**a_m - 100**	**a_m - 100**	**0.1 - 0.5**	**0.2 - 2.3**	**0 -0.9**	**0 -0.9**	**0-60/120-180**	**0**	**0 -180**	**0**	**0**	**0.005**	**2x 5:1 MMR**
Triple	**S3**	-	$\mathbf{10^5}$ - $\mathbf{10^6}$	**0.01**	**0.01a_m - 100**	**a_m - 100**	**0.001 - 0.5**	**0.001 - 2.2**	**0 -0.7**	**0 -0.7**	**0-60/120-180**	**0**	**0 -180**	**0**	**0**	**0.005**	**Eqn. (54)**
Binary	S1	-	10^5 - 10^6	0.01	-	-	.001 - 1	-	0 -0.7	-	-	0	0 -180	0	0	0.005	0.9a_1
Binary	P1	-	10^5 - 10^6	1	a_m - 100	a_m - 100	0.1 - 1	-	0 -0.9	-	-	0	0 -180	0	0	0.005	2x 5:1 MMR

(1) Excluding high-inclination cases

TP - test particle cloud, a_m - Mardling limit

Table 86. Comparison with variable ranges used in previous empirical studies

4.7.2 Comparison of results

The data are shown in Table 87. The number of significant figures shown are as per the sources. In the comparisons we use both mean critical semi-major axis ratios and the regression constants. They contain dissimilar but useful information and both are necessary, since only a minority of previous studies provided a regression constant. Our regression coefficients are not shown as they are not comparable with the different regression models used in other studies.

System	Orbit type	Reference	Critical semi-major axis ratio*		Constant range (P1 orbits)		Constant range (S1 orbits)	
			Prograde planets	Retrograde planets	Prograde planets	Retrograde planets	Prograde planets	Retrograde planets
Previous work								
Triple	**P2**	**Verrier 2007**[1]	**2.92**		**2.92**			
Triple	**P1**	**Verrier 2007**[1]	**0.466**				**0.466**	
Binary	S1	Holman 1999	0.464				0.464	
Binary	P1	Holman 1999	1.60		1.60			
Binary	P1	Pilat-Lohinger 2003	2.1 - 3.85[2]		2.1 3.85			
Binary	P1	Musielak 2005	1.75 - 2.45		1.75 2.45			
Binary	S1	Musielak 2005	0.22 - 0.46				0.22 0.46	
Binary	S1	Mudryk 2006	0.32 - 0.34				0.32 0.34	
Binary	P1	Doolin 2011	2.3 - 3.9	1.3 - 2.7[3]	2.3 3.9	1.3 2.7		
Binary	S1	Morais 2012	0.4	0.6				
Averages	S1	-	0.384	0.6			0.33 0.40	
for binaries	P1	-	2.44	2.00	2.56	1.3 2.7		
This work (prograde stellar orbits only)								
Triple	**S1**	-	**0.180**	**0.185**			**0.390**	**0.393**
Triple	**P1**	-	**0.383**	**0.519**	**0.439**	**0.573**		
Triple	**P2**	-	**2.94**	**1.98**	**2.38**	**1.48**		
Triple	**S3**	-	**0.289**	**0.361**			**0.392**	**0.441**
Binary	S1	-	0.257	0.289			0.360	0.378
Binary	P1	-	2.70	1.69	0.195	0.21		

* Note that for our work these are mean values over a large parameter space and may not be fully comparable to previous work

(1) Abbreviated model

(2) Assuming binary semi-major axis is 1 AU

(3) Read from their Figure 14

Table 87. Comparison with mean critical semi-major axis ratios and regression constants from previous empirical studies

There is little to compare with, in terms of previous work on triples. Our prograde P1 mean critical ratio of 0.383 is 18% smaller than the 0.466 from Verrier and Evans (2007), while our P2 critical ratio of 2.94 is very close to their 2.92.

The reason for the P1 discrepancy is not clear. The code used, “Moirai”, was not made public so replication is not possible. Also, a relatively limited number of

configurations and test particles were used in the 2007 study. Although a much larger parameter space and much larger clouds of test particles were used in our study, the boundary of P1 orbits is always far more tenuous than that for P2 orbits, and the selection of a density cutoff to define its edge is necessarily arbitrary. So while results should be consistent within a study, a difference of this magnitude across studies is quite possible for P1 orbits.

Another study by Verrier and Evans (2006) can be mentioned, even though it is not of a triple but a close binary with a large planet orbiting one component. Since this is conceptually no different to a triple with a very low-mass inner binary component it provides an interesting, if extreme, example. Their prograde S1 critical ratio was 0.605 compared with our 0.180; they found no prograde P2 bound (versus our 0.383) but a retrograde ratio of 0.234 (compared with our 0.518); their prograde and retrograde P2 ratios of 3.04 and 1.87 respectively were close to our 2.94 and 1.98, but their prograde and retrograde S3 ratios of 0.070 and 0.164 were quite different to our 0.289 and 0.361. It may be expected that the results for orbits *within* this "triple" are quite different because of its unusual configuration, while those for orbits *external* to it are similar, being relatively unconcerned with the inner binary structure of the "triple".

Although the object of this work was to establish the stable planetary regions of triples, for interest we have also included the few historical results for binaries. The results of our integrations where the triple was reduced to a binary are also shown for comparison. The regression constants, where they were provided in other studies, are compared with ours in Figure 94.

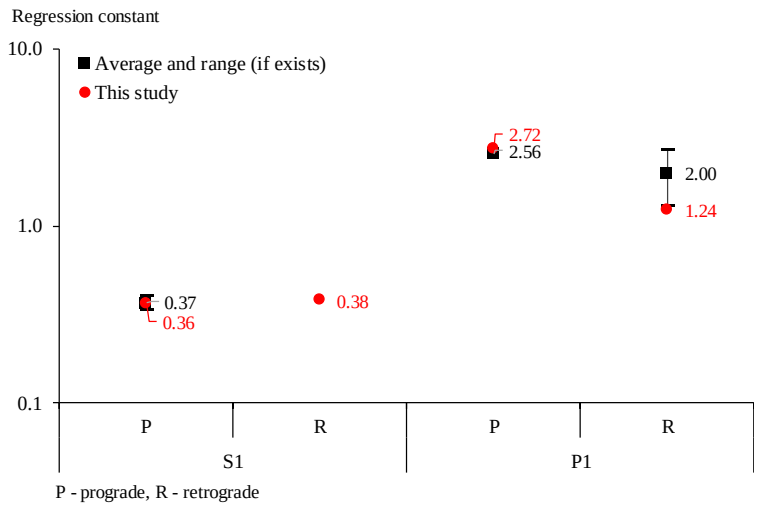

Figure 94. Comparison of results for binaries – regression constants

For prograde S1 and P1 orbits our results are very close to those in previous work. There have been no studies on S1 retrograde orbits. For P1 retrograde orbits there exist only two other results; ours coincides with the lower one, from Doolin and Blundell (2011).

The critical semi-major axis ratios found in previous research are shown in Figure 95, together with both our mean critical semi-major axis ratios and our regression constants.

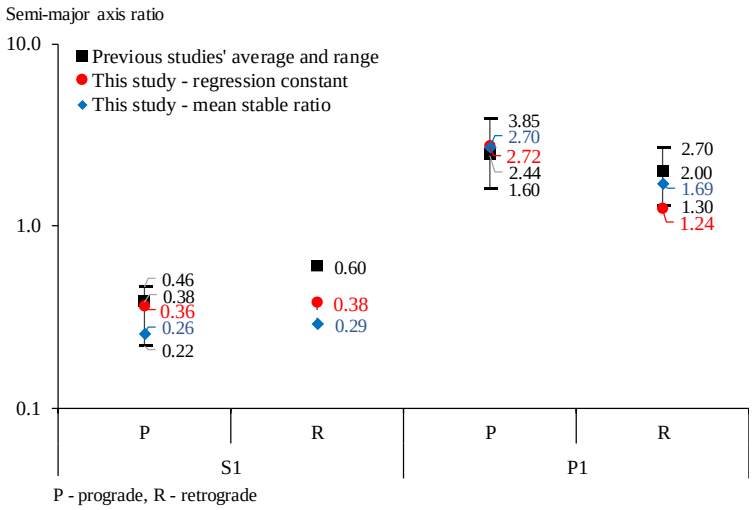

Figure 95. Comparison of results for binaries – critical semi-major axis ratios

Our mean critical ratios shown are the average of the P1/P2, S1 and S3 binary reductions; while the results from these triple reductions should be identical, they did show some differences.

For binary S1 prograde planetary orbits, previous results for the critical semi-major axis ratio varied widely, ranging from $0.22 - 0.46$ and averaging 0.38. Our corresponding mean critical ratio of 0.26 and regression constant of 0.36 are within this range.

For P1 prograde orbits the range was $1.6 - 3.85$, with the important study by Holman and Wiegert (1999) being the lowest. The average is 2.44, close to our mean critical ratio and constant of 2.70 and 2.72 respectively.

Of the two studies that addressed retrograde planetary orbits, the one for S1 orbits found a critical ratio of 0.60. Our results for the mean critical ratio and constant, of 0.29 and 0.38 respectively, are ~45% lower. The results for our S1 prograde and retrograde orbit types should be mutually consistent, however, since the integration procedure was simply repeated with only one number, the prograde/retrograde toggle, changing. The study for P1 orbits, by Doolin and Blundell (2011), found critical ratios in the range $1.3 - 2.7$; our results were comparable, with a mean critical ratio of 1.69 and a regression constant of 1.24.

Despite the small amount of data from previous studies and our integrations, the above results compare well. The one relatively large difference for retrograde S1 orbits is curious and suggests further investigation.

4.7.3 New binary data

The integrations of reduced triples contribute some new results and data points to the analysis of binaries. These results are consolidated in Appendix D.

Chapter 5

Conclusions

5.1 What Was Done In This Study

The main contribution of this work has been to extend the analysis of planetary stability in triples into configurations and parameter ranges that have not been previously researched, as well as to expand the number of variables and the understanding of their influence on stability in these systems.

We first reviewed the current state of knowledge regarding stellar multiplicity, hierarchical orbits and exoplanet multiplicity, before defining the characteristics of the planetary orbit types in triples and documenting the observational discoveries of these planets to date.

We then outlined previous approaches to the problem of planetary stability within triples and discussed the merits of theoretical and computational approaches. In the body of the work, we compared the results of theoretical and numerical analyses in two different situations, to illustrate the inadequacy of the former method.

The preparations for the investigation were then set out, including a review of the observed ranges of parameters for triple stars and their planets; the selection of the types of orbits to be investigated; Kozai resonances; the parameter ranges to be investigated; the selection of numerical method and integrator; the choice of computational parameters and their ranges for planetary orbits, and the development of code for the detection of the edges of planetary stability bounds.

The body of the research then investigated the generalised stability of triple stellar configurations for all S-type and P-type orbital configurations, for prograde and retrograde planetary orbits and prograde and retrograde stellar orbits. We then reduced the triple configurations to binaries and re-ran the integrations, to highlight how the results for triples differ from those for binaries. The results for both triples and binaries were then compared with previous research and with observational examples.

The construction of multiple regression equations resulted in semi-analytical models for each type of orbital configuration studied, 24 in all.

5.2 How This Extended Previous Work

This extended previous research by expanding into, and investigating new areas through

This work expanded into, and investigated new areas through

1. Providing a generalised mapping of the regions of planetary stability in triples, by:
2. examining all four types of orbits – P1, P2, S1 and S3;
3. investigating these orbit types for both prograde and retrograde motion of the planets;

4. investigating them for both prograde and retrograde motion of the outer body of the triple;
5. investigating highly-inclined orbits of the outer star, stellar Kozai resonance and its effect on the region of stability for P1 and P2 orbits;
6. extending the number of parameters used to all relevant orbital elements of the triple's stars, and
7. expanding these elements and mass ratios to wider ranges that will accommodate recent and possible future observational discoveries.
8. To highlight how the stability of planets in triple systems differs from that for binaries, an analysis of these systems over the same parameter space was required, resulting in a contribution to the body of empirical work on binaries as well.

This advanced our understanding of the regions of stability within a significantly extended parameter space. It also enabled comparisons with some observational results which were not possible previously. The small region where our work overlapped with other studies enabled comparison with, and confirmation of, these studies. The correspondence between our work and previous research in these areas of overlap was good, engendering some confidence in the new results, where validation by other work is not yet possible.

5.3 New Findings

Most findings were new, simply because they were made in an area that had not yet been investigated comprehensively. Some of the more interesting or significant ones were as follows.

Low-inclination P1 and P2 orbits

Compared with binaries, the inner and outer critical semi-major axis ratios of triples are further from the central star for both prograde and retrograde planetary orbits. The difference is small but statistically significant, indicating the dominant influence of the outer body over the inner binary. These relatively small differences between triples and binaries results from the Mardling stability limit for triples, which precludes them from becoming too compact.

The difference in critical ratios for prograde and retrograde planetary orbits is significant, ranging from ~30%-70% depending on the eccentricity of the outer star. For highly eccentric orbits of the outer star, the critical semi-major axis of the outer stability bound can expand by over 80% for prograde orbits and more than double for retrograde orbits, while the inner bound shrinks by a quarter for prograde planetary orbits and by over 80% for retrograde planetary orbits.

The outer stability bound increases approximately linearly with increasing outer star eccentricity, with the critical semi-major axis ratios of prograde and retrograde planetary orbits converging to the same value of around 3.1.

The regression constant for the prograde and retrograde inner orbits corresponds approximately with those published by Morais and Giuppone (2012), and those for the outer orbits are similar to those originally found by Holman and Wiegert (1999) and later by Verrier and Evans (2007).

The smallest exoplanet orbits found to date have semi-major axis ratios ~3, which are far outside the smallest ones we found of ~0.1, so the possibility exists of finding planets in much smaller orbits.

High-inclination P1 and P2 orbits

For real bodies that may also be relatively large, Kozai resonance tends to occur when $i_2 > 45^\circ$ and $i_2 < 135^\circ$. Analysis of a limited set of stellar Kozai resonances in triples showed that for larger a, μ_1, μ_2 and i_2, the period of the Kozai resonance is shorter and resonance begins earlier, with the influence of μ_1 on the Kozai resonance period being the largest, followed by μ_2 and i_2, while that of a is small. The period of libration was much shorter for higher a, μ_1 and μ_2, but longer for higher i_2. For retrograde stellar orbits the resonance period and inclination range increased modestly, but the libration period more than doubled and the libration range widened considerably. Comparing the numerical results with the theoretical equations, the libration periods and Kozai resonance periods differed by ~40% while maximum eccentricity was within ~2%.

The number of stable orbital bounds for planets falls exponentially with increasing inclination of the outer body of the triple. For the inner stability bound, the critical semi-major axis ratio had little dependence on the outer star's inclination. For the outer stability bound, there is no dependence at low inclinations, but as stellar inclination increases the critical semi-major axis ratio begins to decline, since the Kozai resonance causes the eccentricity of the inner binary to decrease. This divergence begins at inclinations of around 45°, instead of the theoretical 39°.

For retrograde stellar orbits dependence on i_2 is generally much stronger. For a prograde outer star, stellar Kozai resonance has no effect on the critical ratios of the inner or outer bounds. For a retrograde outer star, however, when Kozai resonance occurs the inner bound contracts inwards, while the outer bound moves outwards, by a larger proportional amount. These movements are in the opposite direction to the general result from a retrograde stellar orbit, indicating that Kozai resonance increases planetary instability.

While the semi-major axis ratio of the outer bound shows an overall decrease as i_2 increases from 0°to 180°, between the $\sim 45° - 135°$ where Kozai resonance occurs, there is an increase of up to ~20%, which appears to be related to the strength of the Kozai resonance.

S1/S2 orbits

On average, the outer star of a triple has a substantial constraining influence on S1-type orbits compared with the binary case, which makes S1 orbits move inwards, with the critical semi-major axis ratio reducing substantially by over 30%, from an average 0.270 to 0.183. The difference in critical ratio between prograde and retrograde planetary orbits also shrinks, by around 10%. The mass ratio has a larger influence in triples than in binaries, while the effect of eccentricity remains the same.

For S1 planetary orbits in triples, the critical semi-major axis ratio is in the range $\sim 0.180 - 0.196$. The sole significant determinants of this ratio are the inner binary's mass ratio and eccentricity, in approximately equal measure, as found by other researchers, although we found that the influence of eccentricity declines

sharply for a retrograde outer star. The critical ratio is generally ~7% greater for retrograde stellar orbits. Retrograde planetary orbits extend slightly further out (by 3%) for prograde stellar orbits, but for retrograde stellar orbits they are essentially unchanged.

Our results for binary S1 orbits corresponded well with the few previous studies on prograde orbits but were different to the single study done on retrograde orbits.

Only three S1 orbits in triple systems have been found to date, with semi-major axis ratios $\sim 0.001 - 0.1$, and they suffer from observational bias. Our results showed stable bounds with semi-major axis ratios that extended to almost 0.8, with the greatest concentration in a "sweet spot" of 0.03 – 0.25, so there appears to be scope for future planet discoveries to be made much further out from their host stars.

S3 orbits

For S3 orbits a triple has a smaller mean critical semi-major axis ratio than a binary, since the outer binary has a larger effect on it than a single body of equal mass at the same semi-major axis. However, this difference is small, at around 5%. This is less than the average 7% and 11% differences for P1 and P2 orbits respectively and much smaller than the average 50% difference found for S1 orbits.

For S3 planetary orbits in triples, the critical semi-major axis ratio is in the range $\sim 0.287 - 0.361$ (compared with $\sim 0.180 - 0.196$ for S1 orbits) and is essentially independent of the direction of motion of the outer star. The critical semi-major axis ratio is ~25% larger for retrograde planetary orbits compared with prograde orbits, significantly larger than the 7% for S1 orbits.

The sole significant determinant of the critical ratio is the eccentricity of the outer star, with very minor contributions from the inner and outer mass ratios. These regression coefficients are virtually identical for prograde and retrograde planetary motions and the direction of motion of the outer star.

The largest and smallest observational values for semi-major axis ratios found to date are 0.265 and 0.000606. The lowest result in our integrations was 0.009, but there were very few critical ratios lying below ~0.1.

The S3 orbits discovered to date also suffer observational bias. In our integrations the majority of mean critical ratios ranged from 0.1 – 0.6, with some as high as 0.9, so there are probably many planets at much greater distances from their host stars that are yet to be discovered.

Effect of the direction of stellar and planetary orbits

The effect on the planetary stability bounds of the outer star being retrograde is quite small, with the difference in critical semimajor axis ratio averaging ~|3%|. Nevertheless, half of the differences are statistically significant.

The effect on the planetary stability bounds of the direction of motion of the planets is much larger, averaging 37% for P1 orbits, 31% for P2 orbits and 25% for S3 orbits. S1 orbits are largely unaffected.

5.4 How The Results Can Be Used

These generalised results can be useful in the investigation of observed systems, providing a fast method of determining their stability bounds within the large parameter space that results from observational uncertainties. The relationships expressed in the regression models can be used to guide searches for planets in triple systems. They can also be used to select suitable candidates for a survey of triple systems. The geometry of the stable zone indicates not only where to look for planets but how to look – whether radial velocity, transit or other methods would be the most suitable.

Chapter 6

Further work

The limited investigation of high-inclination stellar orbits in this work was confined to Kozai resonance in these orbits and then its effect on the three-dimensional shape of the region of planetary stability. Examining Kozai resonance in the planetary orbits themselves would add a further layer of complexity.

Another interesting extension of this work would be to investigate mean motion resonances in the planetary orbits. Since this will occur for only a very small proportion of planets, the test particle clouds we used, consisting of 1 000 – 3 000 test particles, would only find a few instances of resonance. To generate meaningful numbers, the number of test particles would need to increase by an order of magnitude, to around 200 000. Particles in mean motion resonances could then be found by exhaustive search of the test particles or by narrowing the search to the theoretically determined areas where they are most likely to be found. The additional amount of both time and computational resources required did not permit this to be carried out.

Appendices

Appendix A

A.1 Summary Of Stellar Parameters

Parameter ranges	Units	Orbit type P1 and P2		Orbit type P1 and P2 Binary reduction		Orbit type P1 and P2 High inclination		Orbit type S1		Orbit type S3	
Prograde (0) and retrograde (1) outer star	-	0	1	0	1	0	1	0	1	0	1
Prograde (0) and retrograde (1) planets	-	0	1	0	1	0	1	0	1	0	1
Geometry											
Semimajor axis ratio $a = a_2/a_1$	-	a_m	100	a_m	100	a_m	100	a_m	100	a_m	100
Inner mass ratio $\mu_1 = m_2/(m_1+m_2)$	-	0.1	0.5	0.1	0.5	0.1	0.5	0.001	0.5	0.001	0.5
Outer mass ratio $\mu_2 = m_3/(m_1+m_2)$	-	0.2	2.3	0.2	2.3	0.2	2.5	0.001	2.2	0.001	2.2
Star 2											
Eccentricity e_1	-	0	0.9	-	-	0, 0.5		0	0.7	0	0.7
Inclination i_1	deg	0	-	-	-	-	-	0	-	0	-
Longitude of ascending node Ω_1	deg	0	-	-	-	-	-	0	-	0	-
Argument of periapsis ω_1	deg	0	-	-	-	-	-	0	-	0	-
True anomaly v_1	deg	0	-	-	-	-	-	0	-	0	-
Star 3											
Eccentricity e_2	-	0	0.9	0	0.9	0, 0.5		0	0.7	0	0.7
Inclination i_2	deg	0-60	120-180	0-60	120-180	0-180		0-60	120-180	0-60	120-180
Longitude of ascending node Ω_2	deg	0	270	0	270	0, 90		0	270	0	270
Argument of periapsis ω_2	deg	0	270	0	270	0, 90		0	270	0	270

Table A1. Summary of stellar parameter ranges used for various orbit types

A.2 Summary Of Computational Parameters

Parameter		Units	Orbit type P1 and P2	Orbit type P1 and P2 (Binary reduction)	Orbit type P1 and P2 (High inclination)	Orbit type S1	Orbit type S3
Central star mass	m_1	M_S	1	$M = (1-\mu_1)^{-1}$	1	0.01	0.01
Timestep	*dt*	yr	$T_{bin}/20$	Eqn. (29)	$T_{bin}/20$	$T_{bin}/20$	$T_{bin}/20$
Number of test particles		-	1000 - 3000	1000 - 3000	5 000 - 10 000	3 000	2 000
Test particle orbit centres		-	-1 -1 -1	-1 -1 -1	-1 -1 -1	-1 0 0	-1 0 0
Minimum semi-major axis (1)	*amin*	AU	0.01	0.01	0.01	0.02	0.02
Maximum semi-major axis	*amax*	AU	2x 5:1 MMR	2x 5:1 MMR	2x 5:1 MMR	$0.9a_1$	Eqn. (54)
Collision with central body	*rmin*	AU	0.005	0.005	0.005	0.005	0.005
Ejection from system	*rmax*	AU	10^4	10^4	10^4	10^2	10^4

(1) Must be > specified collision distance

Table A2. Summary of computational parameters used for various orbit types

Appendix B

B.1 Comparison With Theory – Outer Restricted Model

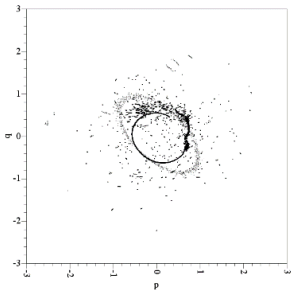

$a)\ \mu_2 = 0.01,\ i_2 = 30°$

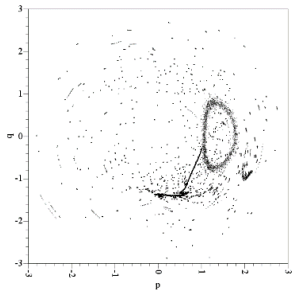

$b)\ \mu_2 = 0.01,\ i_2 = 60°$

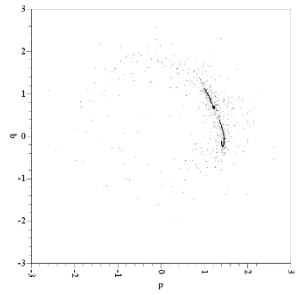

$c)\ \mu_2 = 0.01,\ i_2 = 80°$

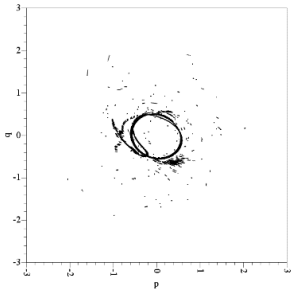

$d)\ \mu_2 = 0.05, i = 30°$

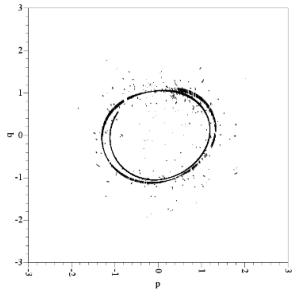

$e)\ \mu_2 = 0.05,\ i_2 = 60°$

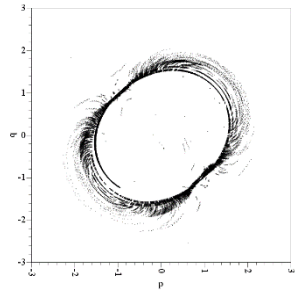

$f)\ \mu_2 = 0.05,\ i_2 = 80°$

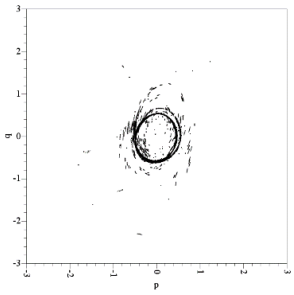

$g)\ \mu_2 = 0.1,\ i_2 = 30°$

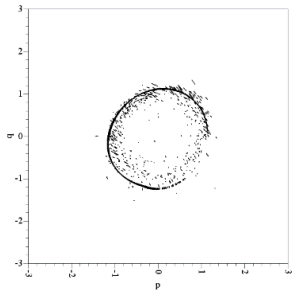

$h)\ \mu_2 = 0.1,\ i_2 = 60°$

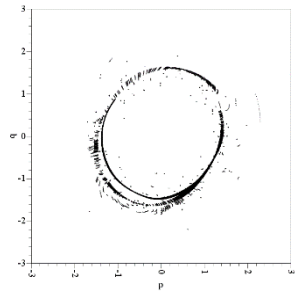

$i)\ \mu_2 = 0.1,\ i_2 = 80°$

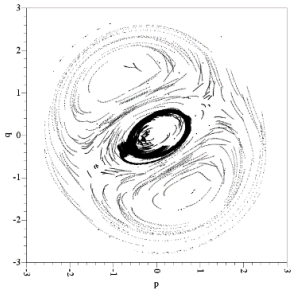

$j)\ \mu_2 = 0.25,\ i_2 = 40°$

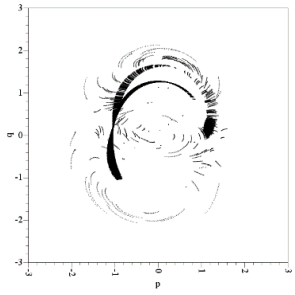

$k)\ \mu_2 = 0.25,\ i_2 = 60°$

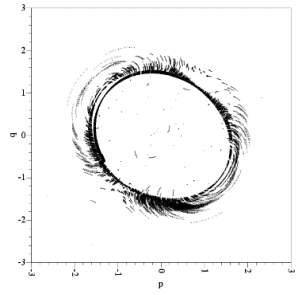

$l)\ \mu_2 = 0.25,\ i_2 = 80°$

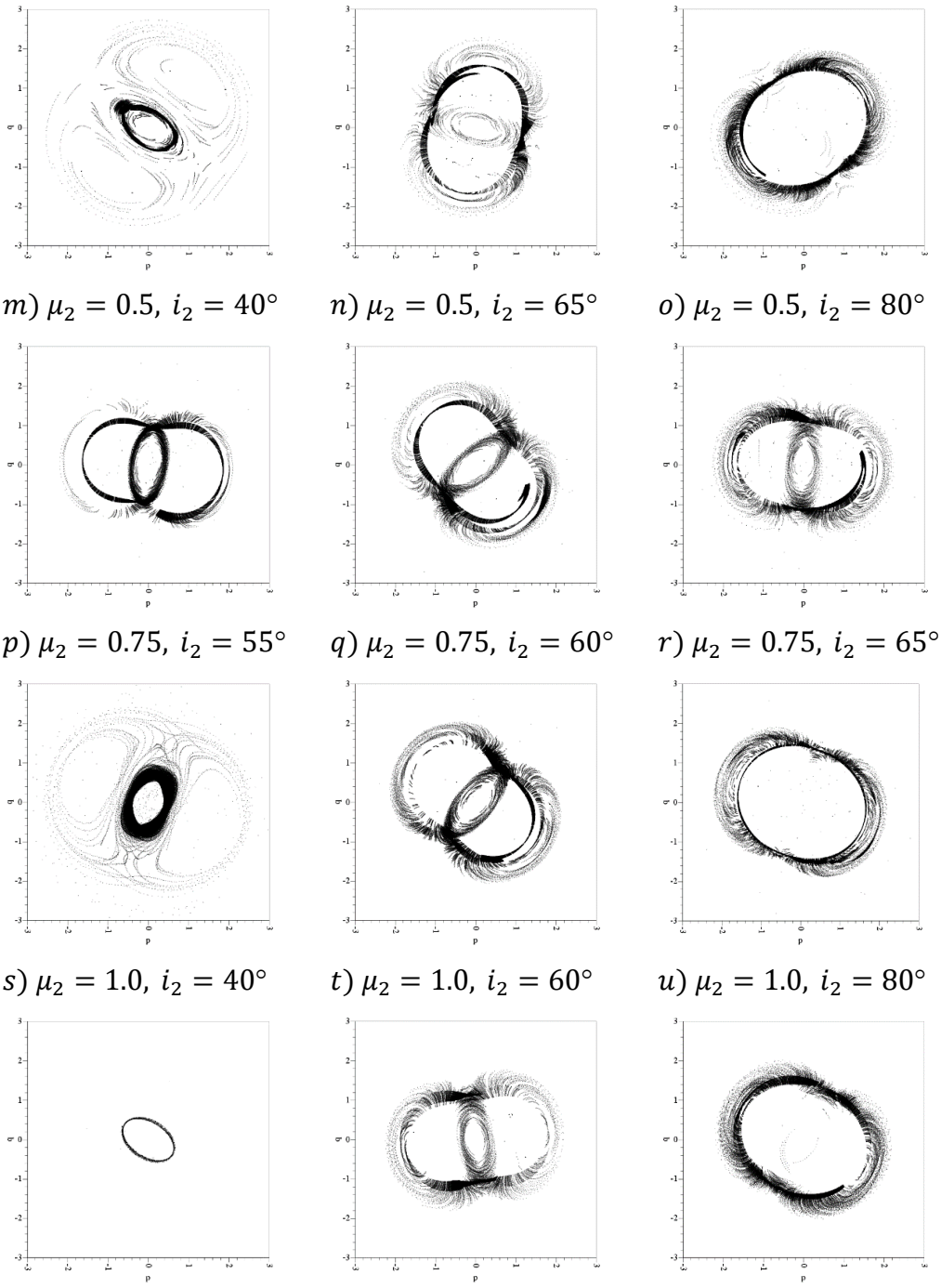

$m)\ \mu_2 = 0.5,\ i_2 = 40°$ $n)\ \mu_2 = 0.5,\ i_2 = 65°$ $o)\ \mu_2 = 0.5,\ i_2 = 80°$

$p)\ \mu_2 = 0.75,\ i_2 = 55°$ $q)\ \mu_2 = 0.75,\ i_2 = 60°$ $r)\ \mu_2 = 0.75,\ i_2 = 65°$

$s)\ \mu_2 = 1.0,\ i_2 = 40°$ $t)\ \mu_2 = 1.0,\ i_2 = 60°$ $u)\ \mu_2 = 1.0,\ i_2 = 80°$

$v)\ \mu_2 = 2.5,\ i_2 = 40°$ $w)\ \mu_2 = 2.5,\ i_2 = 60°$ $x)\ \mu_2 = 2.5,\ i_2 = 80°$

Figure B1. Final test particle distributions in the p-q plane, resulting from an initial disc aligned with the invariable plane. For all cases: $a = 20$ AU, $\mu_1 = 0.5, e_1 = 0.5,\ e_2 = 0.5, i_1 = 0°, \Omega_2 = 90°$ *and* $\omega_2 = 0°$. *Initially 10 000 test particles, integrated for* 10^6 *yr.*

Appendix C

C.1 Regressions – Highly-Inclined Triple Systems

Type	P1 orbits							P2 orbits						
Prograde outer star														
Non-	Model	Coefficients		Coefficients	*t*	Sig.	95.0% Confidence Interval		Model	Coefficients		Coefficients	*t*	Sig.	95.0% Confidence Interval	
		B	Std. Error	Beta			Lower Bound	Upper Bound		B	Std. Error	Beta			Lower Bound	Upper Bound
	C	.545	.032		17.2	.000	.483	.607	*C*	1.921	.009		207.6	.000	1.903	1.940
	a	.000	.000	-.033	-0.5	.610	-.001	.000	*a*	-.001	.000	-.357	-7.6	.000	-.001	.000
	μ_1	-.044	.043	-.064	-1.0	.309	-.128	.041	μ_1	.048	.017	.137	2.9	.004	.016	.081
	μ_2	-.018	.011	-.103	-1.6	.109	-.040	.004	μ_2	.016	.004	.185	3.9	.000	.008	.024
	i_2	-.001	.001	-.106	-1.7	.091	-.002	.000	i_2	.001	.000	.275	5.9	.000	.001	.002
Kozai	Model	Coefficients		Coefficients	*t*	Sig.	95.0% Confidence Interval		Model	Coefficients		Coefficients	*t*	Sig.	95.0% Confidence Interval	
		B	Std. Error	Beta			Lower Bound	Upper Bound		B	Std. Error	Beta			Lower Bound	Upper Bound
	C	.303	.130		2.3	.025	.041	.566	*C*	2.346	.049		47.7	0.000	2.249	2.443
	a	.000	.001	.050	0.3	.748	-.001	.002	*a*	-.004	.000	-.707	-19.2	.000	-.005	-.004
	μ_1	-.170	.101	-.245	-1.7	.099	-.374	.033	μ_1	.066	.044	.055	1.5	.139	-.022	.153
	μ_2	.016	.032	.080	0.5	.631	-.049	.081	μ_2	.044	.011	.143	3.9	.000	.022	.067
	i_2	.003	.001	.320	2.1	.045	.000	.006	i_2	-.003	.001	-.202	-5.4	.000	-.005	-.002
Retrograde outer star																
Non-	Model	Coefficients		Coefficients	*t*	Sig.	95.0% Confidence Interval		Model	Coefficients		Coefficients	*t*	Sig.	95.0% Confidence Interval	
		B	Std. Error	Beta			Lower Bound	Upper Bound		B	Std. Error	Beta			Lower Bound	Upper Bound
	C	.685	.024		28.0	.000	.637	.733	*C*	1.288	.019		67.4	.000	1.250	1.325
	a	-.001	.000	-.222	-3.0	.003	-.001	.000	*a*	-.002	.000	-.413	-10.1	.000	-.002	-.001
	μ_1	.066	.040	.123	1.7	.097	-.012	.145	μ_1	.085	.037	.094	2.3	.023	.012	.158
	μ_2	.029	.011	.197	2.6	.010	.007	.051	μ_2	-.004	.009	-.020	-0.5	.624	-.023	.014
	i_2	-.001	.000	-.093	-1.2	.219	-.002	.000	i_2	.007	.000	.615	15.0	.000	.006	.008
Kozai	Model	Coefficients		Coefficients	*t*	Sig.	95.0% Confidence Interval		Model	Coefficients		Coefficients	*t*	Sig.	95.0% Confidence Interval	
		B	Std. Error	Beta			Lower Bound	Upper Bound		B	Std. Error	Beta			Lower Bound	Upper Bound
	C	.738	.086		8.6	.000	.567	.908	*C*	1.357	.074		18.3	.000	1.211	1.503
	a	.000	.000	-.078	-0.8	.429	-.001	.001	*a*	-.004	.000	-.613	-13.2	.000	-.005	-.004
	μ_1	-.038	.061	-.057	-0.6	.542	-.159	.084	μ_1	.033	.061	.025	0.5	.596	-.089	.154
	μ_2	-.083	.018	-.463	-4.7	.000	-.118	-.048	μ_2	-.016	.015	-.048	-1.0	.302	-.046	.014
	i_2	-.001	.001	-.089	-0.8	.399	-.003	.001	i_2	.009	.001	.439	9.5	.000	.007	.010

Table C1. Regressions for P1 and P2 orbits, with a prograde and retrograde outer body, for non-Kozai and Kozai regimes

Appendix D

D.1 Regressions – Binary Systems

Orbit type	Critical ratio	Motions[1] Planet	Critical semi-major axis ratio Min	-1σ	Avg	SD	+1σ	Max
P1	a_{io}/a_2	P	0.058	0.221	**0.364**	0.143	0.507	0.581
		R	0.026	0.318	**0.471**	0.153	0.624	0.911
P2	a_{oi}/a_2	P	1.030	1.527	**2.703**	1.176	3.879	3.501
		R	1.001	1.326	**1.691**	0.365	2.055	3.478
S1	a_{io}/a_1	P	0.046	0.192	**0.257**	0.066	0.323	0.885
		R	0.047	0.169	**0.289**	0.120	0.409	0.775
S3	a_{io}/a_2	P	0.011	0.129	**0.309**	0.181	0.490	0.907
		R	0.015	0.208	**0.368**	0.160	0.528	0.880

Orbit type	Critical ratio	Motions[1] Planet	Regression coefficients[2] C	a	μ_1	μ_2	e_1	e_2	i_2	Ω_2	ω_2	Integrations Done	Bounds	%	Fit R^2	F	SE	MAPE
P1	a_{io}/a_2	P	0.439	0.000	*-0.005*	-0.020	*-0.004*	-0.114	0.000	-0.001	-0.001	3034	1972	65	0.128	34	0.093	19.4
		R	0.573	0.000	*0.009*	-0.043	*-0.010*	-0.469	0.000	0.000	0.000	2831	859	30	0.668	246	0.062	9.7
P2	a_{oi}/a_2	P	2.377	-0.003	*0.053*	0.044	0.090	1.997	0.000	*-0.002*	*-0.002*	3034	2994	99	0.828	3081	0.239	6.1
		R	1.483	-0.004	*0.131*	*-0.008*	*-0.036*	1.725	*0.002*	0.001	0.001	2831	2831	100	0.860	3881	0.190	6.1
S1	a_{io}/a_1	P	0.390	0.000	-0.746	*0.005*	-0.398	-0.006	0.000	0.000	0.000	2856	1169	41	0.579	142	0.081	34.9
		R	0.393	0.000	-0.667	*0.003*	-0.383	*0.002*	0.000	0.000	0.000	2265	908	40	0.556	124	0.081	36.7
S3	a_{io}/a_2	P	0.385	0.000	-	0.062	-	-0.585	-	0.000	0.000	3218	3195	99	0.724	1676	0.080	30.9
		R	0.446	0.000	-	0.114	-	-0.599	-	0.000	0.000	3092	3040	98	0.813	2639	0.069	22.4
Average[3]/total[4]			-	0.001	0.269	0.037	0.154	0.687	0.001	0.001	0.000	23161	16968	73	0.645	1478	0.112	21

1. P - prograde, R - retrograde
2. Italics indicate wrong sign
3. Of absolute values for regression coefficients
4. Of integrations and bounds

Table D1. Summary of regression statistics for all binary orbital configurations

References

Aarseth, SJ 2003, *Gravitational N-body Simulations: Tools and Algorithms*, Cambridge University Press, Cambridge, UK.

Aarseth, SJ & Scarfe, C 2004, 'Formation and Evolution of Hierarchical Systems', in Revista Mexicana de Astronomia y Astrofisica Conference Series: *proceedings of the Revista Mexicana de Astronomia y Astrofisica Conference Series*, C Allen (ed.), pp. 156-62.

Akeson, RL, Chen, X, Ciardi, D, et al. 2013, 'The NASA Exoplanet Archive: Data and Tools for Exoplanet Research', *Publications of the Astronomical Society of the Pacific*, vol. 125, pp. 989-99.

Alexander, R 2012, 'The Dispersal of Protoplanetary Disks around Binary Stars', *The Astrophysical Journal Letters*, vol. 757.

Alexander, RD & Pascucci, I 2012, 'Deserts and pile-ups in the distribution of exoplanets due to photoevaporative disc clearing', *Monthly Notices of the Royal Astronomical Society*, vol. 422, pp. L82-L6.

Armstrong, DJ, Osborn, HP, Brown, DJA, et al. 2014, 'On the abundance of circumbinary planets', *Monthly Notices of the Royal Astronomical Society*, vol. 444, pp. 1873-83.

Bate, MR, Bonnell, IA, Clarke, CJ, et al. 2000, 'Observational implications of precessing protostellar discs and jets', *Monthly Notices of the Royal Astronomical Society*, vol. 317, pp. 773-81.

Batygin, K, Morbidelli, A & Tsiganis, K 2011, 'Formation and evolution of planetary systems in presence of highly inclined stellar perturbers', *Astronomy and Astrophysics*, vol. 533.

Beuermann, K, Dreizler, S, Hessman, F, et al. 2012, 'The quest for companions to post-common envelope binaries: III. A reexamination of HW Virginis', *Astronomy & Astrophysics*, vol. 543.

Beust, H 2003, 'Symplectic integration of hierarchical stellar systems', *Astronomy and Astrophysics*, vol. 400, no. 3, pp. 1129-44.

Beust, H & Dutrey, A 2005, 'Dynamics of the young multiple system GG Tauri. I. Orbital fits and inner edge of the circumbinary disk of GG Tau A', *Astronomy and Astrophysics*, vol. 439, pp. 585-94.

Beust, H & Dutrey, A 2006, 'Dynamics of the young multiple system GG Tauri. II. Relation between the stellar system and the circumbinary disk', *Astronomy and Astrophysics*, vol. 446, pp. 137-54.

Beust, H, Bonfils, X, Montagnier, G, et al. 2012, 'Dynamical evolution of the Gliese 436 planetary system. Kozai migration as a potential source for Gliese 436b's eccentricity', *Astronomy and Astrophysics*, vol. 545.

Bodenheimer, P 1978, 'Evolution of rotating interstellar clouds. III-On the formation of multiple star systems', *The Astrophysical Journal*, vol. 224, pp. 488-96.

Bonavita, M & Desidera, S 2007, 'The frequency of planets in multiple systems', *Astronomy and Astrophysics*, vol. 468, no. 2, pp. 721-9.

Bonnell, IA & Bate, MR 1994, 'Massive Circumbinary Discs and the Formation of Multiple Systems', *Monthly Notices of the Royal Astronomical Society*, vol. 269, pp. L45-L8.

Borkovits, T, Rappaport, S, Hajdu, T, et al. 2015, 'Eclipse timing variation analyses of eccentric binaries with close tertiaries in the Kepler field', *Monthly Notices of the Royal Astronomical Society*, vol. 448, no. 1, pp. 946-93.

Borkovits, T, Derekas, A, Kiss, LL, et al. 2013, 'Dynamical masses, absolute radii and 3D orbits of the triply eclipsing star HD 181068 from Kepler photometry', *Monthly Notices of the Royal Astronomical Society*, vol. 428, pp. 1656-72.

Boué, G & Fabrycky, DC 2014a, 'Compact Planetary Systems Perturbed by an Inclined Companion. I. Vectorial Representation of the Secular Model', *The Astrophysical Journal*, vol. 789.

Boué, G & Fabrycky, DC 2014b, 'Compact Planetary Systems Perturbed by an Inclined Companion. II. Stellar Spin-Orbit Evolution', *The Astrophysical Journal*, vol. 789.

Chambers, JE 1999, 'A hybrid symplectic integrator that permits close encounters between massive bodies', *Monthly Notices of the Royal Astronomical Society*, vol. 304, no. 4, pp. 793-9.

Chambers, JE, Quintana, EV, Duncan, MJ, et al. 2002, 'Symplectic Integrator Algorithms for Modeling Planetary Accretion in Binary Star Systems', *The Astronomical Journal*, vol. 123, no. 5, p. 2884.

Chenciner, A & Montgomery, R 2000, 'A remarkable periodic solution of the three-body problem in the case of equal masses', *Annals of Mathematics-Second Series*, vol. 152, no. 3, pp. 881-902.

Correia, ACM, Boué, G & Laskar, J 2016, 'Secular and tidal evolution of circumbinary systems', *Celestial Mechanics and Dynamical Astronomy*, vol. 126, pp. 189-225.

Cuntz, M & Yeager, KE 2009, 'On the Validity of the "Hill Radius Criterion" for the Ejection of Planets from Stellar Habitable Zones', *The Astrophysical Journal Letters*, vol. 697, pp. L86-L90.

Cuntz, M, Eberle, J & Musielak, Z 2007, 'Stringent criteria for stable and unstable planetary orbits in stellar binary systems', *The Astrophysical Journal Letters*, vol. 669, no. 2, p. L105.

Derekas, A, Kiss, LL, Borkovits, T, et al. 2011, 'HD 181068: A Red Giant in a Triply Eclipsing Compact Hierarchical Triple System', *Science*, vol. 332, no. 6026, pp. 216-8.

Desidera, S & Barbieri, M 2007, 'Properties of planets in binary systems. The role of binary separation', *Astronomy and Astrophysics*, vol. 462, pp. 345-53.

Desidera, S, Carolo, E, Gratton, R, et al. 2011, 'A giant planet in the triple system HD 132563', *Astronomy and Astrophysics*, vol. 533.

Domingos, RC, Winter, OC & Carruba, V 2012, 'Mean motion resonances and the stability of a circumbinary disk in a triple stellar system', *Astronomy and Astrophysics*, vol. 544.

Dommanget, J & Nys, O 2002, 'CCDM (Catalog of Components of Double & Multiple stars) (Dommanget+ 2002)', *VizieR Online Data Catalog*, vol. 1274.

Dong, S, Katz, B & Socrates, A 2013, 'Exploring a "Flow" of Highly Eccentric Binaries with Kepler', *The Astrophysical Journal Letters*, vol. 763, no. 1, p. L2.

Donnison, J 1999, 'Three-Body Stability Criteria', in *Impact of Modern Dynamics in Astronomy*, Springer, pp. 441-2.

Donnison, J & Mikulskis, D 1994, 'Three-body orbital stability criteria for circular retrograde orbits', *Monthly Notices of the Royal Astronomical Society*, vol. 266, no. 1, pp. 25-30.

Donnison, J & Mikulskis, D 1995, 'The effect of eccentricity on three-body orbital stability criteria and its importance for triple star systems', *Monthly Notices of the Royal Astronomical Society*, vol. 272, pp. 1-10.

Doolin, S & Blundell, KM 2011, 'The dynamics and stability of circumbinary orbits', *Monthly Notices of the Royal Astronomical Society*, vol. 418, no. 4, pp. 2656-68.

Doyle, LR, Carter, JA, Fabrycky, DC, et al. 2011, 'Kepler-16: a transiting circumbinary planet', *Science*, vol. 333, no. 6049, pp. 1602-6, item: 21921192.

Duncan, MJ, Levison, HF & Lee, MH 1998, 'A Multiple Time Step Symplectic Algorithm for Integrating Close Encounters', *The Astronomical Journal*, vol. 116, no. 4, p. 2067.

Duquennoy, A & Mayor, M 1991, 'Multiplicity among solar-type stars in the solar neighbourhood. II - Distribution of the orbital elements in an unbiased sample', *Astronomy and Astrophysics*, vol. 248, pp. 485-524.

Dvorak, R 1984, 'Numerical experiments on planetary orbits in double stars', *Celestial Mechanics*, vol. 34, pp. 369-78.

Dvorak, R, Froeschle, C & Froeschle, C 1986, 'Planetary Orbits in Binaries', in Bulletin of the American Astronomical Society: *proceedings of the Bulletin of the American Astronomical Society* p. 842.

Dvorak, R, Froeschle, C & Froeschle, C 1989, 'Stability of outer planetary orbits (P-types) in binaries', *Astronomy and Astrophysics*, vol. 226, pp. 335-42.

Eastman, JD, Beatty, TG, Siverd, RJ, et al. 2016, 'KELT-4Ab: An Inflated Hot Jupiter Transiting the Bright Component of a Hierarchical Triple', *The Astronomical Journal*, vol. 151.

Eggenberger, A, Udry, S & Mayor, M 2004, 'Statistical properties of exoplanets. III. Planet properties and stellar multiplicity', *Astronomy and Astrophysics*, vol. 417, pp. 353-60.

Eggleton, P 2006, *Evolutionary Processes in Binary and Multiple Stars*, Cambridge University Press, Cambridge, UK.

Eggleton, P & Kiseleva, L 1995, 'An Empirical Condition for Stability of Hierarchical Triple Systems', *The Astrophysical Journal*, vol. 455, p. 640.

Eggleton, PP 2009, 'Towards multiple-star population synthesis', *Monthly Notices of the Royal Astronomical Society*, vol. 399, pp. 1471-81.

Eggleton, PP & Tokovinin, AA 2008, 'A catalogue of multiplicity among bright stellar systems', *Monthly Notices of the Royal Astronomical Society*, vol. 389, no. 2, pp. 869-79.

Fabrycky, D & Tremaine, S 2007, 'Shrinking binary and planetary orbits by Kozai cycles with tidal friction', *The Astrophysical Journal*, vol. 669, no. 2, p. 1298.

Fang, J & Margot, J-L 2012, 'Predicting Planets in Kepler Multi-planet Systems', *The Astrophysical Journal*, vol. 751.

Farago, F & Laskar, J 2010, 'High-inclination orbits in the secular quadrupolar three-body problem', *Monthly Notices of the Royal Astronomical Society*, vol. 401, no. 2, pp. 1189-98.

Fekel, F 1981, 'The properties of close multiple stars', *The Astrophysical Journal*, vol. 246, pp. 879-98.

Ford, EB, Kozinsky, B & Rasio, FA 2000, 'Secular evolution of hierarchical triple star systems', *The Astrophysical Journal*, vol. 535, no. 1, p. 385.

Foucart, F & Lai, D 2013, 'Assembly of Protoplanetary Disks and Inclinations of Circumbinary Planets', *The Astrophysical Journal*, vol. 764.

Fregeau, JM, Cheung, P, Portegies Zwart, SF, et al. 2004, 'Stellar collisions during binary-binary and binary-single star interactions', *Monthly Notices of the Royal Astronomical Society*, vol. 352, no. 1, pp. 1-19.

Gayon, J & Bois, E 2008, 'Are retrograde resonances possible in multi-planet systems?', *Astronomy and Astrophysics*, vol. 482, pp. 665-72.

Georgakarakos, N 2008, 'Stability criteria for hierarchical triple systems', *Celestial Mechanics and Dynamical Astronomy*, vol. 100, no. 2, pp. 151-68.

Gould, A, Udalski, A, Shin, IG, et al. 2014, 'Exoplanet detection. A terrestrial planet in a ~1-AU orbit around one member of a ~15-AU binary', *Science*, vol. 345, no. 6192, pp. 46-9, item: 24994642.

Grimm, SL & Stadel, JG 2014, 'The GENGA Code: Gravitational Encounters in N-body Simulations with GPU Acceleration', *The Astrophysical Journal*, vol. 796.

Grishin, E, Perets, HB, Zenati, Y, et al. 2017, 'Generalized Hill-stability criteria for hierarchical three-body systems at arbitrary inclinations', *Monthly Notices of the Royal Astronomical Society*, vol. 466, pp. 276-85.

Haghighipour, N 2008, '9 Formation, Dynamical Evolution, and Habitability of Planets in Binary Star Systems', *Exoplanets: Detection, Formation, Properties, Habitability*, p. 223.

Hamers, AS, Perets, HB & Portegies Zwart, SF 2015, 'A triple origin for the lack of tight coplanar circumbinary planets around short-period binaries', *Monthly Notices of the Royal Astronomical Society*, vol. 455, no. 3, pp. 3180-200.

Hamers, AS, Perets, HB, Antonini, F, et al. 2015, 'Secular dynamics of hierarchical quadruple systems: the case of a triple system orbited by a fourth body', *Monthly Notices of the Royal Astronomical Society*, vol. 449, pp. 4221-45.

Hamilton, DP & Burns, JA 1991, 'Orbital stability zones about asteroids', *Icarus*, vol. 92, pp. 118-31.

Harrington, RS 1968, 'Dynamical evolution of triple stars', *The Astronomical Journal*, vol. 73, pp. 190-4.

Harrington, RS 1972, 'Stability Criteria for Triple Stars', *Celestial Mechanics*, vol. 6, pp. 322-7.

Harrington, RS 1977, 'Planetary orbits in binary stars', *The Astronomical Journal*, vol. 82, pp. 753-6.

Holman, M, Touma, J & Tremaine, S 1997, 'Chaotic variations in the eccentricity of the planet orbiting 16 Cygni B', *Nature*, vol. 386, pp. 254-6.

Holman, MJ & Wiegert, PA 1999, 'Long-term stability of planets in binary systems', *The Astronomical Journal*, vol. 117, no. 1, p. 621.

Horner, J, Hinse, T, Wittenmyer, R, et al. 2012, 'A dynamical analysis of the proposed circumbinary HW Virginis planetary system', *Monthly Notices of the Royal Astronomical Society*, vol. 427, no. 4, pp. 2812-23.

Innanen, KA 1979, 'The limiting radii of direct and retrograde satellite orbits, with applications to the solar system and to stellar systems', *The Astronomical Journal*, vol. 84, pp. 960-3.

Innanen, KA, Zheng, JQ, Mikkola, S, et al. 1997, 'The Kozai Mechanism and the Stability of Planetary Orbits in Binary Star Systems', *The Astronomical Journal*, vol. 113, p. 1915.

Kaib, NA, Raymond, SN & Duncan, MJ 2011, '55 Cancri: A Coplanar Planetary System That is Likely Misaligned with Its Star', *The Astrophysical Journal Letters*, vol. 742.

Kaib, NA, Raymond, SN & Duncan, M 2013, 'Planetary system disruption by Galactic perturbations to wide binary stars', *Nature*, vol. 493, pp. 381-4.

Kane, SR & Hinkel, NR 2013, 'On the Habitable Zones of Circumbinary Planetary Systems', *The Astrophysical Journal*, vol. 762.

Kane, SR, Barclay, T, Hartmann, M, et al. 2015, 'On the Stellar Companion to the Exoplanet Hosting Star 30 Arietis B', *The Astrophysical Journal*, vol. 815.

Katz, B & Dong, S 2012, 'The rate of WD-WD head-on collisions may be as high as the SNe Ia rate', *ArXiv e-prints*, vol. 1211, p. 4584.

Kennedy, GM, Wyatt, MC, Sibthorpe, B, et al. 2012, '99 Herculis: host to a circumbinary polar-ring debris disc', *Monthly Notices of the Royal Astronomical Society*, vol. 421, pp. 2264-76.

Kiseleva, L, Eggleton, P & Mikkola, S 1998, 'Tidal friction in triple stars', *Monthly Notices of the Royal Astronomical Society*, vol. 300, no. 1, pp. 292-302.

Kozai, Y 1962, 'Secular perturbations of asteroids with high inclination and eccentricity', *The Astronomical Journal*, vol. 67, p. 591.

Kraus, AL, Ireland, MJ, Huber, D, et al. 2016, 'The Impact of Stellar Multiplicity on Planetary Systems. I. The Ruinous Influence of Close Binary Companions', *The Astronomical Journal*, vol. 152.

Krymolowski, Y & Mazeh, T 1999, 'Studies of multiple stellar systems -- II. Second-order averaged Hamiltonian to follow long-term orbital modulations of hierarchical triple systems', *Monthly Notices of the Royal Astronomical Society*, vol. 304, no. 4, pp. 720-32.

Leung, GC & Lee, MH 2013, 'An Analytic Theory for the Orbits of Circumbinary Planets', *The Astrophysical Journal*, vol. 763, no. 2, p. 107.

Levison, HF & Duncan, MJ 1994, 'The long-term dynamical behavior of short-period comets', *Icarus*, vol. 108, pp. 18-36.

Levison, HF & Duncan, MJ 2013, 'Swift: A solar system integration software package', *Astrophysics Source Code Library*, vol. 1, p. 03001.

Li, G, Holman, MJ & Tao, M 2016, 'Uncovering Circumbinary Planetary Architectural Properties from Selection Biases', *The Astrophysical Journal*, vol. 831.

Lidov, M 1962, 'The evolution of orbits of artificial satellites of planets under the action of gravitational perturbations of external bodies', *Planetary and Space Science*, vol. 9, no. 10, pp. 719-59.

Lissauer, JJ, Dawson, RI & Tremaine, S 2014, 'Advances in exoplanet science from Kepler', *Nature*, vol. 513, no. 7518, pp. 336-44, item: 25230655.

Lithwick, Y & Wu, Y 2008a, 'On the Origin of Pluto's Minor Moons, Nix and Hydra', *ArXiv e-prints*, vol. 0802.

Lithwick, Y & Wu, Y 2008b, 'The Effect of Charon's Tidal Damping on the Orbits of Pluto's Three Moons', *ArXiv e-prints*, vol. 0802.

Lithwick, Y & Naoz, S 2011, 'The Eccentric Kozai Mechanism for a Test Particle', *The Astrophysical Journal*, vol. 742, no. 2, p. 94.

Lohr, ME, Norton, AJ, Gillen, E, et al. 2015, 'The doubly eclipsing quintuple low-mass star system 1SWASP J093010.78+533859.5⋆', *Astronomy and Astrophysics*, vol. 578, p. A103.

Malmberg, D, Davies, MB & Chambers, JE 2007, 'The instability of planetary systems in binaries: How the Kozai mechanism leads to strong planet–planet interactions', *Monthly Notices of the Royal Astronomical Society: Letters*, vol. 377, no. 1, pp. L1-L4.

Mardling, R 1999, 'Chaotic Tides in Binary Stars and the Three-Body Problem', in Bulletin of the American Astronomical Society: *proceedings of the Bulletin of the American Astronomical Society* p. 1231.

Mardling, RA 2010, 'The determination of planetary structure in tidally relaxed inclined systems', *Monthly Notices of the Royal Astronomical Society*, vol. 407, pp. 1048-69.

Mardling, RA & Aarseth, SJ 2001, 'Tidal interactions in star cluster simulations', *Monthly Notices of the Royal Astronomical Society*, vol. 321, no. 3, pp. 398-420.

Martin, DV & Triaud, AHMJ 2015, 'Circumbinary planets - why they are so likely to transit', *Monthly Notices of the Royal Astronomical Society*, vol. 449, pp. 781-93.

Mazeh, T & Shaham, J 1979, 'The orbital evolution of close triple systems-the binary eccentricity', *Astronomy and Astrophysics*, vol. 77, pp. 145-51.

Moeckel, N & Veras, D 2012, 'Exoplanets bouncing between binary stars', *Monthly Notices of the Royal Astronomical Society*, vol. 422, no. 1, pp. 831-40.

Moore, A & Quillen, AC 2011, 'QYMSYM: A GPU-accelerated hybrid symplectic integrator that permits close encounters', *New Astronomy*, vol. 16, no. 7, pp. 445-55.

Moore, C 1993, 'Braids in classical dynamics', *Phys Rev Lett*, vol. 70, no. 24, pp. 3675-9, item: 10053934.

Morais, MHM & Giuppone, CA 2012, 'Stability of prograde and retrograde planets in circular binary systems', *Monthly Notices of the Royal Astronomical Society*, vol. 424, no. 1, pp. 52-64.

Moulton, F 1914, 'On the stability of direct and retrograde satellite orbits', *Monthly Notices of the Royal Astronomical Society*, vol. 75, p. 40.

Mudryk, LR & Wu, Y 2006, 'Resonance overlap is responsible for ejecting planets in binary systems', *The Astrophysical Journal*, vol. 639, no. 1, p. 423.

Murray, CD & Dermott, SF 1999, *Solar System Dynamics*, Cambridge University Press, Cambridge, UK.

Musielak, ZE, Cuntz, M, Marshall, EA, et al. 2005, 'Stability of planetary orbits in binary systems', *Astronomy and Astrophysics*, vol. 434, no. 1, pp. 355-64.

Naoz, S, Farr, WM, Lithwick, Y, et al. 2011, 'Hot Jupiters from secular planet-planet interactions', *Nature*, vol. 473, no. 7346, pp. 187-9, item: 21562558.

Naoz, S, Farr, WM, Lithwick, Y, et al. 2013, 'Secular dynamics in hierarchical three-body systems', *Monthly Notices of the Royal Astronomical Society*, p. 302.

Neveu-VanMalle, M, Queloz, D, Anderson, DR, et al. 2014, 'WASP-94 A and B planets: hot-Jupiter cousins in a twin-star system', *Astronomy and Astrophysics*, vol. 572.

Orosz, JA, Welsh, WF, Carter, JA, et al. 2012, 'Kepler-47: a transiting circumbinary multiplanet system', *Science*, vol. 337, no. 6101, pp. 1511-4, item: 22933522.

Pejcha, O, Antognini, JM, Shappee, BJ, et al. 2013, 'Greatly enhanced eccentricity oscillations in quadruple systems composed of two binaries: implications for stars, planets and transients', *Monthly Notices of the Royal Astronomical Society*, vol. 435, pp. 943-51.

Perryman, M 2011, *The Exoplanet Handbook*, Cambridge University Press, Cambridge, UK.

Pichardo, B, Sparke, LS & Aguilar, LA 2005, 'Circumstellar and circumbinary discs in eccentric stellar binaries', *Monthly Notices of the Royal Astronomical Society*, vol. 359, pp. 521-30.

Pichardo, B, Sparke, LS & Aguilar, LA 2008, 'Geometrical and physical properties of circumbinary discs in eccentric stellar binaries', *Monthly Notices of the Royal Astronomical Society*, vol. 391, no. 2, pp. 815-24.

Pilat-Lohinger, E & Dvorak, R 2002, 'Stability of S-type Orbits in Binaries', *Celestial Mechanics and Dynamical Astronomy*, vol. 82, no. 2, pp. 143-53.

Pilat-Lohinger, E, Funk, B & Dvorak, R 2003, 'Stability limits in double stars', *Astronomy and Astrophysics*, vol. 400, no. 3, pp. 1085-94.

Quarles, B & Lissauer, JJ 2016, 'Long-term Stability of Planets in the alpha Centauri System', *The Astronomical Journal*, vol. 151.

Rabl, G & Dvorak, R 1988, 'Satellite-type planetary orbits in double stars - a numerical approach', *Astronomy and Astrophysics*, vol. 191, pp. 385-91.

Raghavan, D, McAlister, HA, Henry, TJ, et al. 2010, 'A survey of stellar families: multiplicity of solar-type stars', *The Astrophysical Journal Supplement Series*, vol. 190, no. 1, p. 1.

Rappaport, S, Deck, K, Levine, A, et al. 2013, 'Triple-star Candidates among the Kepler Binaries', *The Astrophysical Journal*, vol. 768.

Rauch, KP & Hamilton, DP 2012, *HNBody: Hierarchical N-Body Symplectic Integration Package*, Astrophysics Source Code Library, January 1, 2012.

Reche, R, Beust, H & Augereau, J-C 2009, 'Investigating the flyby scenario for the HD 141569 system', *Astronomy and Astrophysics*, vol. 493, no. 2, pp. 661-9.

Rein, H 2012, 'A proposal for community driven and decentralized astronomical databases and the Open Exoplanet Catalogue', *arXiv:1211.7121*.

Reipurth, B & Mikkola, S 2012, 'Formation of the widest binary stars from dynamical unfolding of triple systems', *Nature*, vol. 492, no. 7428, pp. 221-4, item: 23222523.

Roell, T, Neuhäuser, R, Seifahrt, A, et al. 2012, 'Extrasolar planets in stellar multiple systems', *Astronomy and Astrophysics*, vol. 542.

Santerne, A, Hébrard, G, Deleuil, M, et al. 2014, 'SOPHIE velocimetry of Kepler transit candidates. XII. KOI-1257 b: a highly eccentric three-month period transiting exoplanet', *Astronomy and Astrophysics*, vol. 571.

Schneider, J, Dedieu, C, Le Sidaner, P, et al. 2011, 'Defining and cataloging exoplanets: the exoplanet.eu database', *Astronomy and Astrophysics*, vol. 532.

Slawson, RW, Prša, A, Welsh, WF, et al. 2011, 'Kepler Eclipsing Binary Stars. II. 2165 Eclipsing Binaries in the Second Data Release', *The Astronomical Journal*, vol. 142, p. 160.

Smith, AW & Lissauer, JJ 2009, 'Orbital stability of systems of closely-spaced planets', *Icarus*, vol. 201, pp. 381-94.

Soderhjelm, S 1984, 'Third-order and tidal effects in the stellar three-body problem', *Astronomy and Astrophysics*, vol. 141, pp. 232-40.

Sterzik, MF & Tokovinin, AA 2002, 'Relative orientation of orbits in triple stars', *Astronomy & Astrophysics*, vol. 384, no. 3, pp. 1030-7.

Suvakov, M & Dmitrasinovic, V 2013, 'Three classes of Newtonian three-body planar periodic orbits', *Phys Rev Lett*, vol. 110, no. 11, p. 114301, item: 25166541.

Szebehely, V 1980, 'Stability of planetary orbits in binary systems', *Celestial Mechanics*, vol. 22, pp. 7-12.

Tokovinin, A 1993, 'Relative orientation of angular momenta in multiple star systems', *Astronomy Letters*, vol. 19, pp. 383-8.

Tokovinin, A 2000, 'Statistics of multiple stars: some clues to formation mechanisms', in IAU Symposium: *proceedings of the IAU Symposium* pp. 84-92.

Tokovinin, A 2001, 'Statistics of multiple stars: some clues to formation mechanisms', in Formation of Binary Stars: *proceedings of the Formation of Binary Stars* pp. 84-92.

Tokovinin, A 2004, 'Statistics of multiple stars', in Revista Mex. Astron. Astrofis.(Ser. Conf.): *proceedings of the Revista Mex. Astron. Astrofis.(Ser. Conf.)* p. 7.

Tokovinin, A 2008, 'Comparative statistics and origin of triple and quadruple stars', *Monthly Notices of the Royal Astronomical Society*, vol. 389, pp. 925-38.

Tokovinin, A 2014a, 'From Binaries to Multiples. I. Data on F and G Dwarfs within 67 pc of the Sun', *The Astronomical Journal*, vol. 147, p. 86.

Tokovinin, A 2014b, 'From Binaries to Multiples. II. Hierarchical Multiplicity of F and G Dwarfs', *The Astronomical Journal*, vol. 147, p. 87.

Tokovinin, A 2017, 'Orbit alignment in triple stars', *The Astrophysical Journal*, vol. 844.

Tokovinin, A & Kiyaeva, O 2016, 'Eccentricity distribution of wide binaries', *Monthly Notices of the Royal Astronomical Society*, vol. 456, pp. 2070-9.

Tokovinin, A, Gorynya, NA & Morrell, NI 2014, 'The quadruple system ADS 1652', *Monthly Notices of the Royal Astronomical Society*, vol. 443, no. 4, pp. 3082-9.

Tokovinin, AA 1997, 'MSC - a catalogue of physical multiple stars', *Astronomy and Astrophysics Supplement Series*, vol. 124.

Tokovinin, AA 1999, 'VizieR Online Data Catalog: Multiple star catalogue (MSC) (Tokovinin 1997-1999)', *VizieR Online Data Catalog*, vol. 412.

Triaud, AHMJ, Collier Cameron, A, Queloz, D, et al. 2010, 'Spin-orbit angle measurements for six southern transiting planets. New insights into the dynamical origins of hot Jupiters', *Astronomy and Astrophysics*, vol. 524.

Trifonov, T, Lee, MH, Reffert, S, et al. 2018, 'Dynamical analysis of the circumprimary planet in the eccentric binary system HD59686', *ArXiv e-prints*, vol. 1803, viewed March 1, 2018,

Verrier, P & Evans, N 2006, 'Planets and Asteroids in the γ Cephei System', *Monthly Notices of the Royal Astronomical Society*, vol. 368, no. 4, pp. 1599-608.

Verrier, P & Evans, N 2007, 'Planetary stability zones in hierarchical triple star systems', *Monthly Notices of the Royal Astronomical Society*, vol. 382, no. 4, pp. 1432-46.

Verrier, P & Evans, N 2009, 'High-inclination planets and asteroids in multistellar systems', *Monthly Notices of the Royal Astronomical Society*, vol. 394, no. 4, pp. 1721-6.

Verrier, PE & Evans, NW 2008, 'HD 98800: a most unusual debris disc', *Monthly Notices of the Royal Astronomical Society*, vol. 390, pp. 1377-87.

Wagner, K, Apai, D, Kasper, M, et al. 2016, 'Direct imaging discovery of a Jovian exoplanet within a triple-star system', *Science*, vol. 353, no. 6300, pp. 673-8, item: 27386921.

Wang, J, Fischer, DA, Xie, J-W, et al. 2014, 'Influence of Stellar Multiplicity on Planet Formation. II. Planets are Less Common in Multiple-star Systems with Separations Smaller than 1500 AU', *The Astrophysical Journal*, vol. 791.

Wiegert, J, Faramaz, V & Cruz-Saenz de Miera, F 2016, '94 Ceti: a triple star with a planet and dust disc', *Monthly Notices of the Royal Astronomical Society*, vol. 462, pp. 1735-48.

Wisdom, J & Holman, M 1991, 'Symplectic maps for the *N*-body problem', *The Astronomical Journal*, vol. 102, pp. 1528-38.

Wright, JT, Fakhouri, O, Marcy, GW, et al. 2011, 'The exoplanet orbit database', *Publications of the Astronomical Society of the Pacific*, vol. 123, no. 902, pp. 412-22.

Zhuchkov, RY, Orlov, V & Rubinov, A 2006, 'Dynamical stability of the quadruple systems HD 68255/6/7 and HD 76644', *Astronomy Reports*, vol. 50, no. 1, pp. 62-7.